UNCLASSIFIED

MARTIN MARIETTA ENERGY SYSTEMS LIBRARIES
3 4456 0049750 3

CENTRAL RESEARCH LIBRARY
DOCUMENT COLLECTION

ORNL-2432 cy. 8
Reactors—Power
TID-4500 (13th ed. Rev.)

HOMOGENEOUS REACTOR PROJECT

QUARTERLY PROGRESS REPORT

FOR PERIOD ENDING OCTOBER 31, 1957

CENTRAL RESEARCH LIBRARY
DOCUMENT COLLECTION
LIBRARY LOAN COPY
DO NOT TRANSFER TO ANOTHER PERSON
If you wish someone else to see this document, send in name with document and the library will arrange a loan.

OAK RIDGE NATIONAL LABORATORY
OPERATED BY
UNION CARBIDE NUCLEAR COMPANY
Division of Union Carbide Corporation
UCC
POST OFFICE BOX X · OAK RIDGE, TENNESSEE

UNCLASSIFIED

Printed in USA. Price $5.50 cents. Available from the

Office of Technical Services
U. S. Department of Commerce
Washington 25, D. C.

LEGAL NOTICE

This report was prepared as an account of Government sponsored work. Neither the United States, nor the Commission, nor any person acting on behalf of the Commission:

A. Makes any warranty or representation, express or implied, with respect to the accuracy, completeness, or usefulness of the information contained in this report, or that the use of any information, apparatus, method, or process disclosed in this report may not infringe privately owned rights; or

B. Assumes any liabilities with respect to the use of, or for damages resulting from the use of any information, apparatus, method, or process disclosed in this report.

As used in the above, "person acting on behalf of the Commission" includes any employee or contractor of the Commission to the extent that such employee or contractor prepares, handles or distributes, or provides access to, any information pursuant to his employment or contract with the Commission.

UNCLASSIFIED

ORNL-2432
Reactors–Power
TID-4500 (13th ed. Rev.)

Contract No. W-7405-eng-26

HOMOGENEOUS REACTOR PROJECT

QUARTERLY PROGRESS REPORT

For Period Ending October 31, 1957

Project Director – R. B. Briggs
Associate Director – C. E. Winters

Homogeneous Reactor Test – S. E. Beall
Reactor Design and Analysis – J. A. Lane
Engineering Development – J. A. Lane
Reactor Materials Research – E. G. Bohlmann
Chemical Engineering Development – D. E. Ferguson
Supporting Chemical Research – E. H. Taylor
Analytical Chemistry – M. T. Kelley

DATE ISSUED
JAN 7 1958

OAK RIDGE NATIONAL LABORATORY
Operated by
UNION CARBIDE NUCLEAR COMPANY
Division of Union Carbide Corporation
Post Office Box X
Oak Ridge, Tennessee

UNCLASSIFIED

MARTIN MARIETTA ENERGY SYSTEMS LIBRARIES
3 4456 0049750 3

ORNL-2432
Reactors—Power
TID-4500 (13th ed. Rev.)

INTERNAL DISTRIBUTION

1. C. E. Center
2. Biology Library
3. Health Physics Library
4. Metallurgy Library
5–6. Reactor Experimental Engineering Library
7–9. Central Research Library
10–14. Laboratory Records Department
15. Laboratory Records, ORNL R.C.
16. G. M. Adamson
17. J. E. Baker
18. S. E. Beall
19. A. M. Billings
20. D. S. Billington
21. E. P. Blizard
22. E. G. Bohlmann
23. S. E. Bolt
24. C. J. Borkowski
25. G. E. Boyd
26. J. C. Bresee
27. F. R. Bruce
28. W. D. Burch
29. C. A. Burchsted
30. A. D. Callihan
31. D. W. Cardwell
32. W. L. Carter
33. G. H. Cartledge
34. R. A. Charpie
35. R. D. Cheverton
36. H. C. Claiborne
37. W. E. Clark
38. T. E. Cole
39. E. L. Compere
40. F. L. Culler
41. J. S. Culver
42. J. S. Drury
43. W. K. Eister
44. L. B. Emlet (K-25)
45. D. E. Ferguson
46. J. H. Frye, Jr.
47. C. H. Gabbard
48. J. L. Gabbard
49. W. R. Gall
50. H. E. Goeller
51. A. T. Gresky
52. J. C. Griess
53. E. Guth
54. P. A. Haas
55. P. H. Harley
56. P. N. Haubenreich
57. J. W. Hill
58. C. J. Hochanadel
59. A. Hollaender
60. A. S. Householder
61. G. H. Jenks
62. D. T. Jones
63. W. H. Jordan
64. S. I. Kaplan
65. P. R. Kasten
66. C. P. Keim
67. M. T. Kelley
68. R. B. Korsmeyer
69. K. A. Kraus
70. J. A. Lane
71. W. J. Leonard
72. R. E. Leuze
73. S. C. Lind
74. R. B. Lindauer
75. R. S. Livingston
76. R. A. Lorenz
77. M. I. Lundin
78. R. N. Lyon
79. J. L. Marsh (C&CCC, South Charleston)
80. W. L. Marshall
81. H. F. McDuffie
82. J. P. McBride
83. H. A. McLain
84. R. A. McNees
85. J. R. McWherter
86. O. Menis
87. E. C. Miller
88. C. S. Morgan
89. K. Z. Morgan
90. E. J. Murphy
91. M. L. Nelson
92. J. P. Murray (Y-12)
93. L. F. Parsly
94. Sigfred Peterson
95. M. L. Picklesimer
96. L. R. Quarles
97. W. D. Reel
98. P. M. Reyling

99. R. C. Robertson
100. A. M. Rom
101. M. W. Rosenthal
102. H. C. Savage
103. C. L. Segaser
104. E. D. Shipley
105. M. J. Skinner
106. R. W. Stoughton
107. A. H. Snell
108. I. Spiewak
109. C. D. Susano
110. J. A. Swartout
111. E. H. Taylor
112. D. G. Thomas
113. P. F. Thomason
114. M. Tobias
115. D. S. Toomb
116. W. E. Unger
117. R. Van Winkle
118. B. Weaver
119. A. M. Weinberg
120. E. P. Wigner (consultant)
121. G. C. Williams
122. J. C. Wilson
123. C. E. Winters
124. F. C. Zapp
125. ORNL – Y-12 Technical Library, Document Reference Section
126. HRP Director's Office, Y-12

EXTERNAL DISTRIBUTION

127. F. C. Moesel, AEC, Washington
128. Houdry Corporation (Attn: G. A. Mills)
129. Division of Research and Development, AEC, ORO
130–136. TISE for P.A.R.P.
137–666. Given distribution as shown in TID-4500 (13th ed. Rev.) under Reactors–Power category (75 copies – OTS)

Reports previously issued in this series are as follows:

ORNL-527	Date Issued, December 28, 1949
ORNL-630	Period Ending February 28, 1950
ORNL-730	Feasibility Report – Date Issued, July 6, 1950
ORNL-826	Period Ending August 31, 1950
ORNL-925	Period Ending November 30, 1950
ORNL-990	Period Ending February 28, 1951
ORNL-1057	Period Ending May 15, 1951
ORNL-1121	Period Ending August 15, 1951
ORNL-1221	Period Ending November 15, 1951
ORNL-1280	Period Ending March 15, 1952
ORNL-1318	Period Ending July 1, 1952
ORNL-1424	Period Ending October 1, 1952
ORNL-1478	Period Ending January 1, 1953
ORNL-1554	Period Ending March 31, 1953
ORNL-1605	Period Ending July 31, 1953
ORNL-1658	Period Ending October 31, 1953
ORNL-1678	Period Ending January 31, 1954
ORNL-1753	Period Ending April 30, 1954
ORNL-1772	Period Ending July 31, 1954
ORNL-1813	Period Ending October 31, 1954
ORNL-1853	Period Ending January 31, 1955
ORNL-1895	Period Ending April 30, 1955
ORNL-1943	Period Ending July 31, 1955
ORNL-2004	Period Ending October 31, 1955
ORNL-2057	Period Ending January 31, 1956
ORNL-2096	Period Ending April 30, 1956
ORNL-2148	Period Ending July 31, 1956
ORNL-2222	Period Ending October 31, 1956
ORNL-2272	Period Ending January 31, 1957
ORNL-2331	Period Ending April 30, 1957
ORNL-2379	Period Ending July 31, 1957

HRP QUARTERLY PROGRESS REPORT

SUMMARY

PART I. HOMOGENEOUS REACTOR TEST

1. HRT Operations

Following the restoration of the HRT piping to operating condition, the reactor cell was flooded with 18 ft of water for remote-maintenance practice. After successful underwater remote replacement of the purge and circulating pumps, the cell was drained, electrical conduits were purged, and rinsing of the system was begun. The latter half of August and the first week in September were devoted to flushing the piping successively with 3% trisodium phosphate solution, water, 5% nitric acid, and a series of water rinses.

After the phosphate and acid treatments, all flange bolts were replaced and the circulating-pump thermal barriers welded in; then the reactor was hydrostatically tested to 750 and 3000 psi in the low- and high-pressure systems, respectively. A 1950-psi hydrostatic test of the reactor steam system completed the preoperational activity, and the reactor was then charged with condensate for run No. 9.

Run No. 9, begun on September 18, was conducted at 1700 psi and 280°C. It was interrupted on September 19, to flush water, which was high in pH and sodium ion concentration, out of the fuel dump tanks. Operation was resumed on September 23 and was continued to September 30. For run 9 the total operating time at 250°C or above was 155 hr.

After new feed-pump heads were installed, the reactor was filled for run No. 10. High pH and sodium content were again observed in the contents of the fuel dump tanks. Since this phenomenon had been identified with leaching of the catalyst pellets in the iodine-removal section of the fuel recombiner, the recombiner was removed. The run was resumed, with 5.7 kg of uranium being added to the reactor on October 7, and a series of concentration and dilution experiments was conducted to observe the behavior of the dissolved constituents. Another interruption occurred, on October 10, when a leaking chemical-plant sampler valve allowed 200 lb of fuel solution to fill the chemical-plant low-pressure system and discharge to the off-gas system. The entire amount was recovered, as verified by an inventory of the fuel solution. During the final portion of the run, beginning on October 11, operation was maintained without incident for 159 hr at 250°C and above.

The reactor piping is presently being leak-tested with Kr^{85}, to obviate the presence of helium in the system if a need should develop for a more detailed helium leak-test afterward. Activity-breakthrough tests were successfully conducted on two of the four HRT off-gas adsorption beds; the remaining pair will be similarly tested.

A remedy is being sought for the adverse effect on blanket pressurizer control which results from the thermal convection set up in the pressurizer bypass leg (line 204).

Data from the concentration and dilution tests conducted during run No. 10 are being examined for information on the behavior of the ions in solution and the over-all inventory control of the reactor. Inventory balances for the first part of run No. 10 show efficient recovery of the material charged, but analyses of samples collected during high-temperature operation indicate a uranium concentration about 10% lower than expected on the basis of the quantity added to the system.

2. HRT Design

Bolts and nuts received for the HRT were tested to determine asymptotic torque-stress relationship and found to yield results consistent within ±15% after 12 tightening cycles. The pressure-balancing valve was removed from the HRT, leaving only the rupture-disk assembly as protection for the core vessel. A spray system was designed to provide water spray inside the reactor shield as a means of reducing temperature and pressure in event of a gross failure of the reactor system. The piping of the spray system will serve also as a scavenging system for drawing contaminated water away from flanges being opened for underwater maintenance.

3. HRT Component Development

The long-term run of the Westinghouse 400A-1 pump was terminated after 11,605 hr of trouble-free

performance; little wear was noted. The pump has circulated gas-saturated uranyl sulfate solution since that time without difficulty. The 400A-2 shaft seal was improved, achieving a mixing rate of below 2 cc/hr. The 300A-1 pump has operated for 3109 hr since it was last repaired.

No diaphragm or check-valve failures occurred in feed pumps during the quarter. Stellite seats were selected for HRT fuel check valves, and 17-4 PH stainless steel seats for water check valves. Ohio State University fatigue tests indicate annealed 347 stainless steel is the best choice to date for uranyl sulfate feed-pump diaphragms.

The HRT mockup completed a 548-hr run during the quarter, and a second run, which has continued for 1017 hr, was begun. During the first run, Calrod loop heaters gave considerable trouble; this was corrected by substitution of strip heaters. Solution was boiled at 1700 psi in a titanium pipe for 450 hr without any major difficulty. Three stagnant ½-in. lines attached to the mockup high-pressure system have not suffered significant corrosion. Both silvered-alundum pellets and silver-plated Yorkmesh have removed iodine satisfactorily from the HRT mockup.

4. HRT Reactor Analysis

The maximum pressure following a zirconium-water reaction within the HRT core was calculated as a function of the zirconium mass which reacted. If 90% of the reaction energy were quickly dissipated to the aqueous media, kilogram amounts of Zircaloy-2 could react without rupturing the pressure vessel.

HRT critical concentrations were calculated by means of a multigroup, multiregion model. Based on 27 fast groups, a thermal group, and four spacial regions, the "clean" critical concentration was found to be 7.55 g of U^{235} per liter (9.03 g per kilogram of D_2O) at an average temperature of 280°C.

5. HRT Controls and Instrumentation

Armco 17-4 PH alloy has proved to be superior to Stellite No. 6 for letdown-valve plugs. The 17-4 PH alloy is much more resistant to rinse solutions and oxygenated water and has corrosion resistance equal to that of Stellite No. 6 in the uranyl sulfate fuel solution.

Five of the approximately 375 thermocouples in the reactor tank proved unsatisfactory during the last run and will be replaced. All the armored waterproof thermocouples designed for use in thermowells performed satisfactorily.

The reactor nuclear instrumentation was installed and is now undergoing preliminary check-out; check signals have been fed to the pre-amplifiers of the fission-chamber channels for one month.

6. HRT Processing Plant

The final test of the hydroclone system was performed in conjunction with the reactor over a 300-hr operating period. Operation was normal except for an incident following a sampling procedure in which both high-pressure sample valves leaked, permitting fuel solution to pass to the low-pressure system. The processing plant was isolated from the reactor, and one leaking valve was replaced.

Underwater-maintenance procedures were practiced and demonstrated, with the removal and replacement of four components with the cell flooded. Other maintenance procedures were checked for feasibility.

Minor maintenance and construction included seal-welding the thermal barrier and flanges of the circulating pump, installation of new bolts and nuts on high-pressure flanges, installation of the hydroclone-system sampler, and installation of the closed-loop cooling-water system.

Tests of the charcoal adsorber beds are in progress to ascertain whether voids exist which might short-circuit active gases. Beds C and D were shown to be adequate; although tests on the other two beds appeared satisfactory, they will be repeated to obtain more accurate data.

PART II. REACTOR DESIGN AND ANALYSIS

7. HRE-3 Design

In designing the HRE-3, a system requiring no continuous letdown from the high-pressure system and requiring a minimum number of continuously operating components within the reactor cell will be assumed. The plant layout will stress accessibility rather than shortness of lines or proximity to other components in placing the reactor vessel, the pressurizers, circulating pumps, or heat exchangers. Dry maintenance will be considered,

and all components inside the biological shield will be removable. If practicable, following maximum decontamination, major maintenance operations will be performed semidirectly within the biological shield.

8. Reactor Analysis

The prompt-neutron lifetime and the core temperature coefficient of reactivity for the HRE-3 reactor were calculated to be 5.3×10^{-4} sec and -2.9×10^{-3} Δk_e/°C, respectively. For a rate of reactivity addition of 1.5% Δk_e/sec with the reactor initially at source power (0.04 w), the maximum core-pressure rise would be about 400 psi if the piping between the core and pressurizer had a 12-in. diameter, a 40-ft length, and if the vapor volume of the pressurizer were 20 ft^3.

Heat generation rates in the core tank of HRE-3 type reactors were calculated for various core and blanket compositions. With a solution-type core and a D_2O blanket the heat generation rate would be about 15 w/ml. If the D_2O blanket were replaced by a ThO_2-D_2O slurry containing 1000 g of thorium per liter, the corresponding rate would be about 11 w/ml. If this latter reactor had a core region containing 200 g of thorium per liter, the heat generation rate within the core tank would be about 7 w/ml.

Heat generation rates in the HRE-3 pressure vessel resulting from neutron-capture gammas originating in the pressure vessel were calculated for various conditions. At a reactor power of 60 thermal Mw, the maximum heat generation rate obtained with a blanket thorium concentration of 1000 g/liter was about 0.015 w/ml, while with a D_2O blanket the maximum rate was about 1.5 w/ml.

Time-dependent nuclear calculations were performed for HRE-3 type reactors with either U^{233} or U^{235} as the core fuel and with either 500 or 1000 g of thorium per liter in the blanket region. With U^{233} as the fuel and 1000 g of thorium per liter in the blanket, the breeding ratio was on the average about 2% higher during the initial two- to three-year period than for subsequent times. At a core power of 50 Mw, core processing (Thorex) was not required until about 800 days after startup; the corresponding time before the start of blanket processing was about 400 days. With U^{233} as the fuel material the breeding ratio decreased significantly with time until core processing was initiated. Although the breeding ratio was lower on an absolute basis when U^{235} was the fuel material, it varied only slightly during the period before processing. In all cases the total concentration of uranium in the core solution rose very slowly with time and was significantly less than the equilibrium value even after a period of 10 years.

The effect of core length and diameter upon the breeding ratio, wall power density, and critical concentration of cylindrical, two-region HRE-3 reactors was studied. Core diameters were varied from $2\frac{1}{2}$ to $3\frac{1}{2}$ ft, and core lengths from $3\frac{1}{2}$ to 12 ft; the blanket was considered to be 2 ft thick and to contain 1000 g of thorium per liter.

Oracle codes were written for determining the economic characteristics of two-region, time-dependent thorium-breeder reactors, for calculating the critical concentration in bare, annular cylinders, and for calculating the heat generation due to gamma-ray absorption in the core shell of two-region, spherical homogeneous reactors. In the latter code the thermal-flux distribution and hence the prompt-gamma source distribution is calculated by using a two-group model; the decay-gamma source is assumed to be uniformly distributed within the core region. A two-group, two-dimensional, three-region reactor code was converted to comply with present Oracle equipment. A two-group, two-region, spherical reactor code was altered so as to provide more information.

PART III. ENGINEERING DEVELOPMENT

9. Development of Fuel-System Components

The high-pressure recombiner loop was rebuilt, with Inconel material being used in regions where type 347 stainless steel previously stress-cracked, and is ready for operation. Syracuse University has observed little difference between 0.4- and 1.0-in.-dia tubes in H_2-O_2-steam reaction-limit experiments.

Attempts to keep dilute ThO_2 slurry in suspension in the motor of the 20-cfm blower were unsuccessful; consequently, its hydrostatic bearings have not yet been run in slurry service. Investigations of shaft-seal mixing and motor heating on the 4000-gpm Byron Jackson pump are in

progress. A contract was awarded to Reliance Electric Co. for the development and fabrication of a 6000-gpm top-maintenance circulating pump.

After modification by Pressure Products Industries, their diaphragm oxygen compressor has operated satisfactorily. A single-stage Roth turbine pump and a Stellite piston pump containing Haynes alloy 25 piston rings have been operated in efforts to develop 10-gpm feed pumps.

A titanium–stainless steel flanged joint, with satisfactory leakage and thermal-cycling characteristics, has been developed. Chase Brass and Copper Co. has been able to extrude a length of $3\frac{1}{2}$-in. pipe from A-110AT titanium alloy. A titanium heat exchanger is being fabricated for use in the HRT mockup.

Bolting of 19-9 DL, a high-strength austenitic steel, was shown to be satisfactory for joining stainless steel ring-joint flanges. Preliminary data indicate that leak-tight ring joints can be achieved with ASA dimensional tolerances and with nonferruled bolts, provided that the bolts are loaded initially to 45,000-psi stress.

Construction of the thermal-cycle facility is complete except for instrumentation. No failures have occurred to date in tube joints cycled in a water-Cl^--O_2 environment.

Development of HRE-3 gas and steam pressurizers is proceeding. Some sub-assemblies, including a high-pressure jet, are being tested separately.

A 300-gpm slurry loop and a slurry check-valve-materials test system are in various stages of construction.

10. Development of Reactor Slurry Systems

From turbulent-flow pressure-drop measurements it is evident that the substitution of the coefficient of rigidity for viscosity in the Reynolds number gives rise to a unique curve in the conventional Fanning friction-factor plot, lying just below the Newtonian curve for smooth pipe. Laminar-flow data branch off from the turbulent-flow curve at different tube diameters, as they must, according to the Hedstrom relation.

The capillary sampler-viscometer was completed and by means of it pseudo-shear diagrams were obtained at a temperature of about 220°C for the slurry circulating in run T-93. It appears that the coefficient of rigidity and the yield stress are essentially constant over the range of 25 to 220°C.

Heat transfer tests with a slurry containing 685 g of thorium per kilogram of H_2O (yield stress 0.075 lb/ft^2) showed that the change from laminar to transition-type heat transfer occurred at a critical Reynolds number within 10% of that indicated by the Hedstrom criterion. For fully turbulent flows, where the Reynolds number is at least four times the critical value, the conventional heat transfer relations for Newtonian fluids apply with the substitution of the coefficient of rigidity for viscosity.

The 100-gpm loops and the 200-gpm loop were operated for a total of more than 4300 hr during the quarter. Run 200A-14, started last quarter with 1600°C-fired oxide, has accumulated over 2100 hr at 300°C and 2000 psig, with no noticeable change in slurry characteristics. Attack rate based on iron pickup is comparable with that of previous runs where stainless steel impellers were used. Circulation of known sphere-forming oxides at a concentration of 1000 g of thorium per kilogram of H_2O failed to form spheres when uranium and molybdenum oxides were added.

A one-sixteenth-scale Lucite model of a proposed HRE-3 blanket configuration was fabricated, and several flow-visualization techniques were used in initial studies, with injection of bromthymol blue giving the most satisfactory results. These studies showed that the average fluid residence time in the blanket vessel was about 60% greater than the slug (or displacement) flow time for all flow rates examined.

Run SM-3 in the HRT slurry blanket test loop, which had been in progress for 700 hr at the end of the previous quarter, continued for an additional 248 hr before the circulating pump failed and the run was terminated. The gamma surveys indicated relatively uniform thorium distribution at flows of at least 300 gpm, but not at lower flows. After repairs and some improvements to the system, run SM-4 was started as a continuation of run SM-3 and has continued for 800 hr to date. As observed in preceding runs, there is a discrepancy between the calculated thorium charge and the slurry indicated in the system by sampling and gamma measurements. It is believed that the error can be traced to inaccuracies in measuring the thorium charged to the loop. The accuracy with which the gamma transmission through the thorium is measured has been improved to the point where concentrations calculated therefrom are believed to be meaningful.

11. Instrument and Valve Development

A high-differential-range, electric-signal, differential-pressure transmitter incorporating a bellows sensing element performed satisfactorily in calibration checks. Electric-signal differential-pressure transmitters suitable for homogeneous reactor environments are now available in ranges from 50 in. of water to 125 psi.

A survey of pressure and differential-pressure instrument types suitable for a reactor slurry system has been made to aid in the planning of an instrument development program.

A differential transformer for sensing instrument primary-element motions has withstood temperatures to 300°C without insulation failure. The transformer is wound with 30-gage anodized aluminum wire, and the only electrical insulation on the wire is that afforded by the oxide film, which could be expected to be highly temperature and radiation resistant.

Electropneumatic pilot converters and transistorized servo amplifiers are being tested in a program to replace unreliable vacuum tubes with solid-state components.

An industrial television system performed satisfactorily when the camera unit was placed under water in a protective housing.

Slight set-point changes with temperature and time have been observed in the pressure switches used to provide electric alarm and control signals from 3- to 15-psi pneumatic signals.

A 123-in.^{2} pneumatically-powered-bellows valve actuator was tested to 265,000 cycles before developing a leak in the stem sealing bellows.

Electrohydraulic valve actuators for possible application to large control valves in future homogeneous reactors are being tested.

Zircaloy-2 valve trims proved to be very poor in tests performed in the valve test loop but were immune to the ignition reaction experienced with titanium alloys. The tungsten carbide plate on a type 347 stainless steel plug survived 400 "dumps" in the valve test loop; no damage was apparent in a metallographic examination.

PART IV. REACTOR MATERIALS RESEARCH

12. Solution Corrosion

A fifth test was made on the HRT core–pressure-vessel flange and transition-joint mockup. No leakage occurred in 951 hr, for a total of 5069 hr of successful operation.

Metallographic examination revealed stress-corrosion cracks on the outside of a type 347 stainless steel pipe exposed for 20,000 hr to a tap- and demineralized-water spray while circulating solutions at 200 to 300°C. The cracks did not penetrate more than about one-fourth of the wall thickness.

In a study of the effect of additives on corrosion of stainless steel at 250°C in 0.17 *m* UO_2SO_4, the compounds $Ce(SO_4)_2$, $H_7P(MoO_4)_{12}$, As_2O_5, H_3SbO_4, $NaBiO_3$, $(RuNO)_2(SO_4)_3$, $NaNO_3$, and Ag_2SO_4 were found to have no value as inhibitors.

The initial run in the new all-titanium loop, loop H, gave anomalously low corrosion rates for stainless steel coupons. This effect, which is usual in stainless steel loops, may have been due to small differences in pretreatment given the coupons rather than to an effect of the loop itself.

A solution of 0.001 *m* $CuSO_4$ containing 0.003 *m* H_2SO_4 was shown to be satisfactory for the blanket region of the HRT both from a stability and a corrosion standpoint.

Films formed on stressed type 347 stainless steel by exposure in boiling and aerated chloride-free uranyl sulfate solution were found to provide at least some protection from stress-corrosion cracking when the alloy was exposed subsequently in chloride-containing solutions. On the other hand, films formed by heating stainless steel in air at 1250°F did not protect the steel from stress-corrosion cracking in boiling chloride-containing uranyl sulfate solutions. Stressed type 347 stainless steel did not crack during 2500 hr in boiling and aerated distilled water (pH 2.8 and 10.5) containing 100 ppm chloride. However, under similar conditions and with an oxygen overpressure of 150 psi, cracking was produced during the initial 300 hr of test.

The presence of magnesium metal (out of contact with the specimens) or stannous chloride in boiling 42% $MgCl_2$ solution was of no consequence in reducing the susceptibility of type 347 stainless steel to cracking; however, magnesium metal in contact with the stainless steel in the environment completely eliminated the susceptibility of the latter to cracking during a 100-hr test. Chloride-containing marking inks caused cracking of stressed stainless steel when the specimens were exposed to oxygen-containing steam at 300°C.

A number of alloys of zirconium were tested in simulated HRT fuel solution at 300°C. The

best corrosion resistance was shown by a 20% Nb–80% Zr cast alloy. Similarly a preoxidized 33% Nb–67% Zr alloy showed excellent resistance.

Several miscellaneous tests were conducted with material of possible interest to the HRP. Elgiloy, a spring alloy considered for use in the liquid-level control for the HRT pressurizer, was found, in the aged condition, to crack in chloride-free HRT core solution at 300°C. The corrosion rate of AlSiMag 652 was 8 mpy after 1000 hr at 150°C in oxygenated 0.17 *m* UO_2SO_4 solution containing 0.04 *m* H_2SO_4 and 0.03 *m* $CuSO_4$. A ceramic electrical-insulation material, Ceramicite C-100, was completely unsatisfactory in high-temperature uranyl sulfate service. Similarly, Frogalloys C and M corroded excessively in boiling HRT core solution. Nitrided titanium showed excellent corrosion resistance to oxygenated HRT fuel solution at 300°C.

13. Slurry Corrosion

Dynamic-corrosion data and operating observations are reported for five thorium oxide slurry tests in 100A pump loops BS and CS. In two runs in loop BS, oxygenated slurries of a composite of two thoria preparations which were calcined at 1600°C were circulated at 300°C. In one test, made at an average circulating concentration of 944 g of thorium per kilogram of water, an unscheduled shutdown was necessitated after 236 hr of circulation because of erratic operation. Abnormally high attack rates were observed in the test.

A second test made with the same slurry at an average concentration of 630 g of thorium per kilogram of water was terminated as scheduled after 1007 hr of continuous slurry circulation. Moderate specimen attack rates were observed at 21 fps; higher-than-usual rates occurred at 42 fps.

Oxygenated slurries of micropulverized thoria were circulated at 300°C in loop CS in two tests at respective concentrations of 932 and 641 g of thorium per kilogram of water. In the test made at the higher concentration, specimen corrosion rates were normal but pump attack was high. In the second test, an unscheduled shutdown after 168 hr of operation was required because of excessive attack in the circulating pump.

In a 300-hr run in loop CS, sulfated slurry which had been used previously in run SM-2 of the slurry blanket mockup was circulated at 200°C at an average concentration of 488 g of thorium per kilogram of water. Specimen corrosion rates were moderate, but the pump impeller was badly eroded.

Corrosion data are reported for in-line coupon and stress specimens of selected alloys which were exposed in run SM-3 of the slurry blanket mockup.

Higher attack rates of type 347 stainless steel, titanium 75A, and Zircaloy-3A were observed with hydrogenated slurries than with oxygenated slurries in toroid tests with slurries of 1600°C-calcined thoria. Attack of SA-212-B was reduced approximately 30-fold in the hydrogenated runs.

Normal attack rates of type 347 stainless steel, titanium 75A, and Zircaloy-3A were observed in toroid tests in which was studied the effect of the addition of uranyl sulfate to 800°C-calcined thoria slurries.

In toroid tests made to observe differences in attack by slurries of unground and micropulverized thoria, slightly higher attack was observed in runs with the degraded thoria. Slurry spheroids were formed in tests employing the unground thoria.

Generally low attack rates were observed in toroid tests with slurries of jet-precipitated thorium oxalate which was calcined at 650, 1200, 1400, and 1600°C.

Low-to-moderate attack rates were obtained in toroid tests employing slurries prepared from recalcined, 24-μ thoria spheres. Metal attack rates increased with increased slurry concentration and increased circulating velocities.

A standard HB-6-type solution autoclave assembly has been modified to obtain radiation-corrosion data with thorium oxide slurries. An out-of-pile test of the equipment indicates mechanical feasibility of in-pile operation with a thorium oxide slurry containing 500 g of thorium per kilogram of water.

Operation of an in-pile toroid model at 950 to 1000 rpm demonstrated that vibration could be reduced to an acceptable magnitude. However, long-term mechanical reliability has not been achieved. Tests of various heating and cooling systems for temperature control during in-pile operation are continuing.

14. Radiation Corrosion

The construction of loop L-2-19 was completed, and the loop is now in operation in LITR beam hole HB-2. Loop L-2-22 is being constructed. The fabrication of components for an all-titanium loop, L-2-23, was completed. Loop L-4-21 was constructed and is undergoing tests.

In-pile loop experiment L-2-14 has been completed. This was the first loop constructed entirely of titanium. The solution in this loop was 0.17 *m* UO_2SO_4, 0.15 *m* $CuSO_4$, and 0.4 *m* H_2SO_4. The main-stream temperature was 280°C. The in-pile run was terminated when the loop pump failed after 663 hr of circulation of enriched solution. The corrosion rates of Zircaloy-2 core coupons varied from 3.9 mpy at 5.6 w/ml to 7.5 mpy at 13.3 w/ml. Previous experiments with this uranium concentration and at 280°C have had only 0.02 to 0.03 *m* excess acid and 0.015 *m* $CuSO_4$. The Zircaloy-2 corrosion rates in the previous experiments at similar power densities were about twice as great as those in the present experiment. The crystal-bar-zirconium core coupons in the present experiment exhibited corrosion rates in excellent agreement with the Zircaloy-2 data. However, the Zr–15% Nb core coupons exhibited considerably higher corrosion rates than did the Zircaloy-2 coupons. This is in contrast with data from previous experiments in which Zr–15% Nb core coupons exhibited rates lower than those of the Zircaloy-2 coupons. The corrosion rates of the titanium 55A coupons varied from 0.75 mpy at 4.4 w/ml to 1.9 mpy at 21.3 w/ml. The corrosion rates of the titanium–6% Al–4% V core coupons were about twice those of titanium 55A at similar power densities. A heavily deteriorated coupon, tentatively identified as stainless steel, was found in the core annulus. All the other steel coupons had been consumed.

Four autoclave experiments were assembled and operated in the HB-6 facility of the LITR during the past quarter. One experiment was operated in the three-hole HB-5 facility of the LITR. To prevent rubbing and wear of the fixed-plug-hole liner, which was observed in the initial experiment, the fixed plug holes were equipped with Oilite-bronze sleeve bearings before additional experiments were attempted. In addition to the Oilite-bronze bearings in the fixed plug hole, each experimental rocking-autoclave assembly will be equipped with a ball bearing on the nose (reactor) end to further prevent wear of the fixed-plug-hole liner.

A recent autoclave included a Co-Al slow-neutron flux monitor. Good agreement between the flux values from the cobalt monitor and from Zr^{95}-Nb^{95} activity in specimens was obtained. Typical open-hole slow-neutron flux distributions in the HB-5 and HB-6 autoclave facilities at the LITR are given. Three experiments in which stainless steel and Zr–15% Nb–1.5% Sn specimens were exposed in a Zircaloy-2 bomb are discussed briefly. The stainless steel specimens appeared to be covered with a scale similar to that found on Zircaloy-2, indicating that zirconium may be transferred to steel surfaces under the exposure conditions. An example of preferential attack on Zircaloy-2, attributable to flaws in the stock material, is discussed. One autoclave was used to expose samples of zirconia and pin specimens of pure niobium. The zirconia decomposed during exposure. The niobium specimens were covered with a very heavy scale containing 26% uranium and 16% copper. The corrosion rate of the niobium as indicated by defilmed weight loss was 2.5 mpy, as compared with 7.5 mpy for the Zircaloy-2 specimens.

The Zircaloy-2 corrosion rates in a series of reference autoclave tests (that is, in which the solutions were 0.17 *m* UO_2SO_4, 0–0.04 *m* $CuSO_4$, and zero or 0.04 *m* H_2SO_4) have been found to be greater than the corrosion rates of Zircaloy-2 in in-pile loop exposures of similar solutions. It has also been known for some time that Zircaloy-2 surfaces exposed in an autoclave retain a heavy, uranium-containing scale, whereas Zircaloy-2 surfaces exposed in the core section of in-pile loops retain only a very thin film. It is shown that if the power density in the series of reference autoclave tests is corrected by an amount proportional to the amount of uranium found in the scale, rather good agreement between loop and autoclave data both at 250 and 280°C is obtained.

The power-density correction has been applied to autoclave tests, other than the reference series, and earlier conclusions are reviewed. The data, as corrected, indicate no D_2O effect on Zircaloy-2 corrosion and a decrease in corrosion rate (compared with rates in the reference solution) by the use of 0.45 *m* excess H_2SO_4. These two indications are in agreement with loop data. It is indicated that the corrosion rates of Zircaloy-2 in 0.04 *m* UO_2SO_4 and 0.17 *m* UO_2SO_4 solutions are similar at similar corrected power densities. This disagrees with loop observations. Data from an

experiment containing 0.17 *m* $MgSO_4$ and one containing 0.005 *m* $KTcO_4$ in addition to 0.17 *m* UO_2SO_4 indicate no effect by these additives. An experiment in which 0.01 *m* UO_2CO_3 was used with 0.129 Li_2CO_3 demonstrated a corrosion comparable to that expected by the reference media. One experiment of questionable significance indicated that the addition of 0.17 *m* Li_2SO_4 to a 0.17 *m* UO_2SO_4 solution markedly inhibited Zircaloy-2 corrosion. A possible slight inhibitory effect by CrO_3 is indicated.

A test on the effect of fast electrons from a Van de Graaff accelerator on the corrosion of Zircaloy-2 has been carried out. The solution employed was 0.04 *m* in UO_2SO_4, and the test temperature was 300°C. The intensity of the beam was such that the estimated power density in solution at the specimen surface due to absorption of electron energy is 60 w/ml. The total radiation time was 60 hr. Weight and thickness measurements do not show any significant effect of the irradiation on the corrosion of the Zircaloy-2. Similar tests of the effect of electron irradiation on the corrosion of titanium and of stainless steel are proceeding.

15. Metallurgy

Transformation data were obtained on Zr–15% Nb–*X* ternary alloys with additions of Al, Cu, Th, Cr, Mo, Ni, Pd, and V for times up to three weeks at temperatures of 350, 400, and 500°C. All the ternary additions delayed the hardening transformation, molybdenum additions being the most potent, while additions of 1% Al and ½% Cu lowered the maximum temperature for the hardening reaction quite drastically as well.

X-ray diffraction studies of single-crystal and polycrystalline wire specimens, with various diffraction techniques being used, yielded considerable information about the transformation mechanisms occurring in the Zr-Nb binary-alloy system. A transformation mechanism for the hardening reaction is postulated which involves the formation of two body-centered cubic phases from the parent retained-beta matrix. The formation of a transition phase, comparable to the "omega" phase found in the beta-titanium alloys, as an intermediate product between the beta matrix and the two body-centered cubic phases may be occurring. This phase is fairly short lived and, as reported previously, does not seem to be the major hardening phase. The Widmanstätten platelet phase observed in the microstructure has been tentatively identified as body-centered tetragonal in structure.

Subsize tensile specimens of zirconium and titanium alloys were exposed to fissioning uranyl sulfate in the corrosion loops. At the relatively low fast-flux doses in these loops, no change in tensile properties of crystal-bar zirconium or Zircaloy-3A was found. A very few samples indicate that with A-40 and A-110AT titanium an increase in strength and a decrease in ductility are occurring.

Weldments were made in ⅛-in. sheet stock of titanium alloy A-110AT. Guided bend tests made on a 2½ *T* (5/16-in.) radius indicated satisfactory ductility in these weldments. Metallographic examination indicated a second phase present in the as-received base metal, which possibly could lead to unsatisfactory welds in heavy sections of this alloy.

Since titanium and type 347 are used together in contact with water or uranyl sulfate in some HRP designs, the need for joining the metals in final assemblies in the field often arises. Torch-brazing is the only practicable method. Silver or gold filler metal would be required because of corrosive service requirements. A successful method of silver-brazing titanium has not been found. All feasible brazing fluxes investigated failed to function satisfactorily. Thus the possibility of stainless steel–titanium silver brazements appears remote.

Manual welds were made in type 347 stainless steel pipe, simulating the welding sequence which would be used in making machine welds in the field. Results indicate that a machine weld equal to present HRP quality should be obtainable.

With both zirconium and titanium it has been shown that complete combustion of the specimen will occur if they are fractured in high-pressure oxygen. Titanium will ignite and sustain a reaction if ruptured in 350-psi oxygen at room temperature or 250 psi at 300°C. Ignition does not occur under oxygenated water and will be quenched by a bath of water. Reactions of molten zirconium with water and with uranyl sulfate appear to be comparable.

In irons and low-alloy irons, such as carbon steels, in the normalized condition, tensile data indicate a greater loss in ductility in low-carbon alloys with a ferritic structure than in alloys with a pearlitic structure and of higher carbon content.

The uniform elongation in the tensile test is proposed to be a more meaningful and sensitive indication of radiation-induced ductility loss than the conventional elongation, which is the sum of the uniform and necking elongations.

PART V. CHEMICAL ENGINEERING DEVELOPMENT

16. Uranyl Sulfate Fuel Processing

Deposition of ZrO_2 particles from simulated homogeneous-reactor fuel circulating in a glass loop decreased as the Reynolds number of the system was increased by increasing the fuel flow rate. Studies on deposition of ZrO_2 from simulated fuel in a stainless steel loop indicated an HRT fuel solids concentration of 50 to 200 mg/liter.

In a mechanically simple system, adsorption of ZrO_2 on stainless steel surfaces at room temperature was not affected by variations in amount of solids or liquid in contact with a given amount of surface area.

In the HRT mockup, iodine was removed effectively by use of a silvered-alundum trap, located in the low-pressure system. In the laboratory such a trap was more effective when operated at temperatures above 100°C than it was at lower temperatures.

17. Gaseous Fission-Product Disposal

Dynamic studies of the adsorption of fission gases on HRT charcoal showed that xenon was adsorbed 16 times more strongly than krypton. In equilibrium-adsorption studies Linde molecular sieves 5A had about 25% of the capacity of charcoal for krypton adsorption.

18. Uranyl Sulfate Blanket Processing

Several experiments were carried out in the P-1 loop in which ZrO_2 or $Zr(SO_4)_2$ was added to 1.4 *m* UO_2SO_4 circulating at 250°C under 350 to 400 psi O_2. The zirconium was substituted for plutonium, which will be added in later experiments. When preformed ZrO_2 was added, the half-time of ZrO_2 disappearance from the circulating solution was 2 to 4 hr, either with or without the hydroclone operating. Only 6 to 16% of the ZrO_2 was removed by the hydroclone, and 85 to 90% was removed by adsorption on loop walls. When ZrO_2 concentrations were 10 to 100 mg/liter, the calculated hydroclone efficiency was 10 to 20%. When dissolved $Zr(SO_4)_2$ was allowed to hydrolyze in the circulating solution, essentially all the zirconium was adsorbed; only a trace was removed in the hydroclone.

The narrow absorption peak at 835 mμ used for determination of the plutonyl ion in solution was shown to be a nonsymmetrical doublet with a width of 40 Å at half peak height. Both peaks followed the ideal absorption laws.

When 770 mg/liter of Pu(IV) in 1.4 *m* UO_2SO_4 was heated to 90°C, it was partially disproportionated to Pu(III) and Pu(V). Under these conditions, Pu(V) (or PuO^+) is apparently stable.

19. Thorium Oxide Blanket Processing

The adsorption of neodymium from dilute neodymium nitrate solution on thorium oxide in aqueous slurries at 250°C decreased as the ThO_2 calcination temperature increased. Thorium oxide calcined at 650°C adsorbed 7400 ppm Nd from 0.006 *m* $Nd(NO_3)_3$ at 250°C, but that calcined at 1100°C adsorbed only 500 ppm Nd.

20. Thorium Oxide Slurry Development

Ultrasonic energy dispersed dry ThO_2 agglomerates to individual 1-μ particles, but none of the methods tested fed dispersed ThO_2 satisfactorily to a calcination flame. Oxide products prepared by firing thorium hydroxide were gritty, glasslike, and composed of large agglomerates.

Irradiation of a settled slurry of 800°C-calcined micropulverized ThO_2 for 2091 hr at 300°C in the LITR did not markedly impair its slurry properties. The U^{233} content of the slurry solids after 37 days of decay was 0.14%. A slurry of 800°C-calcined ThO_2–0.5% U^{235} prepared from the coprecipitated oxalates and containing 20,000 ppm MoO_3 and 3000 ppm sulfate [$Th(SO_4)_2$] was irradiated for 343 hr in the LITR without apparent damage.

A slurry of 1600°C-fired oxide irradiated for 336 hr at 300°C in the LITR contained nearly five times as much iron and nickel corrosion products as the slurry from an out-of-pile control experiment. Repeated attempts to find chromium in the irradiated slurry were unsuccessful.

In irradiated thorium-uranium oxide slurries (250, 500, and 700 g of thorium per kilogram of H_2O) containing equal ratios of enriched uranium to thorium, gas production and recombination rates, respectively, were directly dependent on power density and slurry concentration. The *G* value for gas production, assuming a neutron flux of

5.3×10^{11} neutrons/cm^2·sec and an energy dissipation of 170 Mev/fission, was 0.7.

In out-of-pile gas-recombination studies it was necessary to calcine thorium-uranium oxides for 16 hr or more at 1000°C in order to obtain satisfactory H_2-O_2 reaction rates (>10 moles of H_2 per hour per liter at 280°C, P_{H_2} = 500 psi) with aqueous slurries prepared from this material and containing 0.05 *m* MoO_3. The mixed oxide calcined at 1200°C for only 4 hr was a satisfactory support for the catalyst in aqueous suspension.

An initial low reaction rate in mixed 1600°C-calcined ThO_2-UO_3·H_2O slurry increased slowly with catalyst concentration, but at 0.048 *m* MoO_3 the reaction rate in the hydrogen-activated slurry was 17.3 moles of H_2 per hour per liter at 291°C and P_{H_2} = 500 psi. The reaction rates in the slurries of thorium-uranium oxide prepared from the coprecipitated oxalates and calcined at 1600°C for 24 hr were low in the absence of the catalyst, but the addition of 0.012 *m* MoO_3 greatly increased the rate in the slurry as prepared to 32.7 moles of H_2 per hour per liter of slurry at 280°C and a partial pressure of 500 psi H_2.

Heating D-16-650 oxide and LO-12 800°C-fired oxide for 1500 hr in water at 300°C did not affect the crystallite size or specific surface area of either oxide. The crystallite growth, on refiring at 900°C, of both oxides was markedly inhibited by the hydrothermal treatment, the effect becoming more pronounced with increasing autoclaving time for the D-16 oxide. The average particle size of the D-16 oxide was considerably decreased by the hydrothermal treatment. The results indicate that the 650°C-fired oxides are more reactive to water at high temperatures than the oxides fired at higher temperatures.

Tap density, particle-size data, and abrasion-test information on thorium-uranium oxides indicate that the presence of uranium promotes sintering and increases the abrasiveness, the effect becoming more pronounced with increasing uranium content and increasing firing temperatures.

Viscosity data obtained with an aqueous suspension of thorium oxide containing 200, 400, and 700 g of thorium per kilogram of H_2O indicates a linear relation between the logarithm of the relative viscosity and the reciprocal temperature. The viscosities of the thorium oxide slurries in the temperature range 25 to 90°C are related to the hindered-settling rates by the equation:

$$\eta = A\, U_0\, e\, 2.85 \times 10^3/T \ ,$$

where η is the slurry viscosity in centipoises, U_0 the settling rate in cm/sec, and T the absolute temperature. The proportionality constant, A, is characteristic of the oxide used and for the oxides tested was 0.003.

Gas-adsorption isotherms for carbon dioxide were obtained for thoria which had been degassed at 450°C. Both enthalpy and entropy appear to play a part in the adsorption, entropy becoming more important as the adsorption temperature is increased. In a study of adsorption on thoria from sulfuric acid solutions, isotherms at 4°C showed an apparent surface saturation of four hydrogen ions and two sulfate ions per surface site. This result is tentatively explained as a displacement of two hydroxyl groups per surface site by hydrogen sulfate groups.

21. In-Pile Slurry Loop

The PAR in-pile slurry loop design and development is proceeding on schedule, with slurry test runs at temperature and pressure in the loop mockup at Westinghouse already in progress. The design of facilities at the ORR reactor is on schedule, with the fabrication of the south facility plug sufficiently far advanced that its completion is assured prior to startup of the ORR. Engineering design of the segmenting facility required for disassembly and inspection of irradiated loops of this size is proceeding according to schedule.

PART VI. SUPPORTING CHEMICAL RESEARCH

22. Aqueous Systems at Elevated Temperatures

Two-liquid-phase transition temperatures were determined for the system $CuSO_4$-UO_2SO_4-H_2SO_4-H_2O. These data indicate maximum temperature and composition limits within which particular homogeneous reactor fuels can be used in order to avoid the appearance of a solid or a second liquid phase. Briefly, in the region of HRT solution composition of $CuSO_4$, UO_2SO_4, and H_2O, an excess amount of H_2SO_4 is necessary, both to eliminate formation of basic (as opposed to acidic) uranium and copper solid compounds and to raise the two-liquid-phase transition temperature.

PART VII. ANALYTICAL CHEMISTRY

23. Analytical Chemistry

Improved methods were devised for the determination of microgram quantities of bismuth and ruthenium in solutions of uranyl sulfate. A volumetric titration method was adapted for use in the determination of microgram quantities of bismuth. A method, more successful than the conventional oxidation-distillation method, was developed in which ruthenium as the nitroso salt is decomposed and separated by pyrolysis in a stream of moist oxygen; the ruthenium is then determined spectrophotometrically.

Development work on the analysis of slurries of thorium oxide of interest in connection with the HRP resulted in the discovery of an improved method for separation of fluoride from stabilizing agents such as clays and related materials. In a procedure developed for the determination of cobalt, an anion exchange technique was applied to the separation of thorium and a number of interfering substances from cobalt; 0.1 ppm of cobalt can be determined by this method.

CONTENTS

SUMMARY v

PART I. HOMOGENEOUS REACTOR TEST

1. HRT OPERATIONS 3
   - 1.1 Reactor Operations 3
   - 1.2 Inventory Control and Chemical Behavior 4
2. HRT DESIGN 5
   - 2.1 Flange Development Program 5
   - 2.2 Pressure-Balancing System 6
   - 2.3 Supplementary Recombination 7
   - 2.4 Cell-Spray and Flange-Scavenging System 7
   - 2.5 Replacement Steam Generator 9
3. HRT COMPONENT DEVELOPMENT 11
   - 3.1 Fuel Circulating Equipment 11
     - 3.1.1 400A-1 Pump and Loop 11
     - 3.1.2 400A-2 Pump and Loop 11
     - 3.1.3 300A-1 Pump 11
   - 3.2 Feed Pumps 11
     - 3.2.1 Feed-Pump Test Loops 11
     - 3.2.2 Purge Pumps 13
     - 3.2.3 Check-Valve Material Test 13
     - 3.2.4 Corrosion Fatigue Tests 13
     - 3.2.5 HRT Replacement Feed and Purge Pumps 13
   - 3.3 HRT Mockup 14
     - 3.3.1 Operation 14
     - 3.3.2 Boiling of Mockup Fuel Solution 14
     - 3.3.3 Corrosion in Stagnant Lines 14
     - 3.3.4 Iodine Removal Tests 15
4. HRT REACTOR ANALYSIS 16
   - 4.1 Reactor Pressure Following Zr-H_2O Reaction 16
   - 4.2 HRT Critical Concentrations Obtained by Multigroup Model 17
5. HRT CONTROLS AND INSTRUMENTATION 19
   - 5.1 Component and System Testing 19
     - 5.1.1 Letdown Valves 19
     - 5.1.2 Thermocouples 19
     - 5.1.3 Nuclear Instrumentation 20
6. HRT PROCESSING PLANT 22
   - 6.1 Underwater-Maintenance Practice 22
     - 6.1.1 Tests Prior to Flooding 22
     - 6.1.2 Underwater Tests 22

6.2 Construction and Maintenance 22
6.3 Final Operation of the High-Pressure System 23
6.4 Holdup Tests on HRT Charcoal Adsorber Beds 23
6.5 Carpenter-20 Pump Test 24

PART II. REACTOR DESIGN AND ANALYSIS

7. HRE-3 DESIGN 27
7.1 Thorium Breeder Reactor (HRE-3) 27

8. REACTOR ANALYSIS 38
8.1 Kinetic Calculations for the HRE-3 38
8.2 Heat Generation Rates in HRE-3 Core Tank 39
8.3 Heat Generation Rates in HRE-3 Pressure Vessel 40
8.4 Time-Dependent Studies of HRE-3 Type Reactors 42
8.5 Cylindrical HRE-3 Reactor Studies 46
8.6 Oracle Programming 46

PART III. ENGINEERING DEVELOPMENT

9. DEVELOPMENT OF FUEL-SYSTEM COMPONENTS 51
9.1 Recombiner Development 51
9.1.1 High-Pressure Recombiner 51
9.1.2 Syracuse Contract 51
9.2 Centrifugal Pumps 51
9.2.1 20-cfm Canned-Motor Blower 51
9.2.2 4000-gpm Loop 51
9.2.3 Reliance 6000-gpm Pump 52
9.3 Oxygen Compressors 52
9.4 10-gpm Fuel Feed Pumps 52
9.5 Titanium Program 52
9.6 Flange Test Program 53
9.7 Thermal-Cycle Facility 53
9.8 Heat Exchanger Tube-Joint Test 54
9.9 HRE-3 Pressurizer Development 54
9.9.1 High-Pressure Jet Test 54
9.10 Development of Slurry Components 54
9.10.1 300-gpm Slurry Loop 54
9.10.2 Slurry Check-Valve Material Test 54

10. DEVELOPMENT OF REACTOR SLURRY SYSTEMS 56
10.1 Rheology of Thorium Oxide Slurries 56
10.1.1 Turbulent-Flow Pressure-Drop Measurements 56
10.1.2 Laminar Flow at Elevated Temperatures 57

10.2 Slurry Heat Transfer 57
10.3 Circulating-Slurry Behavior 59
10.4 Blanket Fluid Mechanics 62
10.5 HRT Blanket System Development 62

11. INSTRUMENT AND VALVE DEVELOPMENT 70
11.1 Instrument Development 70
11.1.1 Differential-Pressure Transmitters 70
11.1.2 Pressure and Differential-Pressure Transmitters for Slurry Systems 70
11.1.3 High-Temperature Radiation-Resistant Differential Transformers 70
11.1.4 Solid-State-Component Instrument Systems 70
11.1.5 Underwater Television 73
11.1.6 Pressure-Switch Evaluation 73
11.2 Valve Development 73
11.2.1 Pneumatic Actuators 73
11.2.2 Hydraulic Actuators 73
11.2.3 Valve Trim 75

PART IV. REACTOR MATERIALS RESEARCH

12. SOLUTION CORROSION 79
12.1 Dynamic Corrosion Studies 79
12.1.1 Fifth Test of the HRT Core–Pressure-Vessel Flange and Transition-Joint Mockup 79
12.1.2 Metallographic Examinations from Previous Experiments 79
12.1.3 Effect of Additives to 0.17 *m* UO_2SO_4 80
12.1.4 Initial Runs in an All-Titanium Loop 81
12.1.5 Chemical Stability and Corrosiveness of Dilute Copper Sulfate–Sulfuric Acid Solution for the HRT Blanket 82
12.2 Laboratory Corrosion Studies 82
12.2.1 Stress-Corrosion Cracking 82
12.2.2 Corrosion Tests with Zirconium Alloys 84
12.2.3 Miscellaneous Corrosion Tests 84

13. SLURRY CORROSION 87
13.1 Pump Loops 87
13.1.1 Loop Engineering 87
13.1.2 100A Pump Loop Tests: Introduction 87
13.1.3 Circulation of 1600°C-Calcined Thoria Slurry 87
13.1.4 Attack by Micropulverized Thoria Slurry 91
13.1.5 Attack by Sulfated Slurry Circulated at 200°C 92
13.1.6 Field Corrosion Tests 93
13.2 Toroids 96
13.2.1 Introduction 96
13.2.2 Tests with Thoria Slurries Containing Uranyl Sulfate 96
13.2.3 Attack by 1600°C-Calcined Thoria Slurries in Hydrogen and Oxygen Atmospheres 97
13.2.4 Pilot Tests with Experimental Preparations of Thoria 98
13.2.5 Toroid Circulation Tests with Thoria Spheres 100

13.3 In-Pile Autoclave Slurry Tests – LITR 104
13.3.1 Development and Construction 104
13.4 In-Pile Slurry Toroid 104
13.4.1 Development Engineering 104

14. RADIATION CORROSION 106
14.1 In-Pile Loops 106
14.1.1 Development and Construction 106
14.1.2 General Description of In-Pile Loop Experiment L-2-14 107
14.1.3 Qualitative Results of Inspection of Loop L-2-14 108
14.1.4 Quantitative Results of Inspection and Evaluation of Loop L-2-14 115
14.1.5 Discussion of Results from Loop L-2-14 and Previous Loops 116
14.1.6 In-Pile Loop L-4-18 119
14.1.7 In-Pile Loop L-2-19 119
14.2 In-Pile Autoclave Solution Tests – LITR 120
14.2.1 Development and Construction 120
14.2.2 Correlation of In-Pile Autoclave Data with In-Pile Loop Data 120
14.2.3 Data from Recent Autoclave Exposures 126
14.3 Supporting Research 130

15. METALLURGY 131
15.1 Physical Metallurgy 131
15.1.1 Zirconium-Alloy Development 131
15.2 Mechanical Metallurgy 134
15.2.1 Tensile Properties of Irradiated Zirconium Alloys 134
15.2.2 Tensile Properties of Irradiated Titanium Alloys 135
15.3 Welding Development 136
15.3.1 Titanium Welding 136
15.3.2 Stainless Steel Welding 137
15.4 Metal-Solution Reactions 137
15.4.1 Titanium 137
15.4.2 Zirconium 137
15.5 Effects of Radiation on Structural Metals and Alloys 138
15.5.1 Equipment and Facilities 138
15.5.2 Test Data 138
15.6 Thorium Oxide Calcination Methods 139
15.6.1 Electric and Gas-Fired Furnace Operations 139
15.6.2 Flame-Spray Calcination 139
15.6.3 Electric-Arc Calcination 140
15.6.4 Spheroidizing of Highly Refractory Materials 140

PART V. CHEMICAL ENGINEERING DEVELOPMENT

16. URANYL SULFATE FUEL PROCESSING 143
16.1 Solids Behavior 143
16.1.1 Loop Studies 143
16.1.2 Laboratory Tests 144

16.2 Iodine Chemistry 145

17. GASEOUS FISSION-PRODUCT DISPOSAL 147

17.1 Dynamic Studies 147

17.2 Equilibrium Studies 147

18. URANYL SULFATE BLANKET PROCESSING 149

18.1 Behavior of Zirconium in the P-1 Loop 149

18.2 Loop P-1 Operation 150

18.3 In-Pile Experiment 150

18.4 Spectrum of PuO_2^{++} 150

18.5 Disproportionation of Plutonium(IV) in Sulfate Systems 151

19. THORIUM OXIDE BLANKET PROCESSING 152

19.1 Cation Adsorption on ThO_2 152

20. THORIUM OXIDE SLURRY DEVELOPMENT 153

20.1 Oxide Preparation 153

20.1.1 Preparation of Small Particles 153

20.1.2 Flocculation Studies 153

20.1.3 Flame Calcination 153

20.1.4 Alternate Preparation Method 153

20.1.5 Grindability of High-Fired Thorium Oxide 155

20.2 Slurry Irradiation Studies 155

20.2.1 Slurry Irradiations in the LITR 155

20.2.2 Postirradiation Analyses 156

20.2.3 In-Pile Gas-Recombination Studies 156

20.3 Gas-Recombination Studies 157

20.3.1 Effect of Calcination Conditions on the Catalytic Activity of Aqueous Thorium-Uranium Oxide Slurries 157

20.3.2 Experiments with Pumped Oxide 158

20.3.3 MoO_3 Concentration Studies with 1600°C-Fired Oxide 158

20.4 Slurry Chemistry Studies 159

20.4.1 Long-Term Hydrothermal Experiments 159

20.5 Thorium-Uranium Oxide Studies 159

20.5.1 Uranium Content 160

20.5.2 Tap Densities 160

20.5.3 Particle Size 161

20.5.4 Crystallite Size and Surface Area 161

20.5.5 Abrasive Characteristics 162

20.6 Slurry Viscosity and Hindered Settling 162

20.7 Surface-Chemistry Studies 163

21. IN-PILE SLURRY LOOP 164

21.1 Slurry Sampling 164

21.2 In-Pile Loop Facility Design 164

21.3 Segmenting Facility 165

21.4 Schedules 165

PART VI. SUPPORTING CHEMICAL RESEARCH

22. AQUEOUS SYSTEMS AT ELEVATED TEMPERATURES 171

22.1 Two-Liquid-Phase Transition Temperatures in the System $CuSO_4$-UO_2SO_4-H_2SO_4-H_2O 171

PART VII. ANALYTICAL CHEMISTRY

23. ANALYTICAL CHEMISTRY 181

23.1 Analysis of Solutions of Uranyl Sulfate 181

23.1.1 Determination of Arsenic 181

23.1.2 Pyrolytic Separation and Spectrophotometric Determination of Ruthenium 181

23.1.3 Determination of Cerium 181

23.1.4 Spectrophotometric Determination of Antimony 181

23.1.5 Spectrophotometric Titration of Bismuth 181

23.2 Analysis of Thorium Oxide 182

23.2.1 Determination of Cobalt 182

23.2.2 Separation of Fluoride by Pyrolysis 182

23.2.3 Particle-Size Distribution in the Range of 10 to 50 μ 184

Part I

HOMOGENEOUS REACTOR TEST

S. E. Beall

1. HRT OPERATIONS

S. E. Beall

H. F. Bauman
N. C. Bradley
N. A. Brown[1]
D. F. Bruley
J. R. Buchanan
J. R. Engel
J. D. Flynn
D. F. Frech
T. H. Gladney[1]
R. H. Guymon
R. J. Harvey
P. N. Haubenreich
J. Hernandez[2]
J. W. Hill, Jr.
S. I. Kaplan
J. O. Kolb
H. M. McLeod
R. M. Pierce[1]
D. M. Richardson
G. W. Rivenbark
H. K. Search[3]
A. J. Sharenberger
W. Terry
K. W. West
R. Van Winkle

1.1 REACTOR OPERATIONS

The extensive repairs and modifications to the HRT, which occupied the previous quarter, were completed during the first week in August. After the flanged joints were leak-checked, the reactor cell was flooded to a depth of 18 ft, and remote replacement of the purge and circulating pumps was demonstrated successfully. The water level was then raised to cover all air lines, air-pressurized conduit, and insulation jackets in the cell, and the location of all leaks was mapped for subsequent repairs. When the cell was drained and after the electrical conduits were superficially dried by air-purging, the circulating-pump and pressurizer-heater wiring was checked and found to be operable.

The period from mid-August to the first week in September was devoted to flushing the reactor piping with hot 3% trisodium phosphate solution, followed by water rinses and a 5% nitric acid wash. After the acid was rinsed from the system, operation was suspended while the zinc-plated flange bolts were replaced with new, unplated material as proposed earlier.[4] At this time, also, the thermal barriers in the circulating pumps were seal-welded. Hydrostatic tests, conducted on the low-pressure systems at 750 psi, the high-pressure systems at 3000 psi, and the reactor steam system at 1950 psi, showed the piping to be mechanically fit for further operation, and the fuel and blanket recombiners were reinstalled to prepare for the high-temperature water and depleted-uranium runs.

Test run No. 9 commenced on September 18, with the reactor operating on condensate at 280°C. A rapid buildup of sodium ion and excessively high pH in the water in the fuel dump tanks dictated a shutdown the following day. The contaminants were found to have been leached from the silver-impregnated alumina Raschig rings in the iodine-removal bed, a chamber in the fuel recombiner. After extensive flushing of the system, the run was restarted on September 23 and was continued until September 30. For run 9 the total operating time at 250°C or above was 155 hr.

Feed-pump heads of improved design were installed on the fuel and blanket systems, following test run No. 9, to provide as much on-site test experience with the new heads as possible before the critical experiments. Test run No. 10 was started on October 3, with condensate in the reactor. A recurrence of the previous leaching trouble caused the run to be discontinued on October 4 long enough for the fuel recombiner to be removed and the fuel-system condensate charge to be replaced. Operation was resumed the same evening; when no further contamination was observed by the following day, the chemical separations plant was started and joint operation resumed. On October 7, 5.7 kg of uranium was injected into the reactor, and a series of concentration and dilution experiments was begun, to study the transient and equilibrium behavior of the ions in the system. Three days later, a leaking chemical-plant sampler valve allowed approximately 200 lb of fuel solution to be transferred to the chemical-plant low-pressure system, which overflowed through the off-gas line, making it necessary to suspend the run. The remaining fuel was removed for inventory, and the discharged portion was completely recovered. Operation was resumed after loading the reactor with fresh fuel

[1]On loan from TVA.

[2]On loan from Puerto Rico Water Resources Authority.

[3]On loan from Pennsylvania Power and Light Co.

[4]S. E. Beall *et al.*, *HRP Quar. Prog. Rep. July 31, 1957*, ORNL-2379, p 3.

and replacing the chemical-plant valves, and a continuous run of 159 hr at 250°C and above was completed. The shutdown at the conclusion of the run was preceded by pumping condensate into the core until essentially complete dilution was achieved; this served both to check out the standard shutdown procedure for critical operation and to remove virtually all the uranium from the high-pressure fuel and chemical processing piping, in preparation for gas leak-testing of the system.

The final leak test of the HRT was originally conceived as a helium leak test. Since the complete system will be tested as a single entity, however, the presence of helium in the reactor would necessitate elaborate purging of the piping if the outcome should indicate the need for a detailed, line-by-line check of the assembly. Hence, the over-all proof test will employ Kr^{85} inside the piping as the detector gas, with nitrogen pressurized to 300 psig as the carrier gas. Detection will be accomplished by extracting gas samples from the sealed shield volume surrounding the piping, and passing them through an activated charcoal adsorption bed cooled to −150°C. The bed will then be outgassed into a sensitive gas counter chamber, and any krypton activity recorded.

Activity-breakthrough tests were successfully conducted on two of the four charcoal beds associated with the HRT. The predicted breakthrough time of a measured slug of Kr^{85}, with 1 liter/min of O_2 as a carrier, matched the actual breakthrough (seven to eight days) within the accuracy of prediction in both cases. Previous tests conducted on the other two beds yielded inconclusive results, and preparations are currently under way to retest those beds.

The bypass line in the blanket pressurizer (line 204), intended to permit heavy-water operation in the blanket without operating the pressurizer purge pump, has adversely affected blanket-pressurizer level control. The difficulties appear to result from temperature differences between line 204 and the pressurizer legs, and means to eliminate the trouble are being studied.

1.2 INVENTORY CONTROL AND CHEMICAL BEHAVIOR

Routine calculations of water inventory were made once per shift, by using pressurizer-level and thermocouple readings and weigh-cell indications. All additions and removals of water were recorded, to provide a "book" inventory figure for the water in each system. Comparison of successive calculated inventories from day to day provided a reliable means of detecting transfer between the fuel and blanket systems, or leakage from the reactor. Although changes in inventory could be determined with satisfactory accuracy, the absolute values of the calculated inventories appeared to be somewhat low. The calculated inventories of water at the end of run No. 10 are compared in Table 1.1 with the amounts in the systems as determined by draining. Shown also for comparison are the "book" balances, which take into account all the measured additions and removals but not the unmeasured transfers between the fuel and blanket systems.

Although the material recovered from the systems agreed very satisfactorily with the amount charged, the concentrations of uranium, sulfate ion, and copper observed from samples during run No. 10 were generally about 10% lower than could be predicted from the inventory of uranium and the apparent inventory of water in the fuel system. (A similar discrepancy existed during the first depleted-uranium run, carried out in the spring of 1957.) During the run, several special experiments, involving concentrating and diluting the fuel solution, were carried out to investigate this situation. Samples were taken at frequent intervals throughout the experiments to provide a record of the transient concentrations of the ions. Results of these experiments, together with all other available data on weigh-cell calibrations, system-volume determinations, and the chemistry of the fuel solution as revealed by analysis of the samples, are presently being studied.

Table 1.1. Water Inventories After Run No. 10

	Fuel System (lb)	Blanket System (lb)	Total (lb)
Calculated	1710	4000	5710
Drained	1750	4090	5840
"Book"	1500	4350	5850

2. HRT DESIGN

W. R. Gall M. I. Lundin

F. C. Bowen[1]
C. A. Burchsted
R. D. Cheverton
C. J. Claffey
C. W. Collins
E. H. Gift
E. M. Guglielmo[1]
H. A. McLain
T. H. Mauney
R. C. Moren[2]
A. C. Phillips[1]
R. G. Pitkin[1]
R. C. Robertson
J. N. Robinson
W. Robinson
C. L. Segaser
R. E. Schappel
D. D. Tarr[1]
W. L. Wright
F. C. Zapp

2.1 FLANGE DEVELOPMENT PROGRAM

It was reported previously[3] that a relationship exists between the number of times a bolt-nut assembly is tightened and the reproducibility of the torque required, as indicated by a torque wrench, to produce a given stress in the bolt. Figure 2.1, in which the torque required is plotted against the number of repetitions of the tightening-loosening procedure, presents the results of tests made with the recently acquired HRT bolts. After several repetitions of the tightening-loosening procedure, the mating surfaces become so conditioned that a minimum torque is required to produce a given stress in the bolt. Table 2.1 presents the torques required to produce stresses of 45,000 psi in conditioned HRT bolts. These torques were determined by tightening each bolt-nut assembly, with a torque wrench and a load cell, a sufficient number of times to reach the horizontal portion of the curves of Fig. 2.1. At this point the bolt was calibrated for the specific torque to be applied upon installation in the HRT flanges. Actual stresses attained when using torque wrenches to tighten the conditioned nuts and bolts in the reactor should be within ±15% of the values specified.

Tests were made to determine the effect of mismatch of flange grooves and ring gaskets in ring-type closures. In four assemblies the pitch

[1]On loan from Vitro Engineering Co.

[2]On loan from Westinghouse Electric Corp.

[3]W. R. Gall *et al.*, *HRP Quar. Prog. Rep. July 31, 1957*, ORNL-2379, p 6, esp 10–11.

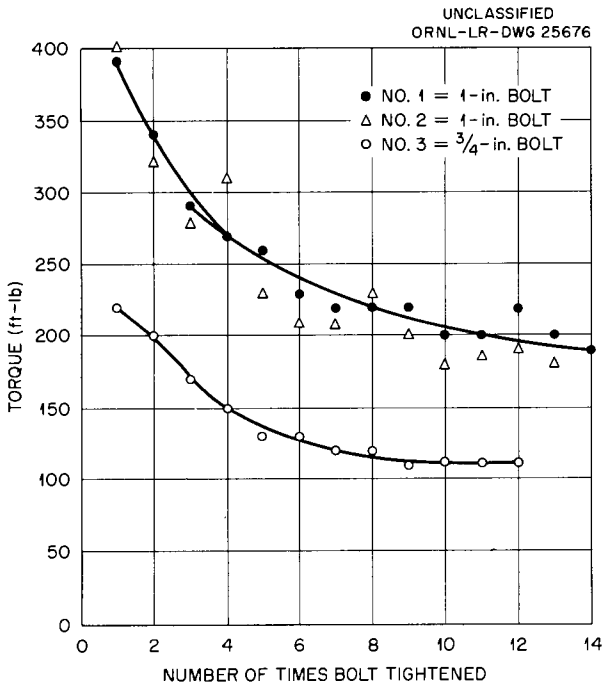

Fig. 2.1. Required Torque to Produce an Initial Bolt Stress of 45,000 psi, as a Function of the Number of Times the Bolt Is Tightened (Experimental Data for Two 1-in. Bolts and One 3/4-in. Bolt).

Table 2.1. Recommended Torque to Produce an Initial Bolt Stress of 45,000 psi

Bolt	Torque (ft-lb)
1/2 – 13 UNC	45
5/8 – 11 UNC	80
3/4 – 10 UNC	115
7/8 – 9 UNC	190
1 – 8 UNC	250
1 1/8 – 8 N	400
1 1/4 – 8 N	700
1 1/2 – 8 N	960

diameters of both sides of each ring were machined to the flange-groove pitch diameter plus 0.010 in., as shown in Fig. 2.2, in effect duplicating the maximum mismatch permissible under the provisions of ASA standard B16.20-1956. In the remaining four assemblies the pitch diameter of one side of each ring was machined to the groove pitch diameter plus 0.010 in., and the other side of each ring was machined to mate exactly with the groove, as shown in Fig. 2.3, thus giving the effect of maximum mismatch of one face only of a pair of mating flanges. The eight assemblies were then thermal-cycled repeatedly between 78°F at atmospheric pressure and 636°F at 2000 psi. No appreciable change of leak rate, as compared with the results of previous tests in the thermal-cycling facility,[3] was observed. There was no noticeable increase in the degree of galling of the seating surfaces of either rings or grooves as the result of the mismatch.

2.2 PRESSURE-BALANCING SYSTEM

A pressure-balancing valve and a rupture disk had been installed in parallel in lines connecting the core and blanket pressurizers of the HRT. Their function was to prevent damage to the Zircaloy core tank by limiting pressure differences between core and blanket to safe values. Experiments with the HRT had shown that the pressure differences could normally be controlled without using the balancing valve. Experience and calculations had shown that if the rupture disk were broken, the reactor could still operate for long periods of time with an open line between the two pressurizers and without serious transfer of fluid between core and blanket systems. Because maintenance of the valve would be difficult and its installation required a complicated piping system, it was decided to remove the pressure-balancing valve, leaving only the rupture disk to limit the pressure differences.[4]

Because corrosion will reduce the thickness of the core-vessel walls, the allowable pressure differential between core and blanket will decrease with time. Table 2.2 presents the recommended rupture-disk burst pressures for the HRT core vessel for several periods of operation.[5]

---

[4]H. A. McLain, *Possibility of Interconnecting the HRT Pressurizers with an Open Pipe*, ORNL CF-57-7-68 (July 17, 1957).

[5]R. D. Cheverton, *Allowable Pressure Differentials for HRT Core Vessel*, ORNL CF-57-9-36 (Sept. 13, 1957).

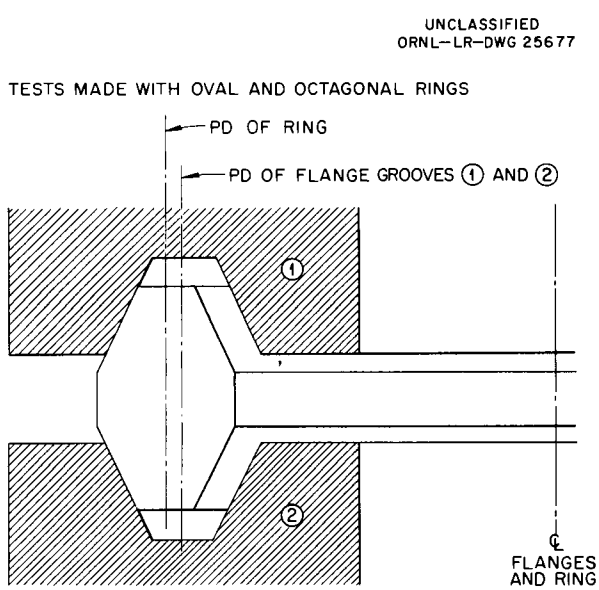

Fig. 2.2. Maximum Mismatch of Ring Gaskets with Flange Groove Under ASA B16.20-1956.

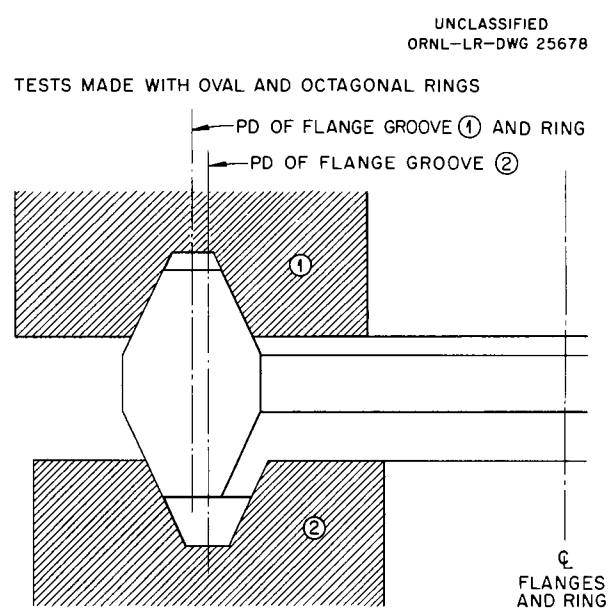

Fig. 2.3. Perfect Fit of Ring Gasket with Flange Groove on One Side, with Maximum Mismatch on Opposite Side.

Table 2.2. Recommended Rupture-Disk Burst Pressures for HRT Core Vessel

Period of Operation (years)	Core to Blanket		Blanket to Core	
	Allowable Working-Pressure Differential (psi)	Burst Pressure (psi)	Allowable Working-Pressure Differential (psi)	Burst Pressure (psi)
0	210	420	110	220
1	190	380	90	180
2	170	340	70	140
3	150	300	55	110
4	130	260	40	80

2.3 SUPPLEMENTARY RECOMBINATION

The decision to operate the HRT with essentially 100% internal recombination in the high-pressure system necessitated a modification of the recombiner system. The recombiners were liberally sized for the design condition of gaseous letdown from the high-pressure system. With liquid letdown only, the concentration of radiolytic gas in the gas-steam mixture entering the recombiner will be reduced from 8 mole % to about 0.8 mole %, and the recombiner efficiency will be reduced because of the lower temperatures which result when the smaller quantities of O_2 and D_2 are recombined.[6,7] Thus small amounts of unrecombined gases could pass to the charcoal adsorption beds, providing a possible explosive mixture in the beds and resulting in a loss of D_2O inventory. Supplementary recombiners, consisting of a roll of platinized stainless steel mesh, 5 in. long, in a 1-in. pipe, were installed in the off-gas piping from the recombiner condensers. These were wrapped with a steam coil to provide the heat necessary to initiate the reaction (see Fig. 2.4). Because the residual gases entering the supplementary recombiners will no longer be diluted with a large volume of steam, the space velocity will be lower and the temperature higher, thus increasing the rate of recombination. Tests were made which indicated that the heat of reaction will be effectively dissipated without overheating the units.[8]

UNCLASSIFIED
ORNL-LR-DWG 25679

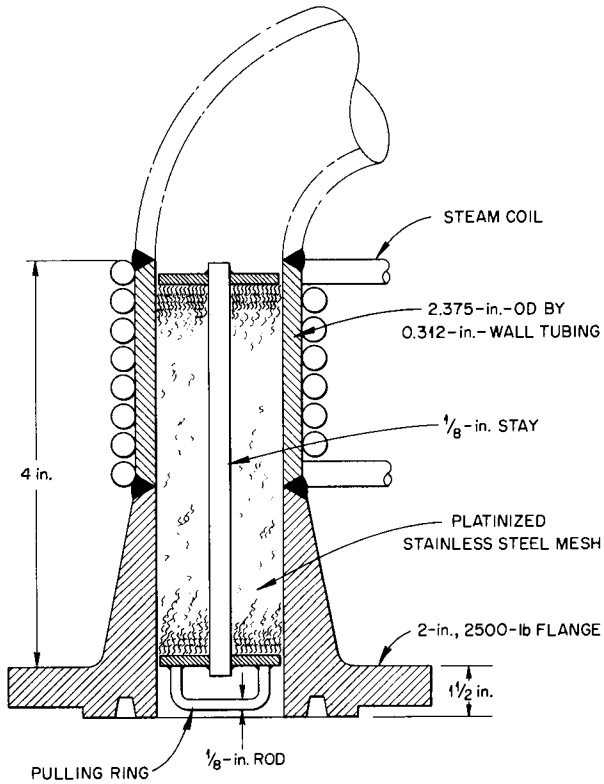

Fig. 2.4. Supplementary Recombiners for HRT.

2.4 CELL-SPRAY AND FLANGE-SCAVENGING SYSTEM

A system was designed which will serve the dual functions of reducing cell pressure following a catastrophic rupture of the high-pressure system and of scavenging residual fluids from flanged joints being opened during maintenance operations.

[6] R. E. Aven, *HRT Recombiner Condenser Design*, ORNL CF-54-11-1 (Nov. 1, 1954).

[7] H. A. McLain, *After Recombiners for the HRT*, ORNL CF-57-8-78 (Aug. 15, 1957).

[8] I. Spiewak *et al.*, *HRP Quar. Prog. Rep. July 31, 1957*, ORNL-2379, p 13, esp 17.

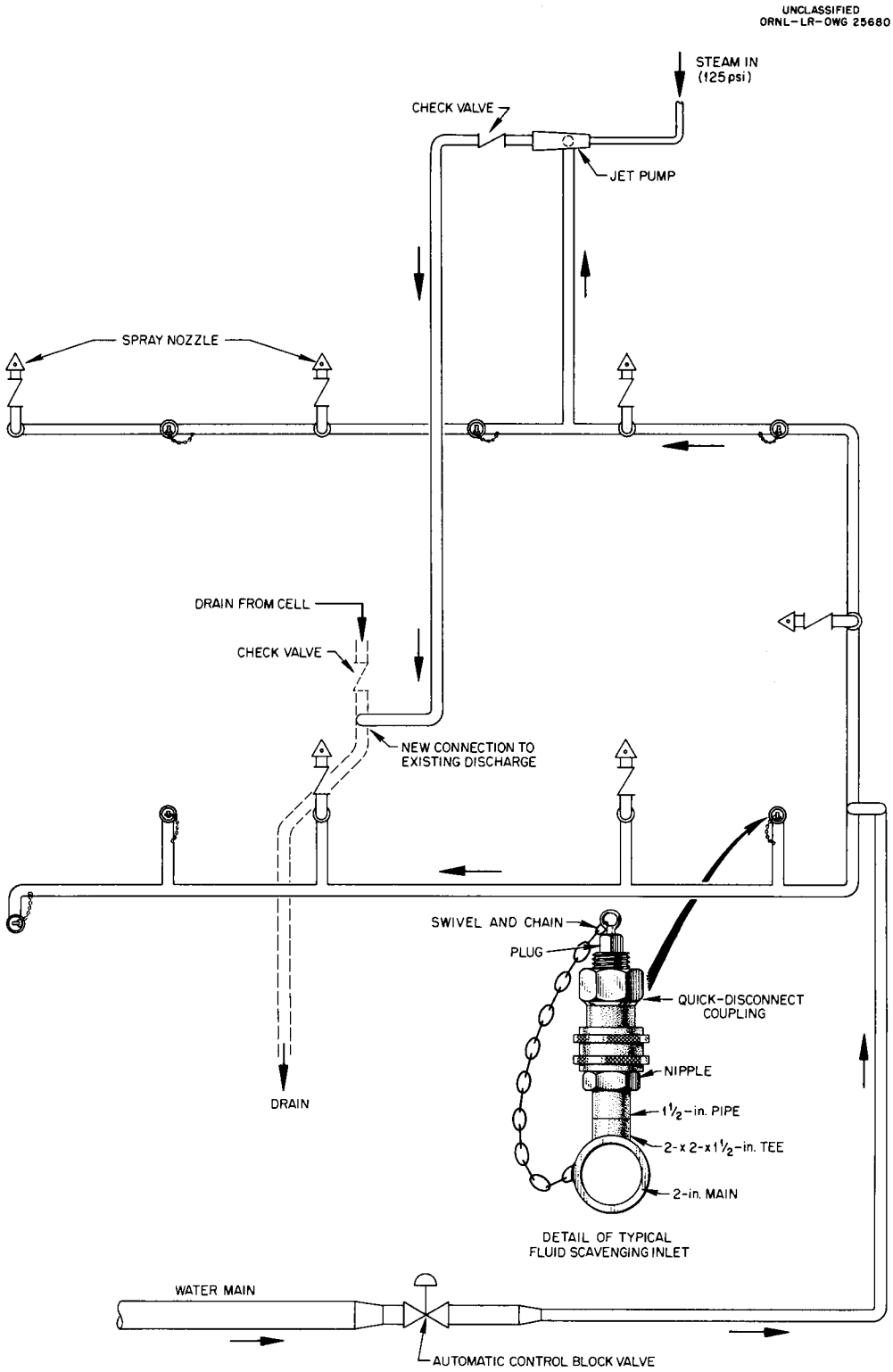

Fig. 2.5. HRT Cell-Spray and Flange-Scavenging System.

Twelve fog-jet nozzles, supplied with water from the mains originally intended for flooding the reactor cell, will produce a water fog in the event of a system rupture. Although the system will not be effective in reducing the peak cell pressure to be expected, it will be effective in reducing the time required for cell pressure to return to atmospheric.[9]

The lines leading to the spray nozzles also contain 24 taps to which suction hoses may be attached by means of standard fluid-line, quick-disconnect couplers to convert the system for scavenging operations. The hoses, in turn, are attached to a suction device on flanges to be scavenged, and vacuum is applied by means of steam-jet eductors exhausting to the waste and vent system. A schematic diagram of the system is presented in Fig. 2.5.

2.5 REPLACEMENT STEAM GENERATOR

Figure 2.6 shows the replacement steam generator for the HRT. Design of this vessel was complicated by the necessity of fitting it into an existing system, with the requirements of fitting existing supports, piping connections, and space limitations. Some alteration to existing structural members and piping will be required on installation, but this will not be extensive.

The design of the heat exchanger was dictated by the desire to prevent stress-corrosion cracking and crevice corrosion of the stainless steel tubes in the secondary side of tube joints. Precautions were taken against crevice corrosion by eliminating the conventional tube sheet and water box which typify the existing exchangers. The tubes in the new design are terminated in external stainless steel headers (Fig. 2.7), to which they are joined by stainless-to-stainless seal welds. The 88 double-U, $\frac{5}{8}$-in. tubes are brought through the carbon-steel shell of the vessel through thermal sleeves which eliminate direct welding between the stainless steel tube and the carbon-steel shell, and eliminate any crevice between the tube and surrounding metal which might be subject to crevice corrosion attack. The only stainless-steel-to-carbon-steel weld is made at a point well away from the carbon-steel shell of the vessel. A detail of the thermal sleeve is shown in Fig. 2.8. The welding detail noted on the junction box, or elbow, at the end of the tube in Fig. 2.8 is typical of the manner in which nozzles are welded to the heat exchanger; the nozzle is machined and installed as a solid piece. After the weld is completed, the nozzle is drilled out to the prescribed internal diameter, as indicated in the detail of Fig. 2.8, thus resulting in a full-penetration weld with no crevice between the nozzle and the parent member.

The vessel will be rigidly fixed at the front support and be free to move with thermal expansion in other directions. A $1\frac{1}{16}$-in.-thick carbon-steel blast shield[9] will surround the vessel as shown in Fig. 2.6.

[9] W. R. Gall *et al.*, *HRP Quar. Prog. Rep. April 30, 1957*, ORNL-2331, p 19–21.

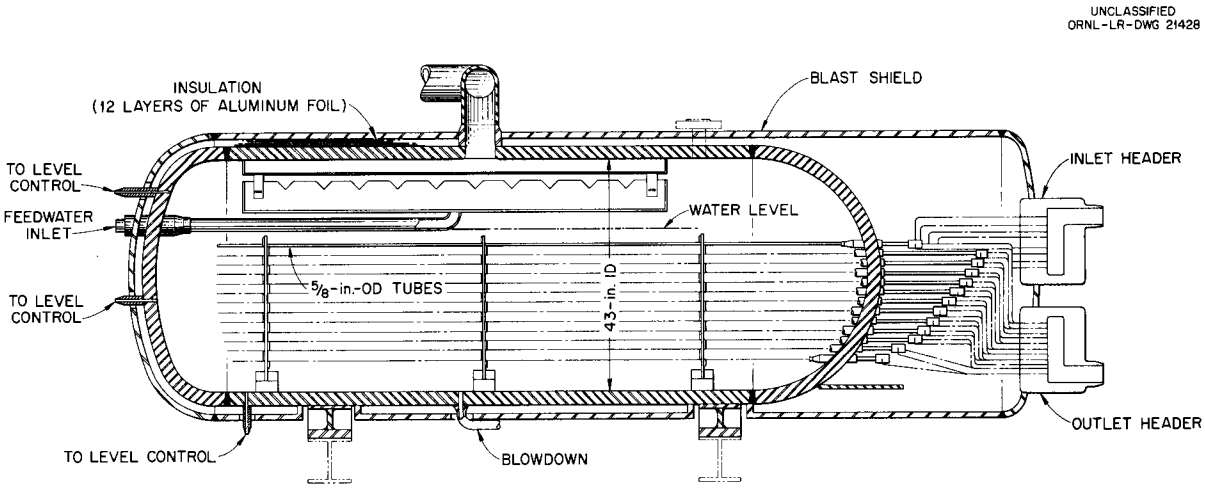

Fig. 2.6. HRT Replacement Steam Generator.

UNCLASSIFIED
ORNL-LR-DWG 25681

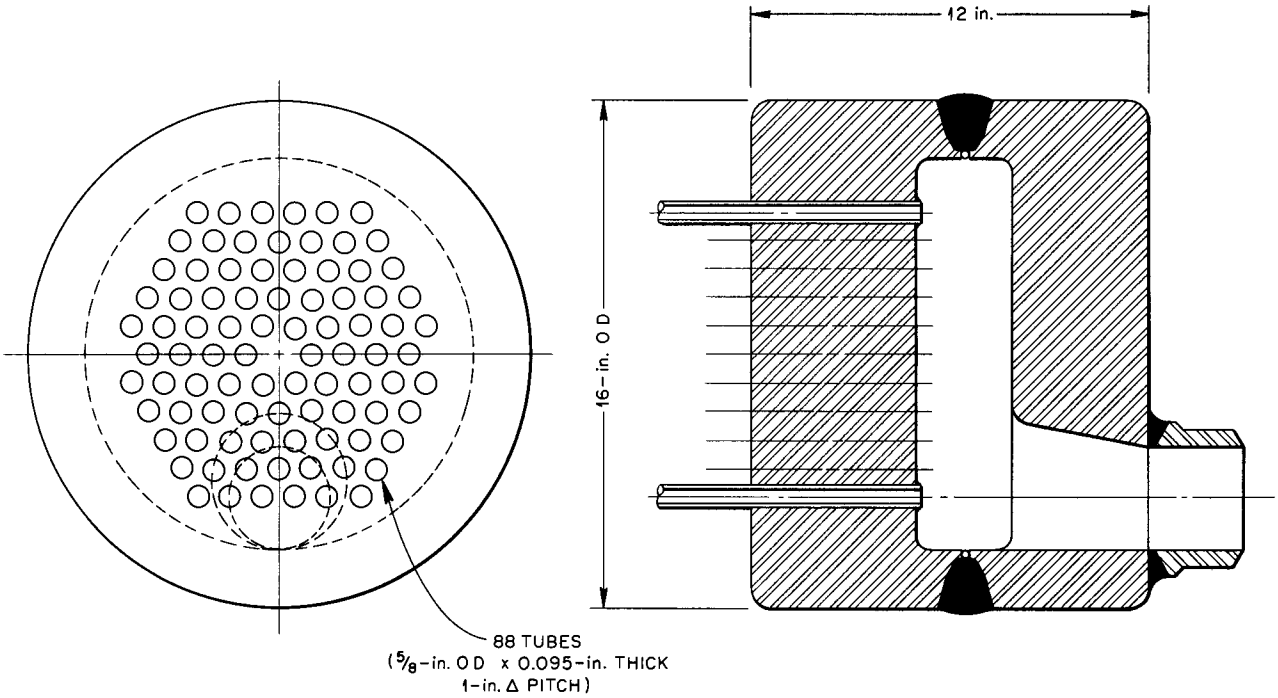

Fig. 2.7. Typical Tube Header for HRT Replacement Steam Generator.

UNCLASSIFIED
ORNL-LR-DWG 25682

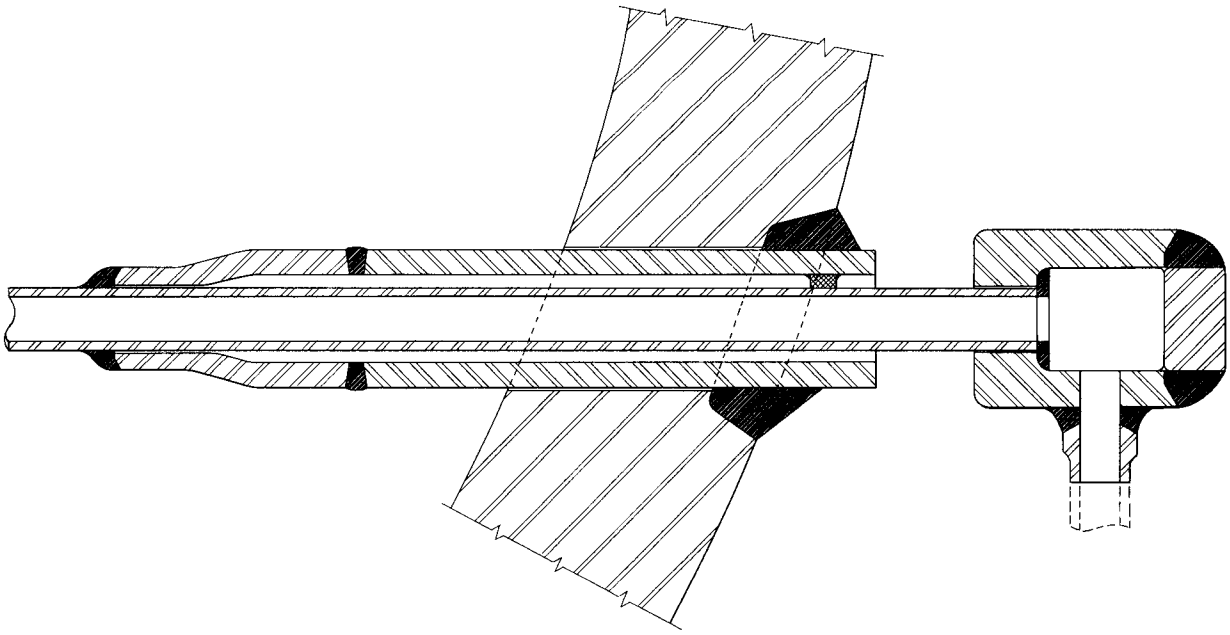

Fig. 2.8. Thermal Sleeve and Special Elbow, HRT Replacement Steam Generator.

3. HRT COMPONENT DEVELOPMENT

I. Spiewak

J. M. Baker
R. Blumberg
J. S. Culver
C. H. Gabbard
P. H. Harley
J. K. Hayes
P. G. Herndon
E. C. Hise
J. C. Moyers
H. R. Payne
D. E. Willis

3.1 FUEL CIRCULATING EQUIPMENT

3.1.1 400A-1 Pump and Loop

The long-term run of the Westinghouse 400A-1 pump was terminated after 11,605 hr of trouble-free performance.[1] This pump was equipped with a titanium impeller and a seal-welded stainless steel thermal barrier which contained a titanium wear-ring insert. A solution containing 0.04 *m* UO_2SO_4, 0.005 *m* $CuSO_4$, and 50 mole % excess H_2SO_4 was circulated at 250°C. The only measurable wear that occurred during the run was an increase in end play, indicating thrust-bearing wear of approximately 0.001 in. per 1000 hr of operation.

The pump was reassembled, and a gas-saturated run was started to determine whether gas bubbles in the circulating uranyl sulfate stream will be harmful to the pump. Experiments completed earlier indicated that gas bubbles will migrate into the motor section of the pump and gas-bind the auxiliary-coolant impeller. During the present run, which has continued for 650 hr, the gas pressurizer has been maintained 5°C below the loop temperature of 250°C. Total pressure is 1100 psi. These operating conditions should theoretically produce some bubble formation in the pump suction, although there are no means of verifying this experimentally. Pump and loop operation have been normal, and gas has not collected in the motor. Pump operation was also normal during several thermal cycles and while cylinder gas was added slowly to the circulating stream.

3.1.2 400A-2 Pump and Loop

Shaft-seal mixing tests were continued with the 400A-2 pump. Best results were obtained by using a shaft sleeve serrated at the top to provide suction ports for the auxiliary-coolant impeller; the sleeve was also securely sealed to the shaft to prevent flow between shaft and sleeve. Mixing flow of 0.48 liter/hr was observed with zero motor purge, and the rate was decreased[2] to below 0.002 liter/hr with a purge flow of 10 liters/hr.

Improved shaft sleeves were installed in the HRT pumps.

3.1.3 300A-1 Pump

The 300A-1 pump has operated in the HRT mockup since the revised thermal-barrier seal weld was made for a total of 3109 hr: 142 hr with 0.13 *m* UO_2SO_4 solution at 260°C, 376 hr with 1.3 *m* UO_2SO_4 solution at 260°C, and 2591 hr with 0.04 *m* UO_2SO_4 solution at 280 to 300°C. The pump has operated satisfactorily, with the condition causing power irregularities, previously reported,[3] apparently correcting itself.

3.2 FEED PUMPS

3.2.1 Feed-Pump Test Loops

Endurance testing of feed-pump heads was continued. No diaphragm or check-valve failures were experienced during the quarter. However, a leak developed in the seal weld on the north head in the HRT mockup. This was an experimental bolted head, and the crack in the seal weld could have been caused by improper reassembly following repair of the cracked nipple reported previously.[3] Tables 3.1 and 3.2 list the test duration for all heads and check valves now in operation.

The reciprocating drive unit of the mockup feed pump was equipped with a variable-speed drive which provides a continuously variable flow up to 2 gpm. The reciprocating drive has continued to operate satisfactorily.

---

[1] J. C. Moyers, *Long-Term Run of Westinghouse 400A-1 Pump*, ORNL CF-57-9-1 (Sept. 3, 1957).

[2] H. A. Rundell, D. H. Roy, and J. C. Moyers, *Investigation of Effect of Seal Configuration on Mixing Flow and Radiation Damage in HRT-Type Circulating Pumps*, ORNL CF-57-10-48 (Oct. 10, 1957).

[3] I. Spiewak *et al.*, *HRP Quar. Prog. Rep. July 31, 1957*, ORNL-2379, p 13.

Table 3.1. Duration of Tests of Feed-Pump Heads Currently Operating

Head Location	Diaphragm (Type 347 Stainless Steel)	Test Duration (hr)
Feed-pump loop No. 1 (water)		
East	0.031-in., annealed, liquid-blasted finish	2184
West	0.019-in., annealed	7847
Feed-pump loop No. 2 (fuel)		
South	0.031-in., annealed, mirror finish	4427
North	0.031 in., ¼ hard, as-rolled finish	4427
HRT mockup (fuel)		
South	0.022-in., ¼ hard, mechanically polished	6111
North	0.031-in., annealed, mirror finish	713
Valve test loop (fuel)	0.031-in., annealed, mirror finish	1074

Table 3.2. Duration of Test of Feed-Pump Check Valves Currently Operating

Location	Material		Test Duration (hr)
	Ball	Seat	
HRT mockup (fuel)			
South			
Suction	Star J	Stellite 6	8791
Discharge	Star J	Stellite 6	4083
North			
Suction	Star J	Stellite 6	8832
Discharge	Star J	Stellite 6	3724
Feed pump No. 1 (water)			
West			
Suction	Star J	Stellite 6	7246
Discharge	Star J	Stellite 6	7847
East			
Suction	Star J	17-4 PH SS	1044
Discharge	Star J	17-4 PH SS	613
Feed pump No. 2 (fuel)			
North			
Suction	Star J	17-4 PH SS	2027
Discharge	Star J	17-4 PH SS	2027
South			
Suction	Star J	Stellite 6	4427
Discharge	Star J	Stellite 6	4427
Valve test loop (fuel)			
Suction	Star J	Stellite 3	2191
Discharge	Star J	Stellite 3	2191

Over a period of 3500 hr of continuous operation, feed-pump loop No. 2 experienced a loss of flow of 0.15 gpm and a noticeable increase in check-valve noise. Replacement of the Scott & Williams slide-valve unit restored the flow and reduced the noise.

3.2.2 Purge Pumps

Purge-pump loops 1 and 2 have resumed operation with new heads having 100-mesh screens and modified closure welds. In loop 1 a 0.019-in. Allegheny Ludlum AM-350 alloy diaphragm and type 17-4 PH stainless steel valve seats are being tested in fuel solution. In loop 2 a full-hard 0.019-in. type 347 stainless steel diaphragm and Stellite valve trim are being tested in water. Both loops are driven by the new Scott & Williams P2 duplex drive unit. The drive unit failed after about 150 hr of operation because of fracture of the plunger return springs. It was returned to the factory, where the trouble was corrected, and has since operated satisfactorily. Total time on these loops is now 556 hr.

The HRT-mockup purge-pump head, containing 100-mesh screen, a 0.019-in. annealed and polished type 347 stainless steel diaphragm, and Stellite valve trim, has operated for 1610 hr without trouble.

3.2.3 Check-Valve Material Test

The screening of check-valve materials for the HRT was completed. Some of the data obtained in this program are summarized in Table 3.3. The facility is continuing to operate in long-term check-valve tests. On the basis of these tests, 17-4 PH seats vs Star J balls were recommended for water service. For uranyl sulfate service, Stellite 3 seats vs Star J balls were recommended on the basis of many years of successful loop operation.

3.2.4 Corrosion Fatigue Tests

Ohio State University has run additional fatigue tests on types 347 and 316-L stainless steel and on Allegheny Ludlum AM-350. Annealed type 347 appears to be the best alloy tested thus far for uranyl sulfate service because of its superior resistance to corrosion fatigue and its ductility. However, some of the other materials may prove superior in water service. Table 3.4 summarizes the results obtained to date.

3.2.5 HRT Replacement Feed and Purge Pumps

The rebuilding of replacement pumps is almost complete. The four feed-pump heads were completed and installed in the reactor, and the purge

Table 3.3. Check-Valve Material Tests

Material		Medium	Time (hr)	Results
Ball	Seat			
Star J	Stellite 6	Water	132	Failed; seat damage
		Fuel	260	Passed; no leakage
	Stellite 1	Water	1070	Passed; no leakage
		Fuel	849	Passed; no leakage
	17-4 PH SS	Water	1740	Passed; no leakage
		Fuel	2207	Passed; no leakage
	347 SS	Water	279	Passed; no leakage
	Carpenter 20 SS	Water	298	Passed; no leakage
Kennametal K 501	Kennametal K 501	Water	283	Questionable; flow loss but no leak
		Fuel	850	Passing; in progress
Aluminum oxide	Aluminum oxide	Water	817	No leakage but balls lost weight
		Fuel	600	Failed; balls and seats lost weight

Table 3.4. Results of Corrosion Fatigue Tests

Material	Endurance Limit (psi)			Elongation (%)
	In 0.04 *m* UO_2SO_4 at 60°C	In Water at 60°C	In Air at Room Temperature	
347 SS				
Annealed	34,000	36,000	39,000	42
¼ hard	30,000	50,000	58,000	14
½ hard	31,000	57,000	67,000	2.5
¾ hard	32,000		88,000	2.5
Full hard	43,000			2.5
316L SS				
¼ hard	32,000			14
½ hard	32,500			10
AM-350 S.B.T.*	39,000		90,000	11

*S.B.T. refers to tempering by refrigeration followed by aging at 650°F.

pumps are now being installed. Three of eight purge-pump check valves indicated static leaks across the seats after assembly; this condition was corrected by one to two days of operation.

3.3 HRT MOCKUP

3.3.1 Operation

During the report period the HRT mockup completed a run of 548 hr circulating 0.042 *m* UO_2SO_4, 0.021 *m* H_2SO_4, and 0.005 *m* $CuSO_4$ at 1400 psi and 280°C. This run was terminated because of a suspected high-pressure solution leak and the failure of 40% of the Calrod loop heaters.

The generalized corrosion rate observed during the first 265 hr of this run was 3.9 mpy. This abnormally high rate was attributed to the presence of 0.2% HNO_3 from a previous HNO_3 rinse. After replacing the fuel solution, the corrosion rate went down to 0.8 mpy for the remainder of the run.

The suspicion of a leak was based on the discoloration of Thermon, a commercial aluminum silicate heat-transfer compound, used as a medium for conducting heat from the Calrod heaters to the pipe walls. The discoloration was traced to material escaping from burned-out heaters. No leak from the system was indicated by hydrostatic and helium leak tests.

The Calrod-Thermon heating system was replaced by strip heaters placed directly on the loop piping. Another run was started, with 0.042 *m* UO_2SO_4 solution at 280°C and 1700 psi; it is still in progress after 1017 hr. The corrosion rate during this period has averaged 1.1 mpy. The only major component failure was that of a feed-pump head described in Sec 3.2.1.

3.3.2 Boiling of Mockup Fuel Solution

Mockup fuel solution was boiled for 450 hr during the present run in a 4-ft-long bypass of ½-in. sched-80, A-40 titanium pipe. Upon removal of the pipe, the preliminary examination showed that a thin rusty scale covered the inside of the section where boiling took place. X-ray analysis showed the film to be mainly an unidentified aluminum compound, plus some TiO_2 and smaller amounts of Fe_2O_3 and Cr_2O_3. The aluminum probably originated in the pellets used in I_2 removal tests.

The titanium pipe had sagged slightly and had enlarged about 0.02 in. in outside diameter. The outside-pipe-wall temperature indication was 430°C; boiling occurred at 325°C. The pipe has been submitted for metallographic examination.

3.3.3 Corrosion in Stagnant Lines

No significant attack was noted in three ½-in. sched-80 lines welded to the high-pressure circulating system after being exposed to stagnant solution in the 548-hr run described in Sec 3.3.1.

The lines were reinstalled for the present run, with added stressed specimens, which may provide further information.

3.3.4 Iodine Removal Tests

Three runs were made in which iodine was injected into the high-pressure system and removed from the vapor phase of the low-pressure system by a 6-in.-dia by 8-in.-deep bed of silvered-alundum Raschig rings or silver-plated stainless steel Yorkmesh installed between the dump tank and the condenser. Iodine concentration within the bed was found to decrease exponentially as shown in Fig. 3.1. Efficiencies estimated from the iodine distributions are listed in Table 3.5. The effectiveness of the silvered-alundum pellets appeared to depend strongly on temperature in the range 110 to 150°C.

Table 3.5. Efficiency of Iodine Removal Beds

Material	Temperature (°C)	Efficiency (%)
Silvered alundum	110	63*
	120	81
	150	98
Silver-plated Yorkmesh	120	97

*Run made during previous quarter; bed was 5 in. deep.

Difficulty with leaching of material from the silvered-alundum bed installed in the HRT suggested development of an alternate material for iodine removal. Several samples of stainless steel Yorkmesh wire were silver-plated and tested by the Chemical Technology Division.

In the first samples tested, only 2.5% of the plated silver was available for reaction, as compared with 100% of the silver deposited on alundum. On a volume basis, this gives silvered alundum seven times the capacity of silver-plated Yorkmesh.

The silver plate did not become brittle after reaction. Soaking the wire in water after reaction did not produce any leaching of iodine or base-metal corrosion. When contacted with moisture and concentrated iodine vapor, extensive corrosion occurred; this is, however, a much more severe environment than is expected in the HRT.

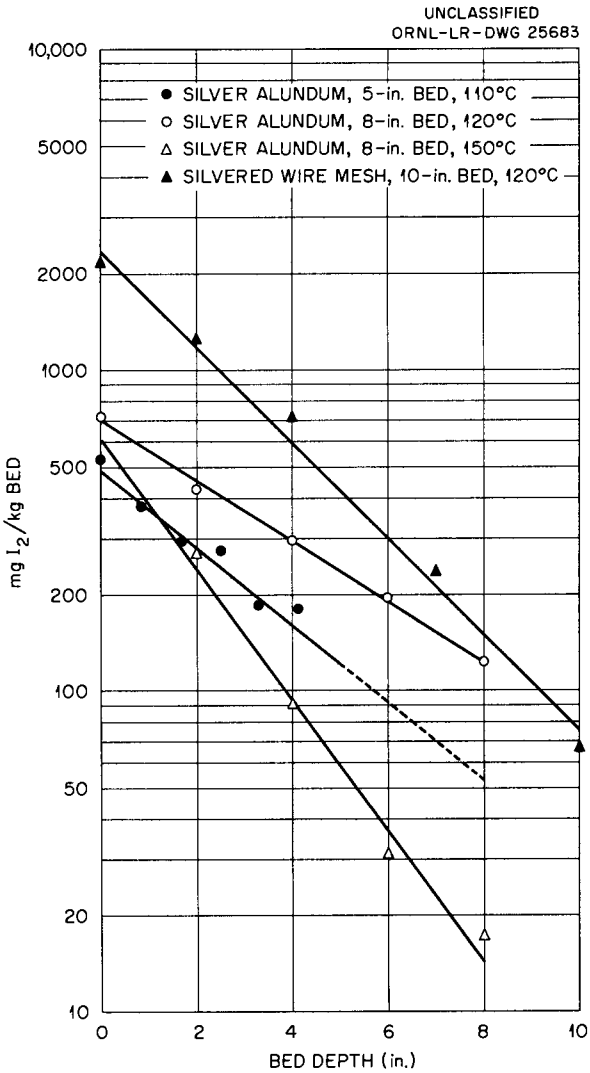

Fig. 3.1. Iodine Distribution in Silvered Bed.

A sample of the silver-plated Yorkmesh was tested in the mockup and gave the good results shown in Fig. 3.1 and Table 3.5. It is concluded that an absorber containing silvered alundum or silver-plated Yorkmesh can be designed to remove iodine from the HRT with an efficiency >>99%.

4. HRT REACTOR ANALYSIS

P. R. Kasten

C. W. Nestor, Jr. B. E. Prince
M. W. Rosenthal

4.1 REACTOR PRESSURE FOLLOWING Zr-H_2O REACTION IN HRT

The Aerojet General Corp. report[1] concerning metal-water reaction experiments was examined for pertinence to the HRP. The major results pertaining to zirconium-water reactions are summarized below:

1. Injection of zirconium or zirconium-alloy droplets which are 200°C above the melting point into water resulted in about 20% reaction when the particles were 1000 μ (40 mils) in diameter and about 50% reaction when they were 100 μ (4 mils) in diameter. No significant difference in behavior of zirconium and its alloys (including Zircaloy-2) was found. These results are similar to those obtained earlier by the same investigators using a different technique.

2. The efficiency of converting the thermal-energy release into work was determined by permitting ejection of water from the test chamber. The highest efficiency obtained (defined as work done over energy liberated) was 7.7%.

3. The authors conclude that metal-water reactions are not high-order explosions, since they required milliseconds ($\sim$10) rather than microseconds to attain peak pressure. In the tests performed, there was no shattering-type damage. However, damaging shock waves are thought to have been produced in earlier experiments in which the specific surface of the molten metal was higher.

4. The reaction of Zircaloy-2 with steam was investigated by using metal-sample temperatures of 800, 1000, and 1200°C. From these tests the authors conclude that the reaction of Zircaloy-2 in steam is not self-sustaining, even when considerable energy for ignition (electric arc formed during experiment) is provided.

These results indicate that any appreciable reaction of Zircaloy-2 and water is unlikely while the metal is present in massive form. However, the behavior with oxygenated uranyl sulfate is still uncertain.

Although the reduction of an appreciable fraction of a core vessel to droplets is extremely unlikely, the production of a small mass of drops is conceivable; for example, consider the following chain of events: uranium is deposited at a spot on the core-tank surface, film boiling occurs at that point, the metal melts and is sprayed into the liquid by a pressure differential between the core and blanket regions. Even this scheme would probably not produce metal drops small enough for a high percentage of reaction.

The pressures which would occur in the HRT following reaction of part of the Zircaloy-2 core vessel have been estimated by using two simple thermodynamic systems. In all computations the pressure vessel was assumed to be a rigid sphere, and no allowance was made for escape of liquid into the pressurizers. Two models were considered:

1. The reaction occurs adiabatically at constant volume, the gaseous product, D_2, then expanding isentropically and compressing the liquid in the pressure vessel.

2. During the reaction, 90% of the energy released is transferred to the liquid. The remaining energy is transmitted to the reaction products and the expansion treated by means of model 1. This reaction was considered to have an efficiency of 10%.

The results are plotted in Fig. 4.1, where the pressures shown are for the quasi-equilibrium condition when the gas and liquid pressures become equal. Because of the assumption of adiabatic reaction and isentropic expansion, plus considering the liquid to be completely retained in the pressure vessel, the upper curve gives pressures higher than would actually occur in the absence of shock waves. If the curve for 10% efficiency is appropriate, kilogram amounts of Zircaloy could react in the HRT without rupturing the pressure vessel.

Failure of the Zircaloy-steam reaction to be self-sustaining suggests that there would be no

[1] H. M. Higgins and R. D. Schultz, *The Reaction of Metals with Water and Oxidizing Gases at High Temperatures*, IDO-28000 (April 30, 1957).

danger to the core vessel from this mechanism if it were to become hot from deposited fission products while full of steam, as might occur after a dump. However, in the experiments performed,[1] the effects of oxygen and deuterium in the steam were not investigated.

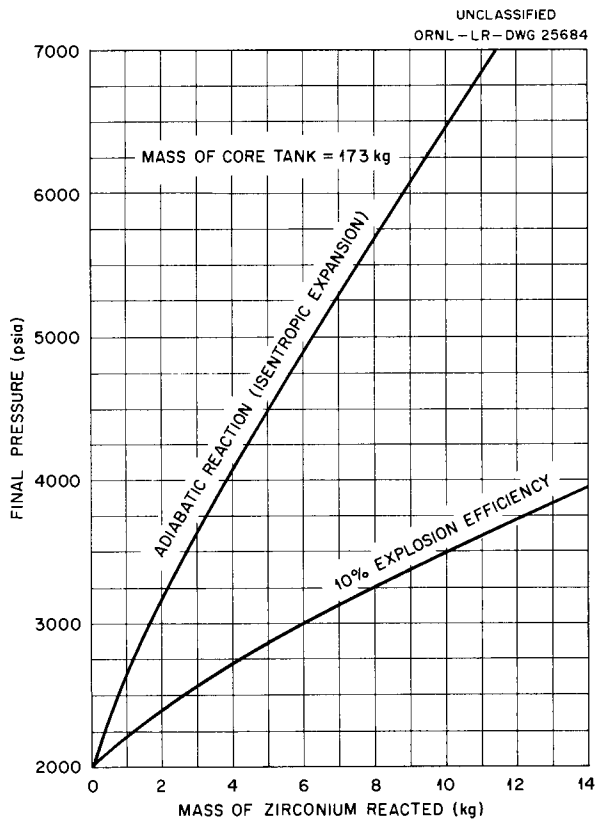

Fig. 4.1. Pressure in HRT Following Zirconium-Water Reaction.

4.2 HRT CRITICAL CONCENTRATIONS OBTAINED BY MULTIGROUP MODEL

Critical concentrations for the HRT were calculated by using the Eyewash multigroup multiregion code.[2] Twenty-seven fast groups, one thermal group, and four space regions were employed. The space regions consisted of the core, Zircaloy-2 core-tank wall, blanket, and pressure vessel. In all cases it was assumed that there were no poisons present. Three fuel loadings at 280°C were considered: (1) U^{235} core solution, D_2O blanket; (2) U^{233} core, D_2O blanket; and (3) U^{233} core, ThO_2-D_2O blanket containing 500 g of thorium per liter. For comparison purposes, the above cases were also calculated by using a two-group, two-region code.[3] Results of both calculations are summarized in Table 4.1, where the multigroup values have been analyzed in terms of a fast effect, ϵ.

The critical concentrations obtained with the two-group model were found to be consistently 20 to 30% lower than those obtained with the multigroup model. The difference arises because the former method of calculation does not take adequate account of fast fissions and fast leakages for a reactor the size of the HRT. For the case of the U^{235}-fueled, D_2O-reflected reactor, an earlier

[2] J. H. Alexander and N. D. Given, *A Machine Multigroup Calculation. The Eyewash Program for UNIVAC*, ORNL-1925 (Sept. 15, 1955).

[3] T. B. Fowler, *Oracle Code for a General Two-Region, Two-Group Spherical Homogeneous Reactor Calculation*, ORNL CF-55-9-133 (Sept. 22, 1955).

Table 4.1. Results of HRT Critical Calculations

Core, Blanket (280°C)	Fuel Critical Concentration				ϵ*
	Eyewash		Two-Group, Two-Region		
	g/liter	g/kg D_2O	g/liter	g/kg D_2O	
U^{235}, D_2O	7.55	9.03	5.63	6.73	1.133
U^{233}, D_2O	5.83	6.97	4.75	5.68	1.173
U^{233}, 500-g/liter ThO_2 in D_2O	12.35	14.8	10.08	12.1	1.404

*ϵ = (neutrons produced by all fissions)/(neutrons produced by fissions resulting from thermal-neutron absorption by fuel); based on multigroup calculations.

estimate of 8.1 g of U^{235} per liter (9.7 g per kilogram of D_2O) calculated by Edlund and Wood[4] using a harmonics method, compares favorably with the multigroup result.

The multigroup value of the breeding ratio for the case of 500 g of thorium per liter of slurry in the blanket was 0.85.

[4] M. C. Edlund and P. M. Wood, ORNL-1780 (Aug. 27, 1954) (classified).

5. HRT CONTROLS AND INSTRUMENTATION

D. S. Toomb

E. H. Bell
A. M. Billings
J. R. Brown
R. L. Moore
R. M. Pierce[1]
K. W. West
H. D. Wills

5.1 COMPONENT AND SYSTEM TESTING

5.1.1 Letdown Valves

A letdown valve utilizing a Stellite No. 6 plug and mounted horizontally in the HRT mockup operated very satisfactorily for 2100 hr. The Stellite No. 6 plug was replaced with one fabricated from Armco 17-4 PH alloy incorporating a step characteristic.[2] This plug was tested for 708 hr; the wear was negligible, as shown in Fig. 5.1. Since 17-4 PH plugs also performed well in the reactor fuel and blanket letdown valves during the last runs with rinse solutions, oxygenated water, and unenriched uranyl sulfate fuel solution, this alloy will be used for subsequent reactor operation. As mentioned in the previous report,[2] Stellite No. 6 plugs were not satisfactory in rinse and oxygenated-water runs.

[1]On loan from TVA.

[2]D. S. Toomb *et al.*, *HRP Quar. Prog. Rep. July 31, 1957*, ORNL-2379, p 21.

Fig. 5.1. Type 17-4 PH Stainless Steel Letdown-Valve Plug After 708 hr of HRT Mockup Loop Operation. Reduced 6%.

5.1.2 Thermocouples

Of the approximately 375 thermocouples (half are spares) in the reactor tank, about 160 had to be replaced and 40 repaired after the flange and tubing replacement program. During the last natural-uranium run five thermocouples were not working; three were grounded in the conduit, and the other two were open-circuited. These will be replaced before operation is resumed.

The thermocouple cable is of the duplex type; each 20-gage conductor is insulated with a phenol formaldehyde varnish and Fiberglas impregnated with a silicone alkyd copolymer. An over-all insulating sheath of similarly impregnated Fiberglas forms the two-conductor cable.

Most of the thermocouples are spot-welded to the reactor piping, and the insulated couples then run to a disconnect which can be broken remotely. From the disconnect the cable is fed into a conduit terminal box through a compression sealing gland. However, several thermocouples in the heat exchangers and pressurizers are installed in wells. The design of these thermocouples is illustrated in Fig. 5.2. The thermojunction is made by Heliarc-welding the 20-gage Chromel-Alumel wire to the stainless steel tubing at the tip. The wire is sealed in the stainless steel protection tube by a modified Conax Co. type PG sealing gland, the seal being effected by a bead of Lava (American Lava Corp.), which is crushed against the wire by the gland follower when the compression nut is tightened. The thermocouple is held in compression against the bottom of the well by the Inconel compression spring. The flexible metallic lead is for protection of the lead wire against abrasion. The connectors on all leads are standard Thermo Electric Co. Chromel-Alumel connectors with Bakelite insulation.

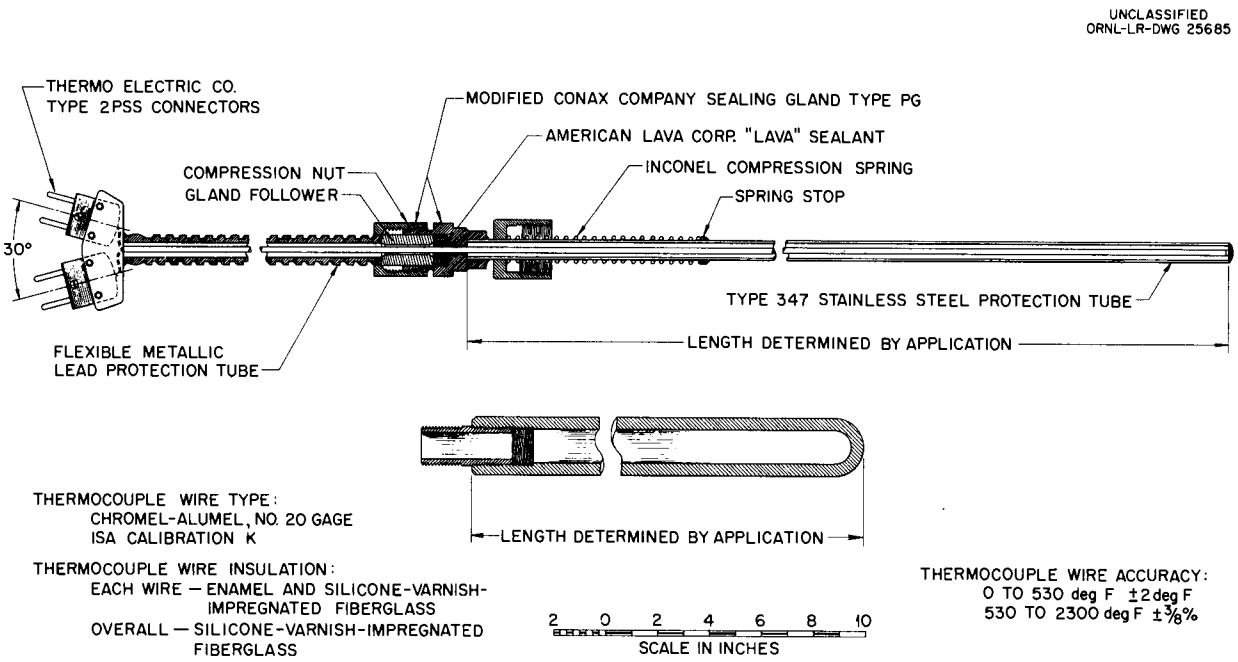

Fig. 5.2. Waterproof Thermocouple for HRT Thermowells.

5.1.3 Nuclear Instrumentation

The HRT nuclear instrumentation system includes the gamma monitors for personnel protection in the control areas; the beta-gamma monitors for sampling air in the control areas; the remote-area gamma-sensitive monitors, which will alarm if radiation leaks into auxiliary process lines such as cooling water, steam, off-gas to the stack, etc.; high-level-gamma radiation monitors inside the reactor cell to indicate ambient radiation levels near equipment; and the neutron-detecting fission chambers and gamma-detecting compensated ion chamber inside the nuclear instrument tube. The last two elements are used to monitor the fission process in the core vessel.

The nuclear instrumentation is now installed and undergoing preliminary tests at the reactor site. The neutron-detecting channels have been operated for one month, with dummy check signals from a pulse generator being fed into the preamplifier. The ORNL-fabricated gamma-ray-detecting compensated ion chamber and the Westinghouse neutron-detecting fission chambers will next be installed in the nuclear instrument tube to check operation in the water which fills the tube and serves as shielding while permitting easy movement of the chambers for sensitivity adjustment.

The junction box which provides the means of sealing the electrical signal leads from the high-level-gamma ionization chambers at the shield-tank wall is shown in Fig. 5.3. The base of the box is welded to the shield tank, and the leads are brought to the terminal strips through Kovar glass-to-metal seals. The box and conduit can be pressurized with air to prevent water from leaking into the conduit during periods when the reactor tank is flooded for equipment maintenance. The box is test-checked at 20 psig to demonstrate leak-tightness. Rear access to the Kovar seals is had by lifting the dust cover, unbolting the hinged plate upon which the seals are mounted, and allowing the plate to rotate down on the bottom hinge.

UNCLASSIFIED
ORNL-LR-DWG 25686

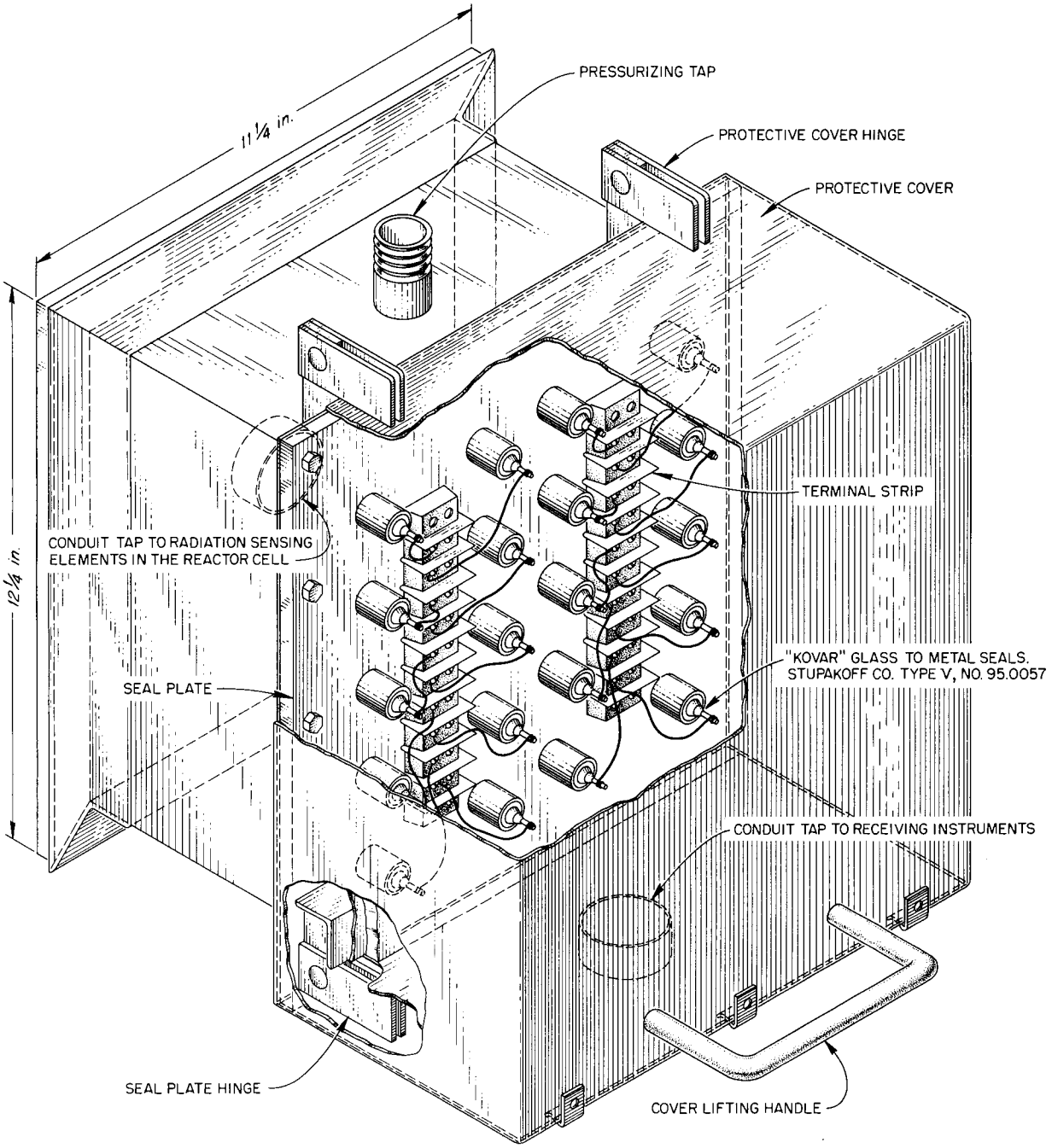

Fig. 5.3. Pressurized Junction Box; Test Pressure, 20 psig.

6. HRT PROCESSING PLANT

W. D. Burch P. A. Haas W. E. Unger
R. E. Adams R. W. Horton H. O. Weeren
W. L. Albrecht C. S. Lisser R. H. Winget
W. E. Browning F. C. McCullough E. L. Youngblood
L. H. Chase A. M. Rom

Effort during this period was expended on (1) an underwater-maintenance practice, (2) minor construction and maintenance in preparation for operation with radioactive solutions, (3) operation with the reactor during the final over-all tests of the systems, and (4) tests of the charcoal beds.

6.1 UNDERWATER-MAINTENANCE PRACTICE

Maintenance philosophy for the processing plant is similar to that for the reactor system. After flooding the cell with water for shielding, equipment is removed and replaced from on top of the cell with special tools. Several specific maintenance procedures were practiced with the cell flooded, and all other equipment designed to be replaceable was checked to ascertain that the proposed procedures are feasible.

6.1.1 Tests Prior to Flooding

All maintenance procedures were given preliminary checks prior to flooding the cell. Several minor changes were found necessary, mainly modifications to equipment supports to permit proper tool alignment and removal of equipment without interference from connecting piping. Conduits and canned insulation were leak-checked, repaired where necessary, and pressurized with air to prevent inleakage of water when the cell was flooded later. The high-pressure-system circulating pump, heater, and filter; the dissolver; and two valves were replaced without flooding to verify the removal procedures.

6.1.2 Underwater Tests

Maintenance practice with the cell flooded was carried out over a period of 10 days. The water, upon standing, gradually became cloudy, making visibility very poor after five to six days and necessitating replacement of the water.

Five of the more complex and inaccessible components were scheduled for replacement during this period. All except the high-pressure filter were removed and replaced. The latter could not be removed without risking damage to flange surfaces because of insufficient flexibility in adjoining piping. This piping has since been modified.

Except for a slightly decreased visibility, replacement of equipment was not complicated by the presence of shield water. This practice period adequately demonstrated this type of maintenance for the processing plant.

The components removed were:

Dissolver. – With seven connecting flanges and extremely limited working space at the bottom of the cell, the dissolver is the most difficult item to replace. No unforeseen difficulties arose, and the vessel was removed and replaced in 12 working hours.

Circulating pump. – Prior to breaking flanges, adjoining lines were frozen with semipermanent freeze coils which, in actual operation, would prevent contamination of heavy water with shield water. The plugs were tested by applying 40-psi pressure from outside the cell. While some difficulties were encountered in relocating the pump on the mounting dowel pins, the maintenance operation was satisfactory.

High-pressure-system heater. – Numerous electrical leads made handling of the 6-ft-long heater assembly awkward, but removal and replacement proved to be routine.

One low-pressure valve. – Removal of one low-pressure valve demonstrated the procedure as typical of maintenance of all low-pressure valves.

6.2 CONSTRUCTION AND MAINTENANCE

Numerous minor maintenance and construction jobs were completed in preparation for further operation. These included:

1. replacement of cadmium-plated nuts and bolts in the high-pressure system with higher quality nonplated nuts and bolts;
2. seal-welding of the thermal barrier and main flanges of the circulating pump;

3. fitting and installation of cell roof plugs and seal sheets; final welding will be delayed until after final leak-testing of process piping;
4. completion and installation of the hydroclone system sampler, including instrumentation and the control panel;
5. installation of the closed-loop cooling-water system, including a 300-gal surge tank, a 50-gpm 150-ft-head circulating pump, and a heat exchanger; the system was cleaned, checked, and placed in operation with distilled water containing 1000 ppm K_2CrO_4 as a corrosion inhibitor.

6.3 FINAL OPERATION OF THE HIGH-PRESSURE SYSTEM

The processing-plant hydroclone loop was operated throughout the final 300-hr nonradioactive run of the reactor in October. Operation was, in general, satisfactory, but serious leakage through the two high-pressure sampler valves following a normal sampling procedure resulted in loss of fuel solution to the chemical-plant low-pressure system through the sampler vent valve. When the leakage was noted, the system was immediately isolated from the reactor, and subsequently the air-operated sample letdown valve was replaced. Leakage rate through the inlet hand valve in the sampler itself is still very high, and this valve will also be replaced. Some difficulties were also experienced with obtaining a normal 5-ml volume during the initial tests of this sampler.

A sizable zero shift of the differential-pressure cell, measuring pressure drop across the hydroclone, occurred during the tie-in with the reactor, but the instrument can be re-zeroed from outside the cell.

6.4 HOLDUP TESTS ON HRT CHARCOAL ADSORBER BEDS

Experimental data from small laboratory charcoal beds indicated that the presence of a horizontal void space in a charcoal bed will reduce the efficiency of the bed significantly. Holdup tests of the HRT charcoal beds are in progress under simulated operating conditions to determine their efficiency before reactor startup. A radioactive-tracer technique developed for use in the laboratory adsorption study is being used. A pulse of Kr^{85} is injected at the entrance of each bed and swept through the bed by a stream of oxygen. Gases leaving the charcoal bed are monitored by a G-M tube, and the activity is measured by a linear count-rate meter.

Results of holdup tests on charcoal beds 10-A and -B during the month of August are not considered valid because of inaccuracies in sweep-gas flow measurements and temperature-induced changes in the field-mounted counting circuits. Holdup tests on these beds are to be rerun at a later date.

Tests on charcoal beds 10-C and -D were started in the latter part of September and completed early in October. The electronic equipment was moved into an air-conditioned building, which eliminated the effect of temperature fluctuation on the components in the counter circuit. Wet-test meters were installed downstream from the counter to measure total gas flow leaving the beds.

A graph of activity in the effluent gas versus time after injection of the pulse of Kr^{85} is given in Fig. 6.1. Activity broke through bed 10-C,

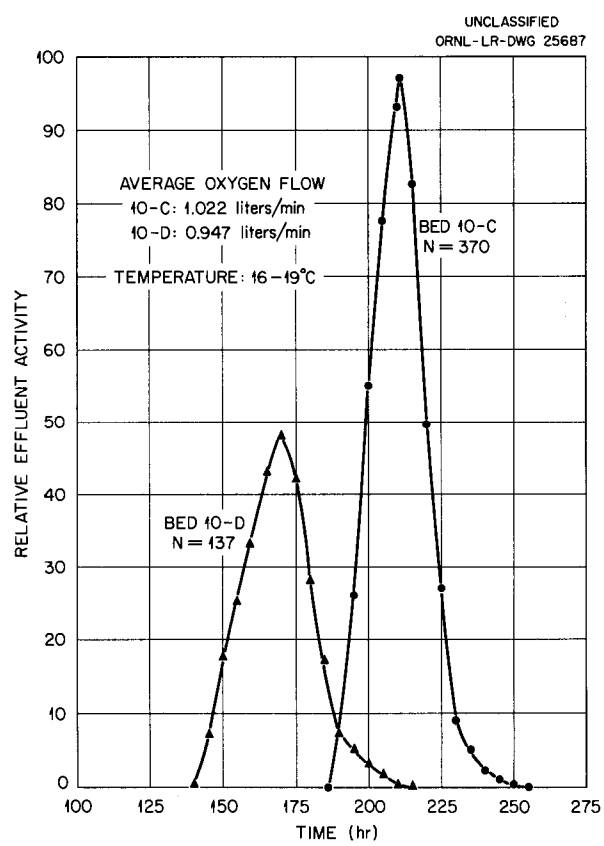

Fig. 6.1. Activity in Effluent Gas vs Time After Injection of Pulse of Kr^{85} in Charcoal Beds 10-C and -D.

containing 520 lb of charcoal, after 186 hr and reached a maximum (t_{max}) after 211 hr. The average gas flow through this bed was 1.022 liters/min. Activity broke through bed 10-D, containing 360 lb of charcoal, after 140 hr and reached a t_{max} after 170 hr. Average gas flow through the bed was 0.947 liter/min. These gas flows are approximately four times the design flow rate of 0.25 liter/min. Calculated values for t_{max}, based on laboratory data from small charcoal traps, are 300 hr for HRT charcoal beds 10-A, -B, and -C at a gas flow of 0.25 liter/min. It should be noted that holdup times are inversely proportional to flow rates, and the efficiency of the charcoal bed, as determined by these holdup tests, is higher than anticipated.

Calculated values[1] for N (the number of theoretical chambers in the bed calculated from the pulse width, not from breakthrough times) were lower than expected. This indicates a possibility of void spaces in the charcoal beds. It should be noted also that the bed temperature was 16 to 19°C during the test and that under reactor conditions the inlet end of the charcoal bed will be heated by decay of fission gases. This will tend to reduce the over-all holdup time of the charcoal bed. However, on the basis of the holdup tests, beds 10-C and -D should be adequate for use under reactor operating conditions.

[1] *Chem. Tech. Monthly Prog. Rep. Sept. 1957*, ORNL-2416, sec 13 (in press) (classified).

6.5 CARPENTER-20 PUMP TEST

A Chempump using aluminum oxide bearings and Carpenter-20 stainless steel for all wetted parts is being tested with 4 M H_2SO_4 dissolver solution at 100°F for possible use in sampling the HRT-CP dissolver-product solution or for transferring stored dissolver solution from cell C. The pump has a capacity of 1 gpm at a 43-ft head, which exceeds the design requirements. No appreciable bearing wear or corrosion of the Carpenter-20 parts was noted after 108 hr of running time.

Part II

REACTOR DESIGN AND ANALYSIS

J. A. Lane

7. HRE-3 DESIGN

W. R. Gall M. I. Lundin

J. C. Bolger
R. H. Chapman
R. D. Cheverton
E. H. Gift
R. O. Maak[1]
E. A. Mason
H. A. McLain
R. C. Robertson
J. M. Trummel
E. H. Volk[2]
D. W. Vroom

7.1 THORIUM BREEDER REACTOR (HRE-3)

In designing HRE-3, it was decided to assume a system requiring no continuous letdown from the high-pressure system and requiring a minimum number of continuously operating components within the reactor cell. The plant layout will stress accessibility rather than shortness of lines or proximity to other components in placing the reactor vessel, the pressurizers, circulating pumps, or heat exchangers. Dry maintenance will be considered and all components inside the biological shield will be removable. If practicable, following maximum decontamination, major maintenance operations will be performed semidirectly within the biological shield, by using supplementary shields or coffins. An investigation will be made, supplementing the PAR welding studies, to determine the feasibility of welding instead of using flanges in the large lines.

A major objective of HRE-3 is the demonstration of breeding. The criteria for the design of the system are presented in Table 7.1.

The most recent flowsheets and the design data for HRE-3 are presented in Figs. 7.1 and 7.2 and in Table 7.2, respectively. The high-pressure-system flowsheet, Fig. 7.1, was modified to show an iodine removal system, and a jet eductor was substituted for the blower to recirculate gases through the blanket-pressurizer system.[3,4] The design data of Table 7.2 incorporate a Newtonian-like slurry which has a yield stress of 0.1 lb/ft^2 and a coefficient of rigidity of 2.42 lb/hr-ft. This change in slurry properties[5] is reflected primarily in the slurry pumping-power requirements, reducing the shaft horsepower from 400 to 237. Other changes in the data include reduction of the core circulating-loop piping to 12 in., schedule 150, and reduction of the blanket circulating-loop piping to 10 in., schedule 150.

Oxygen pressurization of the high-pressure system is shown in Fig. 7.1. This appears the most promising method of pressurization.[6] Figure 7.1 also shows a four-plate stripping column in the high-pressure condensate stream for the removal of iodine from the high-pressure system, which may prove feasible. Calculations indicate that the breeding-ratio loss due to Xe^{135} poisoning can be reduced from about 0.055 to 0.017 through iodine removal.

[1]On loan from Foster Wheeler Corp.

[2]On loan from Combustion Engineering, Inc.

[3]W. R. Gall *et al.*, *HRP Quar. Prog. Rep. July 31, 1957*, ORNL-2379, p 32, Fig. 7.1.

[4]W. R. Gall and M. I. Lundin, *Monthly Report – Design Section – Sept. 1957*, ORNL CF-57-10-79.

[5]W. R. Gall *et al.*, *HRP Quar. Prog. Rep. July 31, 1957*, ORNL-2379, p 31, esp 33–36.

[6]W. R. Gall and M. I. Lundin, *Monthly Report – Design Section – Aug. 1957*, ORNL CF-57-9-37.

Table 7.1. HRE-3 Design Criteria

	Minimum	Maximum	Design
Core power (thermal), Mw		50	50
Core outlet temperature, °C		300	280
Core inlet temperature, °C	240		250
Core ΔT, °C	0		30
Flow velocity, fuel, fps		20	
Pressure, psi			
Operating		2000	1500
Mechanical design			2500, code
Steam pressure, psia			450
Blanket power		10	10
Conversion ratio (with U^{233})	1.05	1.15	1.10
Core-tank life, years	3		
Number of pumps and heat exchangers		2	1
Capacity of heat exchanger, Mw	50		50

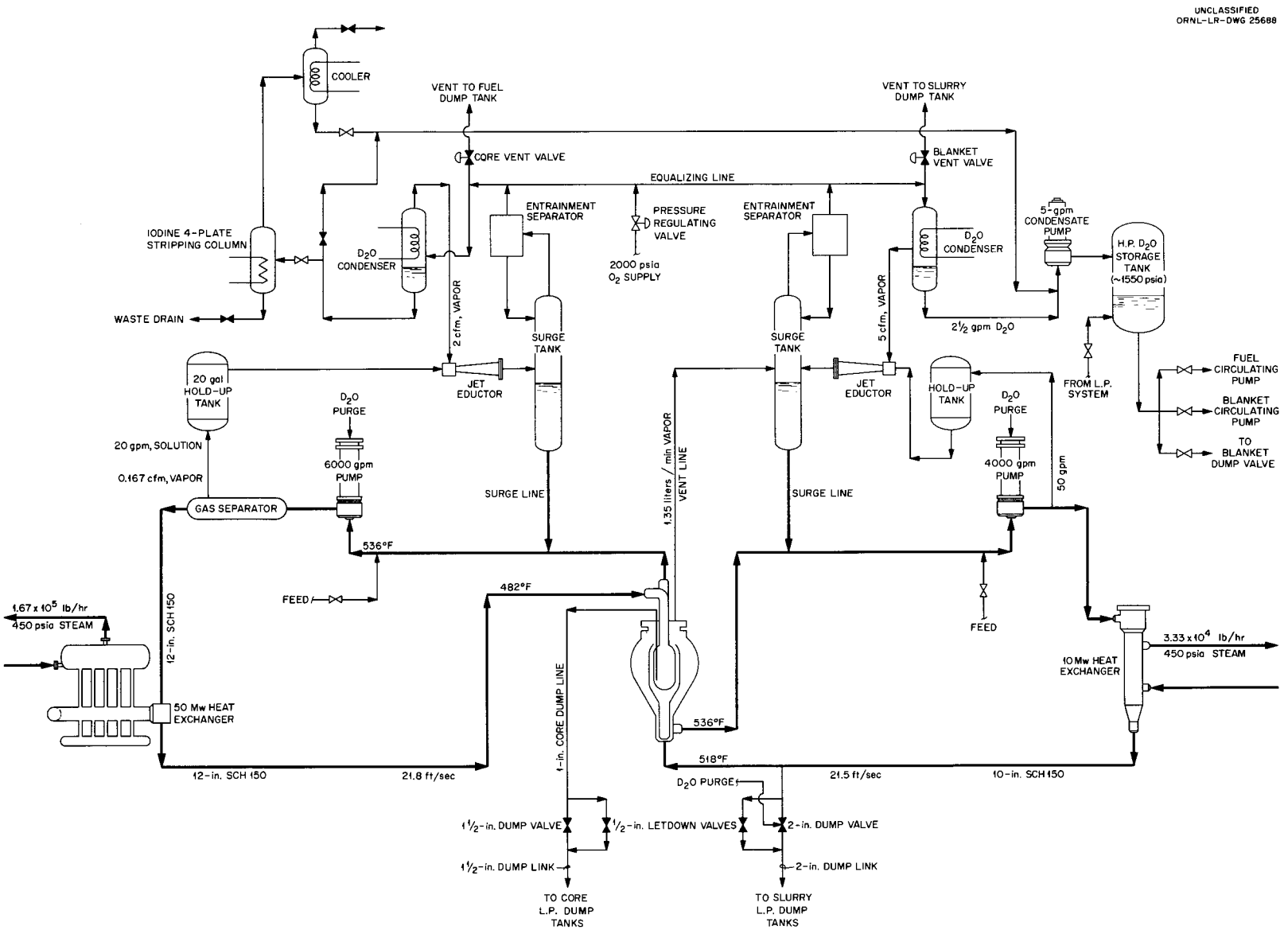

Fig. 7.1. HRE-3 High-Pressure System.

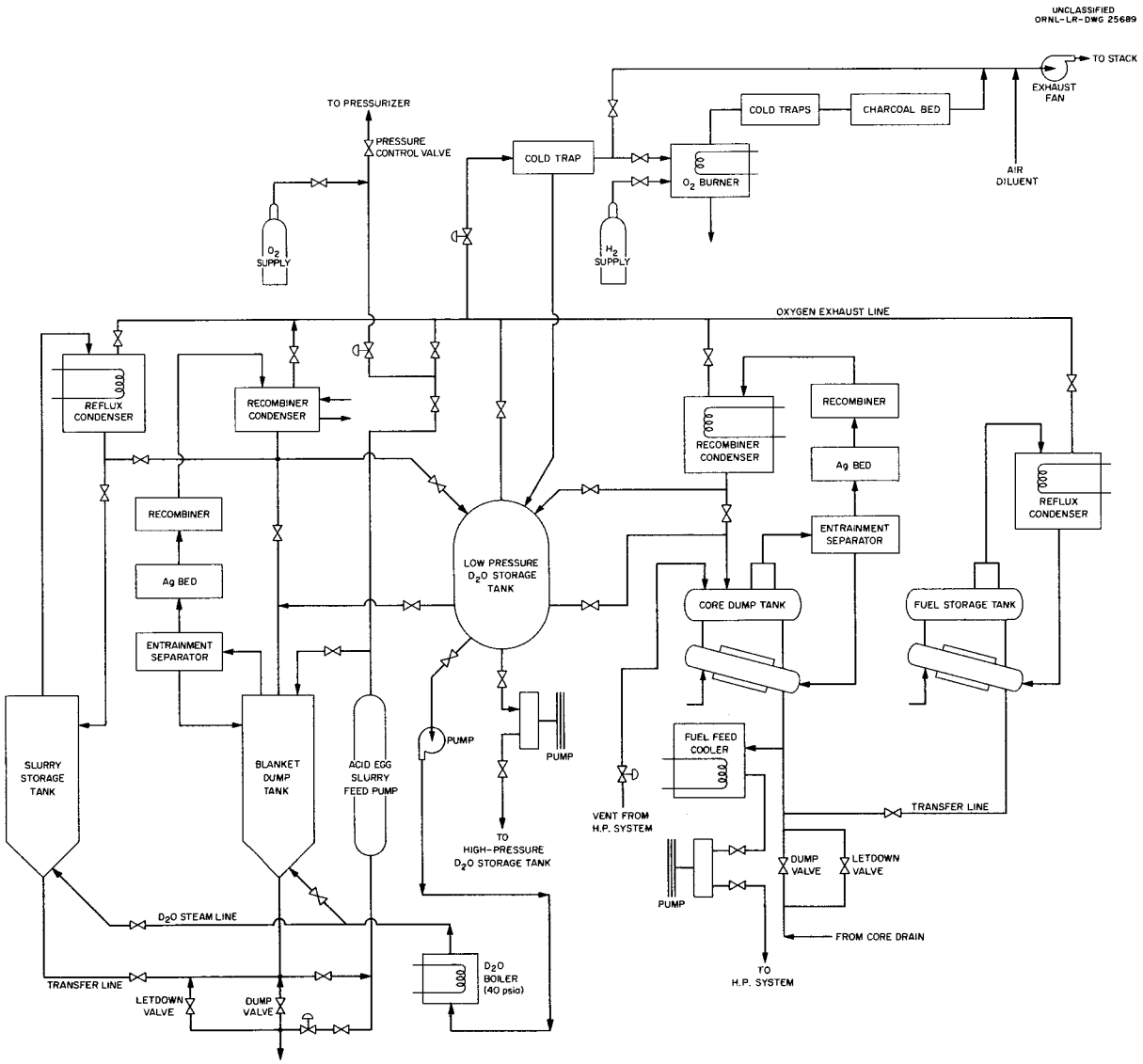

Fig. 7.2. HRE-3 Low-Pressure System.

Table 7.2. Preliminary HRE-3 Design Data

I. GENERAL REACTOR DATA		
A. Type	Two-region; breeding, Th-U^{233}; internal recombination; oxygen pressurized; fuel solution, UO_2SO_4 in D_2O; blanket slurry, ThO_2 in D_2O	
B. Gross Power		
1. Core power (thermal)	Maximum	50 Mw
	Design	50 Mw
2. Blanket power (thermal)	Maximum	10 Mw
	Design	10 Mw
3. Total power (thermal)	Design	60 Mw
(electrical)	Design	~19 Mw
C. Power Densities and Corrosion Rate (at 60 Mw)		
1. Average power density		
Core	52.6 kw/liter	
Blanket	1.04 kw/liter	
2. Power density at Zircaloy-2 wall		
In fuel adjacent to wall	23.0 kw/liter	
Within Zircaloy-2 wall	10.6 kw/liter	
3. Estimated corrosion rate of Zircaloy-2	27 mpy	
D. Breeding Ratio (estimated)[a]		
Minimum	1.05	
Design	1.09	
II. CORE-SYSTEM DATA		
A. General		
1. Solution properties		
Composition	$UO_2SO_4 + CuSO_4 + D_2SO_4$ in D_2O	
Critical concentration in core at $t_{av} = 280°C$		
Initial loading (clean)	4.6 g U^{233}/kg D_2O	
Equilibrium	4.8 g U^{233}/kg D_2O + 0.45 g U^{235}/kg D_2O	
Analysis at equilibrium		
Total uranium	10.5 g U/kg D_2O	
Copper	2.3 g cu/kg D_2O	
Excess acid	40% (0.027 *M*)	

[a]Assumes equilibrium of higher isotopes, 7% total fission-product poisoning, and an average of 2.25 fast neutrons emitted per thermal-neutron capture in U^{233}.

Table 7.2 (continued)

Density	
At 70°F	70.4 lb/ft^3
At 482°F	56.6 lb/ft^3
At 536°F	53.3 lb/ft^3
Thermal conductivity	
At 70°F	0.35 Btu/hr·ft·°F
At 536°F	0.32 Btu/hr·ft·°F
Viscosity	
At 70°F	3.06 lb/hr·ft
At 482°F	0.27 lb/hr·ft
At 536°F	0.24 lb/hr·ft
Heat capacity	
At 70°F	0.99 Btu/lb·°F
Av from 482 to 536°F	1.24 Btu/lb·°F
2. Solution decomposition and recombination data	
Decomposition rate of D_2O	1.67 molecules D_2/100 ev
Rate of formation of D_2 without internal catalyst	5.13×10^{-5} moles D_2/sec-mole solution
Rate of formation of O_2 without internal catalyst	2.56×10^{-5} moles O_2/sec-mole solution
Catalyst ($CuSO_4$) concentration for 100% recombination, design[b]	0.03 g mole/liter
Recombination rate constant with $CuSO_4$ catalyst[c]	
$D_2 + O_2$ at 482°F	K = 0.885 liter/sec·g-mole Cu
at 536°F	K = 3.15 liter/sec·g-mole Cu
Concentration and partial pressure of dissolved gases at core outlet, at 536°F and 1500 psia total pressure	
D_2O vapor pressure	940 psia
D_2 partial pressure	230 psia (0.0427 g-mole/liter)
O_2 partial pressure	330 psia (0.0562 g-mole/liter)

3. Operating temperatures at design power of 50 Mw

	Maximum	Minimum	Design
Core inlet		464°F (240°C)	482°F (250°C)
Core outlet	572°F (300°C)		536°F (280°C)
Core average	572°F (300°C)		536°F (280°C)
Core ΔT			54°F (30°C)

[b]Excess copper is desired to reduce D_2 partial pressure in pressurizer; this excess results in about 1% poisoning due to copper.

[c]Rates for D_2 have been assumed as about one-half those for H_2.

Table 7.2 (continued)

4. Operating pressure	
Normal	1500 psia
Design (at 600°F)	2500 psia
5. Circulation rate	2.547×10^6 lb/hr
At 482°F	5700 gpm
At 536°F	6000 gpm (at pump)
6. Total pressure loss due to flow, high-pressure core system (includes 14 ft for gas separator)	37.3 psi (100 ft fluid at 536°F)
7. Estimated liquid volume of high-pressure core system	4000 liters
B. Core Vessel	
1. Dimensions	4-ft-dia sphere or 3-ft-dia × 6-ft cylinder
2. Material	Zircaloy-2
3. Wall thickness	0.5 in.
4. Flow pattern	Concentric inlet and outlet at top
5. Core volume	950 liters
6. Pressure loss due to flow through core	15 ft fluid
C. Main Heat Exchonger	
1. Quantity	One (design)
2. Type	U-tube, horizontal, shell and tube (fuel solution in tubes)
3. Solution temperatures at 50 Mw of core power	
Inlet to heat exchanger	536°F
Exit from heat exchanger	482°F
4. Saturated-steam conditions at heat exchanger exit	
At 50-Mw core power	450 psia at 456°F
At 5-Mw core power	865 psia at 527°F
5. Feed-water temperature	360°F
6. Duty, at 50 Mw	170.7×10^6 Btu/hr
7. Steam generation rate	
At 50-Mw core power	195.7×10^3 lb/hr
At 25-Mw core power	98.1×10^3 lb/hr
At 5-Mw core power	19.7×10^3 lb/hr
8. Design pressure	
Tube side	2500 psia
Shell side	1250 psia
9. Design temperature	600°F
10. Log mean temperature difference at 50-Mw core power	47°F

Table 7.2 (continued)

11. Tubes	
Material	Type 347 stainless steel
Size	
OD	0.5 in.
Wall thickness	0.065 in. (No. 16 BWG)
Velocity in tube	12 fps
12. Shell material	Carbon steel
13. Hold-up volumes, tube side, total	1200 liters
14. Total pressure loss in heat exchanger (tube side)	20 psi (51 ft fluid)
D. Circulating Pump	
1. Quantity (design)	One
2. Type	Canned rotor
3. Capacity at 100-ft head	6000 gpm (at 536°F)
4. Estimated shaft-horsepower input, at 100-ft head, based on 74% impeller efficiency	176 hp
5. Purge-water requirements, estimated, design	0.5 gpm
6. Electrical characteristics	440-v, 60-cycle three-phase
E. Piping (core circulating loop)	
1. Design temperature	600°F
2. Design pressure	2500 psia
3. Design allowable working stress	14,900 psi
4. Pipe material	Type 347 seamless stainless steel
5. Pipe size	12 in., sched 150
6. Flow rates at 536°F	6000 gpm
7. Velocities at 536°F	21.8 fps
8. Friction losses	
At 536°F	6.7 ft fluid/100 ft
At 482°F	6.1 ft fluid/100 ft
9. Estimated total friction loss in piping and fittings	20 ft fluid
III. BLANKET-SYSTEM DATA	
A. General	
1. Slurry properties	
Composition	$ThO_2 + UO_2 + MoO_3$ in D_2O
Slurry concentration	1,000 g Th/kg D_2O
Uranium concentration at 10 Mw	3 g U^{233}/liter
Catalyst concentration, MoO_3	0.05 *M*

Table 7.2 (continued)

Density	
At 68°F	120.7 lb/ft^3
At 536°F	102.3 lb/ft^3
Thermal conductivity at 536°F	0.370 Btu/ft·hr·°F
Yield stress, τ_y	
Maximum	0.1 lb/ft^2
Minimum	0 lb/ft^2
Design	0.1 lb/ft^2
Coefficient of rigidity	
Maximum	2.42 lb/hr·ft
Average, design	2.42 lb/hr·ft
Heat capacity, average (518°F to 536°F)	0.626 Btu/lb·°F
2. Slurry decomposition and recombination rates	
Decomposition rate	1.0 molecule D_2/100 ev
Rate formation of D_2 without internal catalyst (at 10 Mw)	2.05×10^{-6} g-mole D_2 per mole of slurry per second
Rate formation of O_2 without internal catalyst (at 10 Mw)	1.02×10^{-6} g-mole per mole of slurry per second
Recombination rate constant with 0.05 M MoO_3 as catalyst[d]	
At 536°F	129.5 hr^{-1}
At 518°F	123.5 hr^{-1}
Concentration and partial pressure of dissolved gases at blanket outlet, at 536°F and 1500 psia total pressure	
D_2O vapor pressure	940 psia
D_2 partial pressure	25 psia (0.00412 g-mole)
O_2 partial pressure	535 psia (0.0808 g-mole/liter)

3. Operating temperature at design power of 10 Mw

	Maximum	Minimum	Design
Blanket inlet		464°F (240°C)	518°F (270°C)
Blanket outlet	572°F (300°C)		535°F (280°C)
Blanket average	563°F (295°C)		527°F (275°C)
Blanket ΔT			18°F (10°C)

4. Operating pressure	
Normal	1500 psia
Design (at 600°F)	2500 psia
5. Circulation rate	3.69×10^6 lb/hr
At pump (536°F)	3940 gpm

[d] $K = \frac{1}{p}\frac{dp}{dt} = 1.67 \times 10^3\, e^{-5067/RT}$ (slurry is 1600°C-fired and activated).

Table 7.2 (continued)

6. Total pressure loss due to flow, high-pressure blanket system	60 psia, 75 ft fluid at 280°C
7. Estimated liquid volume of high-pressure blanket system	12,000 liters
B. Pressure Vessel	
1. Dimensions	9-ft-ID sphere with 60-deg-included-angle conical bottom
2. Material	Type-347-stainless-steel-clad carbon steel
3. Wall thickness	4 to 6 in.
4. Flow pattern	Concentric inlet and outlet at bottom; baffle, or shroud, for two-pass flow
5. Pressure-vessel volume	9600 liters
6. Pressure loss due to flow through vessel	15 ft fluid
C. Main Heat Exchanger	
1. Quantity	One (design)
2. Type	U-tube, vertical, shell and tube (slurry in tubes)
3. Slurry temperatures at 10-Mw blanket power	
Inlet to heat exchanger	536°F
Outlet of heat exchanger	518°F
4. Saturated steam conditions at heat exchanger exit	
At 10-Mw blanket power	450 psia at 456°F
At 5-Mw blanket power	665 psia at 497°F
At 1-Mw blanket power	865 psia at 527°F
5. Feed-water temperature	360°F
6. Duty, at 10 Mw	34.1×10^6 Btu/hr
7. Steam generation rate	
At 10-Mw blanket power	39.1×10^3 lb/hr
At 5-Mw blanket power	19.6×10^3 lb/hr
At 1-Mw blanket power	3.9×10^3 lb/hr
8. Design pressure	
Tube side	2500 psia
Shell side	1250 psia
9. Design temperature	600°F
10. Log mean temperature difference at 10-Mw blanket power	69.2°F
11. Apparent over-all heat transfer coefficient, based on tube OD (fouling factors are included)	442 Btu/hr·ft^2·°F

Table 7.2 (continued)

12. Heat transfer surface, based on tubing OD	1120 ft^2
13. Tubes	
Material	Type 347 stainless steel
Size, outside diameter	0.625 in.
wall thickness	0.065 in. (No. 16 BWG)
Velocity in tube	14 fps
14. Shell material	Carbon steel
15. Holdup volumes	
Tube side, total	270 liters
16. Total pressure loss due to flow, tube side	25 psi (31.4 ft fluid)
D. Circulating Pump	
1. Quantity (design)	One
2. Type	Canned rotor
3. Capacity at 75-ft head	4000 gpm (at 536°F)
4. Estimated shaft-horsepower input, at 75-ft head, based on 74% impeller efficiency	190 hp
5. Purge-water requirements, design	1 gpm
6. Electrical characteristics	440-v, 60-cycle, three phase
E. Piping (pressure-vessel circulating loop)	
1. Design temperature	600°F
2. Design pressure	2500 psia
3. Design allowable working stress	14,900 psi
4. Pipe material	Type 347 seamless stainless steel
5. Pipe size	10-in., sched-150
6. Flow rate	
At 518°F	3915 gpm
At 536°F	3950 gpm
7. Velocities	
At 518°F	21.6 fps
At 536°F	21.8 fps
8. Friction losses (at 536°F)	14.4 ft fluid/100 ft
9. Estimated total friction loss in piping and in fittings	29 ft fluid
IV. AUXILIARY-SYSTEM DATA	
A. Turbine-Generator System	
1. Turbine-generator size	20,000 kw

Table 7.2 (continued)

2. Type	Condensing, direct-connected, hydrogen-cooled, extracting, 1800 rpm, with moisture separation (internal or external)
3. Estimated gross electrical power generated at 60-Mw reactor power	19,250 kw
4. Assumed turbine-element efficiencies	
High-pressure	84.8%
Low-pressure	87.2%
Combined electrical and mechanical efficiencies	96.5%
Exhaust loss	20 Btu/lb
5. Steam to throttle at 60-Mw reactor power	450 psia dry and saturated, 234.7×10^3 lb/hr
6. Exhaust pressure	1.5 in. Hg abs
7. Condensing water, assumed in at 70°F and out at 80°F	31,300 gpm
B. Cooling-Water System	
1. Potable water, estimated requirements	
Building sanitary	100 gpm
Cooling tower make-up	300 gpm
Demineralized-system make-up	50 gpm
Miscellaneous	100 gpm
	550 gpm
Size of main	Minimum 8 in.
2. Process water, estimated requirements	
Turbine condenser	32,000 gpm
Demineralized-water heat exchanger	4,000 gpm
Cell space coolers	1,000 gpm
Miscellaneous	3,000 gpm
	40,000 gpm
Size of main	Approximately 4-ft dia
C. Steam Service System	
1. Estimated size of main from X-10 area	8-in. dia
D. Electrical Distribution	
1. Transmission lines	13.8 kv, three-phase, 60-cycle
2. Transformers	480/13,800 v

8. REACTOR ANALYSIS

P. R. Kasten

H. C. Claiborne
T. B. Fowler
M. P. Lietzke
C. W. Nestor, Jr.
M. W. Rosenthal
M. Tobias

8.1 KINETIC CALCULATIONS FOR HRE-3

The safety of HRE-3 was investigated as a function of the vapor volume in the pressurizer and of the length and inside diameter of the piping between the core and pressurizer. Calculations were performed by assuming that reactivity was added either as a step function or as a linear rate addition. The parameter values considered are given in Table 8.1. For nearly all cases, a rate of reactivity addition of 0.015 Δk_e/sec was assumed, with the reactor initially at a power level of 0.04 w (source power). This corresponds to an equivalent instantaneous reactivity addition of 0.02 Δk_e.

The mathematical model assumed was that used for the HRT.[1] The primary variable is the maximum pressure rise within the core region following the reactivity addition. This is plotted in Figs. 8.1 and 8.2 as a function of the parameter values considered. The results indicate that a 2% reactivity addition will not cause a core-pressure rise greater than 400 psi if the vapor volume of the pressurizer is 20 cu ft, the piping between the core and pressurizer is 12 in. in inside diameter and no longer than 40 ft, and if initially there is zero gas volume within the reactor.

[1]P. R. Kasten, *Operational Safety of the Homogeneous Reactor Test*, ORNL-2088, p 4–8 (July 19, 1956).

Table 8.1. Parameter Values* Used in HRE-3 Kinetic Calculations

Parameter	Values
Length of piping between core and pressurizer, L, ft	10, 15, 20, 30, 40
Vapor volume of pressurizer, V_p, ft^3	5, 8, 16
ID of piping between core and pressurizer, in.	10, 12, 14
Instantaneous reactivity addition, Δk_e	0, 0.02, 0.03
Rate of reactivity addition, Δk_e/sec	0, 0.01, 0.015
Initial reactor power, P_0, kw	4×10^{-5}, 1000
Fraction of fission neutrons which are delayed, β	0.0015
Mean lifetime of prompt neutrons, l, sec	5.3×10^{-4}
Temperature coefficient of reactivity, $\partial k_e/\partial T$, Δk_e/°C	-2.9×10^{-3}
Initial density of core fluid, ρ_0, lb/ft^3	52.5
Temperature coefficient of density, $(1/\rho_0)\ \partial\rho/\partial T$, °C^{-1}	-2.1×10^{-3}
Core volume, ft^3	40
Initial core pressure, psia	2000
Core volume heat capacity, kw-sec/°C	3800
Velocity heads lost due to friction and turbulence in piping, n_f	6
Square of velocity of sound in fuel fluid, (ft/sec)^2	5×10^6

*Based on a 4-ft-dia core, 9-ft-dia pressure vessel, 1000 g of thorium per liter in the blanket, and an operating temperature of 280°C.

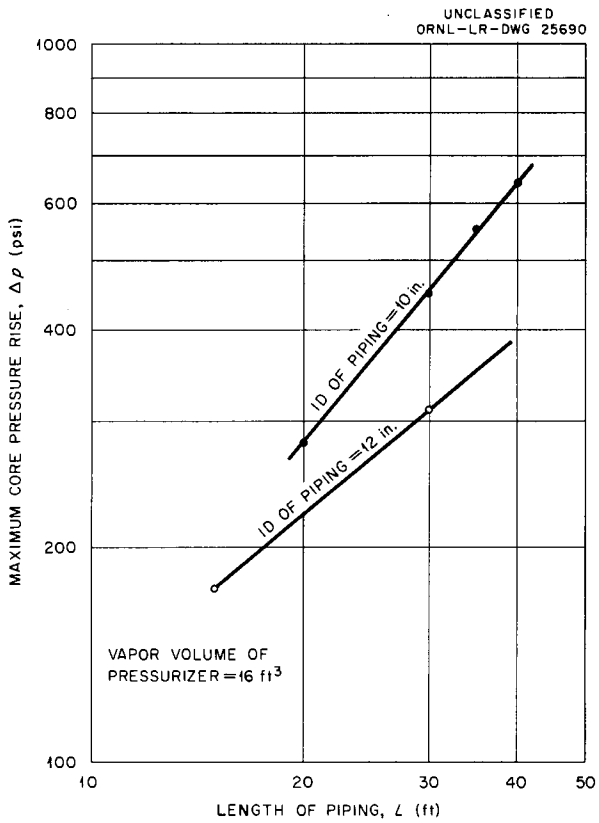

Fig. 8.1. Core-Pressure Rise in HRE-3 as a Function of Length of Piping Between Core and Pressurizer for an Equivalent Reactivity Addition of 2%.

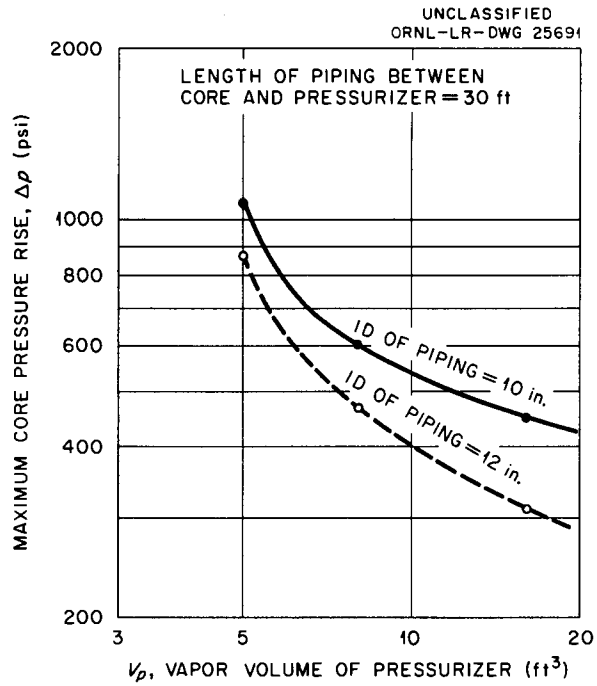

Fig. 8.2. Effect of Vapor Volume of Pressurizer upon Core-Pressure Rise for an Equivalent Reactivity Addition of 2%.

Typical plots of reactor power vs time and core pressure vs time are given in Figs. 8.3 to 8.5. For all cases the power-time curves were similar to the curve given in Fig. 8.3. The variation of pressure with time, however, was significantly dependent upon the parameter values considered; this can be illustrated by comparing Fig. 8.4 with 8.5. As shown, increasing the piping length from 30 to 40 ft resulted in a higher maximum pressure, a lower minimum pressure, and a pressure oscillation with a smaller degree of damping and a lower frequency.

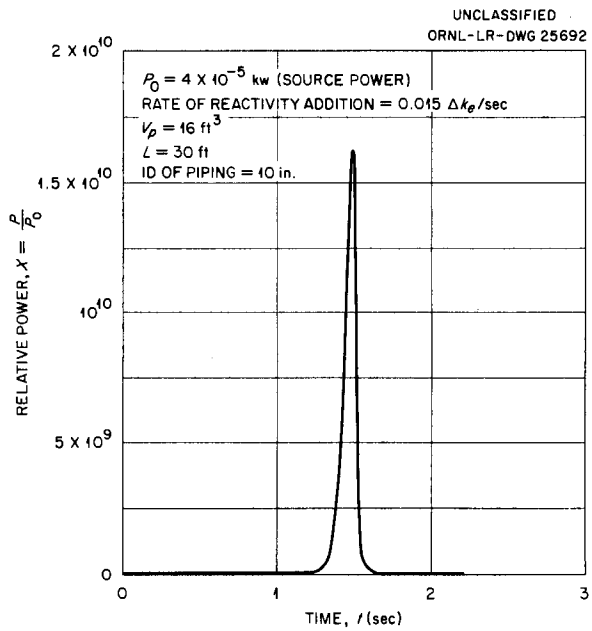

Fig. 8.3. Relative Power vs Time for Reactor Initially at Source Power.

8.2 HEAT GENERATION RATES IN HRE-3 CORE TANK

Heat generation rates in the HRE-3 core tank were calculated for a number of possible operating conditions. The results and the specific conditions considered are given in Table 8.2. Cases 1 through 12 are for a solution core, and

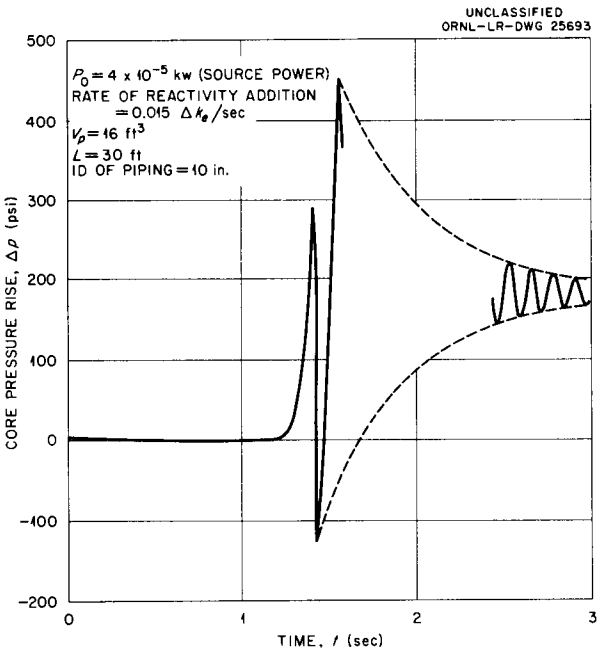

Fig. 8.4. Pressure Rise vs Time for Reactor Initially at Source Power. Length of piping between core and pressurizer, 30 ft.

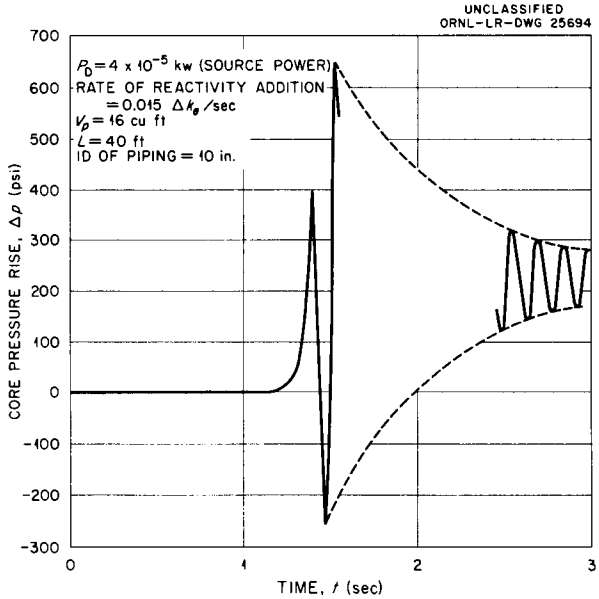

Fig. 8.5. Pressure Rise vs Time for Reactor Initially at Source Power. Length of piping between core and pressurizer, 40 ft.

the remainder are for a slurry core (200 g of thorium per liter plus the required UO_3). The main cause for the variation in the heat generation rates for a particular blanket-thorium concentration is the change in blanket power. If all cases were adjusted to the same total reactor power, the difference in results obtained for a specified blanket-thorium concentration would be only a few tenths of a watt per milliliter. However, a decrease in thorium concentration causes an increase in the heat generation rate, the maximum value occurring with a heavy-water blanket.

Cases 13 through 17 are included in Table 8.2 to indicate the reduction in heat generation that occurs if a mixed ThO_2-UO_3 slurry were to replace the UO_2SO_4-D_2O fuel solution. When the two core types are compared on an equal total-power basis (cases 5 and 14), a 34% reduction in heat generation results from use of a slurry core. If the reactor power level were increased to 500 thermal Mw and the core diameter were 6 ft, the core-tank heat generation rate would be about 30 w/ml for a solution core; this value would be reduced to about 20 w/ml if a slurry core were used.

In the above calculations the experimental results for gamma energy release on fission of U^{235} were used. Corresponding information for U^{233} is not presently available. The calculational method used[2] was previously applied, with good results, in estimating the heat generation rates in parts of the Bulk Shielding Facility.

8.3 HEAT GENERATION RATES IN HRE-3 PRESSURE VESSEL

Heat generation rates in the HRE-3 pressure vessel due to the absorption of gamma rays were estimated for various conditions. Only those gamma rays resulting from neutron capture in the pressure vessel were considered. This energy source appears to be the major contributor to heating the vessel,[3] and therefore the values obtained are an indication of the total heat-release rate. Computations were performed for the various blanket compositions given in Table 8.3.

---

[2] H. C. Claiborne *et al.*, *Nucleonics* 15(10), 114 (1957).

[3] R. H. Chapman, *Analysis of Spherical Pressure Vessel Having an Energy Source Within the Wall*, ORNL-1987 (Oct. 26, 1954).

Table 8.2. Heat Generation Rates Within the Core Tank of HRE-3 Type Reactors*

Case	Core Fuel Type	Core Power (Mw)	Blanket Power (Mw)	Blanket Thorium Concentration (g/liter)	Blanket Uranium Concentration (g/liter)	Fraction Poisons (core, blanket)	Heat Generation Rate (w/ml)
1	Solution	50	0	1000	0	0, 0	10.0
2	Solution	50	11.6	1000	3	0, 0	10.8
3	Solution	50	20.2	1000	5	0, 0	11.4
4	Solution	50	0	1000	0	6, 0	9.8
5	Solution	50	10.9	1000	3	6, 2	10.6
6	Solution	50	0	500	0	0, 0	10.8
7	Solution	50	12.6	500	3	0, 0	11.7
8	Solution	50	22.7	500	5	0, 0	12.5
9	Solution	50	0	500	0	6, 2	10.5
10	Solution	50	11.9	500	3	6, 2	11.4
11	Solution	50	0	0	0	0, 0	14.8
12	Solution	50	0	0	0	6, 0	14.4
13	Slurry**	50	11.7	1000	3	6, 2	6.3
14	Slurry**	55.6	5.3	1000	3	6, 2	7.0
15	Slurry**	50	8.1	1000	5	6, 2	6.5
16	Slurry**	50	14.3	500	3	6, 2	6.9
17	Slurry**	50	0	0	0	0, 0	9.2

*Core diameter, 4 ft; ID of pressure vessel, 9 ft; core-tank thickness, ½-in. Zircaloy-2; moderator, D_2O; temperature, 280°C.

**200 g of thorium per liter.

Table 8.3. Neutron Currents into HRE-3 Pressure Vessel*

Blanket Thorium (g/liter)	Blanket U^{233} (g per kg of Th)	Net Neutron Current into Pressure Vessel (neutrons/cm²·sec)	
		Thermal Current	Total Current
0		8.46×10^{12}	8.48×10^{12}
500	3	1.97×10^{11}	2.67×10^{11}
500	0	1.42×10^{11}	1.62×10^{11}
1000	3	3.33×10^{10}	8.31×10^{10}
1000	0	2.30×10^{10}	4.47×10^{10}

*Based on spherical geometry; 4-ft-ID core; 9-ft-ID pressure vessel; 280°C; and total power of 60 thermal Mw.

The method developed by Enlund[4] was employed, with function values obtained from the expanded plot prepared by Chapman.[3] The pressure vessel was assumed to be type 347 stainless steel. However, the results would not differ appreciably if the vessel were of mild steel clad with stainless steel, since most of the neutrons are absorbed within a short distance from the inner surface. For the same reason the thickness of the wall is not included as a parameter, and in this analysis the vessel was assumed to extend from the inner boundary to infinity.

Net neutron currents into the pressure vessel were obtained by using a two-group multiregion code,[5] with each of the physical sections of the

[4] H. L. F. Enlund, *Energy Absorption of Capture Gammas*, ORNL CF-52-6-99 and Supplement (June 11 and Oct. 16, 1952).

[5] C. W. Nestor, Jr., *Two-Group Analysis of Thermal, One-Dimensional, Multi-Region Spherical Reactors*, ORNL CF-57-5-14 (May 1, 1957); *Two-Group Analysis of Multi-Region Reactors. Part II: Construction and Use of Oracle Code*, ORNL CF-57-5-49 (May 14, 1957).

reactor (core, core tank, blanket, pressure vessel) considered as a region. The fast-neutron current was added to the thermal current and the total treated as being thermal. Seven gamma-energy groups were used, and allowance for buildup was made by dividing the absorption coefficients by 1.2. The compositions considered and the neutron currents obtained are given in Table 8.3. The corresponding heat generation rates are shown in Fig. 8.6.

Also shown in Fig. 8.6 are the results obtained for capture-gamma heating by Chapman[3] using one gamma-energy group, normalized to a neutron current of 10^{12}. Because of the different group treatment used here, it is not surprising that the results are different; however, the agreement between the two methods is good.

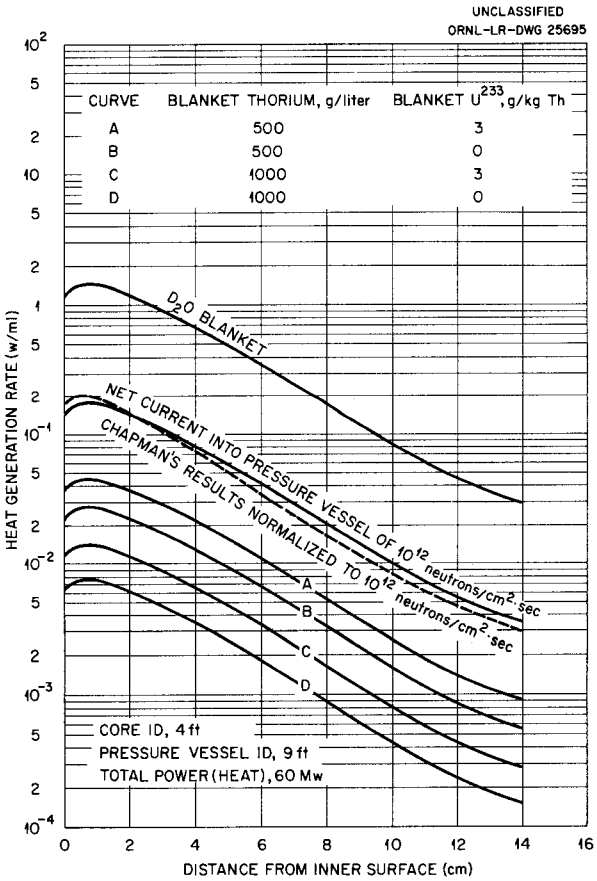

Fig. 8.6. Estimated Heat Generation Rate in HRE-3 Pressure Vessel Due to Capture Gammas Originating in Pressure Vessel.

8.4 TIME-DEPENDENT STUDIES OF HRE-3 TYPE REACTORS

Computations were performed for several spherical HRE-3 type reactors by using an Oracle code[6] for two-region, time-dependent thorium breeder systems. The variation with time of the breeding ratio and the concentrations of U^{233}, U^{234}, U^{235}, U^{236}, Pa^{233}, and fission-product poisons were obtained. Calculations were confined to solution-core reactors initially containing either U^{233} or U^{235}. Core and blanket Thorex processing was considered only when the initial fuel was U^{233}. The use of centrifugal separation (hydroclones) for core-solution processing was assumed in all cases. The time dependence of the concentrations of xenon, the samarium group of poisons, and the poisons removable by hydroclone processing was neglected, since the time required for these poisons to reach near-equilibrium conditions is relatively short. Account was taken of their presence by the use of fixed posion fractions. The effect of copper added for internal gas recombination was also included in this way. Table 8.4 presents the conditions specified for the cases studied.

A simplified flowsheet of the reactor system is shown in Fig. 8.7; it is assumed that processing of the core and blanket regions has started. As indicated, core solution is processed both by hydroclones and by Thorex; the blanket material, a slurry of thorium oxide in heavy water, is processed by Thorex only; fuel produced in the blanket is drawn off from the Thorex plant and returned to the core at a rate sufficient to maintain criticality.

The system was assumed to start "clean," except for the poisons mentioned, with either U^{233} or U^{235} in the core. Make-up fuel (same as initial fuel) was fed as needed while the concentration of fuel in the blanket increased. When the blanket fuel concentration reached a predetermined level, blanket processing was initiated at the rate which would be required if the reactor were at equilibrium; however, for the U^{235}-fueled reactors, calculations were performed only up to the time at which processing would start. At the start of processing, the fuel feed for the core was assumed to come from the processed blanket stream. When the core poison level built up to

[6] P. R. Kasten *et al.*, *HRP Quar. Prog. Rep. July 31, 1957*, ORNL-2379, p 37, esp 44–45.

a predetermined point (8% for the U^{233} reactors), processing of the core solution was started. The processed core-fuel stream was considered mixed with the processed blanket stream; part of the mixture was used as core feed, while the remainder was drawn off as excess fuel. The calculations were continued until most of the concentrations approached equilibrium values. Time lags due to chemical processing holdups were neglected. The chemical processing rates employed were those calculated earlier for equilibrium reactors.[7]

[7] M. W. Rosenthal and T. B. Fowler, *Nuclear Computations for HRE-3 Design; Equilibrium Results*, ORNL CF-57-7-23 (July 10, 1957).

Table 8.4. Specified Conditions for Cases Studied*

Case No.	Core Diameter (ft)	Pressure-Vessel Diameter (ft)	Initial Core Fuel	Blanket Thorium Concentration (g/liter)
1	4	9	U^{233}	1000
2	4	9	U^{233}	500
3	4	9	U^{235}	500
4	4	9	U^{235}	1000
5	4	8	U^{235}	1000
6	4	8	U^{233}	1000
7	5	9	U^{233}	1000

*Core power = 50 Mw; temperature = 280°C; fixed core poisons (per cent of core fission cross section) were assumed as follows: samarium group, 0.8%; xenon, 1%; copper, 0.8%; poisons removable by hydroclones, 1%. Fixed blanket poisons (per cent of blanket fission cross section) were assumed as follows: samarium group, 0.8%; xenon, 1%.

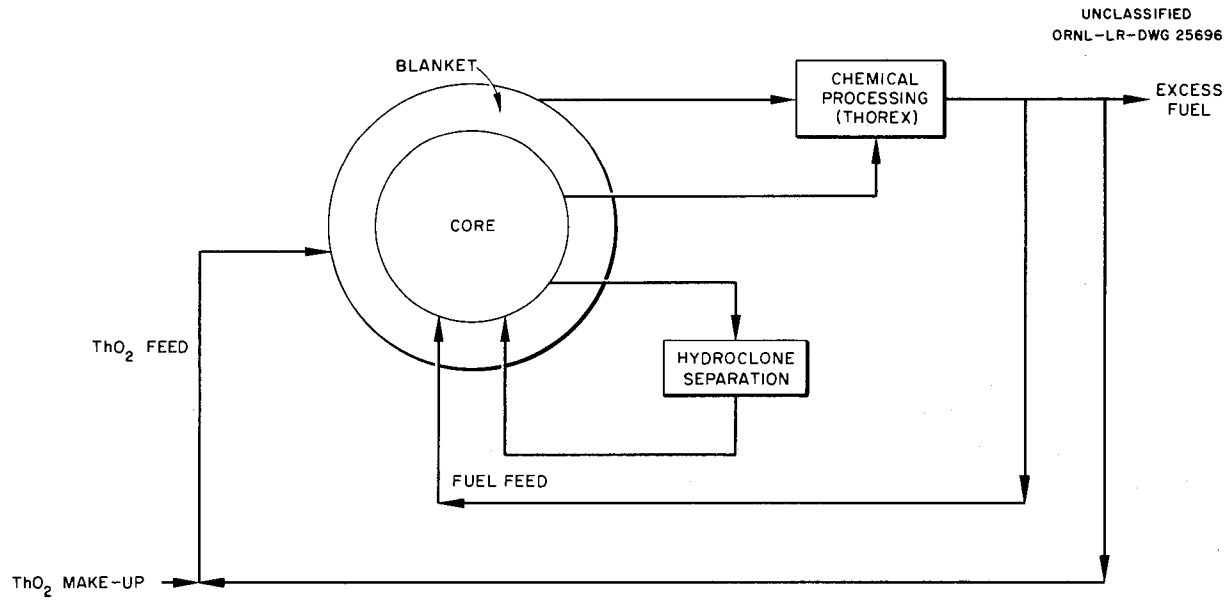

Fig. 8.7. Flowsheet for Reactor System After Fuel Processing Has Been Initiated.

A more complete analysis of this study is reported elsewhere.[8]

The accompanying figures show results for a representative U^{233}-fueled reactor, namely, case 1 of Table 8.4. As shown in Fig. 8.8, the breeding ratio falls steadily for about 900 days until core processing starts. Although blanket processing,

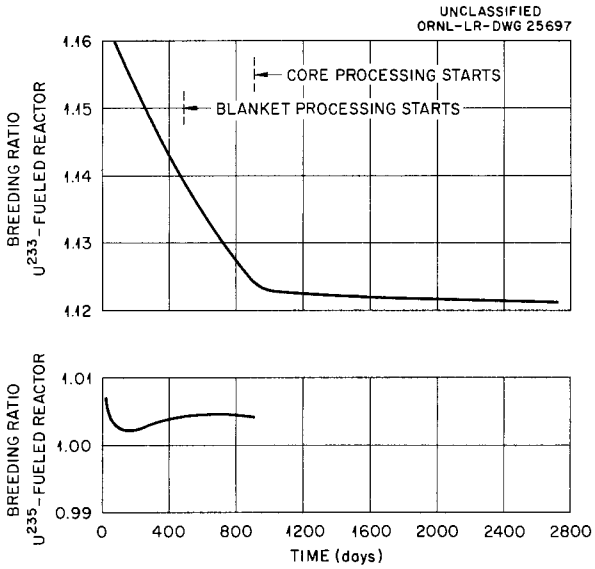

Fig. 8.8. Breeding Ratio vs Time for a U^{233}-Fueled Reactor and a U^{235}-Fueled Reactor. (Core dia = 4 ft; pressure-vessel dia = 9 ft; blanket Th conc = 1000 g of Th per liter; 280°C.)

begun at 490 days, arrests the growth of protactinium and U^{233} in the blanket rather suddenly, as shown in Fig. 8.9, the slope of the breeding-ratio curve does not change markedly because the buildup of core poisons is controlling the breeding ratio. When core processing interrupts the growth of core poisons, the breeding ratio levels off sharply. The variation of relative leakage and poison losses with time is given in Fig. 8.10.

In all cases the time required to reach the 8% core poison level is of the order of two years. The average breeding ratio during this period is about 0.02 higher than the equilibrium value. The effect of poisoning due to buildup of corrosion products is not included in this estimate.

[8] M. Tobias, T. B. Fowler, and M. W. Rosenthal, *Time-Dependent Studies of HRE-3 Type Reactors*, ORNL CF-57-12-1 (to be published).

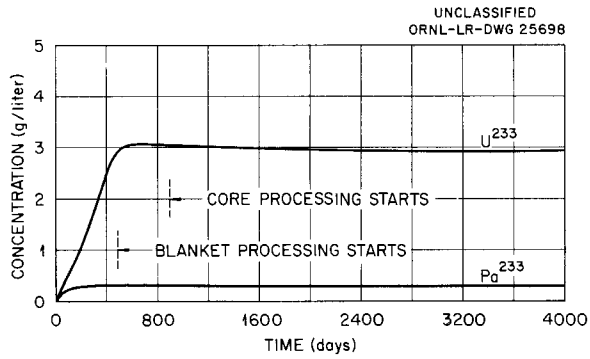

Fig. 8.9. Blanket Concentration of U^{233} and Pa^{233} vs Time for a U^{233}-Fueled Reactor. (Core dia = 4 ft; pressure-vessel dia = 9 ft; blanket Th conc = 1000 g of Th per liter; 280°C.)

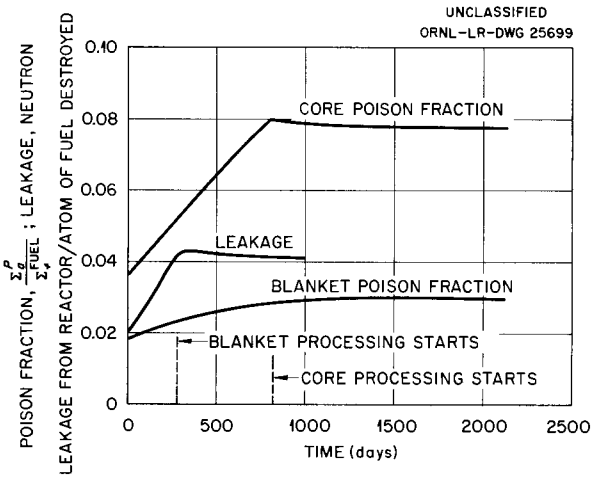

Fig. 8.10. Neutron Leakage and Poison Fraction vs Time for a U^{233}-Fueled Reactor. (Core dia = 4 ft; pressure-vessel dia = 9 ft; blanket Th conc = 500 g of Th per liter; 280°C.)

While the above statements concerning breeding ratio are characteristic of U^{233}-fueled reactors, U^{235} reactors show quite a different variation of breeding ratio with time, due to changes in the effective η for the system with time. As indicated in Fig. 8.8, U^{235}-fueled reactors have appreciably lower breeding ratios than do U^{233}-fueled systems. This is primarily due to the relatively low value of η^{25} compared with η^{23} (η^{23} = 2.25 while η^{25} = 2.08). As U^{233} builds up in the blanket of a U^{235}-fueled reactor, the average value of η for the reactor as a whole increases. This helps compensate for the increase in core poison fraction

and accounts for the strikingly different time behavior of breeding ratio shown in Fig. 8.8 for the two systems considered.

Three types of isotope growth were obtained in this study. First, as illustrated in Fig. 8.11, the concentration of the main fuel isotope, U^{233} or U^{235}, remained relatively constant despite sizable changes in other concentrations. Second,

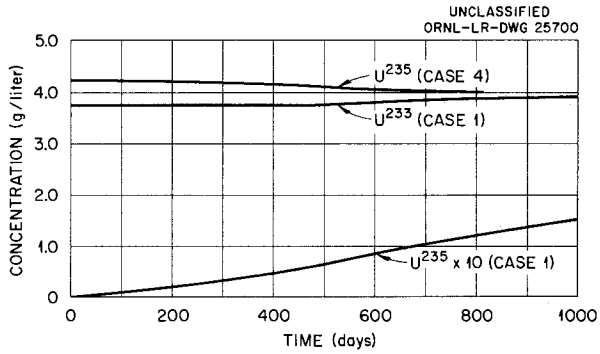

Fig. 8.11. Core Fuel Concentrations vs Time for a U^{233}-Fueled Reactor (Case 4, Table 8.4).

the protactinium concentration was found to reach a steady value even before processing started, as shown in Fig. 8.9. This behavior was due to the radioactive decay rate being several times larger than the chemical processing rates employed. Third, the concentration of the heavier isotopes of uranium built up slowly with time; even after 10 years of operation their concentrations were much less than the equilibrium values. The *total* core concentration of uranium was thus significantly less than the equilibrium value. The isotope concentrations after various operating times are shown in Table 8.5, along with equilibrium values.

While chemical processing sharply discontinues the growth of U^{233} in the blanket, the power level in the blanket may markedly overshoot the equilibrium level, as shown in Fig. 8.12. An overshoot is obtained when the blanket U^{233} concentration reaches its maximum value before core processing starts. Table 8.6 shows the peak values of blanket power computed for the reactors studied, along with the equilibrium values.

Table 8.5. Core Concentration of Uranium Isotopes as a Function of Time for a U^{233}-Fueled Reactor (Case 1) and for a U^{235}-Fueled Reactor (Case 4)

Time (days)	U^{233}	U^{234}	U^{235}	U^{236}	U Total
Concentrations of Isotopes for Case 1 (g/liter)					
0	3.75				3.75
200	3.77	0.33	0.02		4.12
500	3.74	0.74	0.07	0.01	4.56
920	3.91	1.29	0.14	0.04	5.38
2000	3.98	2.06	0.26	0.18	6.48
3000	4.02	2.40	0.31	0.34	7.07
Equilibrium	4.02	2.74	0.37	1.57	8.70
Concentrations of Isotopes for Case 4 (g/liter)					
0			4.21		4.21
200			4.19	0.57	4.76
500			4.12	1.43	5.55
900			4.03	2.54	6.57

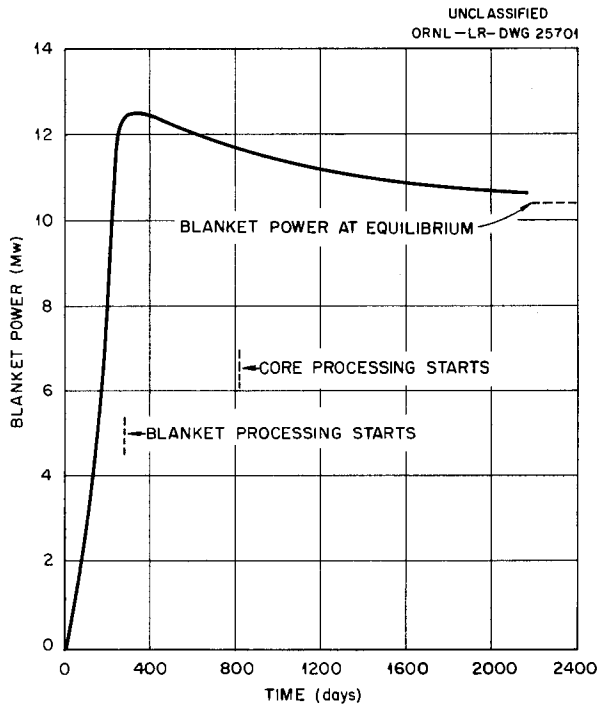

Fig. 8.12. Blanket Power vs Time for a U^{233}-Fueled Reactor (Case 2, Table 8.4).

Table 8.6. Peak and Equilibrium Values of Blanket Power Computed for U^{233}-Fueled Reactors

Case No.	Blanket Power (Mw)		Time at Which Peak Value Occurs (days)
	Equilibrium Value	Peak Value	
1	9.6	10.8	520
2	10.4	12.5	350
6	9.3	10.8	380
7	10.0	11.5	490

8.5 CYLINDRICAL HRE-3 REACTOR STUDIES

Results were obtained supplementing those reported earlier,[9] concerning some of the nuclear characteristics of two-region, cylindrical, thorium breeder reactors. As before, the reactors were assumed to be at 280°C with 7% core poisons, 3 g of U^{233} per liter and 1000 g of Th per liter (as ThO_2) in heavy water in the blanket, and operated at a total power of 60 Mw. A cylindrical core was assumed to be positioned within a cylindrical pressure vessel such that a 2-ft blanket thickness surrounds the core. A two-group, two-region model was used in calculating the critical concentration, breeding ratio, and power density at the core wall. In these calculations the core diameter was considered to be 2½, 3, or 3½ ft, and the reactor length was varied from 3½ to 12 ft.

Table 8.7 summarizes the results obtained for breeding ratio and critical concentration. It is apparent that increasing the reactor length had very slight effect on breeding ratio; also, although the critical concentration declined with increasing length, the corresponding total fuel inventory increased. While not shown, the ratio of blanket power to core power did not vary significantly with length. Figure 8.13 shows the variation of the maximum power density at the core wall as a function of length. Also shown are lines of constant volume corresponding to various core diameters and heights. Increasing the core volume caused a pronounced decrease in core-wall power density and an increase in fuel inventory. Thus, for a 3-ft-dia core, increasing the core length from 4.8 to 8 ft decreased the power density by 36%. However, the core fuel inventory increased by about 40%; the blanket inventory would show an even larger increase.

8.6 ORACLE PROGRAMMING

An Oracle code was completed for calculating the fuel costs in two-region, time-dependent thorium breeder reactors, considering the buildup of U^{233}, U^{234}, U^{235}, U^{236}, Pa^{233}, and fission-product poisons with respect to time. The input parameters include reactor diameter (core and pressure vessel), thorium concentration (core and blanket), operating power (core or total), unit fuel value, and nuclear constants.

[9] P. R. Kasten *et al.*, *HRP Quar. Prog. Rep. July 31, 1957*, ORNL-2379, p 37, esp 43–44.

Table 8.7. Breeding Ratios and Critical U^{233} Concentrations for Cylindrical Reactors of Various Lengths

Length of Core (ft)	Core Diameter (ft)					
	2½		3		3½	
	U^{233} (g/liter)	Breeding Ratio	U^{233} (g/liter)	Breeding Ratio	U^{233} (g/liter)	Breeding Ratio
3.5					4.1	1.10
4.8			4.6	1.12		
6.0			4.2	1.12	3.0	1.12
6.8	6.5	1.13				
8	6.2	1.13	3.9	1.13	2.7	1.12
10	6.0	1.13	3.7	1.13	2.6	1.12
12	5.8	1.13	3.6	1.13	2.5	1.12

A code for calculating the heat generation due to gamma-ray absorption in the core shell of two-region, spherical homogeneous reactors was written for the Oracle. The prompt-gamma source distribution is based on the thermal-flux distribution, while the decay-gamma source is assumed uniformly distributed within the reactor region.

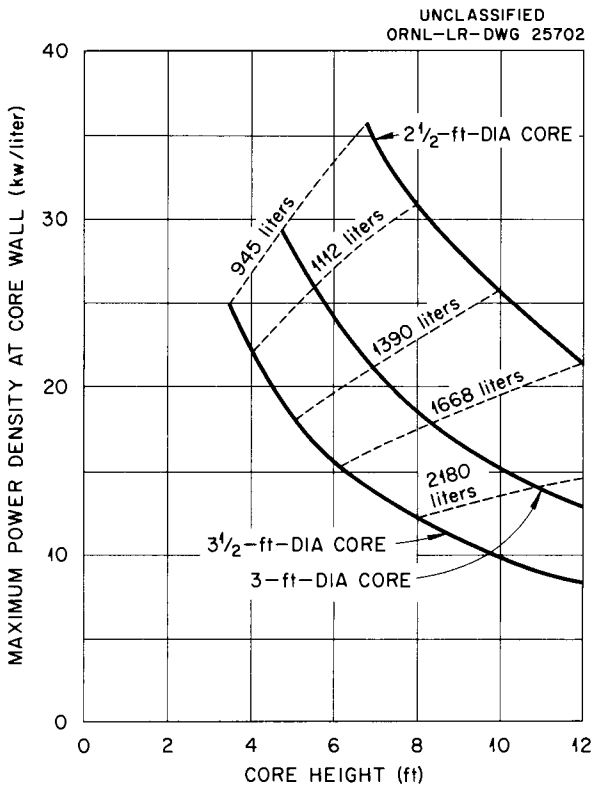

Fig. 8.13. Maximum Power Density at Core Wall for HRE-3 Type Cylindrical Reactors. (Dashed lines represent constant core volume.)

The standard two-region, two-group reactor code was altered to accept additional input parameters, including reactor power, and to compute additional output answers. Additions and changes to the output now permit critical concentration to be given in units of grams per liter for all isotope components in the core and blanket; other values obtained are breeding ratio, average thermal and fast flux in the core and blanket, core and blanket power, power densities (core maximum, core mean, core wall, blanket wall, and blanket mean), neutron absorptions and leakages normalized to 100 absorptions in fuel, and the flux plot associated with the assumed power level. By use of the new Oracle alphameric output, the output format was changed to a more convenient form.

The two-group, two-dimensional, three-region reactor code written by Bradshaw[10] was converted to comply with present Oracle equipment.

An Oracle code was written for calculating the critical concentration within a bare reactor having annular-cylindrical geometry. A two-group model was assumed.

[10] C. L. Bradshaw, *A Three-Region, Two-Group, Two-Dimensional Reactor Code for the Oracle*, ORNL-2047 (March 27, 1956).

Part III

ENGINEERING DEVELOPMENT

J. A. Lane

9. DEVELOPMENT OF FUEL-SYSTEM COMPONENTS

I. Spiewak

J. M. Baker
R. Blumberg
J. S. Culver
B. D. Draper
C. H. Gabbard
B. A. Hannaford
P. H. Harley
P. G. Herndon
E. C. Hise
P. P. Holz
J. C. Moyers
I. K. Namba
H. R. Payne
H. C. Roller
D. L. Snyder

9.1 RECOMBINER DEVELOPMENT

9.1.1 High-Pressure Recombiner

The high-pressure recombiner loop was dismantled and a new loop built, with Inconel material being used where possible in an effort to eliminate stress-cracking, which occurred in the old type 347 stainless steel loop. In addition, flanged sections of type 430 modified stainless steel pipe will replace some existing sections of type 347 stainless in order to determine its suitability for the recombiner environment. A welding procedure for this material is being developed.

Specimens of titanium and zirconium alloys and type 430 modified stainless steel have been placed in the loop; later, they will be examined metallurgically and analyzed for hydrogen. Two sets of thermocouple wells, each set consisting of a titanium-jacketed well and a reference well, were also installed to determine whether the phase change noted in previous titanium specimens was due to a chemical reaction resulting in a rise in metal temperature above loop temperature.

Initial runs will be made with KOH electrolyte containing less than 1 ppm Cl^-.

9.1.2 Syracuse Contract

Syracuse University is continuing to explore the effects of geometry, temperature, and source of ignition on the reaction, explosion, and detonation limits of steam-H_2-O_2 mixtures. There appears to be little difference in the limits observed in 1- and 0.4-in. tubes. Also, varying temperature between 100 and 200°C has little effect. The lower detonation limit appears to be about 50% stoichiometric gas. Between 45 and 50% gas, unstable or partial detonations occur. Some reactions have been observed at as low as 20% gas at 100°C and 15% at 200°C; these are very weak reactions, causing pressure surges of only a few pounds per square inch.

Calculated explosion pressures for complete and partial reactions will be compared with experimental data.

The University has submitted a final report on the detonation loading of thin-walled cylinders.[1] The primary conclusion reached is that pressures required for failure are considerably greater than those required during static loading.

9.2 CENTRIFUGAL PUMPS

9.2.1 20-cfm Canned-Motor Blower

In order to get information on the behavior of its hydrostatic bearings in slurry, the 20-cfm canned-motor blower was operated for 53 hr with sufficient ThO_2 in the bearing-fluid system to provide 30-g/liter slurry. Additional ThO_2 was then added to provide a slurry concentration of 60 g/liter. In both cases, efforts to keep the slurry evenly dispersed were unsuccessful. A method of externally recirculating the bearing fluid to promote better mixing action is to be provided for future runs.

9.2.2 4000-gpm Loop

Following stator-can repair, the Byron Jackson 4000-gpm pump ran for 114 hr before it was shut down owing to short-circuiting of two of the electrical terminals. The failure was probably caused by the combination of cracked insulating bushings and moisture in the junction box. The pump was repaired with new terminals and insulators, which were sealed to prevent the entry of moisture, and has since operated for 500 hr without difficulty. Data on mixing across the motor shaft seal and on heat removal from the stator are now being obtained.

---

[1] S. A. Mosier and J. A. Luker, *Transient Loading of Thin-Walled Cylinders*, SURI-ChE-273-578T (Aug. 2, 1957).

9.2.3 Reliance 6000-gpm Pump

A contract was awarded to Reliance Electric Co. for the development and fabrication of a 6000-gpm top-maintenance pump, which will serve as a prototype for the HRE-3 fuel circulator. It is desired that the same motor be usable for circulating slurry in the HRE-3. A preliminary design study is being made to define the useful range of head-flow characteristics obtainable in solution and slurry service with the proposed motor.

Reliance Electric is fabricating three small canned stators which will be irradiated in the HRT to evaluate the potential life of the insulation. The life of the HRT pump motors will be predicted from the same experiment.

9.3 OXYGEN COMPRESSORS

The diaphragm compressor was modified by the manufacturer, Pressure Products Industries, and was returned to service on the HRT mockup on September 3. It has been in satisfactory operation since that time. Because its capacity exceeds the demand, it operates only about a minute every half hour; it has logged about 60 running hours and 3000 starts. The compressor delivers 0.9 scfm at its present operating conditions of 500 psi suction and 2200 psi delivery.

The floating-piston cylinders for the compressor manufactured by Harwood Corp. are still in the possession of the manufacturer for modification.

A preliminary inquiry has been issued for a reactor-grade compressor capable of delivering 1 to 2 scfm of contaminated oxygen from atmospheric suction to 2500 psi discharge.

9.4 10-gpm FUEL FEED PUMPS

The multipump test facility has been completed and will be used for solution-pump development work.

A single-stage Roth turbine pump has been received and placed in operation delivering 15 gpm against a 300-psi head. As soon as the preliminary run on water has been completed, fuel solution will be placed in the loop for an endurance test.

The Stellite-piston pump[2] was fitted with four rings of Haynes alloy 25. It is pumping 1 gpm of fuel solution against a 500-psi head (the mechanical limit of the drive), with a leak rate of approximately 20 cc/min. Prior to the installation of the rings the leak rate under similar conditions initially was 360 cc/min and after 130 hr of operation was 960 cc/min.

The Koppers Co., in conjunction with Argonne National Laboratory, has developed a carbon circumferential seal for control-rod drives. They state that the seal is suitable for plunger pumps and has an extremely low leak rate. They have proposed a design incorporating two seals plus a high-pressure barrier fluid which will permit no out-leakage of the pumped fluid and an estimated leakage of 1 liter/hr of the barrier fluid. A purchase inquiry was issued to have John Bean Co. build a liquid end utilizing the Koppers seal in conjunction with the triplex power end.

A sintered filter material, Poroloy, is being investigated for use as the screening material in diaphragm feed pumps. Samples of both 20- and 40-μ pore size have been made into screen tubes and placed in heads. These heads will be assembled and operated to determine the hydraulic and plugging behavior of the assembly. Bench tests made on screen tubes 0.75 in. in inside diameter by 11 in. long by 0.032 in. thick gave the following results:

Flow rate, gpm of water	1	3	5	8	10
Pressure drop, in. H_2O					
20-μ pore	4.2	9	13.5		
40-μ pore	0.6	0.9	3.3	7.2	9.0

9.5 TITANIUM PROGRAM

A titanium–stainless steel flanged joint, shown in Fig. 9.1, has been tested in the multiple-flange testing facility and shown to have a leak rate equal to or slightly less than that of the standard HRT type 347 stainless steel flanged joint. It was subjected four times to the standard series of nine thermal cycles between 200 and 635°F. The joint was dismantled and inspected between series. Each time the 17-4 PH ring was removed from the flange groove easily by hand.

Crane Co. has been delayed in completing its 3½- and 20-in. titanium-lined carbon-steel pipe because of an inadvertent substitution of material by one of its suppliers. The blind flanges and O-rings needed to thermal-cycle these pipes at ORNL are on order.

[2] I. Spiewak *et al.*, *HRP Quar. Prog. Rep. April 30, 1957*, ORNL-2331, p 61.

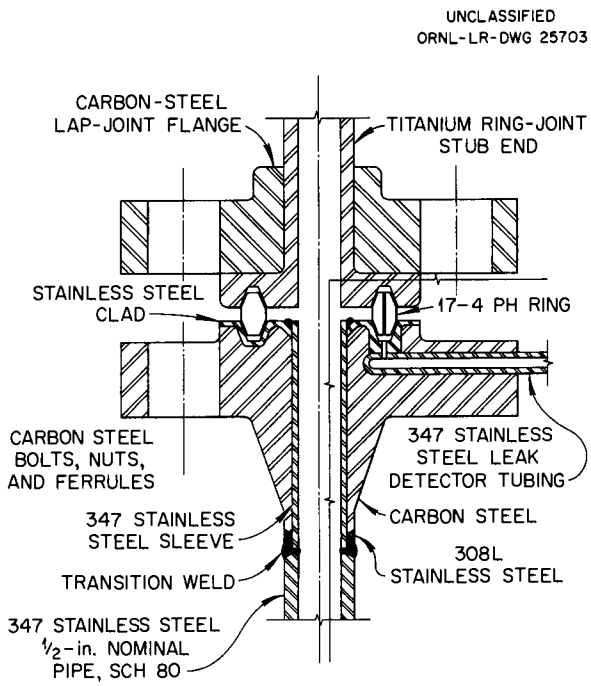

Fig. 9.1. Titanium–Stainless Steel Joint.

Chase Brass and Copper Co. has extruded an 8-ft length of 4-in.-OD × 0.300-in.-wall tubing of high-strength A-110AT titanium alloy. Unfortunately, the wall thickness is not sufficient for the intended application, a boiling uranyl sulfate loop pressurizer. Chase will supply the first piece for ORNL examination and will then extrude a second pipe to specifications.

A replacement letdown heat exchanger for the HRT mockup is being constructed from A-55 titanium pipe and tubing. The design is essentially the same as that of the presently installed unit. The titanium–stainless steel joint described above will be used to install the exchanger in the mockup.

9.6 FLANGE TEST PROGRAM

From experience gained in the flange test program, it became apparent that the torque to produce a given stress in flange bolts decreases as the bolt is tightened and loosened several times. To provide a closer relationship between torque applied and bolt stress, the new bolts for the HRT flanges were all "run in" by being tightened with a torque wrench until the desired stress was achieved as measured by a load cell. This process was repeated from three to seven times, until the torque for a given stress was constant on successive tightenings.

A test of 19-9 DL bolts was run to evaluate this material as a possible bolting material for type 347 stainless steel flanges. This material is a high-strength austenitic stainless steel with the following nominal composition (wt %):

Cr, 18–20	Ti, 0.10–0.35
Ni, 8–11	Cu, 0.50 max
Mo, 1.00–1.75	Mn, 0.75–1.50
W, 1.00–1.75	C, 0.28–0.35
Nb and Ta, 0.25–0.60	Si, 0.30–0.80

Samples of one of the studs tested gave the following physical properties:

Ultimate tensile strength	126,980 psi
Yield strength (2% offset)	93,660 psi
Elongation (1 in.)	41.5%
Reduction in area	56.1%

Bolts tested displayed a yielding characteristic somewhat different from that observed with carbon-steel bolts. All yielding occurred in the first cycle with these bolts, whereas the carbon-steel bolts yield slowly over three or four cycles. The residual room-temperature stress was somewhat higher after thermal cycling of the 19-9 DL bolts than it was with the carbon-steel bolts.

Thermal cycling of HRT flanges, from ½-in. 1500-lb to 3½-in. 2500-lb rating, containing rings mismatched with grooves by 0.010-in. (ASA tolerance), gave leak rates similar to those observed previously with zero to 0.002-in. mismatch (HRP tolerance). Furthermore, ½-in. 1500-lb and 1-in. 2500-lb flanges were sealed just as effectively with standard bolts as with ferruled bolts. While these results are preliminary, they indicate that the most important parameters in sealing a stainless ring-joint flange are (1) the initial bolt loading of 45,000-psi stress and (2) freedom from gross defects in the ring and groove.

9.7 THERMAL-CYCLE FACILITY

All major construction on the thermal-cycle facility is complete except for instrumentation. Testing of the feed-water pumps and flushing of

the low-pressure steam system are proceeding. It is planned to start the high-pressure Besler boiler early in December.

9.8 HEAT EXCHANGER TUBE-JOINT TEST

Since no tube-joint stress-corrosion cracking was observed in previous runs of 500- to 1000-hr duration, five tube bundles are being thermal-cycled with 250-psi steam until failure occurs. The shell-side environment is boiler water containing 50 ppm O_2 and 100 ppm Cl^-. The units have now operated for about 750 hr.

9.9 HRE-3 PRESSURIZER DEVELOPMENT

Two basic types of pressurizers are being developed for HRE-3. The first type, a gas pressurizer, is illustrated in Fig. 9.2. The second type is a steam pressurizer wherein uranyl sulfate (or ThO_2 slurry) is boiled. Titanium or noble-metal material is required to provide adequate corrosion resistance to boiling uranyl sulfate at the required temperature. Prior to operating the two schemes in loops, some subassembly development is being conducted as described below.

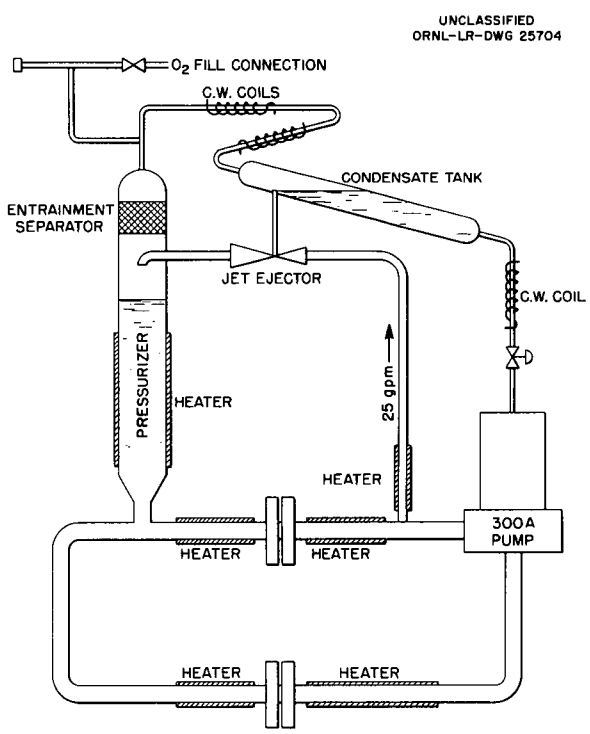

Fig. 9.2. 300A Pump Loop.

A small titanium system has been fabricated from ½-in. sched-80 pipe and will be used to investigate any undesirable long-term effects from boiling uranyl sulfate at 1700 to 2000 psi.

A small stainless steel system has been fabricated and will be used to obtain heat transfer and corrosion information on the heating and cooling of high-pressure steam-oxygen mixtures. The effect of undesirable fission-product vapors such as iodine can be investigated in this system.

9.9.1 High-Pressure Jet Test

A high-pressure ejector is proposed for HRE-3 gas-pressurizers. A commercial water jet ejector, with 1-in. sched-40 connections, was tested at pressures up to 1500 psi to determine its operating characteristics. The motive fluid was water from the discharge of a 5-gpm ORNL pump; the driven fluid was nitrogen gas.

Figure 9.3 describes the variation of efficiency as a function of nitrogen flow rates (absolute volume units) at a single water flow rate. Jet efficiency increased with system pressure to a maximum of about 26% at 1000 to 1500 psi. Had the optimum water flow rate been reached, the maximum efficiency would have been somewhat higher.

The test indicates that efficiencies are sufficiently high to make ejectors practical for use in the HRE-3 pressurizer.

9.10 DEVELOPMENT OF SLURRY COMPONENTS

9.10.1 300-gpm Slurry Loop

The 230A loop is being modified into a 300-gpm slurry loop, in accordance with Fig. 9.2; the loop will be used primarily in the development of slurry pumps, but it will also provide a facility for testing various schemes for pressurization. The loop should be ready for operation by about December 15, 1957.

9.10.2 Slurry Check-Valve Material Test

A facility to evaluate check-valve and letdown-valve materials has been built and is currently undergoing shakedown runs on water. The system contains a capillary letdown device of variable length, demountable check valves, and a dump tank which is agitated by a high-velocity return stream. A 1-LB Scott & Williams pump will permit circulation of about 0.5 gpm of 1000-g/liter ThO_2 slurry at a head of 2000 psi.

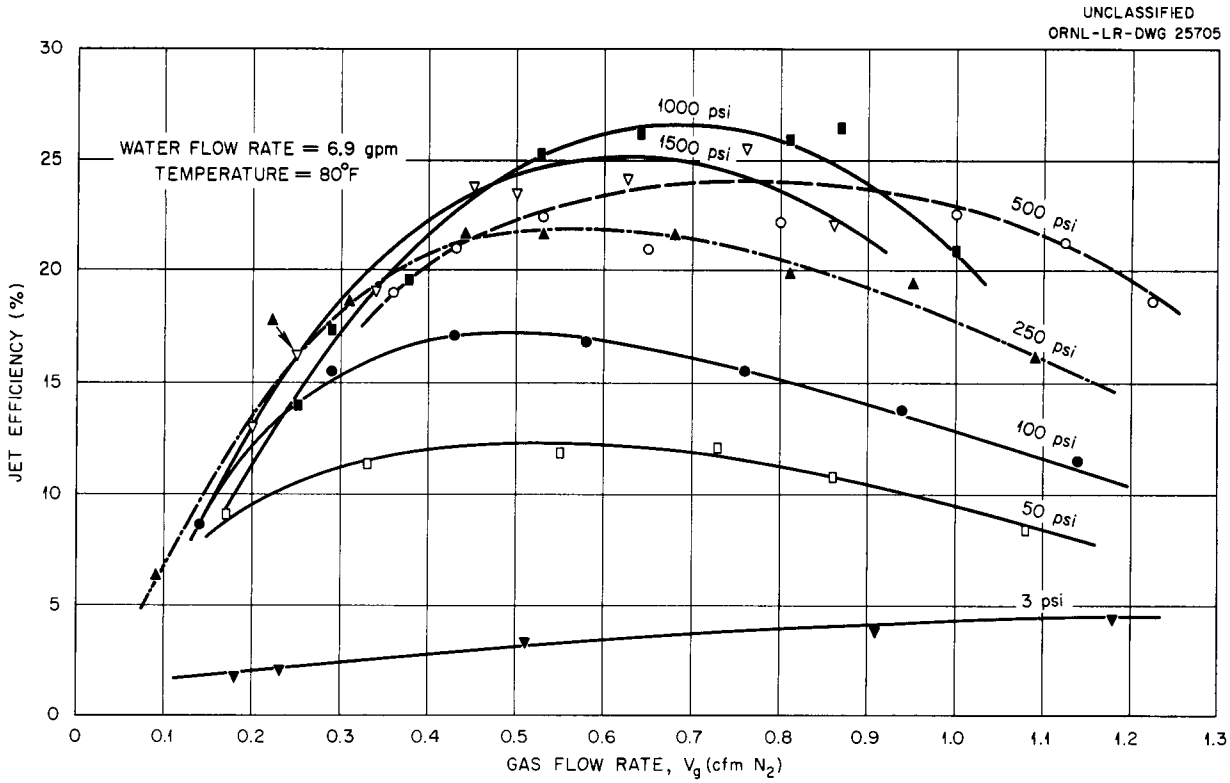

Fig. 9.3. Jet Efficiency as a Function of Gas Flow Rate.

10. DEVELOPMENT OF REACTOR SLURRY SYSTEMS

R. B. Korsmeyer

L. L. Bennett
D. G. Davis
H. L. Falkenberry[1]
R. B. Gallaher
C. H. Gibson
V. L. Kenyon
C. G. Lawson
W. R. Mixon
C. S. Morgan
R. H. Nimmo
L. F. Parsly
F. N. Peebles
M. Richardson
A. N. Smith
C. F. VandenBulck[2]
R. P. Wichner[3]

10.1 RHEOLOGY OF THORIUM OXIDE SLURRIES

10.1.1 Turbulent-Flow Pressure-Drop Measurements

Pressure-drop flow measurements were made at room temperature with tubes having inside diameters from 0.124 to 1.030 in. and with a slurry having a yield stress of 0.075 lb/ft^2 and a coefficient of rigidity of 2.9 centipoises at a concentration of 685 g of thorium per kilogram of H_2O. A portion of this slurry was made Newtonian by the addition of sodium silicate, and its flow properties were measured in the 0.124-in.-ID tube. The data are shown plotted on a conventional Fanning friction-factor plot in Fig. 10.1. All the non-Newtonian turbulent-flow data lie below the "smooth tube" line except at the highest Reynolds numbers. The substitution of the coefficient of rigidity for viscosity in the Reynolds number evidently gives a unique curve in the turbulent range for the different tube diameters studied. The laminar-flow data branch off from the turbulent-flow curve at the different tube diameters (as they must if the identity implicit in the Hedstrom[4] relation is correct), with no apparent transition region except for the Newtonian silicated slurry. The data are also plotted by using an apparent viscosity, as defined by the simplified form of the Buckingham equation,[5-8] in Fig. 10.2. This

[1]On loan from TVA.

[2]On loan from Union Carbide Nuclear Co., New York Office.

[3]Attending Oak Ridge School of Reactor Technology.

[4]B. O. A. Hedstrom, *Ind. Eng. Chem.* **44**, 651–656 (1952).

[5]E. C. Bingham, *Fluidity and Plasticity*, 1st ed., McGraw-Hill, New York, 1922.

[6]H. E. Babbitt and D. H. Caldwell, *Univ. Ill. Eng. Exp. Sta. Bull.* **323** (1940).

[7]R. V. Bailey, *Forced Convection Heat Transfer to Slurries in Tubes*, ORNL CF-52-11-189 (Nov. 24, 1952).

[8]R. J. Atkins, B. Hoffman, and G. R. Taylor, "Some Rheological and Engineering Aspects of Non-Newtonian Slurries," Paper 14-6, *3rd Annual American Nuclear Society Meeting, Pittsburgh, Pa., June 10–12, 1957.*

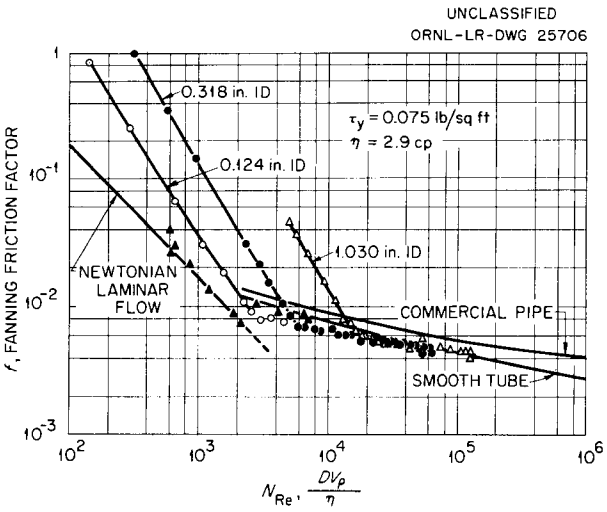

Fig. 10.1. Fanning Friction-Factor Plot for ThO_2 Slurries.

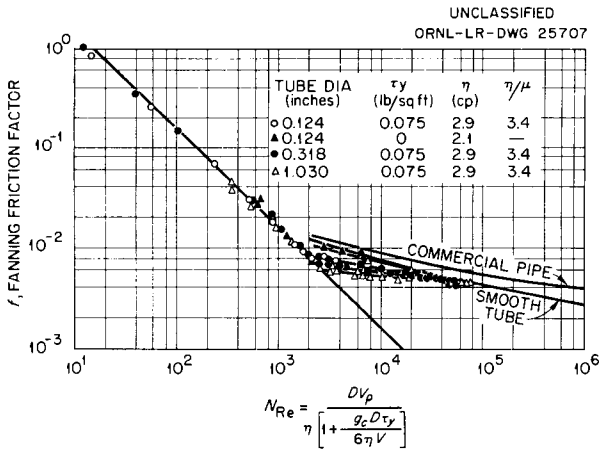

Fig. 10.2. Modified Fanning Friction-Factor Plot for ThO_2 Slurries.

treatment superimposes all the data for the laminar region on the data for Newtonian fluids. However, the data in the turbulent region are fanned out with tube diameter as a parameter. In subsequent tests the velocity and the yield stress will be increased.

10.1.2 Laminar Flow at Elevated Temperatures

The capillary sampler-viscometer[9] was completed and is shown installed at T-loop in Fig. 10.3. Pseudoshear diagrams for the slurry from run T-93 are shown in Fig. 10.4; data were taken at 220 ± 20°C by using the sampler-viscometer and at 25 and 80°C by using a horizontal-tube viscometer. Values of yield stress and coefficient of rigidity are given in Table 10.1. The determination of the yield stress is more precise than that of the coefficient of rigidity; however, it appears that both values are essentially constant in the range 25 to 220°C. Subsequent tests will be made with improved temperature control, and attempts will be made to improve the precision of the coefficient-of-rigidity determination.

10.2 SLURRY HEAT TRANSFER

Heat transfer tests were made with the slurry described in Sec 10.1.1, by using apparatus previously described.[10] The range of conditions covered is given in Table 10.2. Data for two different tube diameters are shown in the form of a *j*-factor plot in Fig. 10.5. The change from laminar- to transition-type heat transfer occurred

[9] R. B. Korsmeyer *et al.*, *HRP Quar. Prog. Rep. July 31, 1957*, ORNL-2379, p 52–54.

[10] R. B. Korsmeyer *et al.*, *HRP Quar. Prog. Rep. Jan. 31, 1957*, ORNL-2272, p 61–63.

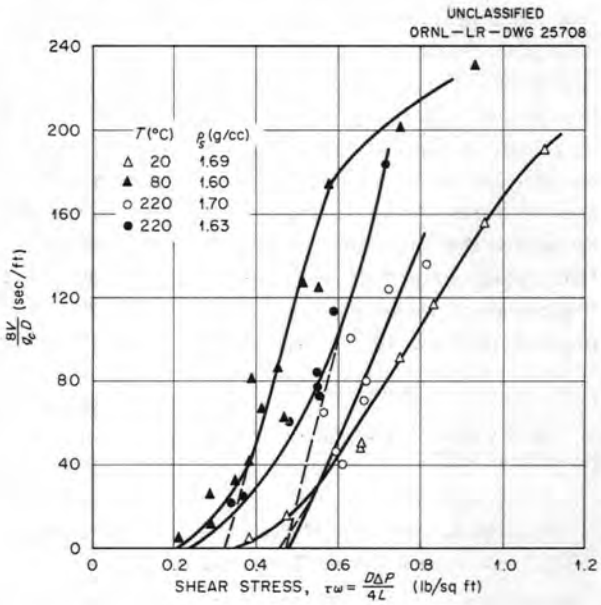

Fig. 10.4. Pseudoshear Diagrams for Slurry from Run T-93.

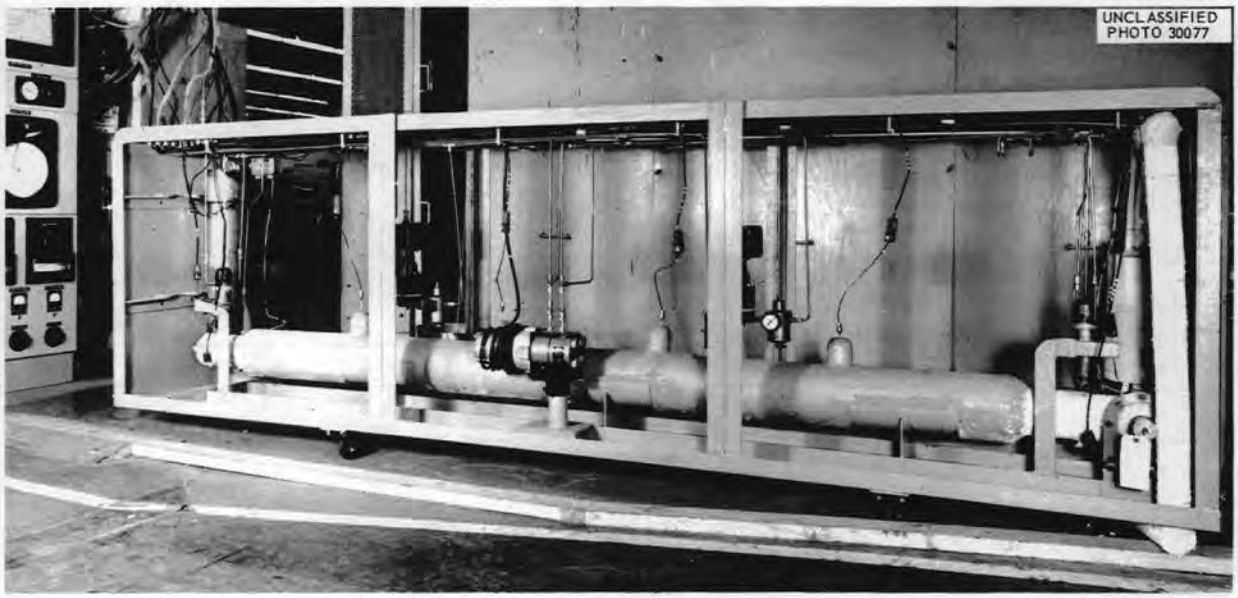

Fig. 10.3. Capillary Sampler-Viscometer.

at a critical Reynolds number within 10% of that given by the Hedstrom criterion[4] for both sets of data. The data from Fig. 10.5 for Reynolds numbers greater than four times the critical Reynolds number are shown in Fig. 10.6, superimposed on the j-factor curve for Newtonian fluids.[11] (The Newtonian-fluid heat-transfer transition region extends to Reynolds numbers from four to five times the critical Reynolds number.) The data cluster around the Newtonian-fluid curve, indicating that the coefficient of rigidity, η, is the proper viscosity term to use in conventional correlations for fully developed turbulent flow. In an attempt to superimpose the slurry data for the two different tube diameters on the Newtonian curve for the transition and fully developed turbulent region, the data were recalculated, by using the apparent viscosity previously defined,[5-8] and plotted in Fig. 10.7. As with the pressure-drop

[11] G. G. Brown *et al.*, *Unit Operations*, p 443, Wiley, New York, 1950.

Table 10.1. Rheological Properties of T-93 Slurry at Elevated Temperatures

Temperature (°C)	Slurry Density (g/cc)	Coefficient of Rigidity (centipoises)	Yield Stress (lb/ft^2)
20	1.69	4	0.35
80	1.60	2	0.25
220 ± 20	1.70	3	0.36
220 ± 20	1.63	2	0.35

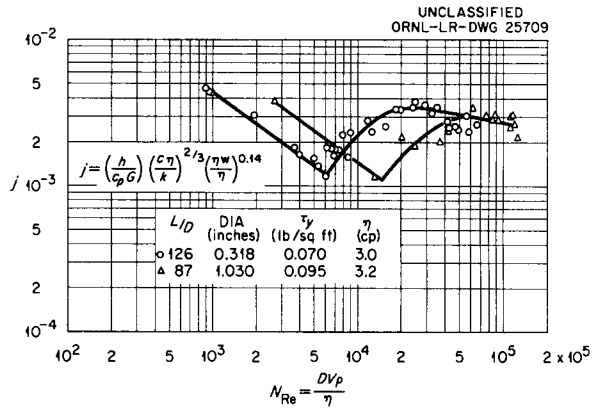

Fig. 10.5. Heat Transfer Characteristics of ThO_2 Slurries.

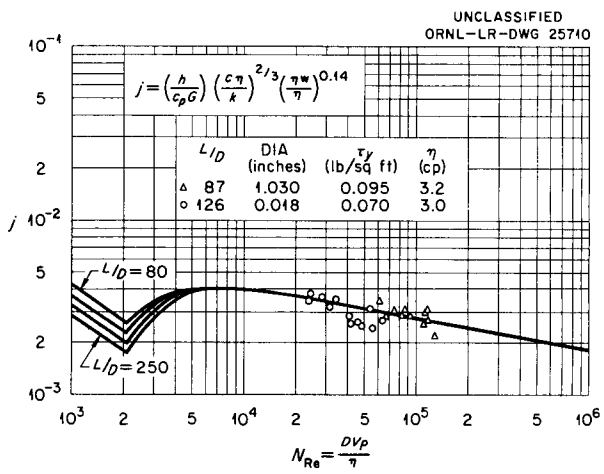

Fig. 10.6. Heat Transfer Characteristics of Fully Turbulent ThO_2 Slurries.

Table 10.2. Operating Conditions in Slurry Heat Transfer Tests

Tube Diameter (in.)	Heated-Section Length-to-Diameter Ratio	Velocity Range (fps)		Reynolds No. Range, $DV\rho/\eta$		Critical Reynolds No.
		Minimum	Maximum	Minimum	Maximum	
0.318	378	2.08	44.4	3.0×10^3	6.7×10^4	6×10^3
	252	0.25	47.0	3.9×10^2	6.7×10^4	6×10^3
	126	0.64	45.7	9.0×10^2	6.47×10^4	6×10^3
1.030	175	0.26	30.9	1.0×10^3	1.58×10^5	1.3×10^4
	87	0.71	28.9	2.66×10^3	1.29×10^5	1.3×10^4

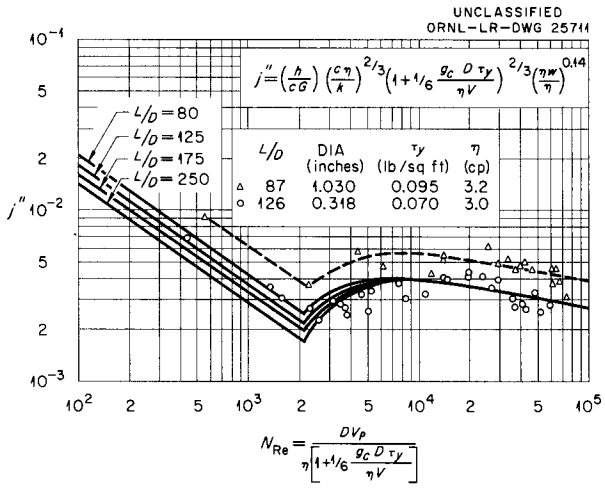

Fig. 10.7. Heat Transfer Characteristics of ThO_2 Slurries, Based on Apparent Viscosity.

data, the critical Reynolds number for the onset of turbulence is shifted to about 2100; however, the fully developed turbulent data are on different lines for different tube diameters. Future tests will be made at higher velocities and with slurries having higher yield stresses.

10.3 CIRCULATING-SLURRY BEHAVIOR

Slurry and water were circulated in S, T, and 200A loops for over 4300 hr during the quarter. These runs are summarized in Table 10.3.

Run 200A-14, begun last quarter as a study of the degradation characteristics of 1600°C-fired oxide, has continued for more than 2100 hr at 300°C and 2000 psig, with no difficulties attributable to the slurry. However, some troubles have been encountered with leaks through valves and tubing fittings and with instrument failures. The oxide used in this run is batch LO-22 which was fired originally at 800°C and then refired at 1600°C for 2 hr, passed through the micropulverizer four times, and dry-screened through a 170-mesh screen.

All samples withdrawn during the first 1500 hr had a mean particle diameter of 2.5 μ, indicating no degradation of the oxide. A few spheroidal particles of 15 μ have been observed. These do not appear to be growing. Photomicrographs of the slurry before loading and after 1500 hr of circulation show some rounding of the sharp points, as seen in Figs. 10.8 and 10.9. The room-temperature hindered-settling rate of the slurry containing 600 g of thorium per kilogram of H_2O has remained unchanged at 0.065 cm/sec for 2000 hr.

During the run the average circulating concentration has been 600 g of thorium per kilogram of H_2O. Samples withdrawn from the top and bottom of a horizontal run of the loop indicate a concentration gradient across the flowing stream. However, gamma surveying methods show a symmetrical distribution, suggesting inaccurate sampling procedures because of the high settling rate. An improved sampling system has been designed for installation before another run is started.

The iron-to-thorium ratio has increased linearly with time during the first 2000 hr according to the equation: $Fe/Th = 0.0024t + 0.1$, where t is the time in hours, Fe/Th is grams of iron per kilogram of thorium, and the constant represents iron contamination in the oxide as charged. This rate is comparable with rates in previous runs where stainless steel impellers were used. All the chromium removed from the equipment is not associated with the slurry; some remains in solution and accumulates in the pressurizer. The venturi reading, with density determined by the pump power demand, indicates a decrease in the flow rate from 203 to 198 gpm in 2000 hr.

Two runs were made in the 100A loops to determine the effect on caking and sphere formation of molybdenum and uranium additives to sulfated slurry containing 1000 g of thorium per kilogram of H_2O. One batch of oxide had been fired at 550°C (run S-102), and the other at 800°C (run T-93). After 600 hr of circulation no sphere formation was observed in either run. No cake was found at the end of S-102; T-93 is still in progress.

Two unsuccessful attempts were made in the 100A loops to circulate "standard spheres" which had been refired at 1400°C. Pump failure terminated both runs.

Three service runs were made for the Chemical Technology Division to determine the rate of disappearance of solids from dilute slurries into dead areas in the 100A loops. At concentrations of a few grams of thorium per kilogram of H_2O, the initial concentration decreased to one-half in 4 to 6 hr. A slower rate occurred at concentrations severalfold higher.

Tests were made to determine the effect of slurry concentration on the caking and sphere-forming tendencies of a known sphere-forming oxide. Batch

Table 10.3. High-Temperature Slurry Circulation – Run Summary

	Run No.								
	200A-14	S-102	S-103	S-104	S-105	S-106	S-107	T-92	•T-93
Test dates	7/18 to I*	7/9 to 8/3	8/15	8/26	9/16 to 9/20	9/26 to 9/30	10/2 to I	7/17 to 7/18	9/10 to I
Running time, hr	I	606	5.4	8.8	89.9	96.2	I	5.6	I
Objective	Determine degradation characteristics of 1600°C-fired ThO_2	Determine handling characteristics of sulfated slurry containing uranium and molybdenum oxide	Determine handling characteristics of 1400°C-fired "standard oxide" (spheres ~15 μ in diameter)	Same as S-103	To determine rate of disappearance of solids from dilute slurries	Same as S-105	Same as S-105	To determine the effect of concentration on cake and sphere formation	To determine the handling characteristics of sulfated slurry containing uranium and molybdenum
Charge									
ThO_2, kg	30 (LO-22)	14.4 (LO-17)	4.9 (LO-12)	4.3 (LO-12)	Incremental amounts of LO-7	Incremental amounts of LO-7	Incremental amounts of LO-7	16.1 (LO-23)	15.4 (LO-23)
Water, kg	71	11	12	12	12.5	12.5	12.5	14.4	14.5
Additives	75 liters O_2	80 g $Th(SO_4)_2$ 87 g MoO_3 184 g $UO_3 \cdot H_2O$ 25 liters O_2	25 liters O_2	25 liters O_2	25 liters O_2	25 liters O_2	25 liters O_2	25 liters O_2	86 g $Th(SO_4)_2$ 197 g $UO_3 \cdot H_2O$ 97 g MoO_3 25 liters O_2
Temperature, °C	300	290	290	290	250	250	250	200	290
Pressure, psig	2000	1600	1600	1600	1600	1600	1600	1600	1600
Average circulating concentration, g Th/kg H_2O	I	1090	175	130					I
Reason for termination	I	Valve stem backed out of valve body	Pump out of balance	Pump out of balance	Crack in purge-water condenser	Leak in a tubing fitting	I	Pump out of balance	I
Maximum sphere diameter, μ	15	No spheres						Present but not measured	No spheres
Cake location	I	No cake	Light deposit in eye and vanes of impeller	No cake	No observations	No observations	I	Impeller eye, vanes, and balance holes; loop piping	I
Total Fe in slurry, g	I	46.0	92.4	27.0	Not detectable	Not detectable	Not detectable	Not detectable	I
Total Ni in slurry, g	I	7.4	13.5	5.9	Not detectable	Not detectable	Not detectable	Not detectable	I
Total Cr in slurry, g	I	4.6	13.0	3.8	Not detectable	Not detectable	Not detectable	Not detectable	I
Impeller weight loss, g	I	27	66	0	Not weighed	Not weighed	I	2	I
Orifice-plate weight loss, g	I	2.7883	0.004	0	Not weighed	Not weighed	I	0.0106	I

*Incomplete (still running).

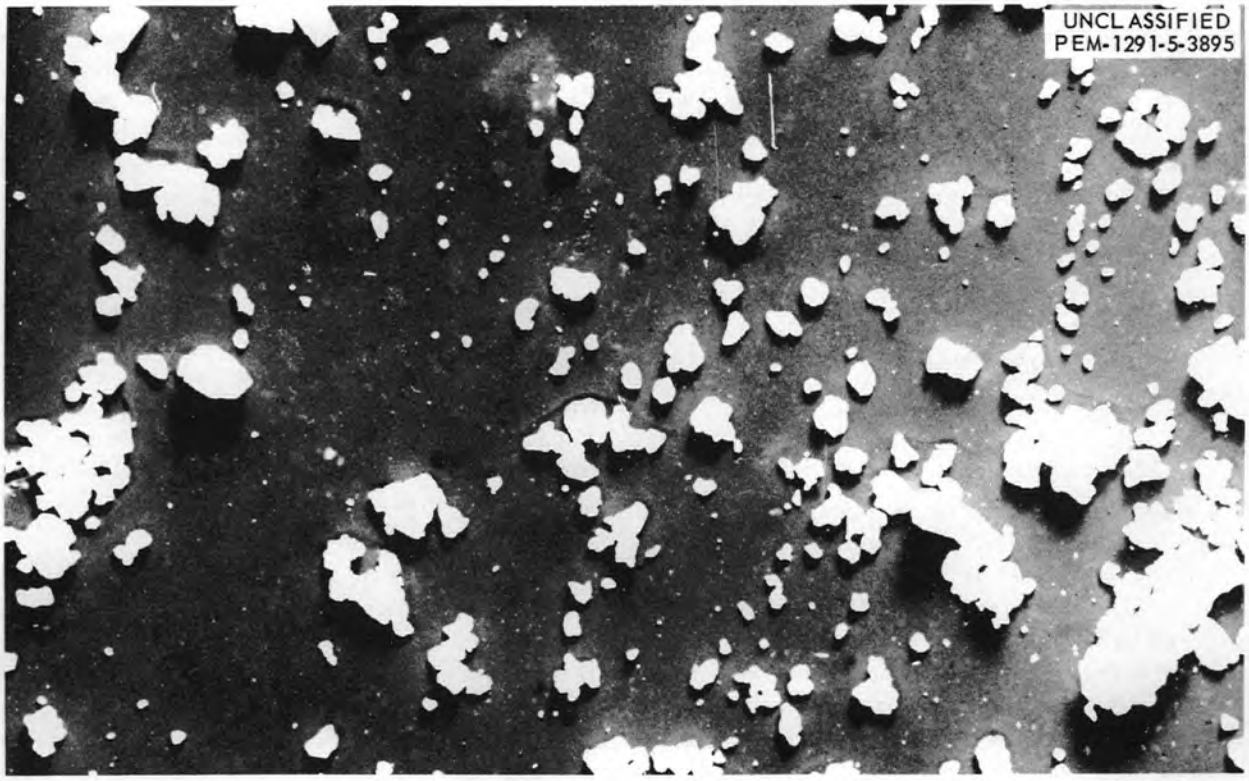

Fig. 10.8. Thorium Oxide Fired at 1600°C and Micropulverized. 8000 X.

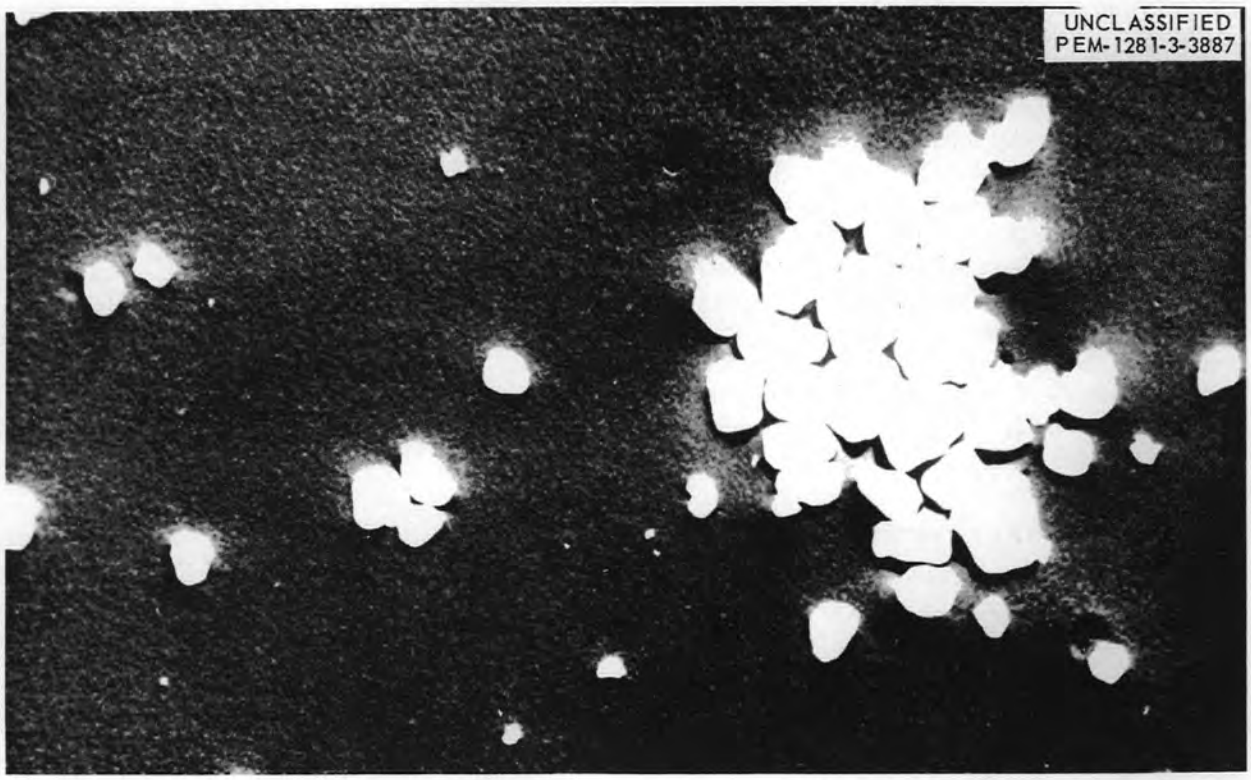

Fig. 10.9. Thorium Oxide Fired at 1600°C After Being Pumped for 1500 hr in 200A Loop. 20,000X.

LO-23 oxide at a concentration of 500 g of thorium per kilogram of H_2O formed 20-μ spheres in 13 hr, together with some cake on the impeller (run T-91). At a 1000-g/kg concentration this batch of oxide was circulated for only 5.6 hr before the pump failed. Spheres had started forming, and heavy cake was found in the eye, the vanes, and the balancing holes of the impeller and on the loop piping. This same oxide failed to form spheres at a concentration of 1000 g per kilogram of H_2O when sulfate, molybdenum, and uranium were added in run T-93.

10.4 BLANKET FLUID MECHANICS

A one-sixteenth-scale Lucite model of a proposed HRE-3 blanket configuration was fabricated (Fig. 10.10). The vessel is 6 in. in inside diameter, with a $2\frac{1}{4}$-in. core and a $\frac{1}{8}$-in. gap between the core and baffle.

Several flow-visualization techniques were used in the initial studies, with the injection of bromthymol blue giving the best results. These studies showed that the average fluid holdup was about 60% greater than the slug flow time for all flow rates studied. (*Fluid holdup time* was determined by injecting dye into the inlet for 2 sec, starting at times as the flow of dye was stopped and stopping the times when the model was clear of dye. *Slug flow time* is the volumetric flow rate divided by the model volume.) During these tests a jet of fluid was observed flowing over the lip of the inner baffle and down the wall of the vessel. The velocity of this jet was about one-half the velocity in the inner annulus over a range factor of 5 in velocities. Data taken on the model indicate that the pressure drop from inlet to outlet is approximately proportional to the square of the flow rate and that the flow patterns are symmetrical for all flows examined. The general flow pattern observed is shown in Fig. 10.11.

10.5 HRT BLANKET SYSTEM DEVELOPMENT

Run SM-3, which had been in progress for 700 hr at the end of the previous quarter, was terminated after an additional 248 hr, when the circulating pump froze; the loop was then dumped to permit disassembly and repair of the pump. During the final 248 hr of the run, the charge was increased to 720 kg of thorium, and sampling and gamma surveys were carried out at that charge level. The gamma surveys continued to give a pattern which was interpreted qualitatively as indicating relatively uniform slurry distribution. The results of blanket samplings taken during circulation at 170 and 200°C are in Table 10.4. The table shows that the observed concentration was approximately 30% below the concentration calculated from the estimated charge.

Samples taken from the circulating loop indicated a concentration of 440 g of thorium per kilogram of H_2O at this time, which corresponds to a charge of 616 kg of thorium. The thorium inventory calculated from measurements of the settled-bed volume and the bed concentration was 610 kg, which checks quite well with the loop sample results, suggesting some bias in the blanket sampling procedure.

The possibility of obtaining quantitative measurements of the thorium distribution from the gamma surveys was investigated near the end of the run. It was found that the thorium contribution to the total radiation received by the counting head was relatively large and that surveys with the source removed would be required to obtain meaningful results. The run had been terminated by the time this determination was made.

On the last day of the run the pump was operated on a variable-frequency power supply for 4 hr at 50 cycles and then for 2 hr at 40 cycles, corresponding to a reduction in flow from 350 gpm to 300 and about 230 gpm, respectively. At 50 cycles, the gamma surveys indicated no significant difference from those taken at 60 cycles. At 40 cycles a difference in the gamma trace was observed, and spot samples were taken. These samples showed that a concentration gradient extending from about 200 to 450 g of thorium per kilogram of H_2O existed from the top to the bottom of the blanket.

The loop was returned to constant-frequency power after the 40-cycle measurements had been completed. Almost 30 min later the pump stopped. After blown fuses were replaced, attempts to restart the pump indicated that the rotor was frozen. The loop was partially dumped 45 min later, and drainage was completed the following morning after removal of water from the dump tanks by decantation.

The slurry residue left in the blanket after this dump was similar to that found after run SM-2. Figure 10.12 is a photograph of the settled bed taken through an upper porthole. The bed, which

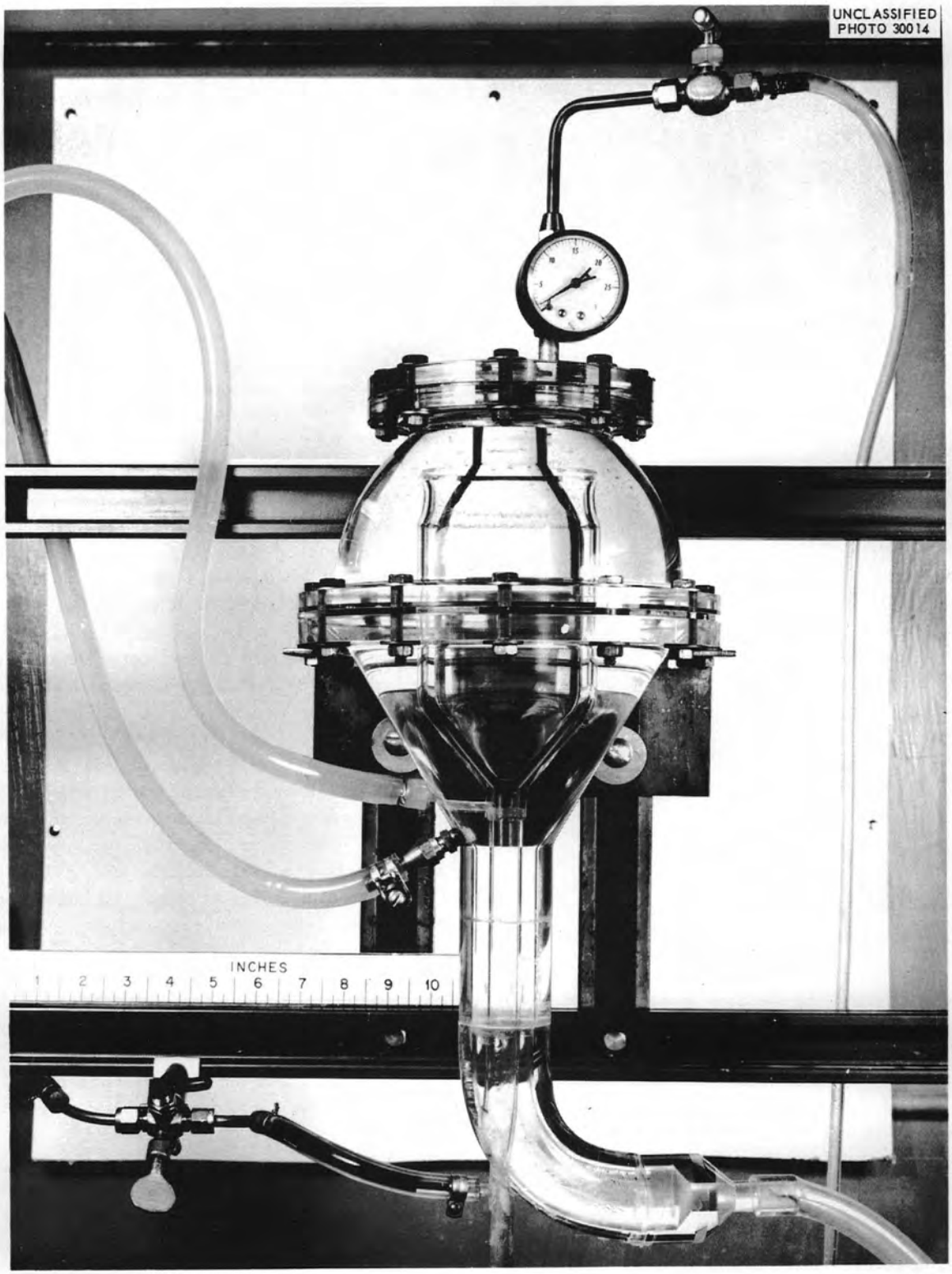

Fig. 10.10. One-Sixteenth-Scale Blanket Model.

UNCLASSIFIED
ORNL-LR-DWG 25712

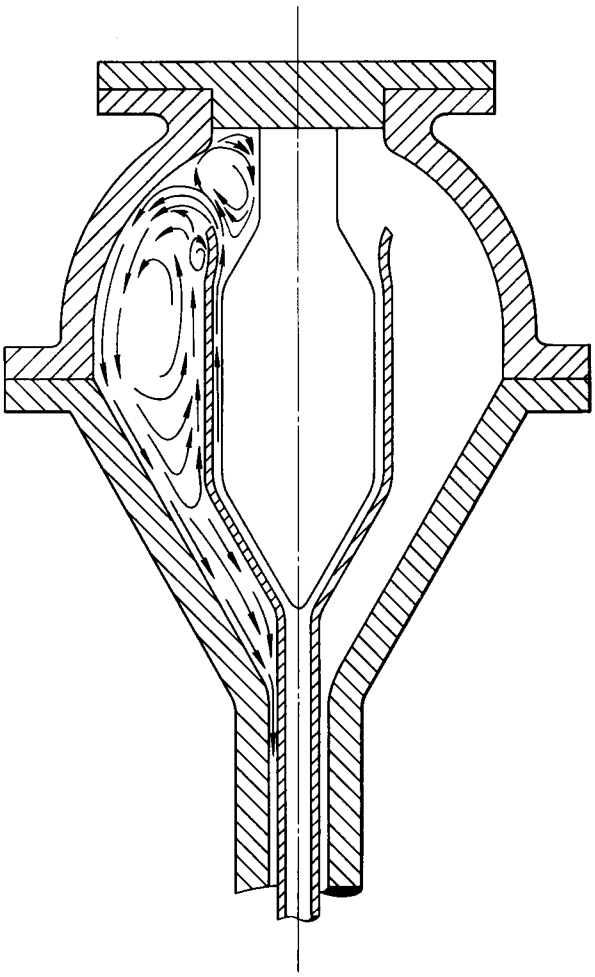

Fig. 10.11. General Flow Pattern Observed in One-Sixteenth-Scale Blanket Model.

is partly obscured by the core vessel, was approximately 12½ in. deep and had a concentration of 1950 g of thorium per kilogram of H_2O. Thus the settled bed contained 350 kg of thorium, or more than half of that which previously had been circulating in the system. Although the bed had the appearance of a cake, it could be dispersed easily in water. There was a thin slurry layer on the upper surface of the core, but otherwise the top part of the system had drained clean. It now seems evident that some means of maintaining a dispersed suspension during dumps is needed with this blanket design, and steam-sparger connections have been installed for this purpose.

Table 10.4. Results of Sampling Slurry Blanket – Run SM-3

	Slurry Concentration (g of Th per kg of H_2O)	
	170°C	200°C
35 deg below top	324	361
30 deg above center line	349	359
30 deg below center line	337	341
35 deg above bottom	398	402
Over-all overage	352	366

Calculated concentration from charge, 500 g of Th per kg of H_2O

After waiting 24 hr for the loop to cool off, the pump was removed and disassembled. The lower journal had cracked along its entire length. Figure 10.13 shows the bearing assembly with the journal in it. When the journal was later removed from the bearing, some 12 additional longitudinal cracks were found on the outside surface. The stainless steel impeller (Fig. 10.14) was found to be badly attacked in a similar way to the impeller used in run SM-2; it had lost 102 out of 1747 g.

During the shutdown the pump was thoroughly overhauled. The rotor shaft, which was found to be slightly warped, was straightened. New upper and lower journals and bearings were installed; the thrust bearing was rebuilt; and a 5-in.-dia titanium impeller was installed. Other changes made to the system included installation of steam spargers in the blanket, replacement of the ¼-in. 16-gage sample tubes projecting into the blanket with ⅛-in. sched-80 pipe (several of the tubes had broken off), installation of a small control valve (C_v 0.025) for venting of the pressurizer and condensate tank, and minor revisions to the piping at the pump to facilitate disassembly and reinstallation.

Run SM-4 was started as a continuation of run SM-3 on September 10; it has continued for 800 hr. Operation for the first 160 hr was on water while some reference data for gamma-survey work were obtained. Over the next 240 hr, 670 kg of thorium were charged into the loop, and the remaining 400 hr have been spent in studying the system behavior at this charge level.

Fig. 10.12. Slurry Residue in Blanket After System Was Dumped.

UNCLASSIFIED
PHOTO 29447

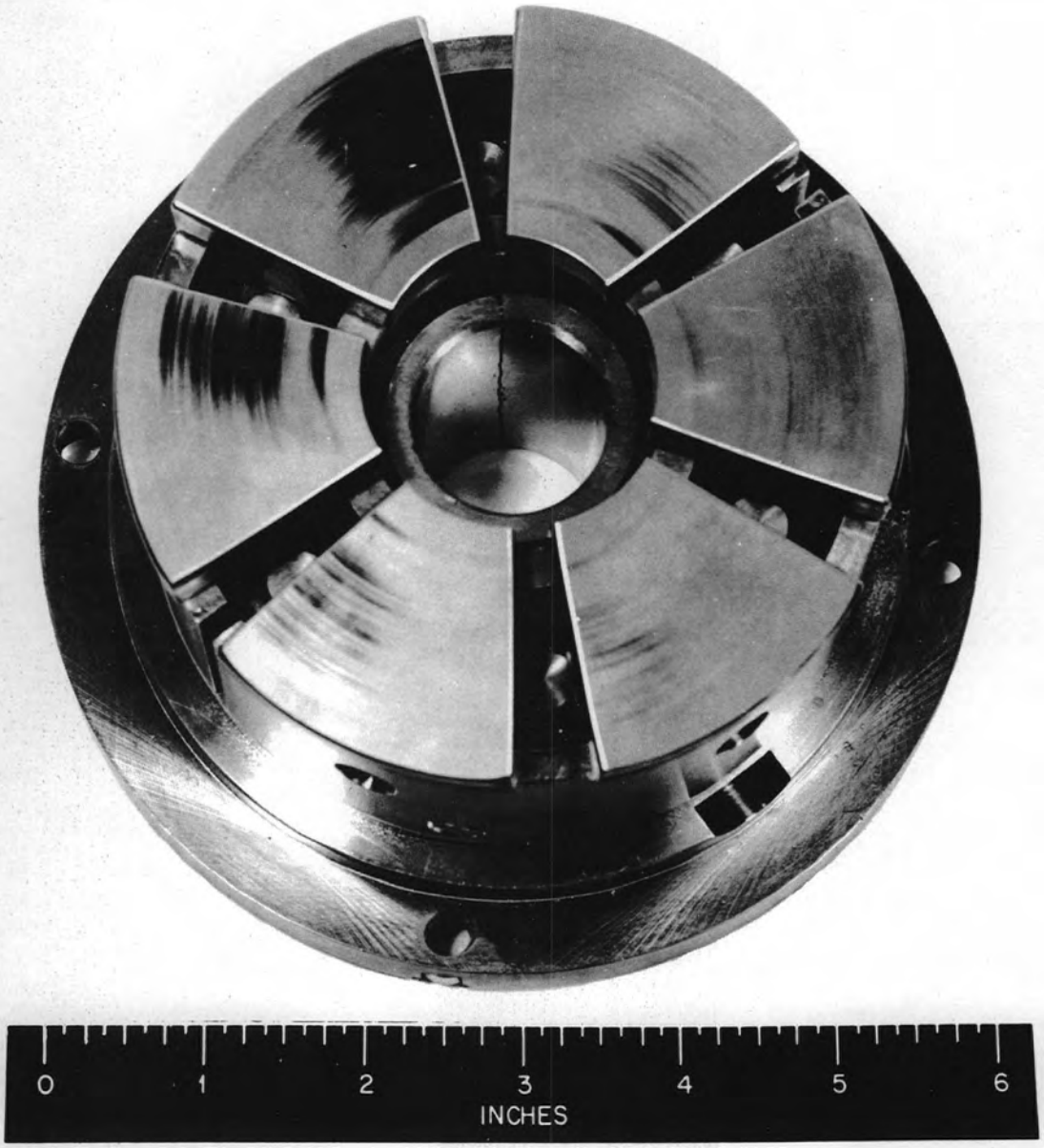

Fig. 10.13. Lower Bearing Assembly After Blanket Pump Failure; Run SM-3.

UNCLASSIFIED
PHOTO 29450

Fig. 10.14. Pump Impeller After Run SM-3.

As observed in preceding runs, there is a considerable discrepancy between the calculated charge and the slurry found in the system. In contrast to the calculated charge of 670 kg, an inventory of 560 kg is estimated from the volume of the settled bed in the blanket when the pump was stopped, 520 kg estimated from samples taken from the piping, and 440 kg from sampling the blanket. The discrepancy exceeds, by an appreciable margin, the amount of thorium which might have been lost from the circulating stream by settling into various stagnant areas; it is believed that no more than 50 kg of thorium could reasonably be expected to be held up in such locations. The discrepancy can perhaps be accounted for by errors in measuring the thorium charged into the loop.

After completing the sampling of the blanket, the loop was changed from constant-frequency power to variable-frequency power and was run at 50 cycles for 24 hr and then at 44.5 cycles for 24 hr. At 50 cycles the slurry distribution pattern was the same as at 60 cycles. At 44.5 cycles, a markedly different pattern became evident approximately 8 hr after the frequency was reduced. A region of high slurry concentration developed approximately 45 deg above the girth flange. After 24 hr at 44.5 cycles, the frequency was raised stepwise, at 2-hr intervals, to 49 cycles. No apparent change occurred until approximately 16 hr after the shift to 49 cycles, when the slurry distribution found at higher frequencies reappeared.

Figure 10.15 shows some typical gamma surveys taken during the present run. In order to estimate the slurry concentration, four curves are necessary: measurements with the source at the center of the vessel with both water and slurry and measurements with the source removed to its lead shield below the blanket with both water and slurry. The net transmission from the source through slurry is

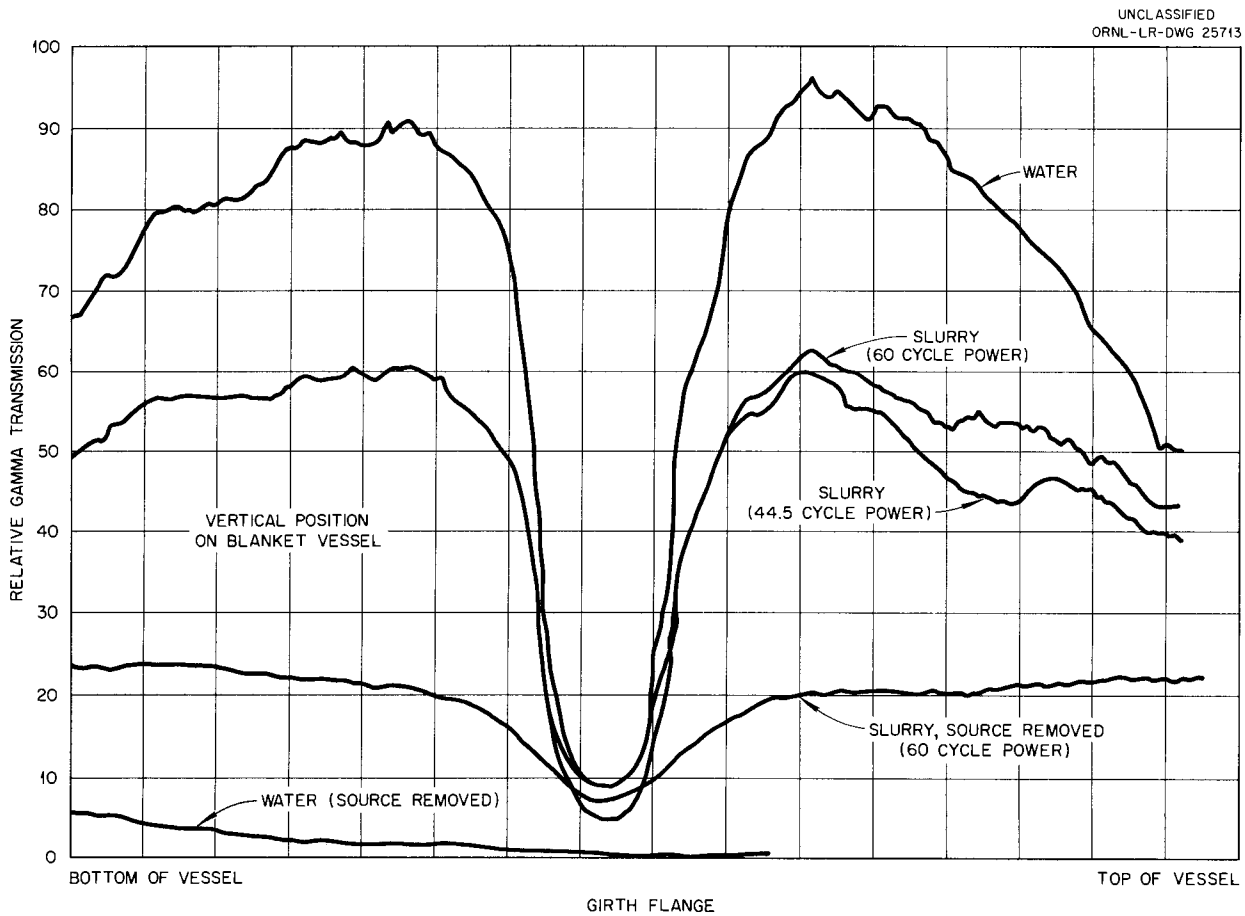

Fig. 10.15. Typical Gamma Surveys, Slurry Blanket Test; Run SM-4.

determined by subtracting the reading with the source out from that with the source in. The water survey with the source in its shield is required to correct the slurry measurement taken with the source in its shield for radiation leakage picked up directly by the scintillation head when located on the lower hemisphere. The slurry concentration is then calculated from the ratio of the net transmission through slurry to the transmission through water. While this calculation involves a number of uncertainties, it probably gives a fair approximation of the actual concentration and a good estimate of the concentration distribution along the survey track. Figure 10.16 shows the distribution patterns obtained at 44.5 and 60 cycles.

Following the above tests, the loop was shut down for 4 hr to obtain data on slurry settling and resuspension. The settling and resuspension behavior was in conformity with previous experience. Initial settling occurred 1 min after the pump was shut down; the slurry interface dropped fairly rapidly during the first hour and at a negligible rate thereafter. The final settled bed volume was 480 liters. The loop was restarted on 60-cycle power, and resuspension occurred within 30 sec.

Microscope slides made from samples taken during the run show a gradual growth of spheroidal particles of 16- to 18-μ diameter in the slurry. The number of such particles appears to have increased about tenfold over the last 400 hr of operation.

Corrosion data accumulated so far indicate an iron pickup rate from carbon steel of 81 g per 100 hr, equivalent to approximately 5 mpy on the inner surface of the pressure vessel. The stainless steel pickup rate is 12.5 g per 100 hr, equivalent to 0.35 mpy on the exposed surface.

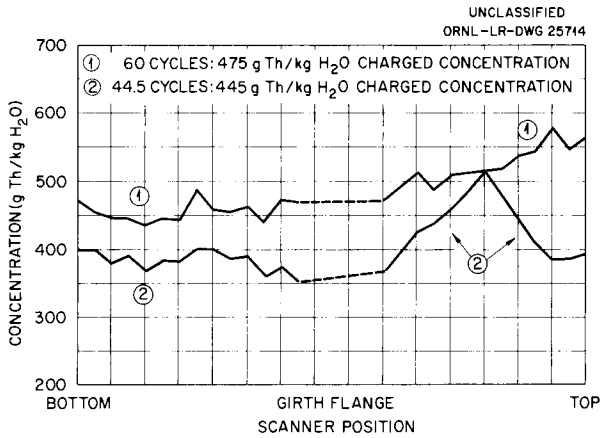

Fig. 10.16. Thorium Concentration vs Position in Blanket Vessel; Run SM-4.

11. INSTRUMENT AND VALVE DEVELOPMENT

D. S. Toomb

A. M. Billings R. L. Moore
E. H. Bell H. D. Wills

11.1 INSTRUMENT DEVELOPMENT

11.1.1 Differential-Pressure Transmitters

An electric-signal differential-pressure transmitter with a high differential range has been received for test and evaluation. The transmitter, which is shown in Fig. 11.1, is available with ranges of 0–50 psi to 0–125 psi and has a static pressure rating of 4000 psi. This unit complements the lower range (50 in. H_2O to 50 psi) transmitter described in an earlier report.[1] A unit of similar design but without the weld-sealing feature of the transmitter illustrated in Fig. 11.1 has been checked, calibrated, and installed in a test loop for a long-term stability test. Electric-signal transmitters are being evaluated, as they eliminate the need for block valves in instrument air-signal lines at the containment-tank wall in reactor applications.

11.1.2 Pressure and Differential-Pressure Transmitters for Slurry Systems

A survey of pressure and differential-pressure instrument types suitable for a reactor slurry system has been made to aid in the planning of an instrument development program.[2] Commercial instruments presently available require connecting lines which are subject to plugging, incorporate fluid fills not compatible with the reactor fluids or piping, or lack a secondary seal behind thin members. It is desired that an instrument system be developed which does not require an auxiliary source of purge water. It is hoped that a transmitter of the type shown conceptually in Fig. 11.2 can be developed or that a suitable fill fluid for the system shown in Fig. 11.3 can be found. Liquid metals are considered a possibility for this fluid as they would not evolve gas or gum under radiation.

11.1.3 High-Temperature Radiation-Resistant Differential Transformers

The development of more-radiation-resistant linear variable differential transformers suitable for sensing instrument primary-element motions in a homogeneous reactor environment is continuing. Another unit, similar in design to the ORNL-developed transformer mentioned in an earlier report[3] but wound with 30-gage anodized aluminum wire supplied by The Sigmund Cohn Co., has withstood temperatures to 300°C without insulation failure. The only electrical insulation on the wire is that afforded by the oxide film on the aluminum, which could be expected to be highly temperature and radiation resistant. Measurements of null voltage and zero shift on the ORNL transformer from 24 to 238°C indicated a null-voltage increase from 0.47 to 5.10 v ac (1000 cps) and a zero shift from 0 to +2%. No decrease in primary-to-secondary resistance was noted over the above temperature range.

11.1.4 Solid-State-Component Instrument Systems

In continuation of the program for the evaluation of instrument systems using solid-state components to replace vacuum tubes, which are subject to sudden failure, frequency-response performance tests have been performed on three commercially available[4] electropneumatic pilot converters. These pilot converters convert a d-c milliampere signal to a proportional pneumatic signal, which is necessary for the presently used bellows valve actuators. Also, a transistorized servo amplifier[5] incorporating a 4500-cycle oscillator, three-stage carrier amplifier, phase-sensitive demodulator, and a d-c power amplifier has been tested for performance. This amplifier requires a 24-v d-c power supply, which can easily be provided by storage

---

[1] D. S. Toomb, E. H. Bell, and A. M. Billings, *HRP Quar. Prog. Rep. April 30, 1957*, ORNL-2331, p 79.

[2] H. D. Wills, *Survey of Pressure and Differential Pressure Instrument Types for Possible Application to HRE-3 Slurry System*, ORNL CF-57-10-88 (to be published).

[3] D. S. Toomb *et al.*, *HRP Quar. Prog. Rep. July 31, 1957*, ORNL-2379, p 21.

[4] Taylor Instrument Componies, Swartwout Co., and Manning, Maxwell and Moore, Inc.

[5] Crescent Engineering and Research Co. model T595.

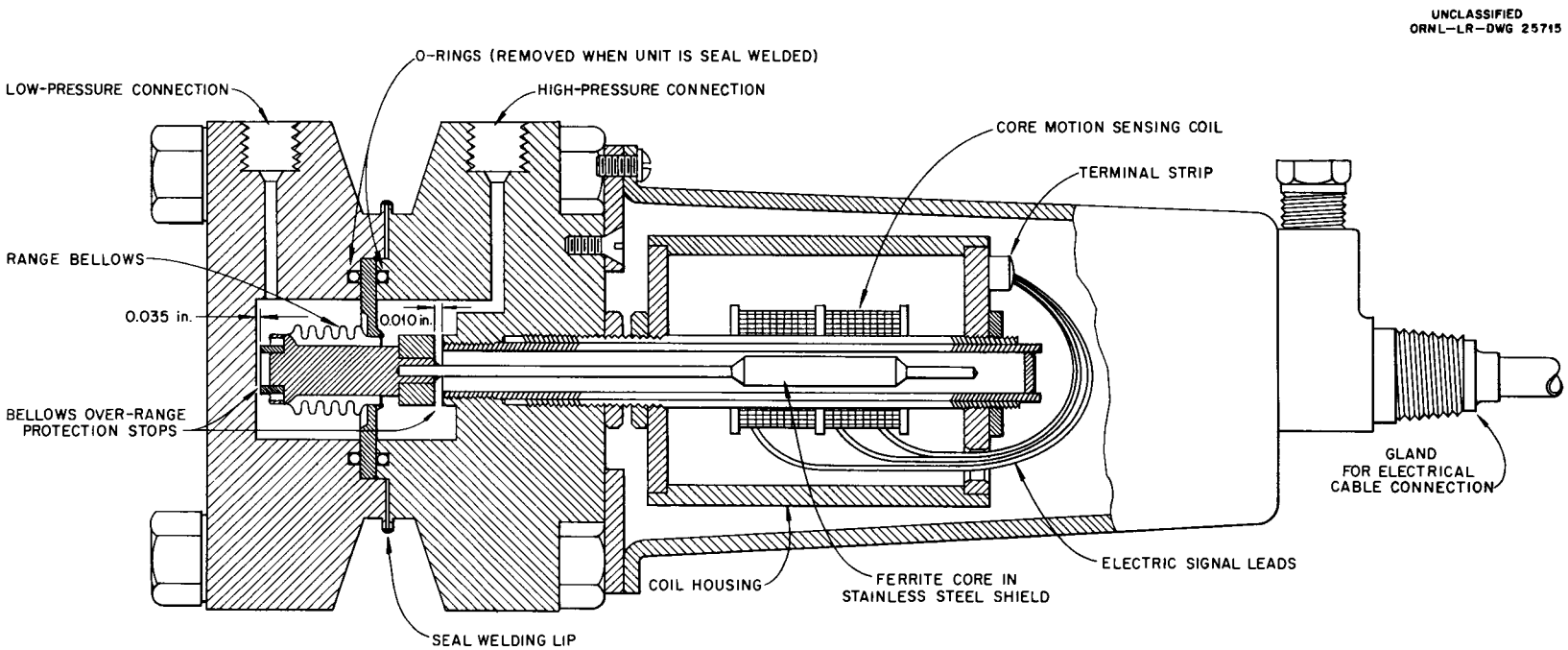

DIFFERENTIAL-PRESSURE TRANSMITTER
TYPE: INDUCTIVE BRIDGE FOR 1000 cps EXCITATION
RANGE: 0–50 psi TO 0–125 psi BY CHANGE OF RANGE BELLOWS
OVER-RANGE: HIGH SIDE–2000 psi, LOW SIDE–500 psi
ACCURACY: 3 %
BODY RATING: 4000 psi DESIGN, 6000 psi TEST
MATERIAL: 347 STAINLESS STEEL
VENDOR: THE FOXBORO CO.

Fig. 11.1. Differential-Pressure Transmitter.

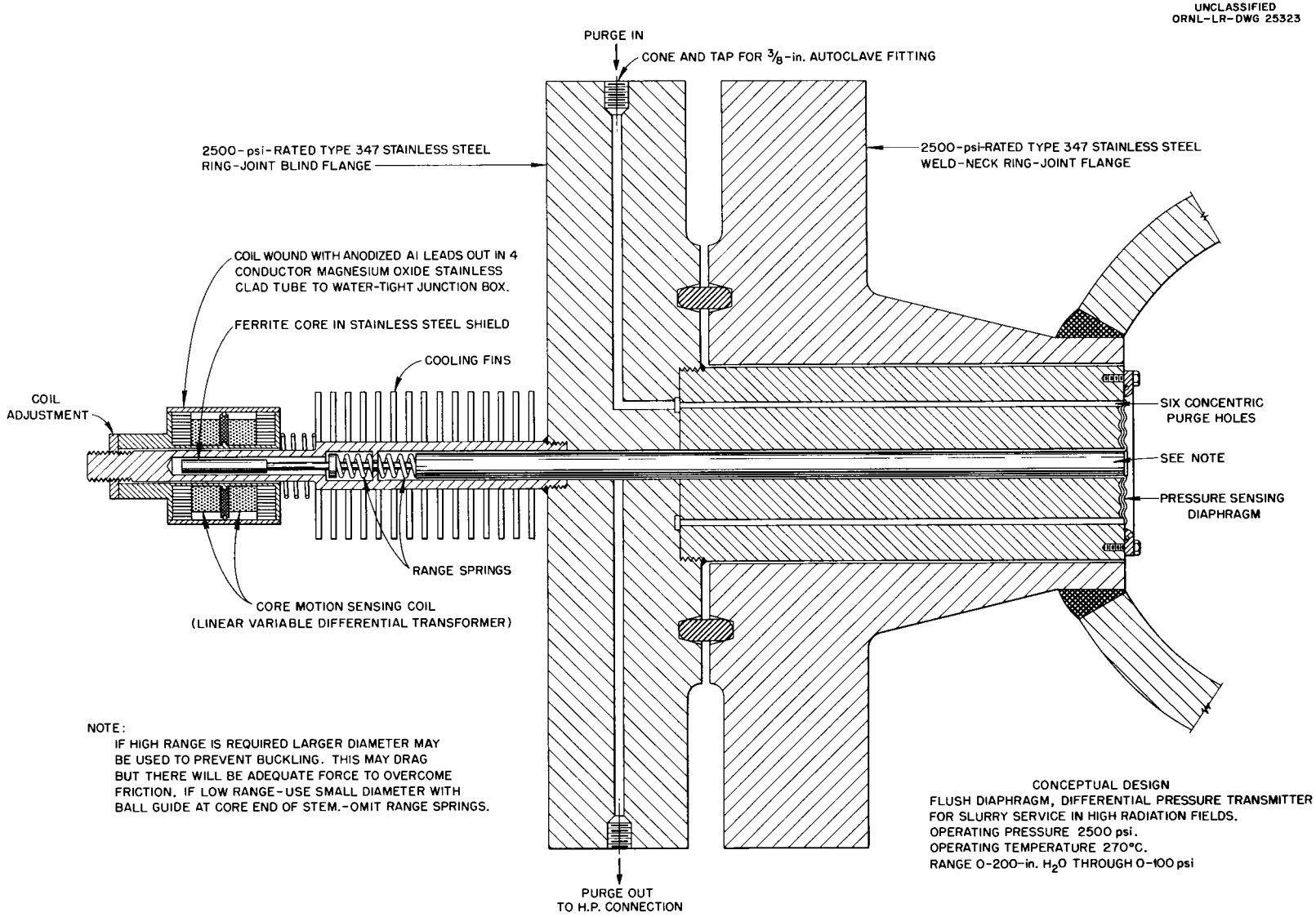

Fig. 11.2. Conceptual Design of Flush-Diaphragm Differential-Pressure Transmitter.

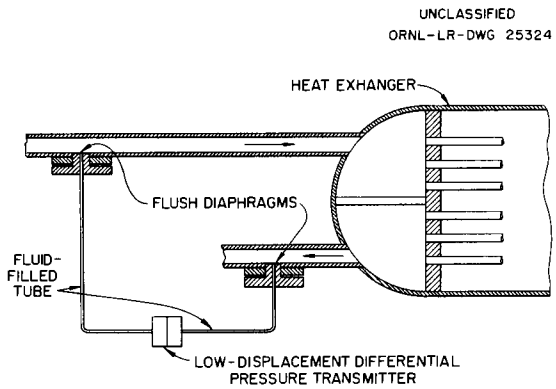

Fig. 11.3. Differential-Pressure Measurement by Sealed Fluid-Filled System.

batteries. This feature would permit instrument operation without an emergency a-c supply in a nuclear power station. The amplifier has now been incorporated into a control-valve positioning system being investigated to eliminate hysteresis effects introduced by valve packing-gland friction.

11.1.5 Underwater Television

The Dage Television Division industrial television camera was tested under water and performed satisfactorily. A protective housing was made with 3-in. pipe and a gasketed Plexiglas end window. The camera was air-purged for cooling, and the electrical leads were brought above the water line in a Tygon plastic tube. The camera was also tested with high-intensity mercury lamps (G-E H250-A5) being used as a source of illumination; the results were slightly better than those obtained with conventional incandescent lamps.

The HRT Operations Section has expressed an interest in the LaSalle Co. Mini TV for possible use in inspecting the HRT core vessel after shutdown. This camera unit is $1\frac{7}{8}$ in. in diameter and about 5 in. long. As the unit incorporates transistors, a literature review was made on the effects of radiation on the transistors and other components in the camera head. Information available indicates that it is very doubtful that the camera could operate for long in the expected 200,000-r/hr radiation field. However, as a relatively short camera life could perhaps be tolerated, the investigation may be pursued further.

11.1.6 Pressure-Switch Evaluation

Pressure switches of the type used to provide electric alarm and control signals from 3- to 15-psi pneumatic signals are being evaluated as to stability of the set point with regard to temperature and time. Preliminary results are as follows:

Switch Type	Set-Point Change Over Four-Month Period with Steady Pressure Signal Applied (psi)	Set-Point Change with Ambient Temperatures from 78 to 120°F (psi)
Minneapolis Honeywell LR404HS7	0.12	0.08
Barksdale Meletron model 424E-10L	0.32	0.30

11.2 VALVE DEVELOPMENT

11.2.1 Pneumatic Actuators

The 123-in.^{2} pneumatically-powered-bellows valve actuator described earlier[6] was cycled four times per minute at a stroke of $\frac{13}{16}$ in. and a pressure of 80 psig for 265,000 cycles before developing a small leak in the stem sealing bellows. Testing was discontinued at this time although the small leak did not impair the operation of the actuator.

11.2.2 Hydraulic Actuators

Because the maximum thrust of sealed air actuators is limited by the existing metal-bellows technology, electrohydraulic valve actuators are being investigated for possible application to the large valves which may be required in future homogeneous reactors. A hydraulic actuator (Fig. 11.4) which utilizes oil as the operating fluid has performed satisfactorily in continuous operation for two months to date. The actuator is incorporated in a package unit 18 in. high and 15 in. in diameter (including side-mounted motor). The signal and motor electrical power leads and the valve-stem mechanical link are the only connections required.

---

[6] D. S. Toomb, A. M. Billings, and E. H. Bell, *HRP Quar. Prog. Rep. July 31, 1957*, ORNL-2379, p 64.

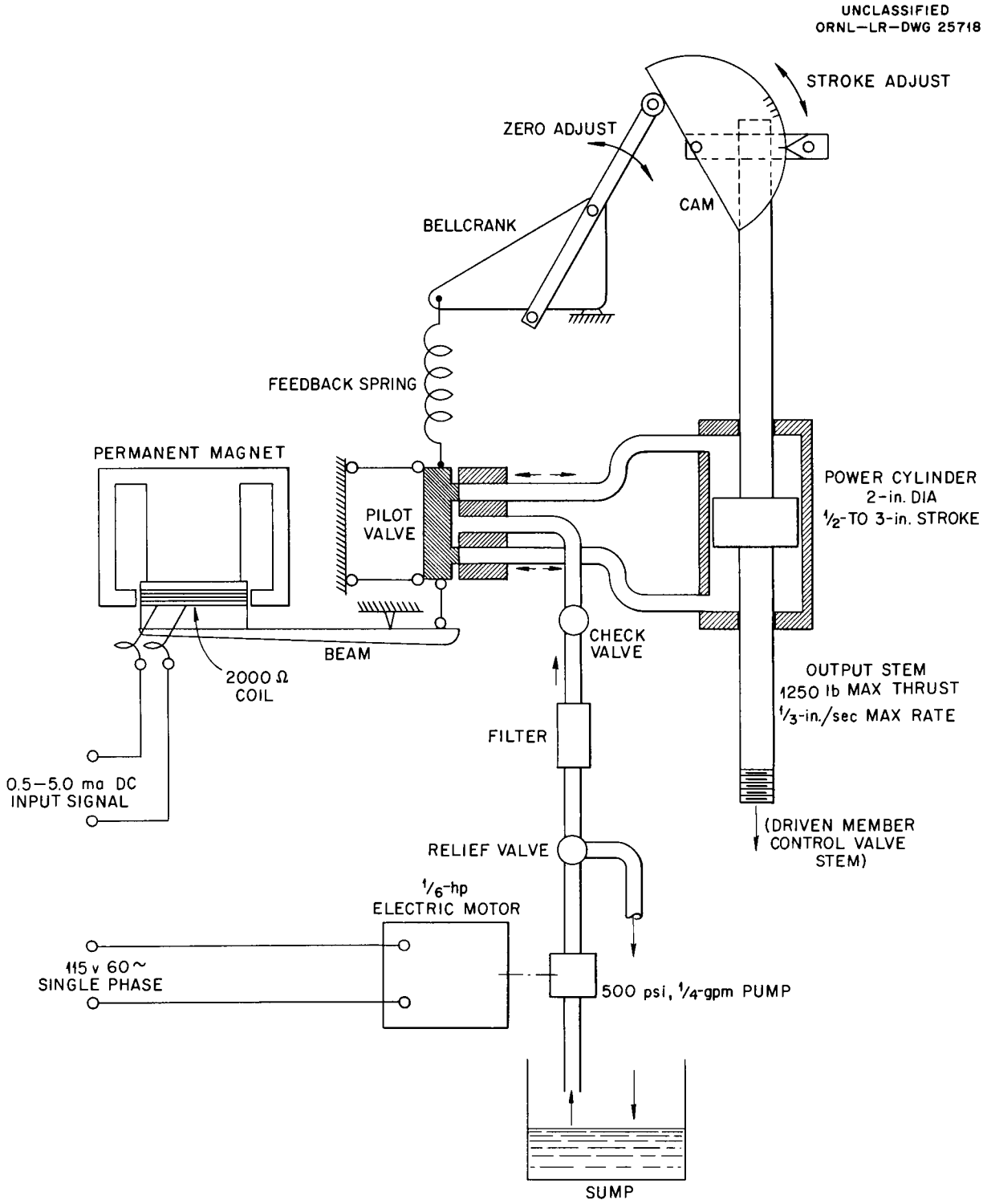

Fig. 11.4. Basic Electrohydraulic Valve Actuator.

A similar system, but with more thrust and utilizing water for the operating fluid, is on order from the Askania Regulator Co.

11.2.3 Valve Trim

Two Zircaloy-2 plugs were cycled for approximately 400 "dumps" each in the valve test loop and gave extremely poor results. The first trim set is shown before and after testing in Figs. 11.5 and 11.6, respectively. Galling is quite evident in the seating line of the plug. There was no evidence of an ignition reaction such as occurred with two titanium-alloy plugs reported earlier.[7]

The type 347 stainless steel plug flame-plated with tungsten carbide by Linde was examined metallographically,[8] and the plate was found to be intact in the seating area, as shown in Fig. 11.7. The plate thickness along the contour of the plug is shown in Fig. 11.8.

[7] D. S. Toomb *et al.*, *HRP Quar. Prog. Rep. July 31, 1956*, ORNL-2148, p 67–68 (classified).

[8] R. L. Fitzgerald, *Metallographic Examination of 347 Stainless Steel Valve Plug*, memo to F. W. Cooks (Sept. 20, 1957).

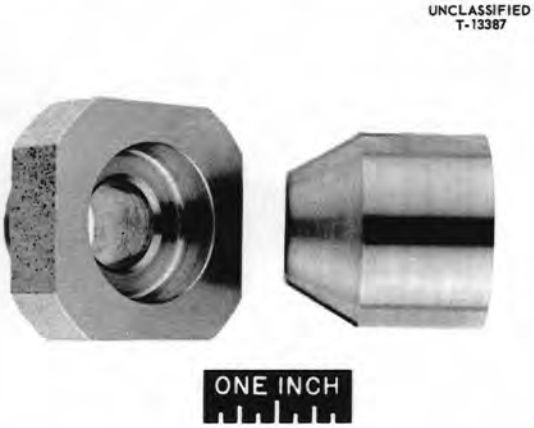

Fig. 11.5. Zircaloy-2 Trim Set Before Test.

Fig. 11.6. Zircaloy-2 Trim Set After Test.

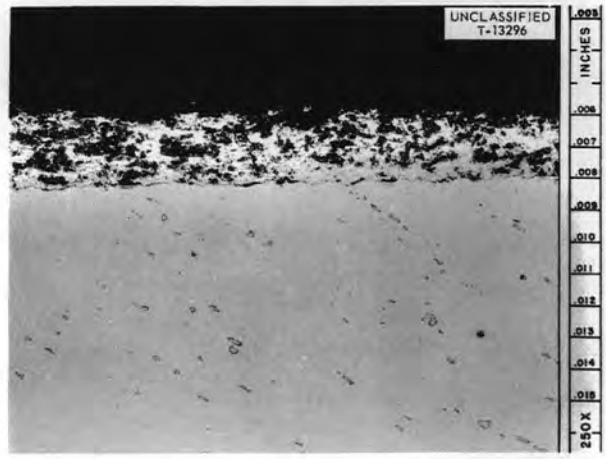

Fig. 11.7. Tungsten Carbide Flame Plate in Seat Area. Reduced 32.5%.

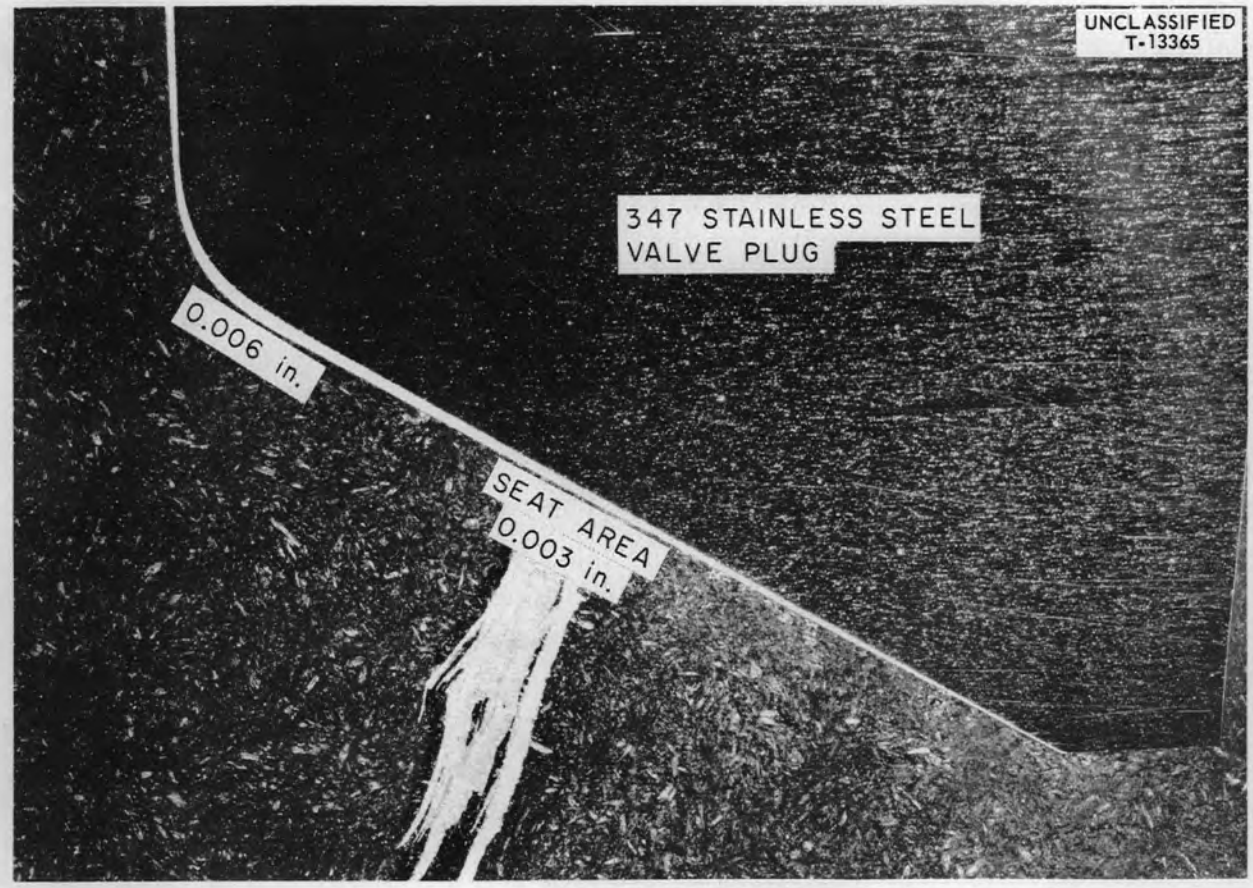

Fig. 11.8. Variation in Thickness of Tungsten Carbide Plate.

Part IV

REACTOR MATERIALS RESEARCH

E. G. Bohlmann

12. SOLUTION CORROSION[1]

J. C. Griess
S. E. Bolt
S. R. Buxton
J. L. English
R. S. Greeley
H. C. Savage
D. W. Hubbard
D. N. Hess
P. D. Neumann
W. C. Ulrich

12.1 DYNAMIC CORROSION STUDIES

12.1.1 Fifth Test of the HRT Core–Pressure-Vessel Flange and Transition-Joint Mockup

A fifth test of the mockup of the Zircaloy-2–stainless steel transition and expansion joint as used in the HRT reactor vessel has been made in 100A dynamic loop F. The first four tests were described previously.[2–5]

This test lasted 951 hr, 23 hr on water and 928 hr on fuel solution (0.04 *m* UO_2SO_4, 0.02 *m* H_2SO_4, 0.005 *m* $CuSO_4$). The test was conducted isothermally at 300°C, and the expansion joint was mechanically deflected $\frac{5}{8}$ in. every 4 hr for a total of 226 deflections. At the conclusion of the run and prior to disassembly, no leakage was detected through the 10-in.-IPS, 1500-lb test-vessel oval-ring joint when tested with 200 psig of helium. Neither leakage of fuel solution into the oval-ring-joint gasket grooves nor leakage of fuel solution through the bellows or across the transition joint was observed during the run. Also, after disassembly the bellows and transition joint were leak-tight to 50 psi of helium.

The pitting attack on the bellows at the edge of the reinforcing rings,[6] which stopped during the previous test in the absence of mechanical deflections, started again. The average depth of the pits increased about 0.003 in. during the fifth test, with three pits now measuring 0.022 to 0.024 in. deep. The recurrence of the pitting attack definitely indicates that the mechanical deflections are the primary cause of the pitting.

The solution remained stable throughout the test. The increase in nickel ion concentration corresponded to a generalized corrosion rate of about 0.1 mpy, the same rate as observed in the previous test.[2] This shows that in this case thermal cycling had little effect on the generalized corrosion rate. However, the stainless steel pins exposed in the loop gained small amounts of weight or lost insignificant amounts of weight at flow rates below 50 fps, in contrast to the previous run with thermal cycling in which weight losses of 1 to 2 mg/cm^2 occurred.

The total exposure of the mockup has been 5069 hr, including 4545 hr on fuel solution, 168 thermal cycles, and 374 mechanical deflections.

12.1.2 Metallographic Examinations from Previous Experiments

Metallographic results from several previous experiments have become available. In general, these corroborate other data previously reported.

A section of $1\frac{1}{2}$-in.-OD sched-80 type 347 stainless steel pipe from loop H was found to have stress-corrosion cracks about 0.025 to 0.050 in. deep starting from the outside of the pipe. This section of pipe had been exposed for about 20,000 hr to a demineralized-water spray, with frequent periods of tap-water spray, on the outside for cooling purposes. During this time, various solutions were circulated inside the loop at 200 to 300°C. The inside of the pipe was corroded fairly uniformly and had no cracks. Evidently the cracks propagated from the outside, owing to chloride in the water spray, until the surface stresses in the metal were relieved, and then the rate of cracking slowed or stopped. This behavior is in contrast to a previous failure[7]

[1] Reported in greater detail by J. C. Griess *et al.*, *Quarterly Report of the Solution Corrosion Group for the Period Ending Oct. 31, 1957*, ORNL CF-57-10-80 (to be published).

[2] J. C. Griess *et al.*, *HRP Quar. Prog. Rep. July 31, 1957*, ORNL-2379, p 69.

[3] J. C. Griess *et al.*, *HRP Quar. Prog. Rep. April 30, 1957*, ORNL-2331, p 83.

[4] J. C. Griess *et al.*, *HRP Quar. Prog. Rep. Jan. 31, 1957*, ORNL-2272, p 77–79.

[5] H. C. Savage *et al.*, *HRP Quar. Prog. Rep. Oct. 31, 1956*, ORNL-2222, p 75–76.

[6] J. C. Griess *et al.*, *HRP Quar. Prog. Rep. Jan. 31, 1957*, ORNL-2272, p 75, esp 78.

[7] E. C. Miller, W. O. Harms, and T. W. Fulton, *HRP Quar. Prog. Rep. April 30, 1954*, ORNL-1753, p 117–119 (classified).

where the pipe exposed to the water spray had been cold-formed into a bend and where the stresses induced throughout the wall of the pipe caused the cracks to penetrate the entire wall. The significance of the cracks in the cooler from loop H is that stress-corrosion cracking did occur even on supposedly unstressed straight austenitic stainless steel pipe in contact with water containing small amounts of chloride (the tap water contains between 5 and 8 ppm of chloride), although the cracks did not propagate through the entire wall thickness.

A commercially pure titanium (75A) corrosion sample holder which had become severely pitted beneath a stainless steel clamping band during a 151-hr exposure to 1.3 *m* UO_2F_2 at 250°C was found to have been severely hydrogen-embrittled in the pitted area. The sample holder snapped at the pitted area when clamped in a vise for repair. Figure 12.1 illustrates the microstructure of the material away from the pitted area, and Fig. 12.2 illustrates the microstructure below the pitted area; the hydride is clearly evident in the latter photomicrograph. The hydride extended throughout the thickness of the holder (about $\frac{3}{8}$ in.) and was not concentrated in a surface layer next to the pits. This indicates that massive titanium can become hydrogen-embrittled within a few hundred hours under certain corrosive conditions. The attack appeared to be a form of crevice corrosion, since titanium pins insulated with Teflon also corroded severely in the crevice region. In the crevice, in the absence of oxygen, hydrogen would be a product of the corrosion reaction.

Hydrogen pickup by titanium in a crevice region was also found on a titanium insert described previously.[8] In this case the titanium insert was used to protect a stainless steel loop in a turbulent area and had been exposed for 9900 hr to 0.04 to 1.3 *m* UO_2SO_4 solution at 175 to 300°C. Oxygen exhaustion had occurred in the crevice between the titanium insert and the stainless steel pipe wall. The hydrogen concentration of the titanium increased only from 42 ppm to 120 ppm, but photomicrographs showed definite amounts of hydride. The hydrogen pickup by the titanium insert did not impair the usefulness of the insert in this instance. This observation that titanium can absorb hydrogen under certain conditions in uranyl sulfate solutions raises some question as to the use of titanium as a pressure container in crevice regions.

12.1.3 Effect of Additives to 0.17 *m* UO_2SO_4

A large number of compounds have been tested previously in the 100A loop program as additives to uranyl sulfate to inhibit the corrosion of stainless steel. The testing has been continued recently in an attempt to find inhibitors other than

Fig. 12.1. Microstructure of Titanium 75A Corrosion Specimen Holder Away from Corroded Area. Reduced 32.5%.

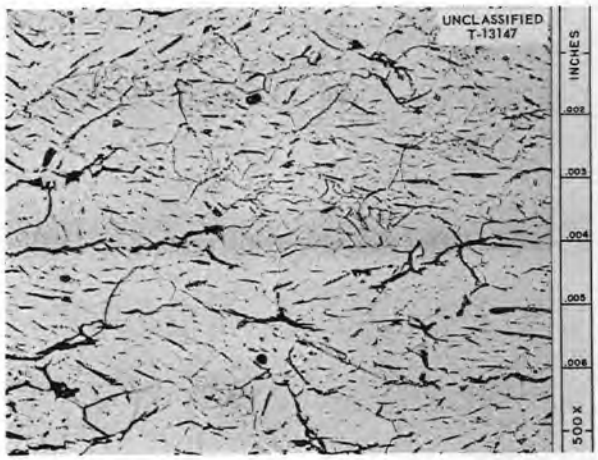

Fig. 12.2. Microstructure of Titanium 75A Corrosion Specimen Holder in Pitted Area After 151 hr at 250°C in 1.3 *m* UO_2F_2. Dark areas are hydride. Reduced 32.5%.

[8] J. C. Griess *et al.*, *HRP Quar. Prog. Rep. Jan. 31, 1957*, ORNL-2272, p 77, esp 81.

compounds containing or forming hexavalent chromium, which is unstable under radiation. All the tests were conducted for 200 hr at 250°C with 0.17 *m* UO_2SO_4 containing the compound to be tested and about 1000 ppm of oxygen. Table 12.1 lists the compounds tested and the stability of the solutions of which they were constituents.

None of the additives gave a significant improvement in the corrosion resistance of stainless steel except the ruthenium nitrososulfate. Weight losses of type 347 stainless steel coupons up to the critical velocity of 30 to 35 fps were 5 to 10 times lower in the presence of 100 ppm ruthenium as the nitroso complex than in uranyl sulfate alone. However, the ruthenium was lost from solution rapidly; less than 3 ppm remained after 24 hr. It appeared that the inhibition of corrosion was caused by the ruthenium catalyzing the oxidation of chromium from the steel or oxide scale to the hexavalent state. The chromium(VI) concentration increased rapidly during the run, reaching 820 ppm in 200 hr, and very likely was the effective agent in causing the inhibition. Therefore it does not appear that any of the compounds tested would be of value as corrosion inhibitors.

12.1.4 Initial Runs in an All-Titanium Loop

It has been found[9] that loop history, in particular whether a loop is new or used, can affect the corrosion results obtained in stainless steel loops. In order to investigate further the effect of loop history on corrosion of stainless steel, the initial runs in loop H, a new all-titanium loop,[10] were made to determine whether new titanium surfaces would have as great an effect on corrosion of stainless steel coupons as new stainless steel surfaces. In the first run, type 347 stainless steel coupons in the titanium loop were exposed to the "standard" pretreatment of 4 hr with 3% trisodium phosphate at 100°C, 12 hr with 5% nitric acid at 100°C, and 24 hr with oxygenated water at 250°C. The loop was then charged with 0.17 *m* UO_2SO_4 containing 0.04 *m* H_2SO_4 and 0.03 *m* $CuSO_4$, and the solution was circulated at 250°C for 200 hr. Corrosion rates were very low – 0.3 to 0.6 mpy – and no velocity effect was observed on the coupons even at the maximum flow rate of 43 fps.

[9] J. C. Griess *et al.*, *HRP Quar. Prog. Rep. April 30, 1957*, ORNL-2331, p 83, esp 89.

[10] J. C. Griess *et al.*, *HRP Quar. Prog. Rep. July 31, 1957*, ORNL-2379, p 69.

Table 12.1. Possible Inhibitors Added to 0.17 *m* UO_2SO_4 at 250°C; All Runs Were for 200 hr and Contained 1000 ppm O_2

Additive	Concentration		Remarks
	m	ppm	
$Ce(SO_4)_2$	0.0008	110 Ce	Stable solution
$H_7P(MoO_4)_{12}$	0.001	100 Mo	Phosphomolybdic acid decomposed and uranyl phosphate precipitated
As_2O_5	0.0005	70 As	Arsenic lost from solution
H_3SbO_4	0.0008	100 Sb	Less than 1 ppm Sb soluble at 250°C
$NaBiO_3$	0.0005	100 Bi	Bi_2O_3 precipitated
$(RuNO)_2(SO_4)_3$	0.001	100 Ru	Ru metal and RuO_2 precipitated
$NaNO_3$	0.01		Stable solution
	0.1		Stable solution
Ag_2SO_4	0.005		Stable solution

The second run was identical to the first. In this case, however, a sharp velocity effect was observed, and the type 347 stainless steel coupons at 32 to 43 fps corroded at 40 to 50 mpy. The corrosion was a pitting type of attack similar to that observed previously[11] and indicated the breakdown of the pretreatment film. Therefore, even in the case of a titanium system, the initial run was for some reason anomalous in giving low corrosion and no velocity effect. It is believed that the effect might have been due to a small difference in pretreatment in the first and second runs rather than to an effect of the loop itself.

In the third run the pretreatments were omitted and the type 347 stainless steel coupons were exposed directly to 0.17 *m* UO_2SO_4 containing 0.04 *m* H_2SO_4 and 0.03 *m* $CuSO_4$ for 200 hr at 250°C. Corrosion rates were high – 100 to 500 mpy – and a sharp velocity effect was observed. The "standard" pretreatment used in the first and second runs was of value in decreasing the corrosion. However, as the second run showed, pretreatments cannot be depended upon to increase the critical velocity under all conditions.

12.1.5 Chemical Stability and Corrosiveness of Dilute Copper Sulfate–Sulfuric Acid Solution for the HRT Blanket

There exists the likelihood that a small amount of copper sulfate will have to be added to the D_2O blanket of the HRT in order to recombine radiolytic gases. It has been calculated that about 0.001 *m* copper (60 ppm) would be sufficient. A previous run[12] showed that a 0.0005 *m* copper sulfate solution containing 0.002 *m* H_2SO_4 was stable at 300°C. Therefore 0.002 *m* H_2SO_4 was added to the solution containing 0.001 *m* $CuSO_4$ in the first run and 0.003 *m* H_2SO_4 was added in the second run in order to determine the acid concentration necessary to prevent hydrolytic precipitation of 60 ppm of copper. Both runs were made at 300°C.

About 15 ppm of copper was lost from solution within 32 hr in the first run, although the solution was stable for 168 hr with 45 ppm of copper. The solution in the second run was entirely stable for 343 hr. In both runs corrosion of stainless steel specimens was less than 2 mpy up to 70 fps. Therefore it appears that a 0.001 *m* $CuSO_4$ solution containing 0.003 *m* H_2SO_4 would be satisfactory from a stability and corrosion standpoint.

12.2 LABORATORY CORROSION STUDIES

12.2.1 Stress-Corrosion Cracking

(a) Stress-Corrosion Cracking in Uranyl Sulfate Solutions. – A test program was initiated to examine the effect of preformed films on the stress-corrosion cracking behavior of type 347 stainless steel in boiling chloride-containing 0.04 *m* UO_2SO_4 solution with 0.02 *m* H_2SO_4 and 0.005 *m* $CuSO_4$ present. The chloride content of the solution was 50 ppm as KCl. Previous experience indicated that stressed specimens pre-exposed in boiling chloride-free uranyl sulfate solution were highly resistant to cracking when later placed in a similar solution containing chloride ions.[13] Stressed specimens free of preformed films were not resistant to cracking.

In the present study, preformed films on specimens were produced by two methods: (1) exposing for 500 hr in boiling and aerated chloride-free 0.04 *m* UO_2SO_4 solution containing 0.02 *m* H_2SO_4 and 0.005 *m* $CuSO_4$ and (2) heating for 1 hr in air at 677°C (1250°F). The stress specimens were of a U-bend type, cold-formed from 0.019-in.-thick type 347 stainless steel strip. The specimens were placed under elastic stress by means of a type 347 stainless steel tie-bolt through the ends of the U. Pickled and electropolished specimens were used for the films produced in chloride-free uranyl sulfate solution; pickled specimens only were used for the 677°C air-formed films.

In order to determine whether film rupture would accelerate the time required for cracking in chloride-containing uranyl sulfate solution, the stress specimens for the preformed-film study in chloride-free solution were prepared in two ways. In one case, duplicate pickled and duplicate electropolished unstressed specimens were exposed for 500 hr in the boiling chloride-free uranyl sulfate solution and elastically stressed *after* completion of the pre-exposure. In the second case, pickled

[11] J. C. Griess and R. E. Wacker, *HRP Quar. Prog. April 30, 1954*, ORNL-1753, p 61, esp 76 (classified).

[12] J. C. Griess *et al.*, *HRP Quar. Prog. Rep. April 30, 1956*, ORNL-2096, p 81, esp 84.

[13] J. L. English and J. C. Griess, *Quarterly Report of the Solution Corrosion Group for the Period Ending Jan. 31, 1956*, ORNL CF-56-1-167, p 38.

and electropolished specimens (two each) were elastically stressed *before* the start of the 500-hr pre-exposure.

All specimens were placed in the boiling and aerated uranyl sulfate solution containing 50 ppm chloride. After 400 hr the specimens elastically deformed after pre-film-formation have exhibited no tendency toward cracking. Similarly, the specimens elastically stressed before pre-film-formation have run for 500 hr without showing signs of cracks. Control specimens with no preformed film have been found to crack in the chloride-containing environment in periods of 400 hr and less, generally after 25 to 50 hr from the start of the exposure. The tests will be continued.

The second type of preformed film was prepared by heating elastically stressed specimens for 1 hr in air at 677°C (1250°F). Without removing the air-formed film, the specimens were then placed in the chloride-containing uranyl sulfate environment. During the exposure period between 150 and 205 hr, both specimens developed cracks in areas of near-maximum stress. Although additional work is planned to study the effect of films formed at elevated temperature, indications were that films formed at 677°C were not sufficiently protective to resist chloride-induced stress-corrosion cracking in boiling uranyl sulfate solution.

(*b*) Stress-Corrosion Cracking in Chloride-Containing Water. – Stressed specimens of type 347 stainless steel were exposed in distilled water containing 100 ppm of chloride at temperatures ranging between 100 and 300°C. As reported previously, cracks were produced at 300°C in periods from 200 to 400 hr.[14] At 250°C, the time required for cracking of four specimens varied between 100 and 300 hr, while at 200°C the same number of specimens cracked in less than 100 hr. Present work has been concerned with the susceptibility to cracking in pH 2.8 and 10.5 distilled water at 100°C. Sixteen stressed specimens have been exposed in boiling (~100°C) distilled water containing 100 ppm of chloride for 2500 hr without any indications of cracking. The tests were run with air bubbling through the solution. On the other hand, when the same solution at 100°C was pressurized with 150 psi of oxygen in an autoclave, two out of six stress specimens were cracked during the initial 300 hr of exposure. The remaining four specimens are continuing in test. Although the results are not complete, it does appear that at 100°C the concentration of oxygen in solution is important. This has not been the case at higher temperatures.

(c) Stress-Corrosion Cracking in 42% $MgCl_2$ Solution. – Continuation of tests with stressed type 347 stainless steel in boiling (154°C) 42% $MgCl_2$ solution has shown that reducing the applied stress to a level of 10,000 psi did not appreciably affect the time required for crack initiation. However, the rate of crack propagation appeared to decrease.

It was also found that the reported immunity[15] to stress-corrosion cracking of austenitic stainless steels in boiling 42% $MgCl_2$ solution by (1) placing magnesium metal in the solution and not in contact with the test specimen or by (2) the addition of stannous chloride ($SnCl_2$) to the solution was not achieved in laboratory tests. In all cases, the time required for crack initiation was no different from that observed in tests with 42% $MgCl_2$ solution containing neither metallic magnesium nor stannous chloride. However, coupling of magnesium metal with a stressed type 347 stainless steel specimen was found to render the latter immune from cracking during a 100-hr test.

(*d*) Stress-Corrosion Cracking Tests with Marking Inks. – A number of marking inks used to identify stainless steels and other constructional materials were submitted for chloride analyses. The chloride contents were found to range from 3,000 to 19,000 ppm. In order to determine whether such chloride-containing inks were capable of inducing stress-corrosion cracking in type 347 stainless steel, tests were conducted in which stressed specimens were painted with the different inks and exposed in oxygen-rich saturated steam at 300°C. All specimens cracked after periods of 300 hr and less. Presently, similar tests are being run with different inks containing from 20 to 1100 ppm of chloride.

[14] J. C. Griess *et al.*, *HRP Quar. Prog. Rep. July 31, 1957*, ORNL-2379, p 69, esp 78–79.

[15] K. W. Leu and J. N. Helle, "On the Mechanism of Stress Corrosion of Austenitic Stainless Steels in Hot Aqueous Chloride Solutions," paper presented at the 13th Annual Conference of National Association of Corrosion Engineers, St. Louis, March 11–15, 1957.

12.2.2 Corrosion Tests with Zirconium Alloys

The corrosion test program for the evaluation of zirconium-base alloys was completed during the past quarter. The program, a conjoint effort with the HRP Metallurgy Group, was undertaken for two reasons: (1) to determine the general corrosion behavior of a number of zirconium-base alloys in high-temperature uranyl sulfate solution and (2) to provide suitable specimens for film-structure studies by the HRP Metallurgy Group. Corrosion data for other zirconium alloys tested in the program have been reported.[16–18]

The present tests were concerned with the behavior of rolled and oxidized zirconium-base alloys; a number of tests were also run with non-oxidized as-cast alloys. The oxidizing treatment consisted of heating the specimens for 3 to 5 min at a temperature of 1000°C. The treatment produced films that were found to be highly resistant to acid pickling solutions.

All specimens were exposed for 1000 hr at 300°C in oxygenated 0.04 *m* UO_2SO_4 solution containing 0.02 *m* H_2SO_4 and 0.005 *m* $CuSO_4$. The results are included in Table 12.2. No attempt was made to defilm the specimens upon completion of the tests.

Of the three as-cast alloys, the 20% Nb–80% Zr composition exhibited a corrosion rate, <0.1 mpy, comparable with that for Zircaloy-2 under similar conditions of exposure. The other two as-cast alloys, 1% Fe–15% Nb–84% Zr and 2% Y–2% Sn–8% Nb–88% Zr, exhibited weight gains ranging from 1.8 to 4.9 mg/cm^2 and films that were appreciably bulkier than the highly lustrous, dark blue-black thin film formed on the 20% Nb–80% Zr alloy.

The preoxidized casting alloy of 33% Nb–67% Zr composition possessed excellent corrosion resistance; no measurable attack occurred during the 1000 hr in high-temperature uranyl sulfate solution. Several of the cast and rolled preoxidized alloys exhibited promising corrosion behavior, with corrosion rates of 0.7 mpy and less for the 1000-hr exposure. These alloys were the 7% Mo–20% Nb–73% Zr, 2% Sn–2% Mo–15% Nb–81% Zr, and 1% Ni–20% Nb–79% Zr compositions. The remaining preoxidized alloys were corroded at rates ranging between 1.8 and 27.8 mpy. The highest corrosion rate, 27.8 mpy, was for the 10% Mo–90% Zr alloy.

12.2.3 Miscellaneous Corrosion Tests

A number of materials of possible interest to the Homogeneous Reactor Project were subjected to corrosion tests in specific environments. Some of the materials had been tested previously in certain environments, and others were tested for the first time.

Elgiloy, an alloy possessing good spring properties at high temperatures, had been shown previously to be susceptible to stress-corrosion cracking in uranyl sulfate solutions.[19] In recent tests Elgiloy was subjected to aging treatments after which specimens were either electropolished or pickled. Subsequent corrosion tests in 0.04 *m* UO_2SO_4 containing 0.02 *m* H_2SO_4 and 0.005 *m* $CuSO_4$ at 300°C showed that the aging treatment had little or no effect in reducing the tendency of the alloy to stress-corrosion cracking. Both stressed specimens and those to which no stress was applied developed many cracks during exposure. Although the general corrosion behavior of the alloy was acceptable, its susceptibility to cracking precludes its use for reactor applications involving contact by high-temperature uranyl sulfate solution.

Sintered aluminum oxide, specifically AlSiMag 652, produced by the American Lava Corp. had been tested previously in highly concentrated uranyl sulfate solution and shown to have corrosion resistance comparable to that of sintered aluminum oxide produced by the Kearfott Company.[20] Recent tests have been concerned with the corrosion resistance of AlSiMag 652 in a solution containing 0.17 *m* UO_2SO_4, 0.04 *m* H_2SO_4, and 0.03 *m* $CuSO_4$, a solution composition similar to that used in several in-pile loops. The test was conducted at 150°C with a partial pressure of 150-psi oxygen. The corrosion rate of AlSiMag 652 decreased with time; the rate was 19 mpy after 50 hr and 8 mpy

[16] J. C. Griess *et al.*, *HRP Quar. Prog. Rep. Jan. 31, 1957*, ORNL-2272, p 77, esp 86–88.

[17] J. C. Griess *et al.*, *HRP Quar. Prog. Rep. April 30, 1957*, ORNL-2331, p 83, esp 93.

[18] J. C. Griess *et al.*, *HRP Quar. Prog. Rep. July 31, 1957*, ORNL-2379, p 69, esp 79.

[19] J. L. English *et al.*, *Quarterly Report of the Solution Corrosion Group for the Period Ending Jan. 31, 1957*, ORNL CF-57-1-144, p 41.

[20] J. L. English *et al.*, *Quarterly Report of the Solution Corrosion Group for the Period Ending April 30, 1957*, ORNL CF-57-4-55, p 44.

Table 12.2. Corrosion of Preoxidized[a] Zirconium-Base Alloys During 1000 hr at 300°C in 0.04 *m* UO_2SO_4–0.02 *m* H_2SO_4–0.005 *m* $CuSO_4$ Solution

Laboratory No.	Material Identity	Alloy Composition (wt %)	Specimen No.	Corrosion Rate (mpy)
W-83	Zr-18	10 Mo–90 Zr	1	27.8
T-95	Zr-22	20 Nb–80 Zr[b]	1	0
			2	<0.1
W-81	Zr-42	33 Nb–67 Zr[c]	1	Negligible
T-82	Zr-20	1 Fe–15 Nb–84 Zr[d]	1	(+1.8 mg/cm^2)
			2	(+1.9 mg/cm^2)
W-80	Zr-17	5 Mo–15 Nb–80 Zr	1	4.8
W-78	Zr-12	5 Mo–10 Nb–85 Zr	1	4.8
X-3	Zr-47	7 Mo–20 Nb–73 Zr	1	0.3
W-79	Zr-14	5 Mo–5 Ta–10 Nb–80 Zr	1	2.9
W-85	Zr-28	1 Pd–15 Nb–84 Zr	1	1.8
W-84	Zr-27	2 Pd–15 Nb–83 Zr	1	12.5
X-6	Zr-80	2 Sn–2 Mo–15 Nb–81 Zr	1	(+0.4 mg/cm^2)
X-6	Zr-80	2 Sn–2 Mo–15 Nb–81 Zr[e]	1	0.4
W-82	Zr-67	3 Sn–15 Nb–82 Zr	1	2.7
X-4	Zr-48	1 Ni–20 Nb–79 Zr	1	1.0
			2	0.3
X-5	Zr-68	3 V–15 Nb–82 Zr	1	8.8
T-97	Zr-77	2 Y–2 Sn–8 Nb–88 Zr[f]	1	(+4.5 mg/cm^2)
				(+1.9 mg/cm^2)

[a]Preoxidizing treatment: 3 to 5 min in air at 1100°C.

[b]Alloy prepared from Bureau of Mines sponge zirconium; all other alloys prepared from high-purity crystal-bar zirconium. Specimens cast and mechanically abraded; no oxidizing treatment.

[c]Cast specimen; oxidized.

[d]Cast specimens homogeneized for 3 hr in air at 1000°C; oxide film removed by mechanical abrasion prior to test.

[e]Specimen chemically polished before oxidizing.

[f]Cast specimens; no oxidizing treatment.

(cumulative) at the completion of the 1000 hr test. All the aluminum lost from the specimens was found in solution.

A ceramic electrical-insulation material, Ceramicite C-100, produced by the Consolidated Electrodynamics Corp., was tested in a high-temperature uranyl sulfate solution. The material reportedly has superior electrical characteristics and high-pressure integrity at temperatures as high as 438°C (820°F) and has the ability to form a molecular bond with the 400 series stainless steels. Several beads of Ceramicite C-100 were bonded to platinum or type 347 stainless steel by gradual heating at 621 to 649°C. The resulting specimens were exposed to 0.04 *m* UO_2SO_4 containing 0.02 *m* H_2SO_4 and 0.005 *m* $CuSO_4$ at 300°C. The corrosion rates of the ceramic material varied between 930 and 970 mpy.

Preliminary tests were performed on nitrided titanium and Frogalloy, materials of interest to

the HRP injection-pump development program. The nitrided titanium was prepared by Horizons, Inc. During a 1000-hr exposure to 0.04 *m* UO_2SO_4 containing 0.02 *m* H_2SO_4 and 0.005 *m* $CuSO_4$, the specimen showed a small weight gain and darkened slightly. There was no evidence of corrosion attack.

Frogalloy is an alloy produced by the McKay Co. Frogalloy C, with a nominal composition of 0.4 to 0.6% C, 4% Mn min, 18 to 21% Cr, 9 to 10.5% Ni, 0.5% Mo, and balance iron, and Frogalloy M, which has a similar composition except for the presence of molybdenum, were tested in boiling 5% HNO_3 and in boiling HRT fuel solution. In the 5% HNO_3 solution both alloys corroded at rates between 43 and 49 mpy during a 500-hr exposure; in boiling HRT fuel solution corrosion rates of 500 to 580 mpy were observed during a 100-hr exposure.

13. SLURRY CORROSION

E. L. Compere
S. E. Bolt
G. W. Eckerd
D. W. Hubbard
D. T. Jones
H. C. Savage
S. A. Reed
J. A. Russell, Jr.
W. C. Ulrich
R. M. Warner
L. F. Woo

13.1 PUMP LOOPS

13.1.1 Loop Engineering

During the operation of loop BS at 300°C in runs BS-15, -16, and -17, leakage from the pressurizer vapor space of the loop was indicated.[1] Repeated pressure checks at room temperature failed to reveal the leak. It was assumed, therefore, that this leak resulted from distortion of the 4-in. 1500-lb ring-joint flange at the top of the pressurizer at the operating temperature of 300°C. The flange was removed and a straight pipe section welded in its place. This repair apparently remedied the leak, as evidenced by run BS-18, a 1007-hr run at 300°C and ~1500 psig, during which no leakage was noted.

13.1.2 100A Pump Loop Tests: Introduction

Tests in the 100A pump loops this quarter continued to be concerned with the evaluation of the suitability of various thoria preparations for use as circulating aqueous slurries under reactor blanket conditions. The relationship between corrosion-erosion properties and degradation of the thoria particles with continued pumping was of particular interest.

During the report period five dynamic slurry corrosion tests were made in pump loops BS and CS, with three different batches of thoria. These included thoria calcined at 800°C and subsequently micropulverized, sulfated 800°C thoria which had been pumped in the slurry blanket mockup, and a mixture of 1600°C-calcined thoria batches. Four of the runs were made with oxygen pressurization at 300°C, and one run, on the sulfated mockup slurry, with steam pressurization (oxygenated) at 200°C.

A run duration of 1007 hr was achieved in loop BS with the 1600°C-calcined mixed thoria slurry, after modifications corrected leaks which had caused the early termination of several previous runs (one this quarter). This run permitted an examination of the relationship between the degradation and the corrosion-erosion properties of the high-fired thoria preparation.

The use of micropulverized 800°C thoria was of interest, since previous loop runs on unground thoria had indicated that much of the loop corrosion occurred during the period when the thoria particles underwent their greatest size degradation. Size reduction before loop use would thus be expected to result in less slurry corrosion. Two runs with micropulverized thoria were made this quarter, the second employing the same slurry that was pumped in previous runs, to permit further observation of its degradation behavior on continued pumping.

The run with sulfated 800°C-calcined thoria slurry previously circulated in the slurry blanket mockup was carried out at 200°C, simulating the operating conditions of the slurry blanket mockup.

13.1.3 Circulation of 1600°C-Calcined Thoria Slurry

Very favorable handling properties and moderate attack rates of pin corrosion specimens were observed in two previously reported[1] loop tests in which oxygenated slurries of 1600°C-calcined thoria were circulated at 300°C at average circulating concentrations of ~400 g of thorium per kilogram of water. However, those tests were of short duration under unsteady operating conditions, resulting from difficulties due to leakage of water from the system during the runs.

Slurry circulated in those tests was prepared from a special pilot lot, batch TO-10-1000, of thorium oxide produced by calcining thorium oxalate which was made by precipitating thorium nitrate with oxalic acid at 10°C. This lot was recalcined at 1600°C. The mean particle size of the oxide was 1.3 μ.

[1] E. L. Compere *et al.*, *HRP Quar. Prog. Rep. July 31, 1957*, ORNL-2379, p 84, esp 92–93.

It was desirable in the evaluation of high-fired thoria slurries to observe the effects of extended circulation, under reactor blanket conditions, on the properties and behavior of such slurries. Runs BS-17 and BS-18, described below, were for this purpose. Because of the limited quantity of the 1600°C-recalcined batch TO-10-1000 thoria preparation, loop tests at concentrations above 500 g of thorium per kilogram of water were not possible. Therefore supplementary material was prepared by degrading batch LO-17 (70°C-precipitated, 550°C-calcined) thoria for 4 hr in a Waring Blendor and subsequently refiring at 1600°C. Prior to loop circulation tests, the recalcined product was slurried in water and again blended for 1 hr in a Waring Blendor.

The charge to run BS-17 consisted of a composite of 8.1 kg of batch TO-10-1000 which had been recalcined at 1600°C and circulated for a total of 350 hr in runs BS-15 and BS-16 and 9.2 kg of degraded and recalcined batch LO-17 thoria, resulting in a load concentration of 1088 g of thorium per kilogram of water. The mean particle size of the mixed batches was 1.3 μ.

Two sets of pin corrosion specimens were placed in series in the main circulating stream of the loop, which had a bulk flow, measured on water at room temperature, of 27 gpm. The pump suction line contained only a venturi to monitor flow during the test.

After 127 hr of slurry circulation at 300°C (with oxygen added), the loop temperature controller, which provides both heating and cooling control for the system, failed to operate properly. The system temperature dropped to 245°C and the system pressure fell to ~900 psi. The pump became gas-bound. The controller was readjusted, but proper operation was not obtained after that time. Temperature and pressure levels in the system were re-established only for a short period, and pump noise increased markedly. The trend in operational difficulties suggested leakage of liquid from the system as had been experienced in several previous tests. Therefore the system was shut down.

A check of the liquid level in the loop showed that 2 liters of liquid had been lost from the system. After 2 liters of water was added to the loop, an attempt was made to resume the test. The slurry was readily resuspended, but the circulating pump was badly out of balance; so the run was terminated. Total slurry circulation time was 236.4 hr.

The system was drained, rinsed with water, and disassembled for routine inspection. No deposits were found in the loop or pump.

The concentration of the flowing stream, calculated from chemical analysis of samples withdrawn from the system, varied from 1215 to 758 g of thorium per kilogram of water. The average concentration for the run was 944 g of thorium per kilogram of water. Particle-size distribution data gave no evidence of particle degradation during circulation.

When the pump was disassembled, the forward ring in the front set of titanium seal rings was not in place. The ring, which was in three pieces, was found wedged in the downstream specimen holder in the pump discharge line. The ring was not excessively eroded, which indicated it was probably dislodged because of improper installation rather than by attack of slurry. The other front rings were enlarged 55 mils. The rear seal rings, of type 347 stainless steel, were worn 115 mils. The front Graphitar bearing was enlarged 0.0028 in. The dimensions of the rear Graphitar bearing had not changed.

The type 347 stainless steel impeller lost 18 g during the test.

Incremental system corrosion rates, calculated from corrosion products detected in slurry samples and from circulating slurry inventory, indicated a pronounced increase in attack during the latter period of the test when pump performance was poorest. Incremental rates showed a gradual downward trend from 43 to 1.4 mpy until pump trouble began, after which time it rose to 11 mpy. The over-all system attack rate for the run was 7 mpy.

Specimen attack rates, shown in Table 13.1, were higher than had been anticipated. Compared with attack data obtained in runs BS-15 and BS-16, using only 1600°C-calcined TO-10-1000 slurry, the rates were about twofold higher than would be estimated from the increased concentration. Rates for gold and platinum were increased more. It is not known whether the increased attack was caused by the addition of batch LO-17 thoria to the TO-10-1000 preparation or whether it was due to the erratic flow conditions in the system resulting from water loss.

Table 13.1. Corrosion by Circulating Thorium Oxide Slurries in Loop Tests

	Run Number					
	CS-38[a]	CS-39	CS-40	CS-41[b]	BS-17	BS-18
Hours	300	300	168	300	236	1007
Temperature, °C	300	300	300	200	300	300
Concentration, g Th/kg H_2O						
Load	590	850	638	734[c]	1088	730
Average	591	932	641	488	944	630
Calcination temperature, °C	800 micro-pulverized	800 micro-pulverized	800 micro-pulverized	800	1600	1600
Thoria batch No.	LO-27	LO-27	LO-27 from CS-38, -39	Mockup slurry	TO-10-1000 and LO-17 recalcined at 1600°C (see text)	From BS-17
Additives	None	None	None	H_2SO_4[d]	None	None
Atmosphere	O_2 + A	O_2 + A	O_2	O_2	O_2 + A	O_2
Average particle size, μ						
Prerun	1.0	1.0	0.8	0.9	1.3	1.3
Postrun	0.5	0.8	0.8	0.7	1.3	1.3
Impeller weight loss, g	31 (hub pits)	49	24	20 (pits)	18	21.5
Loop corrosion rate, mpy	4.5	7.3	4.8	2.9	7.0	1.9
Range of pin attack rates, mpy, at given flow velocity						
Velocity, fps						
Austenitic Stainless Steels						
19, coupons		1–3	< 1	< 1		
21–26	1–2	2–5	1–2	< 1	8–10	1–2
39–45	3–11	11–19	3–8	2–5	40–58	16–23
46–73, coupons		11–58	1–32	5–27		
Ferritic Stainless Steels						
23–26				2–7		
40–42				5–18		13
Carbon Steels						
19, coupons		3–4	24–27	9		
21–26	13–16	7–15	30–59	100–241		
29–42	13–18	10–13	26–38	248–560		
Titanium Alloys						
19, coupons		< 1	< 1	< 1		
21–26	0 (coupon)		1	< 1	7–9	1
39–45			4	1	47–54	9–13
Zirconium Alloys						
19, coupons		0.0	0.0	< 1		
21–26	0.7	2–3	1	< 1	8–9	< 1
39–45	3	5–6	2	1	67	10
Gold and Platinum						
19, coupons						
21–26	0.3–0.4	1–2	< 1	< 1	10–31	1–4
39–45	1–2	1–6	1–5	< 1	100–270	13–30

[a]Previously reported, ORNL-2379.

[b]Steam pressurized.

[c]Based on estimated circulating volume.

[d]H_2SO_4 added prior to slurry blanket mockup test.

The slurry from run BS-17 was recharged to the test loop for run BS-18 to a load concentration of 755 g of thorium per kilogram of water. The oxygenated slurry was circulated at 300°C for 1007 hr at an average concentration of 630 g of thorium per kilogram of water. The continuous run was made without difficulty and was shut down on schedule.

Attack of the components of the circulating pump was relatively moderate in view of the 1007-hr duration of the run. The type 347 stainless steel impeller lost 21.5 g. The front Graphitar bearing was worn 3 mils. There was no measurable wear of the rear Graphitar bearing. The front seal rings, fabricated of type 347 stainless steel, were enlarged 0.0315 in.; the rear seal rings were not enlarged.

The slurry withdrawn from the test loop at the completion of the run was flocculated, quite fluid, and appeared near-Newtonian in character. Particle-size distribution data, determined by sedimentation analysis, showed no evidence of thoria degradation during the test.

The average system attack rate for the run was 1.9 mpy. Incremental rates ranged between 12 and 0.2 mpy, but were relatively without trend.

The average attack rate of pin specimens was as follows:

	Corrosion Rate (mpy)	
	At 21 fps	At 42 fps
Austenitic stainless steels	2	19–22
Titanium alloys	1	9–13
Zircaloy-2	0.5	10
Gold	4	30
Platinum	1	13

At the higher velocity, abrasive attack on the upstream surfaces of all specimens was clearly evident. A photograph of several of the specimens is shown in Fig. 13.1.

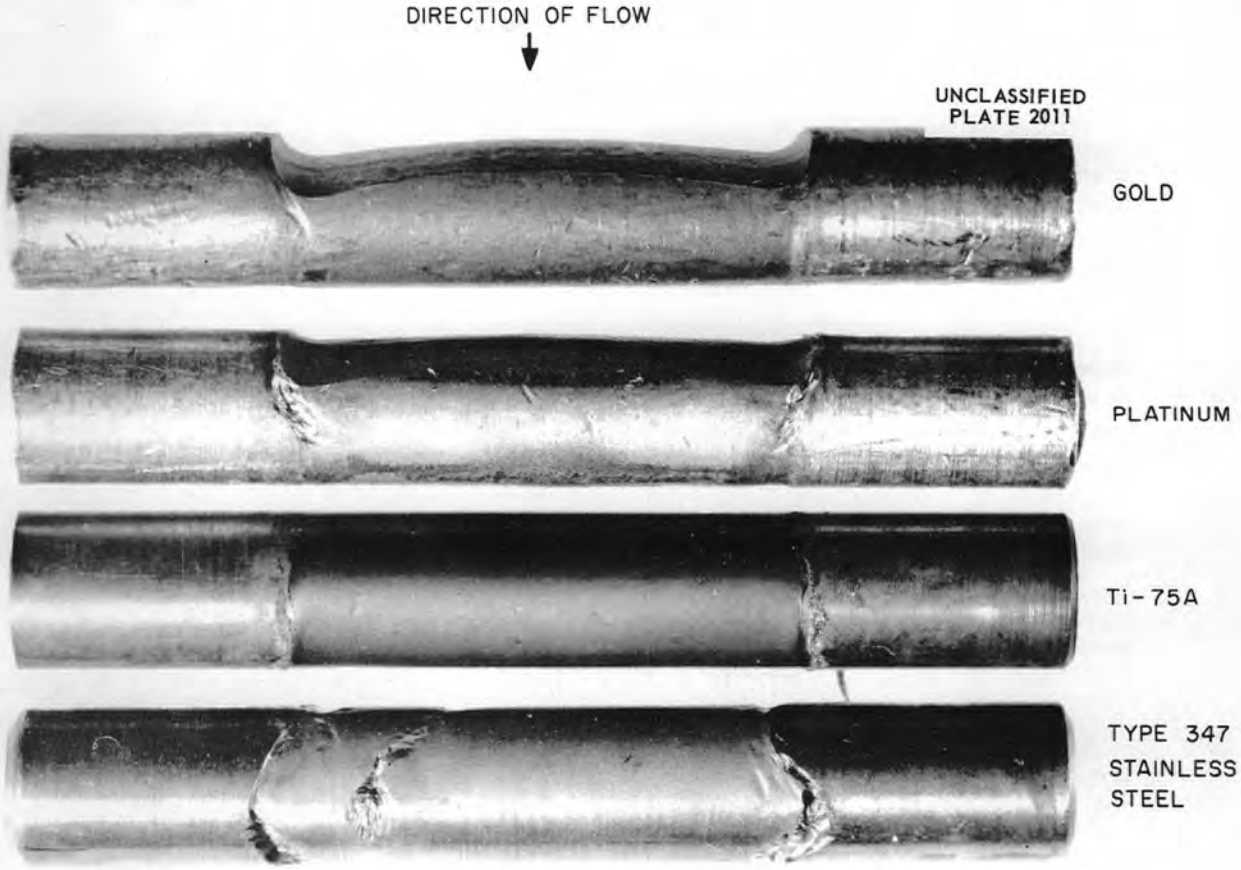

Fig. 13.1. Pin Corrosion Specimens Exposed at 42 fps in Slurry Corrosion Run BS-18.

With the exception of the gold and platinum pins, all specimens were covered with thin, adherent corrosion films. Very small localized areas of bare metal were visible on several specimens of the austenitic stainless steel pins exposed at a velocity of 42 fps. These areas were located principally on the upstream surfaces of the specimens.

The unusually increased attack noted at the higher velocity in this run may be regarded as being due primarily to erosion, as evidenced by strong attack on such materials as gold, platinum, and Zircaloy-2. It may serve as an indication of the interacting tendency of the variables in slurry corrosion. Thus the high calcination temperature of the thoria resulted in slurry particles which did not undergo degradation to smaller particle sizes. Although the attack rate by such particles was not excessive at moderate velocities, above certain velocities the particles are estimated to be able to break through flow streamlines to impinge directly on the metal with resultant erosion. The velocity at which this would be predicted to occur would depend on many factors, including particle size, metal specimen size, and flow and fluid characteristics.[2,3]

Thus the handling properties of 1600°C-calcined thoria slurries still appear to be satisfactory, while the corrosion-erosion behavior indicates a requirement for careful control of particle size and flow characteristics to permit the achievement of circulation without undue corrosion.

13.1.4 Attack by Micropulverized Thoria Slurry

The degradation of thoria particles by circulation of aqueous slurries in pump loops has been observed[4,5] to result in smaller particles and reduced corrosion rates, in the case of thoria calcined at 800°C. It was, therefore, of interest to ascertain whether useful effects could be obtained by reducing the thoria particle size by grinding prior to loop circulation, and thus produce a less aggressive thoria of more uniform properties and behavior.

One convenient apparatus for grinding thoria in substantial quantities after calcination is the Mikro-pulverizer. A quantity of thoria (batch LO-27) prepared by the Chemical Technology Division from thorium oxalate precipitated at 70°C, calcined at 800°C, and ground using the Mikro-pulverizer, has been obtained.

The results of one previous test, run CS-38, in which an oxygenated slurry of the batch LO-27 (800°C-calcined) micropulverized thoria was circulated at 300°C at an average concentration of 591 g of thorium per kilogram of water have been reported.[4] Two additional tests, runs CS-39 and CS-40, were made during the quarter at 300°C with batch LO-27 thoria at an average circulating slurry concentration of 932 and 641 g of thorium per kilogram of water, respectively. Oxygen atmospheres were used in both tests. Run CS-39 was made to determine the effect of increased concentration. Run CS-40 was carried out, using the slurry pumped in runs CS-38 and CS-39, to observe the effect of degradation by loop pumping on the thoria.

For run CS-39, the loop was charged to a concentration of 850 g of thorium per kilogram of water by injecting three batches of concentrated slurry into the system during operation at 300°C. The mean particle size of the micropulverized thoria was 1 μ.

Several periods of erratic operation occurred during the test and were attributed to leakage of liquid from the system. After 59 hr of slurry circulation, the run was temporarily stopped to inspect the system for leaks, but none were located. Consequently, the run was resumed, and water was added intermittently, as leakage indications were noted, to maintain proper operating performance. The run was shut down on schedule at 300 hr. As a result of the leakage and water replacement, the average circulating concentration for the run was 932 g of thorium per kilogram of water, as compared with a charge concentration of 850 g of thorium per kilogram of water.

During the routine inspection of the system after shutdown, a small crack was found in a weld (later determined to be faulty) in the venturi barrel inserted in the pump suction line of the

---

[2] D. G. Thomas, *Comments on the Erosiveness of ThO_2 Slurries*, ORNL CF-55-4-36 (April 5, 1955).

[3] C. E. Lapple, "Dust and Mist Collection," p 1013, esp 1022, in *Chemical Engineers Handbook*, 3d ed., ed. by J. H. Perry, McGraw-Hill, New York, 1950.

[4] E. L. Compere *et al.*, *HRP Quar. Prog. Rep. July 31, 1957*, ORNL-2379, p 84.

[5] E. L. Compere *et al.*, *HRP Dynamic Slurry Corrosion Studies: Quarter Ending April 30, 1957*, ORNL CF-57-4-139 (to be published).

main circulating loop. Although no thoria had passed through the microcrack, the insulation on that section of piping was wetted. Presumably leakage had occurred at that location.

Attack of pump components was abnormally high. Possibly as a result of unsteady loop operating conditions, of the 105.9 g of corrosion products (Fe, Cr, Ni) calculated from analyses to be in the circulating slurry, 49 g was contributed from the type 347 stainless steel impeller. The type 347 stainless steel wear rings and pump head were also heavily attacked.

As a result of high attack in the circulating pump, differential system attack rates, calculated from corrosion products detected in samples withdrawn from the system and from the circulating slurry inventory, remained high throughout the run. Incremental attack rates ranged from an initial 25 to a final 4 mpy. The over-all rate for the 300-hr test was 7.3 mpy.

Attack of pin and coupon specimens exposed in the test was moderate (Table 13.1). Rates were comparable to those observed in previous tests made under similar conditions with slurries of unground 800°C-calcined thoria.

During circulation, the pattern of degradation of the thoria particles was similar to that observed in the previous test, run CS-38. Particle breakdown was slower than on slurries that had not been micropulverized. Little detectable degradation was noted until circulation had proceeded for 60 to 70 hr. With unground 800°C-calcined thoria slurries, major degradation normally occurs within the first 30-hr period of circulation. In run CS-38 the final mean particle size of the thoria after 300 hr of circulation was 0.5 μ, whereas in run CS-39 the mean particle size was 0.8 μ at the conclusion of the 300-hr test.

Previous tests in pump loops have shown that a rapid decrease in the rate of attack by aqueous oxygenated slurries of 800°C-calcined thoria occurs after the thoria particles are degraded by circulation.[4,5] It was of interest to determine whether a similar reduction in attack rate occurred with precirculated micropulverized slurry. Therefore the slurries from runs CS-38 and CS-39 were combined and used as the charge for run CS-40. The mean particle size of the combined slurries was 0.8 μ.

The load concentration for run CS-40 was 638 g of thorium per kilogram of water. Operation proceeded routinely at 300°C until a noise developed in the circulating pump. The run was terminated after 168 hr of slurry circulation.

Little variation in circulating slurry concentration occurred during the test. The average concentration was 641 g of thorium per kilogram of water.

After shutdown the pump was disassembled for routine inspection. The type 347 stainless steel impeller, which lost 24 g during the 168-hr test, was heavily attacked along the front hub and on the front surface. The adjacent seal rings, of type 347 stainless steel, were also badly worn. The front Graphitar bearing, worn 0.0433 in., was not re-usable.

The system differential corrosion rate, calculated from corrosion products detected in slurry samples and circulating slurry inventory, showed a gradual downward trend from 7 to 3 mpy during the first 94.8 hr of circulation. After that time the corrosion rate increased sharply to a final value of 48 mpy. The increased rates were apparently the result of the high attack of pump components during the latter period of the run. The over-all loop attack rate for the test was 4.8 mpy.

Specimen corrosion rates, shown in Table 13.1, were moderate. No notable reduction of attack was apparent as a result of using previously pumped micropulverized thoria. For purposes of comparison, data are included in Table 13.1 from an earlier test, run CS-38, in which unpumped micropulverized thoria was circulated at comparable conditions.

It may be concluded that the micropulverization of the thoria used in these tests did not result in lower specimen corrosion rates and may have resulted in somewhat more severe pump attack.

13.1.5 Attack by Sulfated Slurry Circulated at 200°C

Run CS-41 was carried out as a base-line corrosion test under conditions paralleling those of the slurry blanket mockup test SM-2 (ref 6) operated by the Engineering Research Section, and used sulfated slurry circulated in that mockup test. A comparison may also be made with the

[6] L. F. Parsly, Jr., H. L. Falkenberry, and I. M. Miller, *Report of Slurry Blanket Test Run SM-2*, ORNL CF-57-4-87 (April 29, 1957).

results of the field test in run SM-3 (ref 7) reported in Sec 13.1.6. In addition, run CS-41 marks the beginning of the systematic accumulation of slurry corrosion data at 200°C.

The slurry which had been circulated in the mockup test, mostly in the temperature range 170 to 200°C, for a total of 1730 hr was a composite of ten batches of ORNL-produced, LO-series thoria which had been prepared from 70°C-precipitated thorium oxalate calcined at 800°C. Sulfuric acid had been mixed with the slurry, as a possible deflocculating agent, for the mockup test. By chemical analysis, the slurry circulated in run CS-41 contained ~1750 ppm SO_4^{--} based on thorium. The mean particle size of the thoria was 0.9 μ.

To parallel as closely as possible the conditions of the mockup test, loop CS was operated, with steam pressurization, at 200°C with pressurizer temperatures of 240 to 280°C. Furthermore, low concentrations of oxygen were maintained throughout the run. The charge concentration for the run was 734 g of thorium per kilogram of water, based on a circulating volume estimated from survey-meter scans indicating the thoria level in the pressurizer. The first sample indicated agreement with this charge concentration. However, thoria was indicated by subsequent gamma survey-meter scans to have accumulated in the pressurizer and in a low-velocity sample barrel. The circulating concentration was, consequently, decreased until the thoria in the pressurizer was dislodged by a gas addition at hour 172. The run was continued for a total of 300 hr with an average circulating concentration of 488 g of thorium per kilogram of water.

During the test the average concentration of dissolved oxygen in samples withdrawn from the loop was 62 μg per milliliter of slurry. Slurry pH values, measured at room temperature, ranged from 7 to 5. The slurry supernatant liquid contained 6 to 11 ppm SO_4^{--}.

When the circulating pump was disassembled, the type 347 stainless steel pump scroll, impeller, and thermal barrier had a bright metallic appearance. The scroll and thermal barrier were highly polished. Numerous pits were located on both surfaces immediately downstream of the balance pads. The impeller, which lost 20 g during the test, was markedly eroded along the periphery on both front and back surfaces. On microscopic examination the eroded areas appeared to consist of numerous conical pits ranging in depth from 12 to 24 mils and interconnected by narrow valleys 4 to 6 mils in depth. A photograph of the impeller is shown in Fig. 13.2. The type 347 stainless steel front and rear seal rings in the pump were worn 34 and 20 mils, respectively. The Graphitar pump bearings were not measurably worn.

Loop differential attack rates ranged from an initial value of 30 mpy gradually downward to a final rate of 2 mpy. The average system attack rate for the 300-hr period was 3 mpy.

Specimen attack rates (Table 13.1) were generally low. Exceptions were the high attack rates shown by mild-steel specimens.

Austenitic stainless steels displayed rates from 0.3 to 27 mpy over the velocity range 19 to 71 fps. Rates of ferritic stainless steels exposed at velocities of 23 to 42 fps ranged from 2 to 10 mpy. Zircaloy-2 and titanium alloys showed rates from 0.1 to 1 mpy over the velocity range 19 to 42 fps.

Carbon steel showed substantially higher corrosion in this test, with pin corrosion rates ranging between 100 and 560 mpy for velocities from 21 to 42 fps and with 9 mpy noted for coupons at 19 fps. The higher corrosion rates of this material are believed to be associated with the addition of sulfuric acid to the slurry.

At the test conditions very thin corrosion films were formed on the stainless steel, titanium, and Zircaloy-2 specimens. The films, which were dull gray, were adherent but appeared to be porous in nature. Loose, voluminous films were formed on the mild-steel specimens.

The results of this experiment are in general agreement with the observations made during the slurry blanket mockup run, SM-2, and the field test of run SM-3, reported in Sec 13.1.6. In these tests also, impeller pitting, bright stainless steel surfaces, and high carbon-steel corrosion rates were noted. Further studies at 200°C will be required before the causes of all such effects can be reliably assigned.

13.1.6 Field Corrosion Tests

In cooperation with the Engineering Research Section, two sets of corrosion specimens were exposed in run SM-3 (ref 7) of the slurry blanket

[7] L. F. Parsly, Jr., *et al.*, *Report of Slurry Blanket Test Run SM-3*, ORNL CF-57-10-2. (to be published).

UNCLASSIFIED
PHOTO 29920

DETAIL OF ERODED SURFACE
(12X)

Fig. 13.2. Erosion of Type 347 Stainless Steel Pump Impeller; Slurry Run CS-41. Reduced 18%.

mockup.[6] One set of 16 in-line coupon-type corrosion specimens and a set of 8 stress specimens were exposed in the 948-hr test.

The in-line specimens, which were exposed at a relative velocity estimated as approximately 20 fps, consisted of four coupons each of type 347 stainless steel, SA-212-B carbon steel, titanium RC-55, and Zircaloy-2. The stress specimens, placed in the system pressurizer, consisted of two samples each of type 347 stainless steel, type AM-350 stainless steel, titanium AV, and Zircaloy-2. One specimen of each of the materials was suspended in the gas-vapor space of the vertical pressurizer, while the comparison specimens were placed on the lower section of the specimen holder, which was normally below the level of liquid in the pressurizer. Flow over these specimens was negligible. The coupons, contained in a type 347 stainless steel holder, were not insulated. The stress specimens were mounted, uninsulated, on a type 347 stainless steel holder by using type 347 stainless steel bolts.

Each coupon was machined to the dimensions of 2.35 × 1.00 × 0.20 in. from special ¼-in. plate from controlled-materials stock. Projecting tabs were machined on both ends of each coupon for appropriate clamping in the specially built holders for insertion in the mockup.

The in-line assembly is shown, after removal from the test, in Fig. 13.3. It was inserted in a flanged section of 3-in. sched-40 pipe in the main loop stream of the mockup. The flow rate past the specimens was 360 gpm except for a 6-hr period when the circulating pump was operated at a slightly reduced speed by using a motor-generator set.

The specimens were exposed for a period of 270 hr in oxygenated water before slurry charging was begun. Total exposure to slurry was 678 hr.

During slurry loading and circulation, loop temperatures varied from 170 to 210°C. The system was initially charged, at 170°C over a period of 160 hr, to 238 g of thorium per kilogram of water. After 210 hr of circulation at 200°C at that concentration, an additional loading, which required 36 hr, was made to increase the charge concentration to 500 g of thorium per kilogram of water. The mockup ran at the higher concentration for 161 hr at 170°C and an additional 91 hr at 200°C.

The slurry charges consisted of a number of batches of LO-series 800°C-calcined thoria to which was added 3700 ppm SO_4^{--}, based on thorium, as sulfuric acid. The pH of the slurry ranged from 5.4 to 6.3 during the test.

An oxygen atmosphere was maintained in the system for the first 780 hr of the test. Hydrogen was detected in samples withdrawn from the system during the final 168-hr period of operation.

Corrosion rates, except for SA-212-B carbon steel, were low. Attack of type 347 stainless steel ranged from 0.18 to 0.28 mpy on three specimens; the fourth, the coupon at the entrance in the specimen array, showed 1.9 mpy. The higher attack of that coupon was attributed to

UNCLASSIFIED
PHOTO 29443

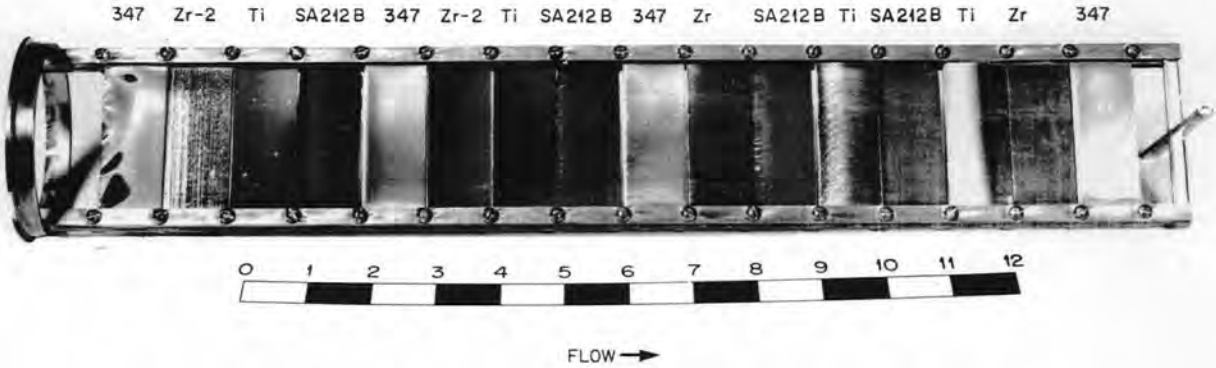

Fig. 13.3. In-Line Corrosion Specimens After Exposure in Slurry Blanket Mockup Run SM-3.

entrance effects and increased abrasive attack by the slurry particles. The pattern of attack may be seen in Fig. 13.3. Attack of titanium RC-55 ranged from 0.16 to 0.26 mpy; Zircaloy-2, from 0.10 to 0.24 mpy; and SA-212-B carbon steel, from 455 to 637 mpy. The high attack of SA-212-B steel appeared to be due, in part, to galvanic action between the uninsulated coupons and the stainless steel specimen holder. Both ends of each specimen were markedly corroded. It is also probable that the presence of sulfuric acid in the slurry contributed to the aggressive attack of the carbon steel.

No evidence of stress-corrosion cracking was observed with any of the specimens exposed in the pressurizer. One specimen of type 347 stainless steel, exposed in the gas-vapor space, and one specimen of type AM-350 stainless steel, which was immersed in the liquid, showed slight weight losses. Corrosion rates of these specimens were 0.11 and 0.47 mpy, respectively. No detectable weight losses occurred with the other specimens.

The results of this field test are in good general agreement with the results of loop run CS-41, reported in Sec 13.1.5.

13.2 TOROIDS

13.2.1 Introduction

The effect of hydrogen and oxygen atmospheres on the attack by slurries of 1600°C-calcined thoria in toroids has been studied. In the tests in which hydrogenated slurries were used, type 347 stainless steel, titanium 75A, and Zircaloy-3A displayed higher attack rates. A marked reduction in attack of carbon steel was noted.

Normal corrosion rates of type 347 stainless steel, titanium 75A, and Zircaloy-3A were observed in tests made in toroids to study the effect of the addition of uranyl sulfate to aqueous oxygenated slurries of 800°C-calcined thoria. Attack of SA-212-B mild steel was increased approximately tenfold.

In toroid runs made to investigate the attack by slurries prepared from thorium oxide before and after micropulverization, slightly higher than normal attack was observed in tests using the attrited oxide. Slurry spheroids were formed in tests in which the unground thoria was circulated, but none were detected in the tests with micropulverized thoria.

Low attack rates were observed with slurries of thoria prepared from jet-precipitated thorium oxalate which was calcined at 650, 1200, 1400, and 1600°C.

Attack rates in toroid tests were in good agreement with corrosion rates obtained in loop runs with slurries of 1600°C-calcined thoria. No apparent degradation of the thoria particles occurred in any of the tests.

Low-to-moderate attack rates were obtained in toroid runs in which were circulated slurries prepared of recalcined, 24-μ thoria spheres. Metal attack rates increased with increased slurry concentration.

13.2.2 Tests with Thoria Slurries Containing Uranyl Sulfate

In a breeder reactor employing a thorium oxide slurry blanket and uranyl sulfate solution in the core, it is conceivable that the uranium solution could contaminate the slurry blanket. Furthermore, experiments involving the addition of uranium trioxide, thorium sulfate, or sulfuric acid to various slurries suggested that observation of the effects of suitable uranyl sulfate additions would be of interest. Three toroid runs were made to ascertain what effects, if any, the addition of uranyl sulfate would have on the corrosivity and circulation properties of a circulating slurry.

Slurries of 800°C-calcined thoria containing 0.02 *m* uranyl sulfate were circulated for periods of 300 hr at 250°C and 26 fps. For comparison, companion toroids contained solutions of uranyl sulfate, slurries with comparable levels of sulfate added as thorium sulfate, and slurries without additives. All tests were made with oxygen atmospheres. Pin specimens of type 347 stainless steel, titanium 75A, SA-212-B carbon steel, and Zircaloy-3A were exposed in each test. Results are shown in Table 13.2.

Within the limits of experimental error, no notable differences in attack rates of type 347 stainless steel, titanium 75A, or Zircaloy-3A were observed with slurries to which uranyl sulfate or thorium sulfate had been added. However, attack of SA-212-B carbon steel in these tests was increased approximately tenfold, presumably due to the lower pH of the slurries containing the sulfate additives.

Table 13.2. Summary of Toroid Experiments Studying the Effect of Uranyl Sulfate as an Additive to Aqueous Thorium Oxide Slurries

Batch D-17, 800°C-calcined thorium oxide, average diameter 2.1 μ
Temperature: 250°C
Relative velocity: 26 fps
Atmosphere: oxygen

Concentration (g Th/kg H_2O)	Additive and Concentration	pH of Slurry	Corrosion Rate,* mpy			
			347 SS	SA-212-B Steel	Zircaloy-3A	Ti-75A
500	UO_2SO_4, 0.02 *m*	4.5	0.2	13.7	0.2	4.6
500	UO_2SO_4, 0.02 *m*	4.5	1.3	15.4	0.1	1.1
500	UO_2SO_4, 0.02 *m*	4.9	0.9	16.9	0.3	1.1
500	UO_2SO_4, 0.02 *m*	4.7	1.7	15.6	0.3	1.4
None	UO_2SO_4, 0.03 *m*	2.8	3.0	41.6	Weight gain	Weight gain
None	UO_2SO_4, 0.03 *m*	3.9	1.3	38.6	Weight gain	0.2
500	$Th(SO_4)_2$, 0.006 *m*	5.8	1.0	3.1	0.1	0.4
500	None	6.2	1.7	2.4	0.3	1.0
500	None	7.3	1.5	3.4	0.3	1.2
500	None	8.2	2.3	4.5	0.6	2.1

*Based on exposed area, uncorrected for slug flow. 45% fill at 250°C.

It was interesting to note that in the tests employing only uranyl sulfate the corrosion rates of type 347 stainless steel and SA-212-B were higher than in those tests in which a mixture of thorium oxide and uranyl sulfate was circulated. In the latter tests the pH values of the solutions were 2.8 and 2.9, as compared with a pH range of 4.5 to 4.9 for the mixtures. After circulation most of the uranyl sulfate was found, by chemical analysis, to be associated with the slurry solids, rather than in the supernate.

No changes were detected in slurry properties as a result of the addition of uranyl sulfate.

13.2.3 Attack by 1600°C-Calcined Thoria Slurries in Hydrogen and Oxygen Atmospheres

The results of several toroid tests with oxygenated slurries of 1600°C-calcined thoria were reported previously.[8] Additional tests were made during the quarter to compare the corrosivity of these slurries in hydrogen and in oxygen atmospheres. Runs were made at 250°C and 26 fps at concentrations of 500 and 1000 g of thorium per kilogram of water using slurries of 1600°C-calcined batch TO-10-1000 thorium oxide.

In four tests, toroids were charged with slurries which contained 0.08 *M* hydrazine, as an oxygen scavenger, and hydrogen at atmospheric pressure. For the comparison tests, oxygen atmospheres were provided by the thermal decomposition of hydrogen peroxide which was added to the slurries. The results are shown in Table 13.3.

It should be noted that the pH values of the hydrogenated slurries were about five units higher (pH 10 to 11) than those of the oxygenated slurries (pH 5 to 6), owing to the presence of hydrazine and its thermal decomposition product, ammonia. With the exception of the SA-212-B carbon-steel specimens, higher corrosion rates were observed with the hydrogenated slurries. A marked reduction in attack of carbon steel occurred in the hydrogenated runs.

[8] E. L. Compere *et al.*, *HRP Quar. Prog. Rep. April 30, 1957*, ORNL-2331, p 96, esp 109.

Table 13.3. Attack by 1600°C-Calcined Thoria Slurries in Hydrogen and Oxygen Atmospheres

Toroids: type 347 stainless steel
Temperature: 250°C
Velocity: 26 fps
Thoria: batch TO-10-1000; recalcined at 1600°C; average particle diameter, 1.2 μ

Concentration, g Th/kg H_2O	500				1000			
Atmosphere	O_2		H_2(0.08 *M* N_2H_4)		O_2		H_2(0.08 *M* N_2H_4)	
pH of slurry (postrun)	5.6	5.2	10.5	10.8	5.8	5.9	10.5	10.3
Corrosion rate,* mpy								
Titanium 75-A	1.3		2.8		1.5		1.6	
Zircaloy-3A	WG**		0.9		WG**		0.4	
SA-212-B steel	123		3.7		113		2.1	
Type 347 SS	1.5	1.3	19.7	6.5	2.7	4.1	10.3	14.0
		3.1		9.7		3.9		13.8
		2.5		6.1		6.0		14.2
		2.3		10.0		2.8		9.9
347 SS toroid	0.2	0.2	5.8	1.6	0.5	0.5	2.5	4.6

*Based on exposed area, uncorrected for slug flow. 45% fill at 250°C.
**WG = weight gain.

No detectable change in particle size was observed in any of the tests.

13.2.4 Pilot Tests with Experimental Preparations of Thoria

In some cases prior to certain 100A pump loop tests, and also in cooperation with groups in the Chemical Technology Division and the Engineering Research Section who are participating in the development of reactor slurry systems, toroid pilot runs were made with aqueous slurries of six different experimental preparations of thoria. All tests were run for 300 hr at 26 fps and 250°C with oxygenated slurries. Data from these runs are summarized in Table 13.4.

One series of tests was made with batch LO-22 thorium oxide, which is currently being circulated in run 200A-14 in the Engineering Research Section[9] (see Sec 10.3). The thoria was recalcined at 1600°C for 2 hr and degraded by passing the dry powder four times through a Mikro-pulverizer. The mean particle size of the batch was 2.2 μ.

Tests were made at concentrations of 20, 200, 500, and 1000 g of thorium per kilogram of water. Generally mild attack of type 347 stainless steel, titanium 75A, SA-212-B, and Zircaloy-3A occurred in all tests. The attack rates observed for type 347 stainless steel and titanium 75A in the test with slurry at a concentration of 500 g of thorium per kilogram of water were slightly higher than those in the test made at a concentration of 1000 g of thorium per kilogram of water. During microscopic examination it was noted that localized abrasive attack was pronounced on the pins exposed to the 500-g/kg concentration. Bright areas of bare metal were seen on the upstream surfaces of most specimens exposed at the other concentrations, but the attack was considerably less severe.

Two preparations of 800°C-calcined thoria, which were prepared for 100A loop tests, were circulated in toroids during the quarter. Both batches, LO-27

[9] R. B. Korsmeyer *et al.*, *HRP Quar. Prog. Rep. July 31, 1957*, ORNL-2379, p 52, esp 56.

Table 13.4. Attack by Thoria Slurries of Experimental Preparations

Test conditions: 300 hr, 26 fps, 250°C, oxygen atmosphere

Thoria Batch Designation	Calcination Temperature (°C)	Slurry Concentration (g Th/kg H_2O)	Particle Size (μ)		Slurry pH, Postrun	Corrosion Rate,* mpy				
			Prerun	Postrun		347 SS	SA-212-B Steel	Ti-75A	Zircaloy-3A	347 SS Toroid
LO-22 micropulverized	1600	20	2.2		4.5	WG**	0.2	WG**	WG**	0.1
		200	2.2	1.6	4.2	2.3	0.2	1.2	WG**	0.7
		500	2.2	1.7	4.9	4.1	0.2	2.5	0.3	1.2
		1000	2.2		5.9	2.4	2.1	1.6	0.4	0.6
LO-27 before micropulverization	800	500	4.0	0.7***	7.2	WG**	2.2	<0.1	WG**	0.2
		1000	4.0	12.0***	7.2	1.1	1.9	WG**	1.6	0.4
LO-27 micropulverized	800	500	1.0	1.0	7.0	1.1	2.8	1.0	0.1	0.3
		750	1.0	1.7	7.0	3.5	2.8	3.2	0.3	2.0
		1000	1.0	1.0	6.4	7.5	3.8	3.8	2.3	1.5
LO-28 before micropulverization	800	500	3.7	7.0***	6.7	0.7	10.7	WG**	WG**	0.7
		1000	3.7	8.5***	7.0	2.5	10.1	WG**	0.9	0.4
Jet precipitated	650	1000	0.6	0.6	6.5	2.4	2.1	1.6	0.4	0.6
	1200	642	0.5	0.8	4.8	1.0	1.7	0.8	0.0	0.3
	1400	642	0.5	0.9	5.0	0.9	6.8	0.3	0.1	0.4
	1600	642	0.9	1.2	6.0	1.4	9.7	1.4	3.0	0.7
TO-10-1000 and LO-17, recalcined	1600	500	1.2	1.2	4.9	2.6	3.6	0.8	0.5	0.6
		750	1.2	0.9	5.3	2.4	5.7	1.0	0.7	0.5
		1000	1.2	1.0	5.5	3.5	2.5	3.3	0.8	1.0
		1500	1.2	0.9	5.3	2.8	3.9	1.1	1.2	0.6

*Based on exposed area, uncorrected for slug flow; 45% fill at 250°C; pin specimens defilmed.

**WG = weight gain.

***Spheroids formed during circulation.

and LO-28, were prepared in the pilot plant of the Chemical Technology Division by precipitation of thorium nitrate with oxalic acid at 70°C and calcination for 4 hr at 800°C. Each preparation was to be degraded, prior to loop circulation, by passing the dry powders twice through a Mikropulverizer. It was of interest to test each material before and after micropulverization.

In both runs which circulated these preparations before micropulverization, thoria spheroids formed during circulation. Attack rates were moderate except with SA-212-B mild-steel specimens exposed in the test with LO-28 slurry at a concentration of 500 g of thorium per kilogram of water. These specimens showed a rate approximately five times greater than the rate for duplicate specimens exposed to the LO-27 thoria slurry. Both pins were severely pitted.

Thin, hard, translucent films of thoria formed on all specimens exposed in these runs. The deposits, shown in Fig. 13.4, were characteristic of those films which usually occur when spheroids are formed. Somewhat heavier deposits were noted in the run with LO-27 thoria. It is possible that the lesser attack of mild-steel specimens exposed in this test may be attributed to the heavier thoria deposits formed on the specimens in that run.

In the tests with LO-27 micropulverized-thoria slurry, no spheroids were formed. It is interesting to note that attack rates were generally slightly higher in these tests than with slurries of the unmicropulverized preparation, even though the micropulverization had reduced the mean particle size of the batch from 4 μ to 1 μ. Unusually high attack of pump components has also occurred in 100A loop tests with this batch (see Sec 13.1.4).

One test was completed during the quarter with slurries prepared of thoria produced by calcining jet-precipitated thorium oxalate. The thoria, furnished by the Chemical Technology Division, had a mean particle size of ~0.6 μ (see Sec 20.1.2).

Portions of the pilot lot were calcined at 650, 1200, 1400, and 1600°C and circulated as oxygenated aqueous slurries in a 300-hr test at 250°C and 26 fps. As shown in Table 13.4, relatively low attack rates resulted in each test. There was little change in thoria particle-size distribution as a result of circulation.

Corrosion rates for type 347 stainless steel, titanium 75A, SA-212-B carbon steel, and Zircaloy-3A were in close agreement with rates obtained at similar test conditions in other toroid runs[10,11] using thorium oxide prepared from 10°C-precipitated $Th(C_2O_4)_2$. Slurry of the jet-precipitated oxide calcined at 1600°C which had a higher mean particle size, 0.9 μ, gave slightly higher attack rates.

Prior to loop tests, pilot toroid runs were made with oxygenated slurries of the 1600°C-calcined mixed-oxide charge for 100A loop tests BS-17 and BS-18 (see Sec 13.1.3). The tests were made at the standard condition: 300 hr, 250°C, and 26 fps. Although the toroid tests do not afford a direct comparison with pump-loop run BS-18, which was made at 300°C, the specimen rates observed at 26 fps in the toroid test, when corrected for slug flow, closely approximate the rates obtained in loop run BS-18 at 21 fps.

13.2.5 Toroid Circulation Tests with Thoria Spheres

Recently a group of toroid runs was made to investigate the circulation behavior and attack by aqueous slurries of thoria spheres. The spheres used in these tests were obtained by calcining slurry spheroids produced, inadvertently, in 100A loop run BS-11 in which batch LO-14 thorium oxide was circulated.[12] The spheroids produced in this run were quite uniform in size. After they were washed, dried, and recalcined at 1200, 1400, or 1600°C, their mean diameters, determined by sedimentation in 19.5 cp glycerol solution using neutron activation analysis, were 23 to 24 μ. The density of the spheres, determined by use of a pycnometer and by using carbon tetrachloride, benzene, or water, varied from 7.8 to 8.5. The specific surface area, measured by nitrogen adsorption, ranged from 0.9 to 0.1 m^2/g.

To determine the integrity of the spheres, initial scouting tests were made with slurries of the 1200, 1400, and 1600°C firings. The tests were made for 300 hr at 250°C and 26 fps using oxygen atmospheres. No detectable degradation of the spheres was observed. Attack of corrosion specimens in these tests was very low.

---

[10] J. P. McBride *et al.*, *HRP Quar. Prog. Rep. July 31, 1957*, ORNL-2379, p 145, esp 152.

[11] E. L. Compere *et al.*, *HRP Quar. Prog. Rep. April 30, 1957*, ORNL-2331, p 96, esp 109.

[12] E. L. Compere *et al.*, *HRP Quar. Prog. Rep. April 30, 1957*, ORNL-2331, p 96, esp 101.

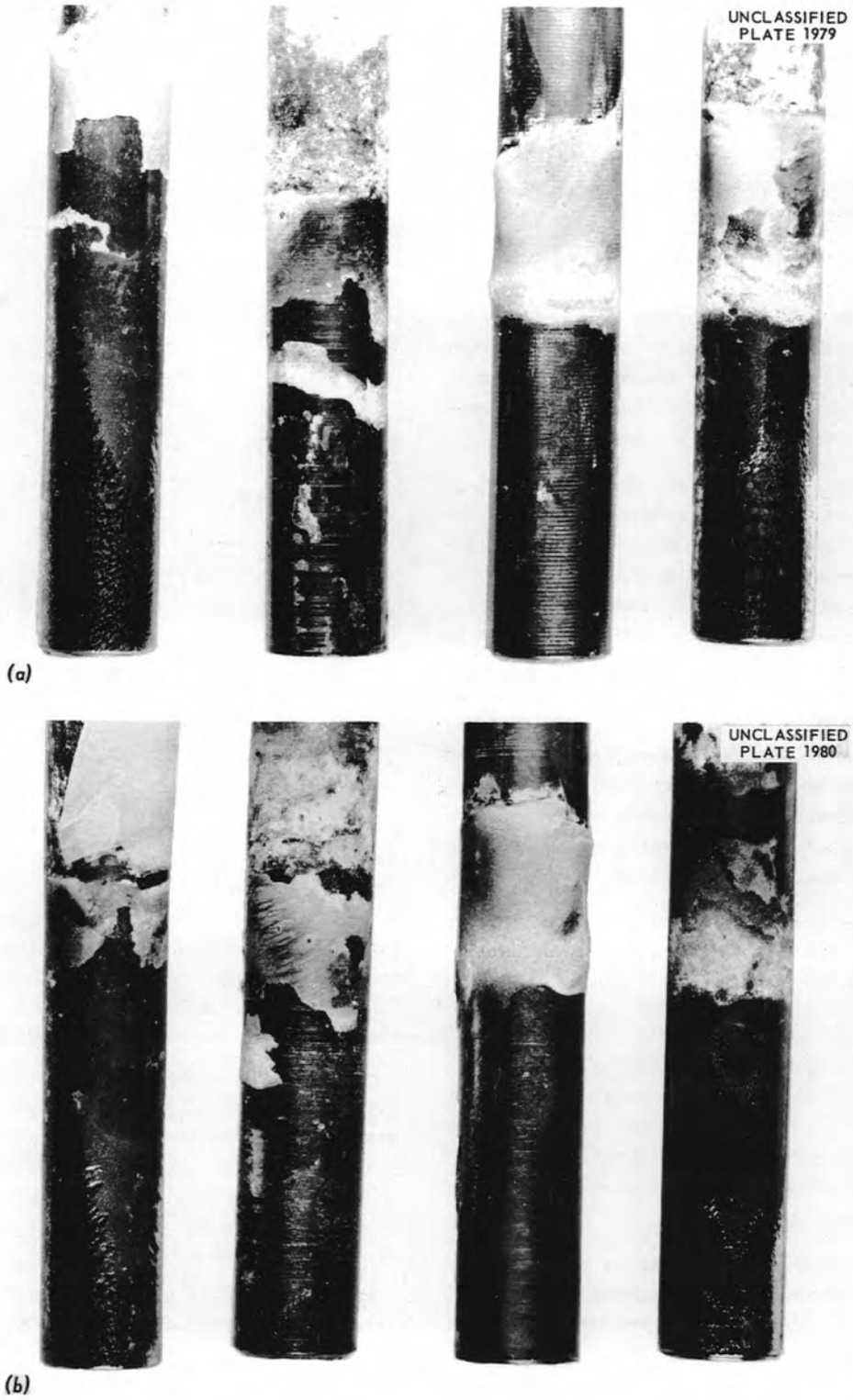

Fig. 13.4. Toroid Pins Exposed in Tests with Thoria at a Concentration of 1000 g of Thorium per Kilogram of H_2O. (*a*) Batch LO-27 thoria. (*b*) Batch LO-28 thoria.

A series of runs was then conducted with 1600°C-calcined material to study the effects of slurry concentration and circulation velocity on the degradation of, and attack by, the spheres. Tests were run in oxygen atmospheres at concentrations of 10 to 1430 g of thorium per kilogram of water and at relative velocities of 10 to 29 fps. Each test was run for 300 hr.

No detectable particle degradation was observed in the runs. Occasionally, microscopic examination of the circulated slurries revealed isolated chipped or cleaved spheres, but in none of the tests were there a sufficient number of these to significantly change the particle-size distributions that were determined by sedimentation analysis.

Thin, glassy films of thoria were deposited on the surfaces of the pin specimens in many of the tests. These films presumably resulted from the extremely fine material (0.1 to 0.05 μ) which was not removed by washing the material before re-calcination. Usually these deposits appeared to have formed and then to have been worn away from the upstream surfaces of the specimens. In the runs made at the higher concentrations and at the higher velocities, the upstream surfaces of the pins were polished, whereas the downstream surfaces were glazed. In the runs at low velocity and concentration, the pins were usually uniformly coated with a thin deposit of thoria.

Attack rates at all concentrations and velocities were low. Metal weight losses of specimens of type 347 stainless steel and SA-212-B carbon steel were consistently higher than losses of Zircaloy-3A or of titanium 75A. However, the corrosion rates calculated for all specimens were normally less than, or only slightly above, 1 mpy. Corrosion rates of SA-212-B steel increased from 2 to 9 mpy in some tests, as a result of random pitting or localized undercutting at the roots of the specimens.

A mild but definite increase in attack of all alloys was noted as the concentration of slurry was increased. A slight velocity effect may also be present, but this is less clear. Data which depict the changes in the attack of type 347 stainless steel specimens at the various velocities and slurry concentrations investigated are shown graphically in Fig. 13.5.

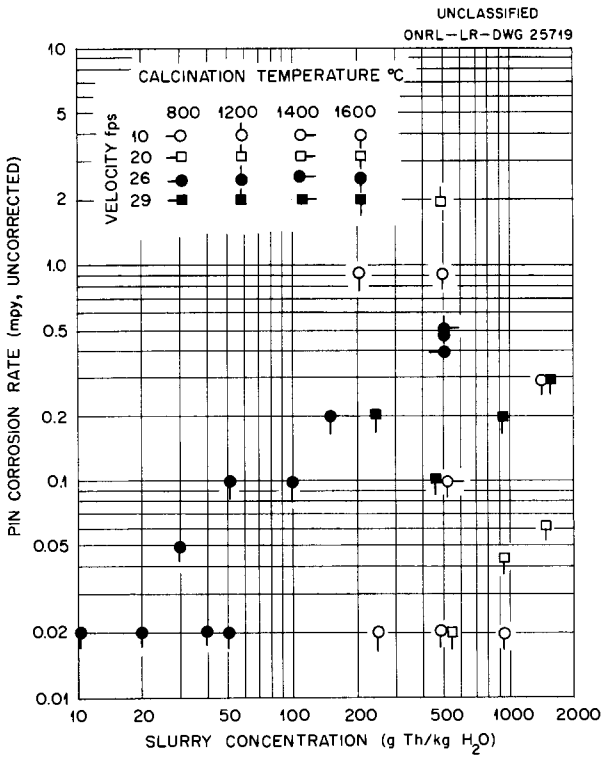

Fig. 13.5. Corrosion of Type 347 Stainless Steel Pins in Toroid Circulation Tests of Thoria Spheres.

Because of the very low attack observed in these tests, considerable relative scatter in data points is to be expected. Normal metal weight losses of the defilmed specimens ranged from 0.2 to 5 mg; therefore relative experimental errors were high. It appears evident, however, that specimen attack rates were affected by changes in both concentration and velocity.

Further confirmatory evidence indicating that the spheres were circulated in the tests as homogeneous or near-homogeneous slurries was obtained by taking high-speed photographs, using a Strobotac attachment on the camera, of an aqueous slurry of the spheres circulated in a plastic toroid at room temperature.

Figure 13.6 is a photograph of a slurry of the spheres at a concentration of 200 g of thorium per kilogram of water during circulation at 20 fps. A well-defined slug of slurry may be seen in the left half of the toroid, with a typical turbulent trailing end in the upper right-hand section of the photograph.

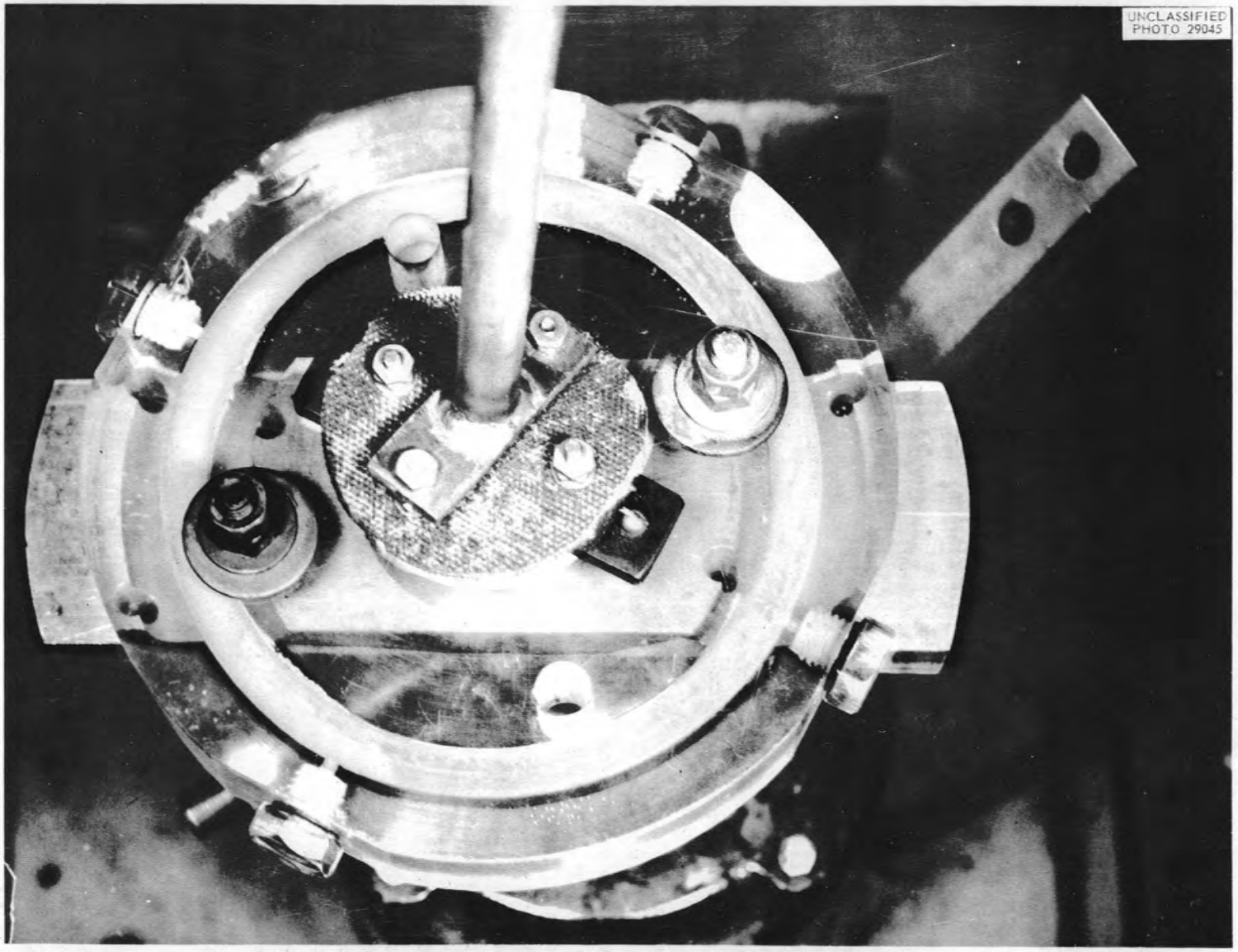

Fig. 13.6. Slurry of Thoria Spheres Circulating in Plastic Toroid at 20 fps.

13.3 IN-PILE AUTOCLAVE SLURRY TESTS – LITR

13.3.1 Development and Construction

In order to obtain radiation-corrosion data with thorium oxide slurries of interest in the HR program and to evaluate the effect of reactor radiation on the physical properties of thorium oxide slurries, the feasibility of using the present in-pile rocking autoclave in a manner similar to the in-pile solution tests is being investigated.

The apparatus used to rock the slurry test autoclave is the same as that used in the autoclave solution experiments, but modified to rock the autoclave through an angle of 120 deg at a rate of 18 cycles/min. The autoclave solution experiments have been rocked through an angle of 60 deg at a rate of 9 cycles/min. The increased agitation (rocking angle and rate) was found necessary to prevent settling of the thorium oxide in preliminary tests made in a Lucite model of the autoclave.

A standard HB-6 autoclave assembly[13,14] containing pin-type corrosion test specimens and charged with a thorium oxide slurry to a concentration of 500 g of thorium per kilogram of water has been successfully rocked for 90 hr at 280°C and 1600 psia in an out-of-pile test. No plugging of the capillary-tube line connecting the autoclave to the pressure transmitter was observed during operation or venting. The autoclave was loaded with dry thorium oxide, water, and the pressurizing solution of hydrogen peroxide. The thorium oxide used in this test was from batch TO-10-1000 which was recalcined at 1600°C and subsequently pumped for approximately 200 hr at 300°C in 100A loop runs BS-15 and BS-16. The average particle size of the material was 1.3 μ. From this test it appears feasible to expose a thorium oxide slurry in the standard HB-6 autoclave assembly. In-pile experiments in the LITR are now being planned for the same thorium oxide preparation as in the out-of-pile test.

13.4 IN-PILE SLURRY TOROID

13.4.1 Development Engineering

The major effort during the past quarter was directed toward the "rotating-arm" model[15] in-pile toroid rotator. Preliminary operation of a unit which had both gimbals frames enclosed within a cylindrical retaining structure, mentioned previously,[16] demonstrated that undesirable operational vibrations could be eliminated during high-speed operation by positioning properly sized counterweights along the rotator arms. However, initial runs indicated that a constant-velocity universal joint instead of a fork-and-tee type is required to obtain sustained long-term operation. Only 8 hr of continuous service at 950 to 1000 rpm was achieved before operational difficulty necessitated a shutdown. During this 8-hr test period, mechanical wear of the rotator mechanism was evidenced by a continual increase in the diameter of the toroid-ring rotational circle. The wear occurred in the radial thrust bearings installed in the gimbals and was believed to have been caused by indeterminable forces created in the fork-and-tee universal joint used to connect the rotator arms. To counteract this difficulty, a rotator model containing a constant-velocity universal joint and heavy-duty spherical bearings in the gimbals has been fabricated and is being assembled for test and evaluation.

Tests to develop a suitable heating and cooling system for temperature control of the toroids during in-pile operation are still in progress. Based on the encouraging preliminary results obtained with air-water coolant mixtures in $\frac{1}{8}$-in.-dia tubing wrapped around the toroid rings,[17] attempts were made to further increase the cooling capacity of the system by casting the $\frac{1}{8}$-in. cooling tubing in aluminum around the toroids for improved over-all heat transfer. Resistance heating wire was wrapped around the outside of the aluminum casting. Repeated failure of the heating wire prevented sufficient data from being obtained. However, preliminary values indicate that the increased cooling capacity obtained with the cooling coils cast in aluminum is not sufficient to remove the additional gamma-heat load which would be created in the added mass of the

---

[13] G. H. Jenks *et al.*, *HRP Quar. Prog. Rep. July 31, 1957*, ORNL-2379, p 99, esp 114–115.

[14] K. S. Warren and R. J. Davis, *In-Reactor Autoclave Reactor Studies – LITR. I. Outline of Methods and Procedures*, ORNL CF-57-5-110 (May 22, 1957).

[15] E. L. Compere *et al.*, *HRP Quar. Prog. Rep. April 30, 1957*, ORNL-2331, p 110, Fig. 12.12.

[16] E. L. Compere *et al.*, *HRP Quar. Prog. Rep. July 31, 1957*, ORNL-2379, p 84, esp 98.

[17] E. L. Compere *et al.*, *HRP Quar. Prog. Rep. July 31, 1957*, ORNL-2379, p 84.

aluminum casting during in-pile operation. This method of cooling requires further evaluation.

A second method of toroid temperature control investigated during the past quarter involves isolating the toroid bundle in a controlled ambient temperature. A heated and/or cooled air-steam or air-water mixture is used to maintain the ambient temperature and thus the toroid temperature. An ORR in-pile-loop type of heater-cooler unit[18] was used to control the temperature of the air-steam mixtures. One test of this method was encouraging, and additional tests will be made.

---

[18] T. H. Mauney and H. C. Savage, *Test Results on a Heater-Cooler Unit for the ORR In-Pile Loop*, ORNL CF-57-6-66 (June 8, 1957).

14. RADIATION CORROSION

G. H. Jenks H. C. Savage

A. L. Bacarella
J. E. Baker
S. E. Bolt
J. W. Brown
R. J. Davis
V. A. DeCarlo
B. O. Heston
D. T. Jones
R. A. Lorenz
J. R. McWherter
A. R. Olsen
J. A. Russell
M. D. Silverman
W. C. Ulrich
F. J. Walter
K. S. Warren
A. Weitzberg
S. H. Wheeler
W. C. Yee

14.1 IN-PILE LOOPS

14.1.1 Development and Construction

(a) HB-2 Loop Package. – The construction and pretreatment of loop L-2-19 (ref 1) were completed, and the loop is now in operation in beam hole HB-2 of the LITR.

Components for loop L-2-22 are being fabricated. This will be a stainless steel loop containing a large variety of zirconium-alloy corrosion specimens prepared by the HRP Metallurgy Group.

The fabrication of components for loop L-2-23, an all-titanium loop, was completed. Assembly of the loop has been deferred.

(b) HB-4 Loop Package. – The construction of loop L-4-21 (ref 1), a type 347 stainless steel loop utilizing a Byron-Jackson 5-gpm pump,[2] was completed, and the loop is undergoing out-of-pile pretreatment and testing. Zircaloy-2 tapered-channel coupon holders in the core and line positions contain Zircaloy-2, titanium 110AT, and type 347 stainless steel corrosion samples. Stress specimens of titanium 110AT and type 430L stainless steel are installed in the core, in-line holder, and pressurizer. Five low-velocity coupon holders[1] in the core and two in the line contain coupon specimens of a variety of zirconium alloys of different heat treatments. Zirconium oxide specimens are also included in the low-velocity holders. One Zircaloy-2 and one type 347 stainless steel coupon are mounted in the forward section of the core, where the neutron flux is the highest. A cobalt-aluminum flux monitor encased in type 347 stainless steel is located in the core.

(c) ORR Loop Package. – Development of the ORR loop package and fabrication of components continued during the quarter. The mockup panel board was installed and is now being wired.

(d) Byron-Jackson 5-gpm Pump. – A Byron-Jackson pump[2] was installed in in-pile loop L-4-21 after preliminary tests indicated acceptable performance. A second pump satisfactorily circulated a uranyl sulfate solution at 250°C for 215 hr. No excessive corrosion of the pump was indicated in this test. Head-capacity tests of the pump before and after the high-temperature uranyl sulfate run showed no change in flow characteristics. Although the output of the Byron-Jackson pumps is below design requirements, they may be adequate for use in selected in-pile loop experiments in place of the present ORNL 5-gpm pumps. To demonstrate corrosion resistance and reliability prior to use in in-pile loops, each Byron-Jackson pump will be run under in-pile loop conditions of temperature and pressure while circulating a representative fuel solution.

(e) ORNL 5-gpm Pump. – Tests of an ORNL 5-gpm pump with a redesigned stator were completed. The stator winding was changed from a 110-v single-phase capacitor type with class A (Formvar) electrical insulation to 220-v three-phase with class H (glass, mica, and silicone varnish) electrical insulation. Greater hydraulic output and motor torque are obtained with the 220-v three-phase stator. In addition, the class H insulation is more resistant to thermal breakdown than the previous class A insulation. These characteristics should reduce the incidence of pump failures, which have resulted from electrical short circuits in the pump stator and/or minor mechanical drag of the rotating parts during in-pile operation.

ORNL 5-gpm pumps used in in-pile loop L-2-22 and subsequent loops will contain the 220-v three-phase stator. Control-panel boards are being modified to supply the 220-v three-phase current.

[1] G. H. Jenks *et al.*, *HRP Quar. Prog. Rep. July 31, 1957*, ORNL-2379, p 99.

[2] G. H. Jenks *et al.*, *HRP Quar. Prog. Rep. July 31, 1956*, ORNL-2148, p 92 (classified).

A detailed report of the test results for a pump equipped with the new stator was issued.[3]

14.1.2 General Description of In-Pile Loop Experiment L-2-14

With the exception of metallographic examination, the twelfth in-pile loop experiment, L-2-14, has been completed. This was the third loop irradiated in the HB-2 hole at the LITR and the first experiment in which the entire loop was constructed of titanium.

The objective of this experiment was to determine the effect of a solution with a high excess H_2SO_4 content on the radiation corrosion of zirconium alloys. During reactor operation the loop contained an enriched-uranium solution which was 0.17 *m* UO_2SO_4, 0.4 *m* excess H_2SO_4, and 0.15 *m* $CuSO_4$. The previous HB-2 experiment, L-2-15 (ref 4), which had the same uranium concentration, contained 0.03 *m* excess acid and 0.015 *m* $CuSO_4$. The $CuSO_4$ concentration was increased in L-2-14 to compensate for an anticipated reduction in catalytic activity with the increase in acid concentration.

The make-up solution used to replace solution removed in sampling had the same uranium concentration as the charge solution. However, to prevent excessive corrosion of the valve stems during solution addition, the make-up solution was only 0.07 *m* in H_2SO_4 and 0.015 *m* in $CuSO_4$ and also contained 100 ppm chromium.

The main-stream operating temperature was controlled at 280°C, and the pressurizer temperature at 300°C.

Because of the variety of specimen types, methods of mounting, and locations, a code has been established for the location and types of mounting as follows:

- CC Core channel holder coupons
- CA Core annulus specimens
- LC In-line channel holder coupons
- LA In-line specimens similar to the CA specimens

Sets of corrosion coupons (25 each) in titanium-75A tapered-channel coupon holders were installed in the core and in-line positions. Coupons were of titanium-55A, titanium–6% Al–4% V, type 347 and 309 SCb stainless steel, crystal-bar zirconium, Zircaloy-2, and Zr–15% Nb. Two types of Zr–15% Nb specimens were included in this loop. Type I was beta quenched. Type II was cold worked and then aged by holding at 600°C for 24 hr. The arrays were identical as to the numbers of coupons of each material, but the arrangement of coupons in each holder was not identical. The core annulus contained a ladder coupon array of 16 coupons. These coupons were made from the same alloys as the channel coupons. In addition, the core annulus contained one tensile specimen of titanium RC-A-40, two tensile specimens of titanium C-130 AM, and four impact specimens of titanium RC-A-40.

The structure of the loop was essentially the same as for previous experiments. Since the loop was titanium 75-A and the thickness of the core was the same as in previous steel loops, the maximum allowable working pressure at operating temperature was reduced from the nominal 2000 psi to 1340 psi. The 5-gpm ORNL titanium circulating pump had Kearfott aluminum oxide bearings and journal bushings.

In the out-of-pile testing of this loop, four runs with natural uranium were made. The solution employed with the first two was 0.17 *m* UO_2SO_4, 0.04 *m* H_2SO_4, and 0.03 *m* $CuSO_4$. The main-stream temperature was maintained at 250°C during the first run and at 280°C during the second run. The runs lasted 96 and 23 hr, respectively, and the corrosion rates of the stainless steel coupons based on the nickel in solution were 127 and 90 mpy, respectively. The solution employed with the third and fourth out-of-pile tests was 0.17 *m* UO_2SO_4, 0.4 *m* H_2SO_4, and 0.15 *m* $CuSO_4$, the same concentrations as the enriched-solution charge. The main-stream operating temperature was maintained at 280°C, the same as during the in-pile run. The stainless steel corrosion rate based on the nickel analyses of the solution was 5660 mpy during the first 20 hr and 1075 mpy during the next 80 hr of the third out-of-pile run. This run was continued for a total of 150 hr, with no additional nickel found after the first 100 hr. It was assumed that all the steel coupons had been consumed during the run. Initially, there were 15 g of steel coupons containing an estimated 1.5 g of nickel. Only 1.2 g of nickel could be accounted for in the solution analyses of these

[3] A. Weitzberg and H. C. Savage, *Performance Test of 220-v, Three-Phase Stator for use with 5-gpm In-Pile Loop Pump*, ORNL CF-57-10-24 (Oct. 4, 1957).

[4] G. H. Jenks *et al.*, *HRP Quar. Prog. Rep. July 31, 1957*, ORNL-2379, p 99–114.

runs. For the fourth out-of-pile test a fresh solution was used. After 100 hr the analyses of the solution indicated a negligible buildup of nickel. The over-all titanium corrosion rate, assuming that oxygen was consumed in the corrosion of only titanium during the fourth test, was 2 mpy. Following the uranyl sulfate operation, a high-temperature run was made with water at 280°C before the loop was charged with the enriched solution.

Enriched solution was circulated in the loop for about 46 hr before irradiation was initiated. The experiment was terminated when the pump failed after a total circulation time of 663 hr with enriched solution. The energy output of the LITR during the inserted time was 1530 Mwhr, essentially all of which was liberated at the 3-Mw reactor level.

During full-power operation the average fission power of the loop, as determined from Cs^{137} analyses, was 2480 w. The average fission and gamma heat was 3030 w, as determined from the difference in electric-heater power requirements with the reactor down and at full power.

The thermal-neutron fluxes in the core were determined from measurements of the induced activities of representative Zircaloy-2 and Zr–15% Nb CC and CA coupons. These determinations indicated a radial gradient of flux. The fluxes in the core channel ranged from 1.7×10^{13} at the front to 3.2×10^{12} neutrons/cm^2/sec at the rear of the coupon array. The fluxes in the core annulus at positions radial to the first and last core channel coupons were 2.0×10^{13} and 3.9×10^{12} neutrons/cm^2/sec, respectively. These values indicate a 15 to 18% radial thermal-neutron flux depression at the front and rear ends of the core channel coupon holder. Fission power densities at the specimens were calculated by using the thermal-neutron fluxes as determined.

The solution power density at a given position was corrected to include the estimated power density associated with moderation of the fast neutrons at the position. The corrected power densities ranged from 21.3 w/ml for the leading CC coupon to 4.4 w/ml for the rear CC coupon and from 21.1 w/ml for the leading CA coupon to 7.7 w/ml for the rear CA coupon. These values included estimated contributions from fast-neutron moderation of 0.5, 0.1, 0.4, and 0.2 w/ml, respectively. The estimated solution power density at the nose of the core was 34.5 w/ml.

No evidence of solution instability was observed during this experiment. No nickel was detected in a solution analysis after 35 hr of circulation of enriched solution. Analysis of the solution sample taken after 91 hr of circulation indicated that 0.114 g of nickel had gone into solution. The final solution sample was taken after 498 hr of circulation, which was 135 hr before termination of the run. An analysis of this sample indicated that 0.347 g of nickel had gone into solution. These data indicate that some of the steel coupons may have been present during the in-pile run. No titanium was detected in any of the solution analyses.

14.1.3 Qualitative Results of Inspection of Loop L-2-14

The loop was dismantled without major difficulties. Components cut from the loop were the core, both in-line sample holders, the pressurizer, and the pump. In addition, sections of the pressurizer heater, the pressurizer outlet tubing, the main loop cooler, the main loop heater, and the main loop piping at the inlet and outlet of the pump were removed. An attempt was made to remove the pump stator windings intact for electrical measurements. However, the windings were damaged in removal, and no electrical measurements were made.

Because of a misunderstanding as to the exact location of the annulus specimen arrays in the core, the rear of the impact and tensile specimens and the core annulus coupon holder were partially cut when the core was sectioned. Figure 14.1 is a photograph of the core specimen assembly and core reducer following removal of the core body. The cuts are visible in this photograph. None of the CC or CA coupons were damaged during this operation. Sectioning of the loop cores in the future will be carried out only after reference to x-ray photographs of the assembled cores.

Some difficulty was encountered in removing the specimen assemblies from the core and in-line positions because of burrs formed when the titanium was sectioned.

The impact and tensile specimens from the loop were transferred to the HRP Metallurgy Group for testing and evaluation.

Several coupons of each material from the core and in-line coupon arrays, together with the above listed sections from the loop components, were

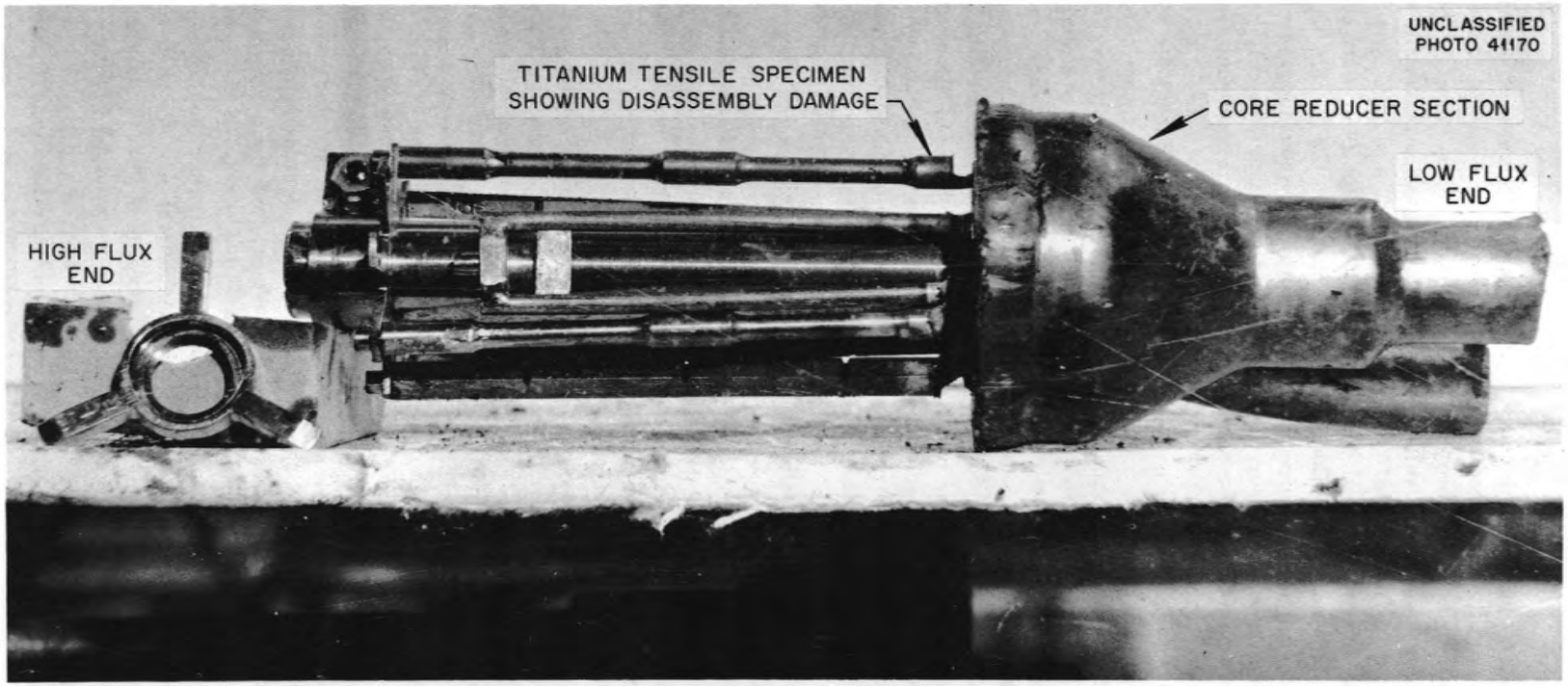

Fig. 14.1. Core Assembly, In-Pile Loop L-2-14.

sent to the Solid State Division for metallographic examination.

In an effort to determine the cause of the pump failure, the pump was carefully sectioned and examined in the manner employed in dismantling loop L-4-16 (ref 5). After removal of the volute, the pump impeller was found to be jammed. All efforts to turn the impeller failed. Lack of end-play in this component was also noted. During removal of the thermal-spacer flange the impeller was tilted with reference to the shaft. Examination of the end of the stub shaft showed that the head of the mounting screw was missing. A photograph of this part, in which the retained portion of the screw can be seen, is shown in Fig. 14.2. This screw has been submitted for metallographic examination to determine, if possible, the origin and time of occurrence of the fracture. Examination of the pump rotor and aluminum oxide bearings showed that there was no evidence of mechanical failure of these parts which could account for the pump failure. Examination of the shaft in the seal-ring region revealed no evidence of scoring. A photograph of the disassembled pump is shown in Fig. 14.3.

As with previous loops, all the components and specimens outside the core region were covered with a uniform dark-brown rustlike scale. This scale was very thin in the vapor region of the pressurizer, but an accumulation of scale was noted at the vapor-solution interface. This accumulation can be seen clearly in the photograph of the interior surface of the sectioned pressurizer shown in Fig. 14.4. Examination of the pump impeller and volute also showed a uniform deposit of rustlike scale. A photograph of these parts is shown in Fig. 14.5.

A very careful examination of the interior surfaces of the titanium core body and cap was made by use of the remote stereomicroscope at 5X magnification. Well-defined machine marks were seen along the entire length of the body, and a sharp edge was found at the spider retaining shoulder of the core cap. The core cap showed some signs of very shallow pits near the center. These pits may have been caused by abrasive from the cutting wheel during the splitting operation.

The interior surfaces of the titanium core and all titanium specimens and coupons in the core area were covered with the typical thin brass-colored film. The crystal-bar zirconium and Zircaloy-2 core coupons were predominantly gray in color, with some interference colors showing. The Zr–15% Nb alloy type I (beta-quenched) core coupons revealed a distinct grain pattern of interference colors, while the type II (cold-worked and aged at 600°C for 24 hr) core coupons were similar in appearance to the Zircaloy-2.

As with previous loops the standard cathodic defilming technique was only partially effective on the zirconium-alloy coupons, and some scale was retained.

It was assumed that all the steel coupons in this loop were consumed in the out-of-pile tests of the completed loop. However, after the core was sectioned a badly deteriorated coupon was found in the annulus and has been tentatively identified as one of the steel CA coupons. Most of the CA coupons fell from the holder upon removal from the core. No other stainless steel coupons were found either in the core or in the in-line positions.

Examination of the in-line holder showed damage in the clamping region near the outlet end. This damage may have been the result of fretting by loosely held coupons. This is indicated by the unusually high weight losses exhibited by the coupons in that section of the holder. The seven coupons of zirconium and titanium alloys in this section exhibited much higher corrosion rates than similar coupons in the undamaged portion of the in-line holder.

Before the in-line holder was dismantled, one of the crystal-bar zirconium coupons, originally in the damaged portion of the holder, was found on the dismantling-cell floor. When this coupon may have dropped from the holder is not known.

In an effort to determine the distribution of corrosion products in the scale throughout the loop, samples of bulk scale were scraped from the rear of the core, the special in-line holder, the pressurizer liquid-vapor interface region, the pressurizer vapor region, and the pump volute. These samples, along with a portion of the front and rear aluminum oxide journals from the pump, were submitted to the Analytical Chemistry Division for analyses. The results of these analyses indicate that the scale ranged from 3.1 to 10.8% Ni and from 0.35 to 12.3% Fe. Very little uranium was found in the scale and no zirconium. The results of the journal analyses were inconclusive.

[5] G. H. Jenks *et al.*, *HRP Quar. Prog. Rep. July 31, 1957*, ORNL-2379, p 99 esp 104–105.

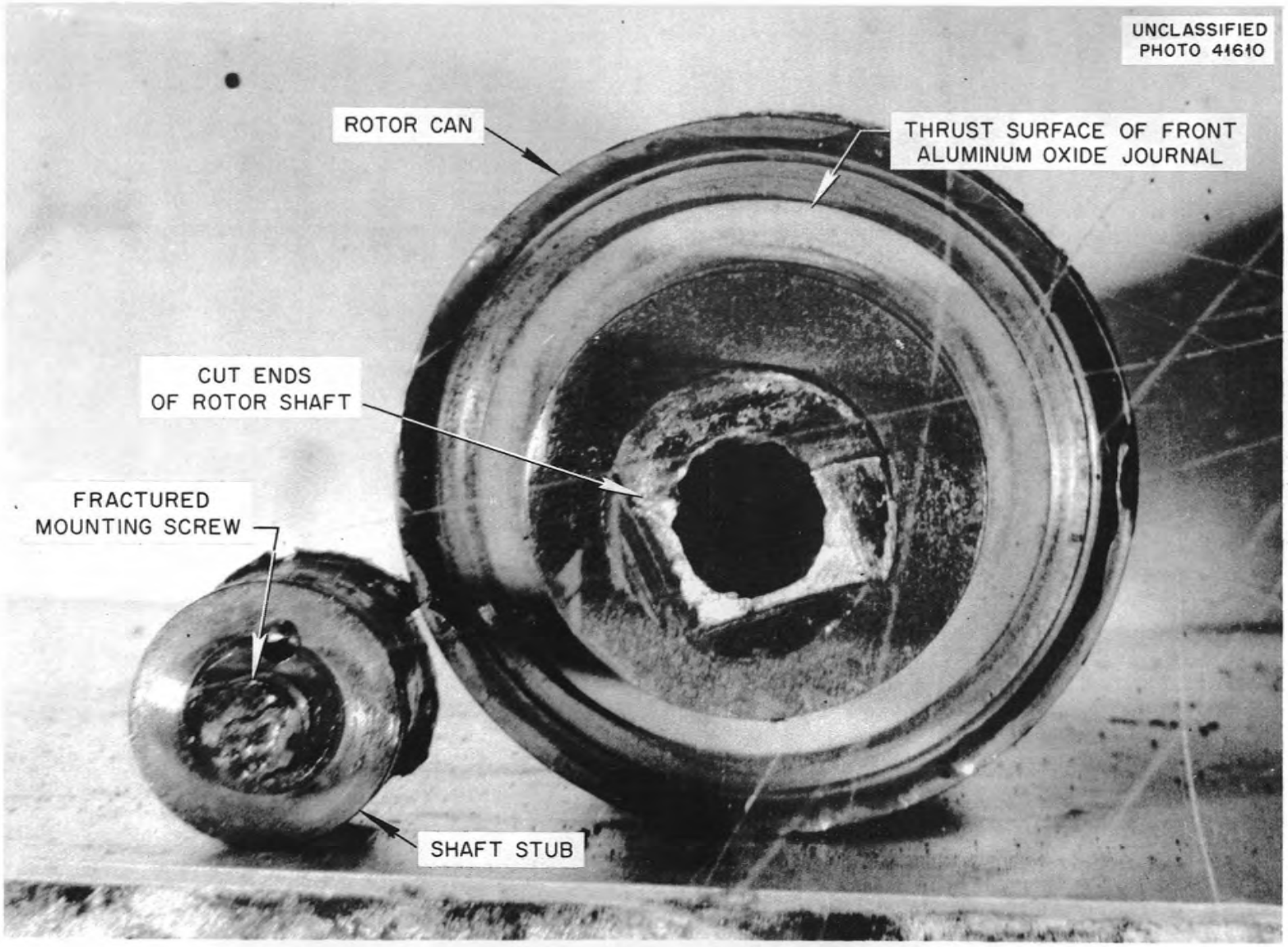

Fig. 14.2. Pump Parts, In-Pile Loop L-2-14.

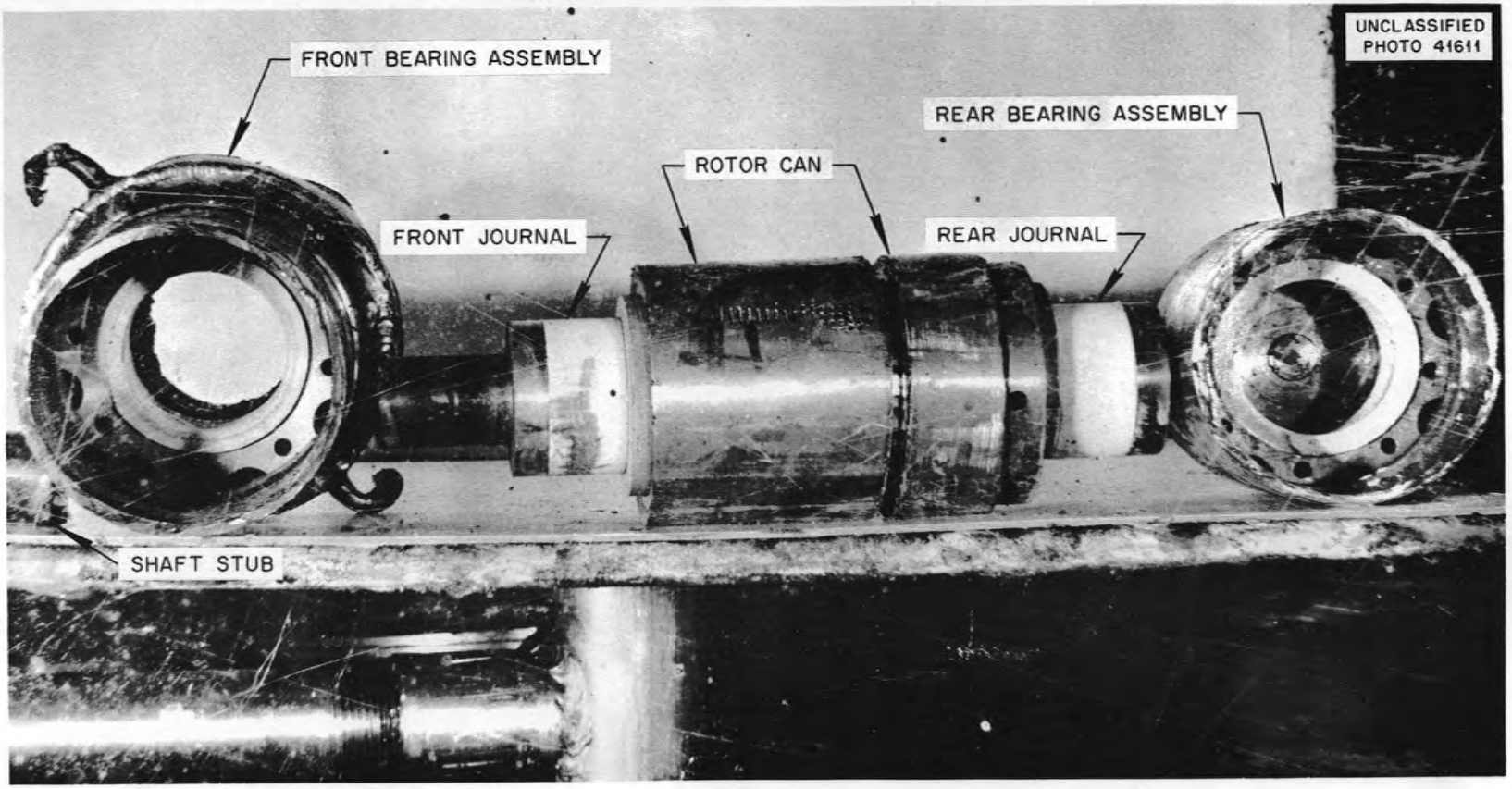

Fig. 14.3. Pump Sections, In-Pile Loop L-2-14.

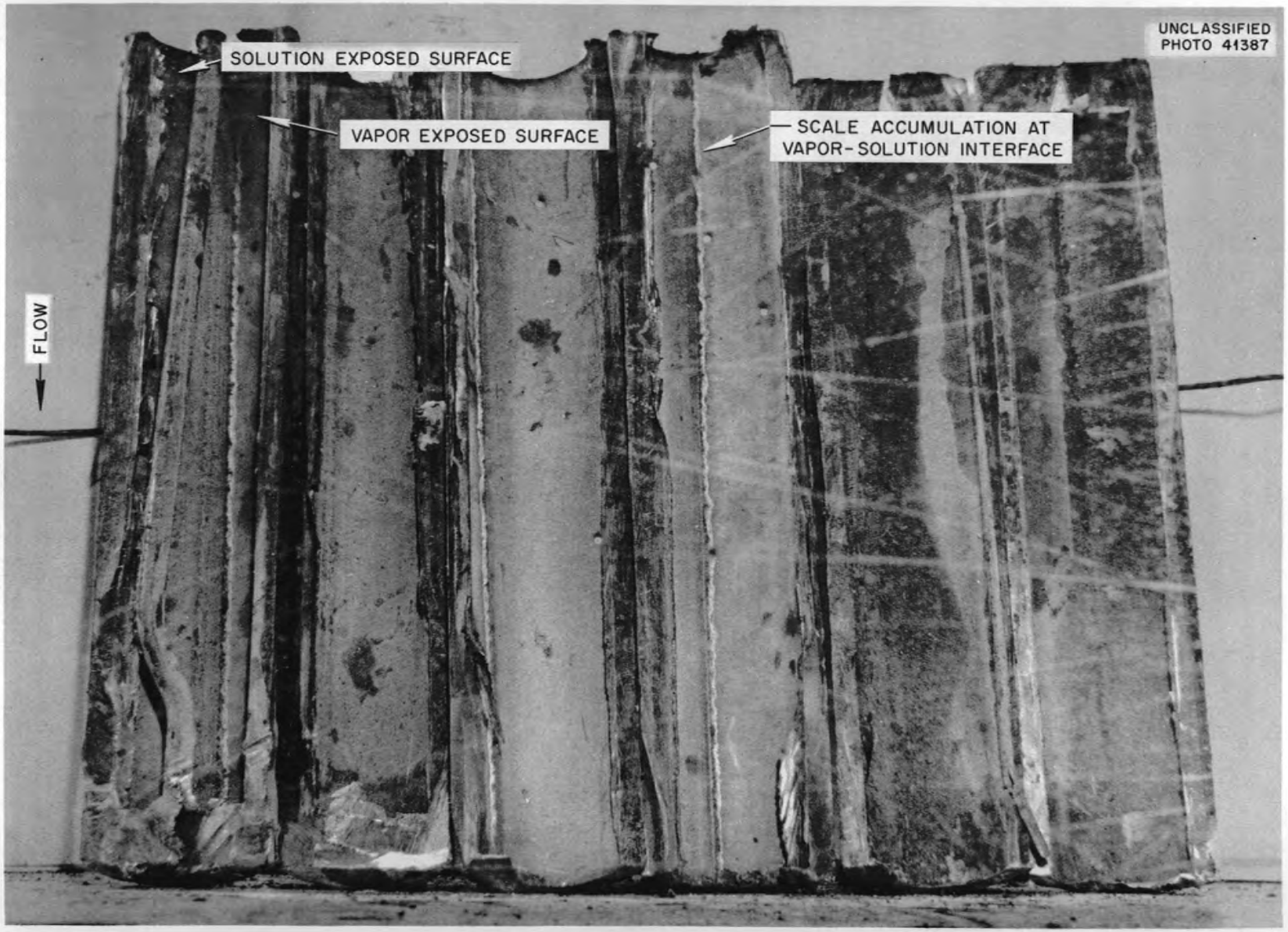

Fig. 14.4. Pressurizer, In-Pile Loop L-2-14.

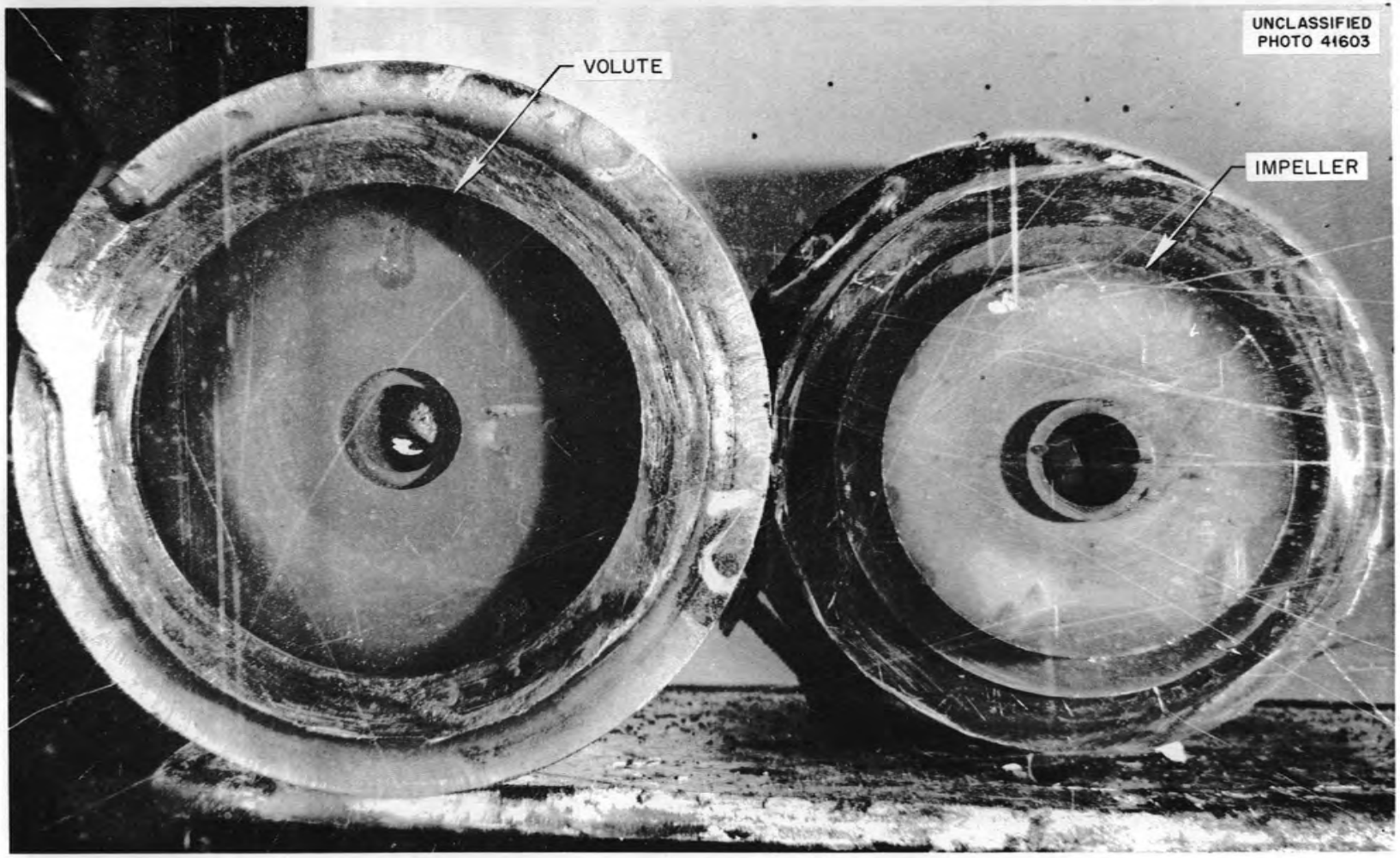

Fig. 14.5. Pump Impeller Region, In-Pile Loop L-2-14.

14.1.4 Quantitative Results of Inspection and Evaluation of Loop L-2-14

All corrosion rate values reported below were calculated from weight-loss data, with the exposed specimen area and total radiation time (equivalent to 510 hr of LITR operation at 3 Mw) used as the bases for the calculations. Average solution velocities across the coupons contained in the tapered-channel holders were from 9.4 to 42.9 fps. Power-density values for the core specimens include the estimated contribution from fast neutrons at the specimen position.

(*a*) **Zircaloy-2.** – Corrosion rates observed on the Zircaloy-2 core coupons are given in Table 14.1. The solution velocity across the CC specimens varied from 14.2 to 39.4 fps and produced no apparent effect. The three Zircaloy-2 LC coupons all showed weight increases ranging from 1.1 to 6.0 mg, following defilming. The average weight increase for these specimens was 3.5 mg. The solution velocities across these specimens varied from 11.9 to 36.2 fps.

(*b*) **Crystal-Bar Zirconium.** – Corrosion rates observed on the core coupons of crystal-bar zirconium are given in Table 14.1. The solution velocity across the CC specimens varied from 13.2 to 32.2 fps and produced no apparent effect on the relative corrosion rates.

Two of the three crystal-bar-zirconium LC coupons showed weight increases of 3.1 and 5.4 mg. Solution velocities across these specimens were 42.9 and 11.0 fps, respectively. The third coupon, which was in the damaged portion of the in-line holder and exposed to a solution velocity of 16.1 fps, exhibited the extremely high corrosion rate of 50.5 mpy.

(c) **Zirconium–15% Nb.** – Corrosion rates exhibited by both type Zr–15% Nb alloys in the core are given in Table 14.1. The solution velocity across the CC specimens varied from 10.2 to 42.9 fps.

Two of the three Zr–15% Nb (type I) LC coupons showed weight increases of 1.7 and 4.1 mg. Solution velocities across these specimens were 32.2

Table 14.1. Zirconium-Alloy Corrosion Data from Loop L-2-14

Material	Core Channel Coupons		Core Annulus Coupons	
	Power Density (w/ml)	Corrosion Rate* (mpy)	Power Density (w/ml)	Corrosion Rate* (mpy)
Zircaloy-2	13.33	7.54	13.02	7.93
	9.48	6.00	7.72	4.90
	5.61	3.94		
Crystal-bar zirconium	16.26	8.05	14.08	7.49
	10.94	6.17	8.25	4.82
	5.34	3.60		
Zr–15% Nb (type I)**	18.78	22.10	21.10	23.49
	9.08	16.27	12.23	18.34
	4.81	15.07		
Zr–15% Nb (type II)**	19.84	25.86	19.64	26.17
	12.54	21.75	11.43	22.03
	6.41	19.01		

*Based on exposed area and radiation time.

**Heat treatment: type I, beta quenched; type II, cold worked and then aged by holding at 600°C for 24 hr.

and 10.2 fps, respectively. The third coupon, which was also in the damaged portion of the in-line holder and exposed to a solution velocity of 13.6 fps, exhibited a corrosion rate of 15.5 mpy.

Two of the three Zr–15% Nb (type II) LC coupons showed weight increases of 3.8 and 7.7 mg. Solution velocities across these specimens were 31.9 and 14.7 fps, respectively. The third coupon, which was also in the damaged portion of the in-line holder and exposed to a solution velocity of 11.3 fps, exhibited a corrosion rate of 5.9 mpy.

(*d*) **Titanium-55A.** – Corrosion rates observed on four titanium-55A CC coupons varied from 0.75 mpy at 4.4 w/ml to 1.9 mpy at 21.3 w/ml. The solution velocity across these specimens varied from 9.4 to 36.2 fps and produced no apparent effect on the relative corrosion rates.

Two of the LC coupons of this material were in the damaged portion of the in-line holder. These coupons corroded at rates of 2.7 and 5.6 mpy at solution velocities of 9.7 and 9.9 fps, respectively. Of the two other titanium-55A LC coupons, one showed no weight change and the other exhibited a corrosion rate of 0.25 mpy. The specimen showing no weight change was exposed to a solution velocity of 39.4 fps, and the other specimen was exposed to a solution velocity of 16.6 fps.

The two titanium-55A CA coupons exhibited corrosion rates of 2.4 and 1.6 mpy at power densities of 17.3 and 10.1 w/ml, respectively.

(e) **Titanium–6% Al–4% V.** – CC and CA coupons of titanium–6% Al–4% V exhibited corrosion rates approximately twice as great as those observed for the titanium-55A core coupons at comparable power densities.

Three titanium–6% Al–4% V CC coupons exhibited corrosion rates of from 1.9 mpy at 7.4 w/ml to 4.0 mpy at 15.5 w/ml. The solution velocity across these specimens varied from 14.7 to 27.1 fps. Two of the three LC coupons of this material showed no weight change following defilming. Solution velocity across these specimens was 19.0 and 40.0 fps. A corrosion rate of 1.1 mpy was observed on the third coupon, which was in the damaged portion of the in-line holder and exposed to a solution velocity of 18.3 fps.

The two titanium–6% Al–4% V CA coupons exhibited corrosion rates of 4.0 and 2.6 mpy at 18.4 and 11.4 w/ml, respectively.

14.1.5 Discussion of Results from Loop L-2-14 and Previous Loops

The radiation-corrosion behavior of Zircaloy-2 channel coupons observed in experiments L-2-15 and L-4-16, the only previous loops with 0.17 *m* UO_2SO_4 at 280°C, was shown to be described reasonably well by the following equation:[6]

$$(1) \qquad R = 1.04\,P\,(1 - e^{-95/R^{1.5}}) ,$$

where R = corrosion rate, mpy, and P = power density, w/ml. As shown in Fig. 14.6, the corrosion rates exhibited by the Zircaloy-2 channel

[6] G. H. Jenks *et al.*, *HRP Quar. Prog. Rep. July 31, 1957*, ORNL-2379, p 99, esp 107–110.

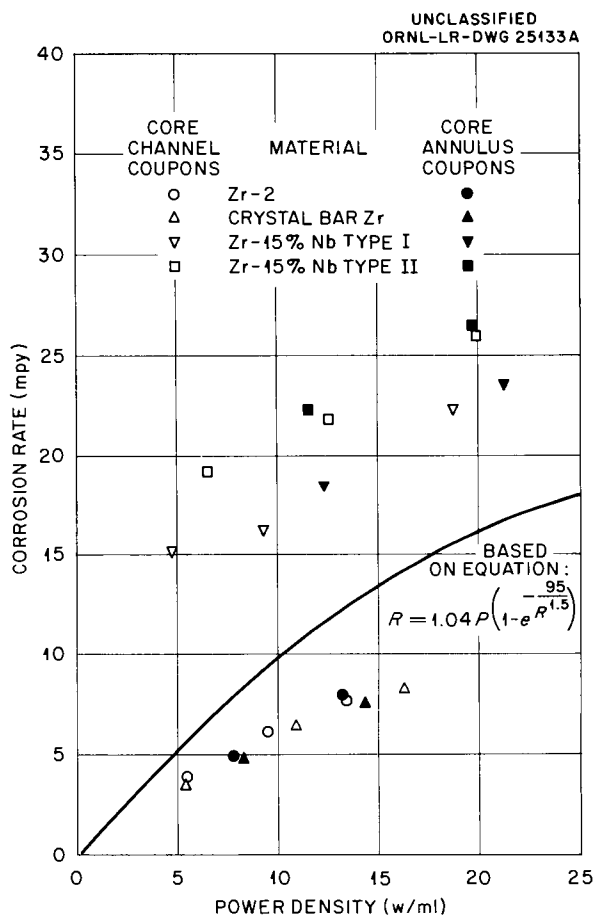

Fig. 14.6. Zirconium-Alloy Corrosion Rates, In-Pile Loop L-2-14.

coupons in the present experiment range between about 50 and 60% of those predicted by this equation. The crystal-bar-zirconium core channel coupons exhibited corrosion rates in excellent agreement with the Zircaloy-2 data. The rates observed for core annulus coupons of each of these materials are in near agreement with core-channel-coupon results. Although the solutions employed with the previous two experiments, L-2-15 and L-4-16, had the same uranium concentration as the present experiment, the $CuSO_4$ and excess H_2SO_4 concentrations were different. The previous experiments contained solutions which were 0.015 *m* in $CuSO_4$ and 0.02–0.03 *m* in excess H_2SO_4, as compared with copper and acid concentrations of 0.15 *m* and 0.4 *m*, respectively, in the present experiment. It appears likely that the lower rates observed in the present experiments are a result of the high concentration of excess H_2SO_4. It is not known whether this effect is a result of the high bisulfate or hydrogen ion concentration. It is assumed that the dissociation constant of the bisulfate is so low at 280°C that the sulfate ion concentration is negligible. An in-pile loop experiment, L-2-19, now in progress, is being conducted to help determine the effect of the sulfate or bisulfate ion on the Zircaloy-2 corrosion. The solution employed with L-2-19 is 0.17 *m* in UO_2SO_4, 0.02 *m* in $CuSO_4$, 0.1 *m* in excess H_2SO_4, and 0.2 *m* in Li_2SO_4.

A decrease in the radiation corrosion of Zircaloy-2 with high excess H_2SO_4 concentration was also observed in an autoclave experiment, Z-3 (ref 7). This autoclave experiment employed a solution of about the same composition as that used in L-2-14, but was exposed at 250°C.

A general discussion and review of the results of the four 280°C loop experiments which have been carried out appears worth while at this time. Some information in addition to that previously reported regarding the behavior of Zircaloy-2 in the core annulus region is available. Also, there are new concepts of the effect on corrosion of uranium adsorbed at the Zircaloy-2 specimen surface, as discussed in Sec 14.2.2a.

Experimental conditions for three of the 280°C experiments, L-2-15, L-4-16, and L-2-14, have been mentioned. The other, L-2-10 (ref 8), was with a solution 0.04 *m* in UO_2SO_4, 0.02 *m* in excess H_2SO_4, and 0.007 *m* in $CuSO_4$. Each of these experiments contained core annulus specimens. In each case, with the exception of L-2-14, the corrosion rate of the annulus specimens, calculated with exposed area as a basis, is greater than that of the channel coupons. As previously reported,[9] metallographic examination of the L-2-15 core annulus coupons showed that the area normally considered unexposed, and not included in the corrosion-rate calculations, was attacked. When the total area of the L-2-15 core annulus coupons and the exposed area of the core channel coupons are used, the calculated corrosion rates are in near agreement. Additional evidence that the attack of Zircaloy-2 in the core annulus region did not exceed that in the core channel has been obtained from the impact and tensile specimens in L-2-15. Two Zircaloy-2 and two crystal-bar-zirconium impact specimens, together with two crystal-bar-zirconium tensile specimens, were included in the core annulus of this loop. With specimens of these types, only a small fraction of the total area is unexposed. No attempt is made to defilm these specimens as is the procedure with corrosion specimens; they are transferred to the HRP Metallurgy Section in the as-removed condition. However, as a general rule, only a negligible change in weight is observed upon defilming Zircaloy-2 or zirconium corrosion specimens from a loop core; observation also indicates the absence of appreciable film. Hence, the weight-change data for these impact and tensile specimens may be regarded as reliable corrosion information. For L-2-15, the average corrosion rate, based on exposed area, of the impact specimens is in near agreement with the average rate predicted from Eq. 1. The average rate of the tensile specimens is below the predicted rate.

However, this agreement between annulus and channel specimens does not extend to the results of L-4-16 and L-2-10. Each of six Zircaloy-2 impact and tensile specimens in the L-2-10 experiment exhibited an average rate equal to or slightly greater than that predicted from the corrosion behavior, based on exposed area, of the core-annulus corrosion coupons. Loop L-4-16 contained only one Zircaloy-2 impact specimen

[7] G. H. Jenks *et al.*, *HRP Quar. Prog. Rep. April 30, 1956*, ORNL-2096, p 92–94.

[8] G. H. Jenks *et al.*, *HRP Quar. Prog. Rep. Jan. 31, 1957*, ORNL-2272, p 102, esp 104–108.

[9] J. O. Stiegler, *Metallographic Examination of Components, Coupons and Stress Specimens from HRP In-Pile Loop L-2-15*, ORNL CF-57-5-103 (May 22, 1957).

and no tensile specimen. The average rate for this impact specimen was about the same as that predicted from the corrosion rates of the annulus corrosion coupons. Here again, the exposed area of the annulus coupons was employed in the prediction. To summarize, there is additional evidence that the corrosion of Zircaloy-2 in the core annulus in L-2-10 and L-4-16 was greater, in each case, than corrosion in the channel. In L-2-15 there is evidence of no difference in corrosion between the two locations.

As previously reported,[6] the corrosion of L-2-10 channel coupons is not described by Eq. 1. At a given solution power density, the rate for an L-2-10 specimen is greater than that given by the equation. Similar differences in corrosion between 0.17 and 0.04 *m* UO_2SO_4 solution have been observed in autoclave experiments. However, as discussed in Sec 14.2.2a, these differences between the results in the two UO_2SO_4 solutions in autoclave tests can be correlated with the amount of uranium in the scale found on specimen surfaces. When a correction to the power density at the surface is made which includes a contribution from scale uranium, the corrosion rate at a given corrected power density is about the same at both solution concentrations. If the validity of the treatment of the autoclave data is assumed, it seems likely that uranium adsorption at a specimen surface also contributes to the results observed in loop L-2-10. A possible explanation for the higher rate of attack in the core annulus region of L-2-10 is that in this low-velocity region (average velocity through the annulus was about 0.8 fps) more scale adhered to a specimen surface than was the case for specimens exposed to higher solution velocities in the channel holder. The same possible explanation may be made for the indicated high rates in the core annulus of L-4-16. The agreement between channel and annulus positions in L-2-15 is an exception for which, with presently available information, no explanation is offered.

The agreement between annulus and channel specimens in L-2-14 is what might be expected if adsorbed uranium has, in fact, been responsible for the difference noted in L-2-10 and L-4-16. Autoclave results have shown that the amount of uranium adsorbed in the scale is reduced when the concentration of excess H_2SO_4 is increased from 0 to 0.04 *m*. In the one autoclave experiment for which the solution was 0.4 *m* in excess H_2SO_4, no uranium was detected in the scale.[7]

Turning now to the results with the Zr-Nb alloys in loop L-2-14, both types of Zr–15% Nb alloy exhibited corrosion rates higher than the rates predicted by Eq. 1. This is in sharp contrast with data from experiment L-4-16, in which the beta-quenched Zr–15% Nb alloy CA coupons exhibited lower corrosion rates than did Zircaloy-2. The Zr–15% Nb alloy also exhibited high corrosion rates in a loop experiment with high excess acid conducted out-of-pile by Greeley and others.[10] The conditions in that experiment were similar to those in L-2-14. The duration of the experiment was 159 hr. Two coupons of Zr–15% Nb alloy in the out-of-pile experiment, one each at solution velocities of 19 and 73 fps, exhibited corrosion rates before defilming of 23 and 31 mpy, respectively. Six crystal-bar-zirconium coupons, three each at the above solution velocities, exhibited negligible defilmed weight losses. All the crystal-bar-zirconium, Zircaloy-2, and Zr–15% Nb in-line coupons in the L-2-14 experiment, with the exception of those in the damaged portion of the holder, showed weight increases. The coupons located in the damaged portion of the holder exhibited high corrosion rates because they were apparently not held firmly in place. Similar damage occurred in a previous loop, L-4-12 (ref 11), which also had titanium in-line coupon holders. The lack of agreement between the in-line Zr–15% Nb corrosion rates in L-2-14 and the Zr–15% Nb corrosion rates in the out-of-pile experiment might be explained by the fact that the out-of-pile experiment contained no steel. Loop L-2-14 initially contained 15 g of steel and was initially tested with a solution containing 0.04 *m* excess acid. Scale from the steel corrosion depositing on the in-line specimens during the initial test may have protected the titanium specimens against attack in the high-acid solution.

The heavily deteriorated coupon, tentatively identified as stainless steel, found in the present loop has been submitted for metallographic examination and identification. It is assumed that all

[10] R. S. Greeley *et al.*, *Summary of Runs H-111, 112, 113 – 0.17 m UO_2SO_4 + 0.4 m H_2SO_4 + 0.15 m $CuSO_4$ at 280°C*, ORNL CF-57-10-85 (in press).

[11] G. H. Jenks *et al.*, *HRP Quar. Prog. Rep. Oct. 31, 1956*, ORNL-2222, p 100, esp 102–103.

the other steel coupons were consumed in the high-acid solution.

The titanium-core-coupon corrosion data are plotted against power density in Fig. 14.7. Both the Ti-55A and the Ti–6% Al–4% V exhibited increasing corrosion rates with increasing power density. In general, the Ti–6% Al–4% V alloy exhibited corrosion rates about twice as great as the Ti-55A at the same power densities. The Ti-55A core-channel-coupon corrosion rates observed in the previous experiment, L-2-15 (ref 7), were in near agreement with, or slightly greater than, those observed in the present experiment. With one exception the in-line titanium coupons not in the damaged portion of the holder exhibited negligible weight changes following defilming. The exception, a Ti-55A coupon, corroded at a rate of 0.25 mpy. In the out-of-pile experiment by Greeley and others,[10] which was similar to the present experiment, the titanium coupons at velocities of 19 and 73 fps exhibited negligible weight changes after defilming. The titanium coupons included types RC-45A and RC-55A and Ti–6% Al–4% V.

The average corrosion rate of the Ti-75A core-channel-coupon holder was about 1.7 mpy based on the defilmed weight loss. The average corrosion rate of the Ti-75A core wall is assumed to be about the same. However, the average power density on the core wall was slightly greater than that on the core coupon holder. The corrosion rate of the Ti-75A in-line channel coupon holder was 0.4 mpy based on the defilmed weight loss.

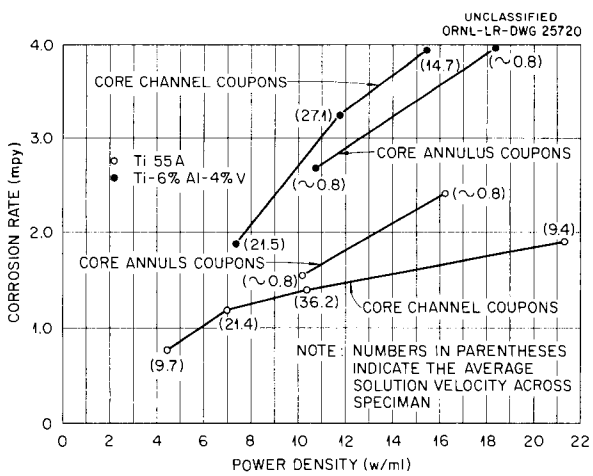

Fig. 14.7. Titanium Corrosion, In-Pile Loop L-2-14.

The over-all corrosion rate of the Ti-75A loop during operation with enriched uranium solution was 2.2 mpy based on oxygen data corrected for the estimated amount consumed in the corrosion of other metals. The total oxygen consumed was 5050 cc at STP. The weight loss of zirconium coupons in this experiment was 0.45 g, which would account for 100 cc of the oxygen. The finding of the coupon, tentatively identified as steel, at the end of the experiment indicates that some steel was present during the entire run. Extrapolation of the nickel data from the last solution analysis to the end of the run indicates that about 0.42 g of nickel went into solution. It is estimated that 4.2 g of stainless steel would contain this amount of nickel. This weight of steel would account for about 1260 cc of oxygen. The remaining 3690 cc of oxygen is assumed to have been consumed in the corrosion of titanium.

14.1.6 In-Pile Loop L-4-18

Irradiation of stainless steel loop L-4-18 was completed in beam hole HB-4 at the LITR. Total circulation time with enriched solution was 860 hr, of which 58 hr was accumulated outside the reactor. The energy output of the LITR during insertion was 1926 Mwhr. Almost all this energy was liberated at the 3-Mw level. The run was terminated when the circulation pump failed.

Operating conditions and contents were reported previously.[12] The solution originally charged to the loop was 0.17 *m* UO_2SO_4 (enriched), 0.07 *m* $CuSO_4$, and 0.02 *m* H_2SO_4 in a heavy-water solvent. The calculated free-acid concentration was maintained reasonably constant during the run. The main-stream operating temperature was 235°C; the pressurizer temperature was 265°C. No evidence of solution instability was observed at these operating conditions. The over-all stainless steel corrosion rate was 0.67 mpy based on oxygen consumption and 0.31 mpy based on the nickel in solution.

14.1.7 In-Pile Loop L-2-19

Stainless steel loop L-2-19 is now being irradiated in the HB-2 beam hole at the LITR. Contents

[12] G. H. Jenks *et al.*, *HRP Quar. Prog. Rep. July 31, 1957*, ORNL-2379, p 99, esp 114.

of this loop were reported previously.[13] The solution originally charged to the loop was 0.17 *m* UO_2SO_4 (enriched), 0.02 *m* $CuSO_4$, 0.1 *m* H_2SO_4, and 0.2 *m* Li_2SO_4 (99.9% Li^7) in a light-water solvent. The main-stream temperature is 280°C, and the pressurizer temperature is 295°C.

14.2 IN-PILE AUTOCLAVE TESTS – LITR

14.2.1 Development and Construction

The assembly and testing of rocking autoclaves for radiation-corrosion studies in beam hole HB-6 of the LITR continued during the past quarter. Four experiments, L6Z-113, -114, -115, and -116, fabricated from Zircaloy-2 and containing zirconium-alloy pin-type corrosion specimens were prepared and operated in the HB-6 facility of the LITR.

Two experiments for use in the HB-5 three-hole facility of the LITR were prepared, as previously reported.[12] One of these experiments, L52Z-107, was operated for a total of 61 hr in the LITR but was terminated at the end of this period because of evidence that the rocking assembly was galling badly. Experiment L53Z-108 was also found to be improperly aligned when inserted in hole No. 3 of the fixed plug. This misalignment caused rubbing between the aluminum can, in which the autoclave assembly is located, and the aluminum sleeve liner.

It was determined that the clearances between the two dry bronze bearings located in the forward section of the hole liner (nearest the reactor) and the aluminum can containing the autoclave were too large. Excessive play in these bearings permitted the can to rub on the sleeve liner at the nose (reactor) end of the assembly. In an attempt to prevent this rubbing and possible failure of the sleeve liner during future experiments, bearings of Oilite-bronze (a porous sintered bronze impregnated with a lubricating oil) were machined to slide into the outer, larger portion of the fixed plug hole to provide additional bearing area for the rocking plug and to help in aligning the autoclave assembly within the sleeve liner (see Fig. 14.8). Three Oilite bearings were placed in each of the three beam holes with tubing spacers between to prevent the bearings from moving axially in the hole. (Hole No. 1 is equipped with brass tubing spacers, and the other two holes of the HB-5 facility have aluminum tubing spacers.) The aluminum can containing the autoclave was also modified by installing a ball bearing on the nose (reactor) end for support and elimination of rubbing between the autoclave container-can and fixed hole liner.

Experiment L51Z-109 was operated successfully for 189 hr in the LITR with the three Oilite-bronze bearings installed in the fixed plug hole (but without the ball bearing on the nose of the aluminum can containing the autoclave). Experiment L53Z-108 is presently being equipped with the ball bearing on the nose of the aluminum can, as will all subsequent experiments. Tests made to date indicate that these modifications will eliminate rubbing and wear in the HB-5 multiple-rocking-bomb facility.

14.2.2 Correlation of In-Pile Autoclave Data with In-Pile Loop Data

(a) Development with Reference Solutions. – Disagreement between loop and autoclave data pertaining to the radiation corrosion of Zircaloy-2 has been apparent for some time.[14] Autoclave results have shown a difference in corrosion rates, depending on whether the excess acid concentration is zero or 0.04 *m* (refs 14, 15); and a bomb experiment, Z-20, to determine the effect of replacing the light-water solvent with D_2O indicated a greater corrosion rate with the D_2O solution.[16] In the one loop experiment which employed D_2O as the solvent, no corrosion effect on crystal-bar zirconium was detected which could be ascribed to the use of D_2O rather than light water.[17] In various loop experiments at 250°C which employed excess H_2SO_4 in the concentration range 0.004 to 0.03 *m*, no significant difference between attack rates at the different acid concentrations has been observed.[14]

It has been suggested previously that at least part of these differences between autoclave and

[13] G. H. Jenks *et al.*, *HRP Quar. Prog. Rep. July 31, 1957*, ORNL-2379, p 99.

[14] G. H. Jenks *et al.*, *HRP Quar. Prog. Rep. Oct. 31, 1956*, ORNL-2222, p 100, esp 110–112.

[15] R. J. Davis, G. H. Jenks, and J. R. McWherter, *HRP Radiation Corrosion Studies: Effect of Uranium in Zircaloy-2 Scale*, ORNL CF-57-10-40 (in press).

[16] G. H. Jenks *et al.*, *HRP Quar. Prog. Rep. Oct. 31, 1956*, ORNL-2222, p 100, esp 108–109.

[17] G. H. Jenks *et al.*, *HRP Quar. Prog. Rep. April 30, 1957*, ORNL-2331, p 112, esp 116–118.

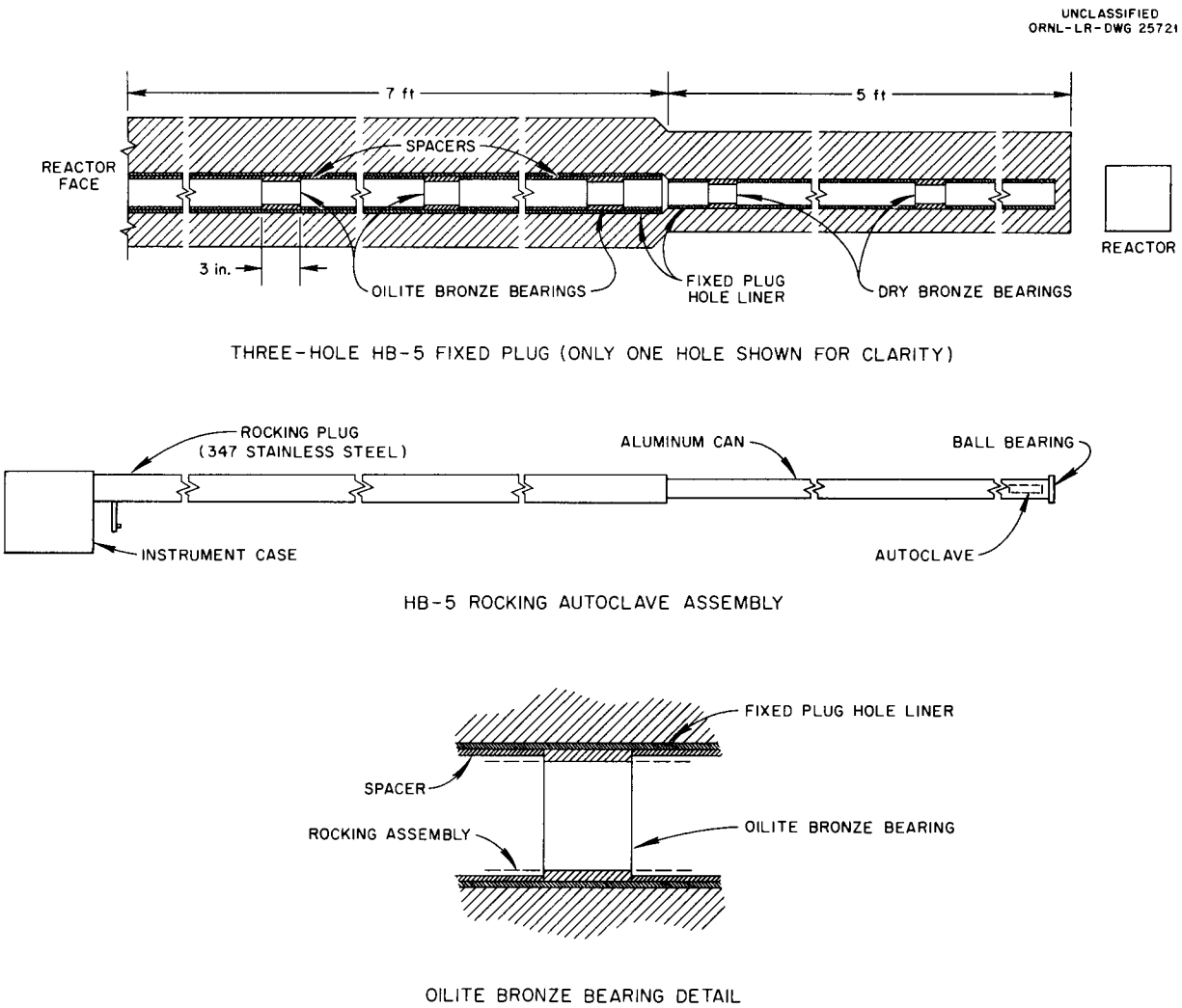

Fig. 14.8. Bearing Inserts for HB-5 Multiple-Rocking-Bomb Facility.

loop results may be connected with the scale found on surfaces of Zircaloy-2 exposed to radiation in autoclaves. Chemical analysis of this scale shows that it usually contains several per cent by weight of uranium, and it can be estimated from consideration of the short ranges of recoiling fission fragments that fissioning of this uranium in the scale contributes appreciably to the intensity of fission-recoil irradiation of the wall. In general, more uranium is found in scales from experiments without acid than from those with acid. Also, some experiments such as Z-20, which have exhibited a higher-than-average rate at a given solution power density, have also shown a higher-than-average uranium concentration in the scales.

Zircaloy-2 exposed in the core of a loop apparently does not form a heavy scale of the type found in autoclaves. As removed from the loop after exposure, a core specimen, in general, has only a thin adherent film. The results of analyses for zirconium in scale removed from portions of a loop external to the core provide[18] additional evidence that large quantities of scale do not accumulate on surfaces of core specimens during exposure.

Efforts to correlate the disagreement between loop and autoclave results with the uranium found

[18] G. H. Jenks *et al.*, *HRP Quar. Prog. Rep. July 31, 1957*, ORNL-2379, p 99, esp 110–114.

in autoclave scale have been quite successful and are discussed in detail in a separate report.[15] It is presumed that the effective power density to which autoclave surfaces are exposed is greater than the power density in solution by an amount related to the quantity of uranium in the scale. A corrected power density, P_c, is considered rather than the power density in solution, P_s. The corrected power density is defined as greater than the solution power density by an amount linearly related to the percentage uranium in the scale. In other words, the effective power density at the wall is assumed to be equal to the sum of the value for the power density in solution and a value which is proportional to the product of the uranium concentration in the scale and the slow-neutron flux during exposure. This relationship is conveniently expressed by the equation:

$$P_c = P_s\left(1 + K\frac{U_f}{U_s}\right), \tag{2}$$

where U_f is the percentage by weight of uranium in the scale, U_s is the concentration of uranium in solution, in grams per liter, measured at the test temperature, and K is a constant. In the calculation of the value of P_s, it is assumed that the concentration of uranium in solution does not change significantly during exposure.

The treatment of the data to test the effect of uranium in the scale has been, in brief, the following: Those experiments were considered first which were exposed at 280°C and were with one of the reference solutions. By "reference solution" is meant a solution of one of the following compositions:

UO_2SO_4	0.17 *m*
H_2SO_4	0 or 0.04 *m*
$CuSO_4$	0 to 0.04 *m*
Solvent	H_2O

It may also be added that the reference solution may or may not be contaminated by several hundred ppm of nitrogen[19] (from atmospheric nitrogen included during fill). The curve expressed by the equation

$$R = 1.04P\left(1 - e^{-95/R^{1.5}}\right) \tag{3}$$

was assumed for the relationship between power density in solution and corrosion rate in the absence of scale. This equation is that established from data for the core-channel-holder coupons in loop experiments L-2-15 and L-4-16 (ref 20). These experiments employed a solution similar to the reference solution, and the exposure temperature in each was 280°C. The constant, K, in Eq. 2 was evaluated as 8.3 for optimum fit of autoclave data to this curve. Using this constant, values for corrected power density were then computed from the data for each experiment.

The above value of the constant K was also used to compute values for corrected power density from data for autoclave experiments at 250°C with the reference solution.

The corrected results for the 280 and 250°C data are shown graphically in Figs. 14.9 and 14.10, respectively. The uncorrected data are also shown in each case and are identified by the open points. The curve shown in Fig. 14.9 is that determined from loop data as mentioned previously (Eq. 3). It should be noted that the power-density range covered in the loop experiments is from about 1 to 20 w/ml. Thus at above 20 w/ml the curve

[19] G. H. Jenks *et al.*, *HRP Quar. Prog. Rep. Jan. 31, 1957*, ORNL-2272, p 114–115.

[20] G. H. Jenks *et al.*, *HRP Quar. Prog. Rep. July 31, 1957*, ORNL-2379, p 99, esp 107–110.

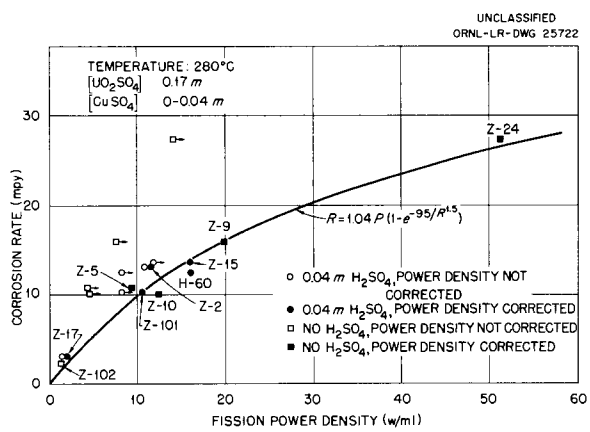

Fig. 14.9. Zircaloy-2 Autoclave Data Corrected for Scale Uranium.

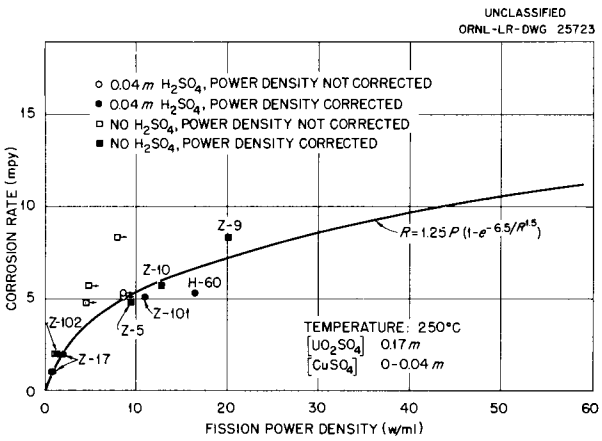

Fig. 14.10. Zircaloy-2 Autoclave Data Corrected for Scale Uranium.

is an extrapolation from lower-power-density data. The curve shown in Fig. 14.10 is that represented by the equation:

$$(4) \qquad R = 1.25P\left(1 - e^{-6.5/R^{1.5}}\right) .$$

This equation has been established primarily from the results of loop experiments at 250°C with solutions similar to the reference solution. Uncorrected autoclave data for solutions containing acid were also employed in the derivation. It is assumed that this curve represents the corrosion-rate–power-density relationship when the Zircaloy-2 is free of scale. The power-density range covered in these loop experiments is from about 0.5 to 6 w/ml. Thus a large portion of this curve represents an extrapolation from lower-power-density data.

Complete analytical data for the amount of uranium contained in the scale from a given experiment are not included in this report, but the following examples are given as illustrations:

Experiment	Uranium in Scale (wt %)
Z-24	9.8
Z-9	6.0
Z-10	6.6
Z-17	1.0
Z-15	1.3

It should be noted that some autoclave experiments with the reference solutions in addition to those shown in Figs. 14.9 and 14.10 have been carried out. For these, however, no analytical data for the concentration of uranium in the scale are available, and no corrections can be applied.

As can be seen in Figs. 14.9 and 14.10, the corrected data fall near the given curve. At each temperature, the fit is considered very good and is probably better than might reasonably be expected if the difficulties inherent in the scale analyses are taken into account. Frequently, only 10 to 20 mg of scale is available for analysis, and this scale is extremely radioactive.

It is concluded, as a result of these correlations, that uranium in the scale indeed influences the corrosion rate of Zircaloy-2 under irradiation in autoclaves. When a correction to the value for the power density is made for this uranium in the scale, the autoclave results are in agreement with the loop results. At a given corrected power density, there is no appreciable difference between the corrosion rate in reference solutions containing 0.04 *m* excess H_2SO_4 and in those free of excess acid.

It is believed that a correction for uranium in the scale is required for proper interpretation of the data. However, there is one aspect of the corrosion behavior of Zircaloy-2 in autoclaves which has been considered as an argument against the concept that scale uranium influences the corrosion to a significant extent, and which should be mentioned here. As indicated by oxygen data, the rate of corrosion under irradiation remains fairly constant after a short period at the start of irradiation during which the rate is, usually, less than the steady-state rate. It may be argued that the amount of scale covering a Zircaloy-2 surface will increase as corrosion proceeds under irradiation and that the amount of uranium adjacent to the wall will also increase as additional scale adsorbs additional uranium. Under these conditions, the corrosion rate might be expected to increase with time. As mentioned above, the observed corrosion rate remains fairly constant.

The explanation for the apparent constancy of the effect of uranium in the scale is unknown. However, it may be postulated that the distribution of uranium in the scale is not uniform. The scale is pictured as forming at the protective oxide-scale interface so that new scale is not exposed to solution to the same extent as the older scale at the solution-scale interface. Hence, the scale adjacent to the protective oxide may contain less uranium

than the outer layer of scale. A given rate of fissioning at the outer layer of scale will contribute less to the fission-recoil irradiation of the protective oxide than fissioning at the same rate in a layer of scale adjacent to the protective oxide. Furthermore, the intensity of fission-fragment irradiation from solution will probably decrease as the scale thickens. Given this picture, it is possible to speculate that the distribution of uranium in the scale is such that the contribution of scale uranium to the fission-recoil irradiation of the specimen surface does not change appreciably with increasing thickness of scale. It should be emphasized that this is a speculation. No accurate calculations to test the validity of the postulated picture have been made.

(*b*) Application to Other Solutions. – The preceding discussion has outlined a new scheme for calculating the fission power density to which rocking autoclave surfaces are exposed. A theoretical treatment of the effect of uranium in the scale is not offered. However, the basic idea that uranium adsorbed in the corrosion scale in autoclaves will increase the local fission power density appears reasonable. The power-density dependence of corrosion found in several autoclave experiments correlates with the power-density dependence found in in-pile loop experiments when corrected power densities are employed. The autoclave results shown in Figs. 14.9 and 14.10 are from comparable experiments, in that each contains solution 0.17 *m* in UO_2SO_4 and solution additives were limited to $CuSO_4$ (0 to 0.04 *m*) and H_2SO_4 (0 or 0.04 *m*). The in-pile loop data shown are from experiments which employed similar solutions. On the basis of these apparently successful correlations of autoclave results with reference solution, it appears worth while to re-examine the data from autoclave experiments which employed other solutions. The corrected power-density value has been calculated for each of these experiments with nonreference solutions for which analytical results for uranium content of the scale are available. Equation 2 above, with the value of the constant *K* determined from the data for reference solutions, was employed in these calculations. The corrected results are plotted in Figs. 14.11 and 14.12 as solid marks in each case. For comparison, uncorrected results are also shown, identified by open marks. The curve shown in Fig. 14.11 for the 280°C data is the same as that shown in Fig. 14.9, and the curve in Fig. 14.12 for the 250°C data is the same as that in Fig. 14.10. The results of data correlation on this new basis are discussed for each experiment in the following paragraphs:

Experiment Z-3. – The solution for this experiment[21-22] was 0.45 *m* in excess H_2SO_4. No other autoclave experiment with more than 0.06 *m* excess H_2SO_4 has been carried out. There was no uranium found in the Z-3 scale and therefore no

[21] W. E. Clark, *Experiment Z-3*, ORNL CF-55-7-143 (July 26, 1955).

[22] G. H. Jenks *et al.*, *HRP Quar. Prog. Rep. April 30, 1956*, ORNL-2096, p 92–94.

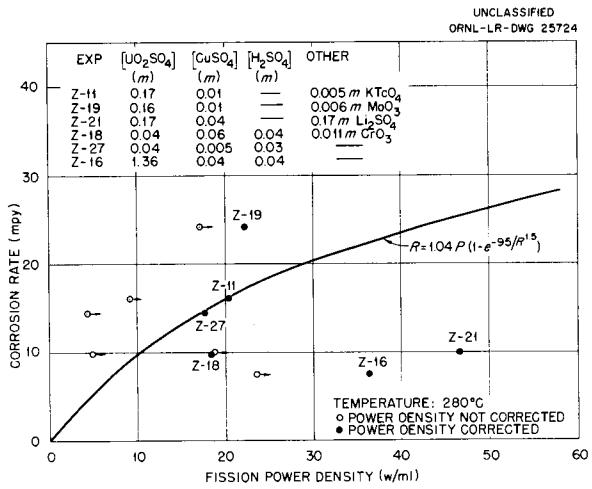

Fig. 14.11. Zircaloy-2 Autoclave Data Corrected for Scale Uranium.

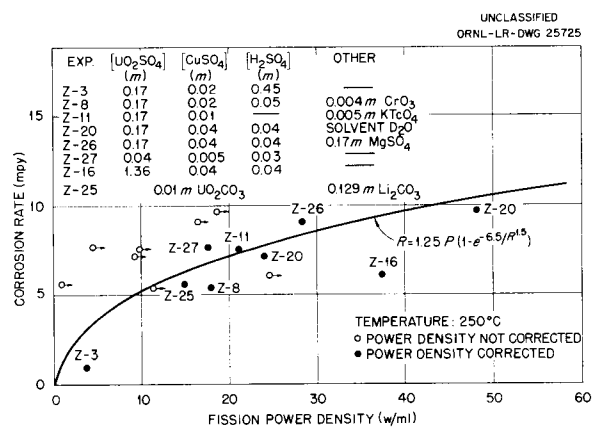

Fig. 14.12. Zircaloy-2 Autoclave Data Corrected for Scale Uranium.

correction to power density from that source. The measured rate of 0.9 mpy is less than that indicated by the curve by a factor of about 3, and this difference is considered significant.

Experiment Z-26. – Magnesium sulfate was added to the solution for this experiment.[23] The earlier interpretation of the result was that the $MgSO_4$ addition increased the corrosion rate. The power-density correction places the Z-26 point very close to the curve, and it would now appear that there was no effect of the addition other than that resulting from a greater uranium concentration in the scale than would be expected without the additive.

Experiment Z-21. – Lithium sulfate additive was employed in this experiment.[24] Unfortunately, the data are open to question, since the solution employed is unstable at 280°C and the run was very short (36 hr). The rate is based on specimen weight losses, since no oxygen-consumption data were obtained. However, if the indicated rate is correct, then Z-21 corroded much more slowly than the standard curve would predict. In this case, the correction for uranium in the film did not change the interpretation of the results.

Experiment Z-11. – Technetium (0.005 *m* $KTcO_4$) was a solution additive in this experiment.[22,25] The earlier conclusion that there was no effect either at 250°C or 280°C by pertechnetate still appears valid. (Note: The previous conclusion was based on a comparison of Z-11 with other 0.17 *m* UO_2SO_4 experiments without excess acid.)

Experiment Z-19. – Molybdenum (0.006 *m* MoO_3) was included in this experiment.[26] The previous comparison with other experiments without acid indicated no effect by the MoO_3. A relatively small amount of uranium was found in the Z-19 scale, yielding a small correction to the power density, and, as now interpreted, the MoO_3 gave rise to a substantial increase in the corrosion rate.

Experiment Z-20. – In this experiment[15] D_2O was used as the solvent. Previous considerations[16] indicated that the corrosion rate in Z-20 was about 30% higher than in comparable light-water exposures. Corrected for uranium in the scale, the Z-20 data fall very close to the standard curve. (Note that Z-20 operated at two power densities, and two Z-20 points are plotted in Fig. 14.12.) A relatively large amount of uranium retained in the scale (6.2% in Z-20 compared with 1–3% in comparable light-water experiments) appears to have been the effect of using D_2O rather than light water. This lack of a direct effect on the corrosion rate, at a given power density, of substituting D_2O for H_2O is in agreement with the results of the L-4-13 loop experiment.[17] This loop experiment employed D_2O and crystal-bar-zirconium specimens. There was no effect on the corrosion of the crystal-bar zirconium which could be attributed to the use of the D_2O.

Experiment Z-8. – Chromium as CrO_3 was an additive in this experiment.[27–28] The data, as now interpreted, seem to re-open the question of a possible beneficial effect by Cr(VI), although the indicated effect (~1.5 mpy less than the predicted 7 mpy) is small and of doubtful significance.

Experiments Z-12, Z-18, and Z-27. – Three autoclave experiments [Z-12 (ref 29), Z-18 (ref 30), Z-27 (ref 23)] have employed 0.04 *m* UO_2SO_4: Z-12, with 0.05 *m* $CuSO_4$ and 0.02 *m* H_2SO_4; Z-18, with 0.06 *m* $CuSO_4$, 0.04 *m* H_2SO_4, and 0.011 *m* CrO_3; and Z-27, with 0.005 *m* $CuSO_4$ and 0.03 *m* H_2SO_4. The uncorrected power densities were 4 to 5 w/ml in each case. Previous considerations indicated that Z-12 (10.3 mpy at 280°C) and Z-18 (9.9 mpy at 280°C) agreed quite well with the data from the loop experiment L-2-10 (ref 31), which employed 0.04 *m* UO_2SO_4, 0.0075 *m* $CuSO_4$, and 0.02 *m* H_2SO_4 at 280°C. The corrosion rate in Z-27 was 14.5 mpy at 280°C and was out of line with these other data. Considerable amounts of uranium were found in the scales from Z-18 and Z-27, 2.6 and 3.5%, respectively. The total amount adsorbed in each experiment was

[23] G. H. Jenks *et al.*, *HRP Quar. Prog. Rep. Jan. 31, 1957*, ORNL-2272, p 102, esp 113–114.

[24] G. H. Jenks *et al.*, *HRP Quar. Prog. Rep. Oct. 31, 1956*, ORNL-2222, p 100, esp 107–108.

[25] G. H. Jenks *et al.*, *HRP Quar. Prog. Rep. Oct. 31, 1956*, ORNL-2222, p 108, Table 13.1.

[26] K. S. Warren, R. J. Davis, and G. H. Jenks, *In-Reactor Autoclave Corrosion Studies. II. Autoclave Z-19*, ORNL CF-57-6-105 (June 27, 1957).

[27] G. H. Jenks *et al.*, *HRP Quar. Prog. Rep. April 30, 1955*, ORNL-1895, p 119–121.

[28] W. E. Clark, *Experiment Z-8*, ORNL CF-55-7-37 (July 13, 1955).

[29] G. H. Jenks *et al.*, *HRP Quar. Prog. Rep. July 31, 1955*, ORNL-1943, p 126, esp 129 (classified).

[30] K. S. Warren, R. J. Davis, and G. H. Jenks, *In-Reactor Autoclave Corrosion Studies. II. Autoclave Z-18*, ORNL CF-57-3-112 (March 22, 1957).

[31] G. H. Jenks *et al.*, *HRP Quar. Prog. Rep. Jan. 31, 1957*, ORNL-2272, p 102, esp 104–108.

sufficient to result in an appreciable lowering of the uranium concentration in solution. Eighty per cent of the uranium charged into Z-18 was found in the irradiated solution, and 60% of the uranium in Z-27 was recovered from the solution. These analytical data are not available for Z-12.

In correcting the power densities in these experiments, Eq. 2 was modified to account for the drop in solution fission power density attending the significant loss of uranium from solution. The corrected power density was calculated as follows:

$$P_c = P_s\left(\frac{U_e}{U_i} + 8.3\frac{U_f}{U_i}\right), \tag{5}$$

where U_e and U_i are, respectively, the average and initial concentration (g/liter) of uranium in solution at the test temperature, and U_f is the percentage uranium in the scale.

Z-18 is plotted in Fig. 14.11, and Z-27 in Figs. 14.11 and 14.12. It should be noted that the corrected power densities are about four times as large as the uncorrected values, which places a large dependence on the scale analyses for uranium. The Z-18 point falls below the standard curve, which may indicate an effect from the CrO_3 additive. The Z-27 results (both 250 and 280°C) are expected to be more clearly indicative of any effect associated with the uranyl sulfate concentration (0.04 *m* compared with the standard 0.17 *m*). It appears that the corrected Z-27 data do not deviate from the standard curve significantly, which is in clear disagreement with the present interpretation of the L-2-10 loop data. For instance, the curve,

$$R = 2.45P\left(1 - e^{-95/R^{1.5}}\right),$$

to which the L-2-10 data can be fitted, extrapolates to a rate of 23 to 24 mpy at the Z-27 corrected power density (17 w/ml) and 280°C. Z-27 corroded at 14.5 mpy at 280°C.

Experiment Z-16. – The Z-16 autoclave[32] employed 1.36 *m* UO_2SO_4. Apparently reliable data were obtained. Z-16 was a duplicate of experiment Z-14 (ref 32) in regard to the solution employed. The corrosion results from oxygen consumption in the Z-14 experiment were confused by a rare example of preferential attack on one specimen. The attack on the other five pins was in agreement with the corrosion rates observed in Z-16. Scale analyses, which are available only from Z-14, showed the scale to be 16% uranium. This analysis was used to correct the Z-16 power density. It is notable that 16% uranium is about eight times the 1 to 3% uranium found after exposures with 0.17 *m* UO_2SO_4–0.04 *m* H_2SO_4 solutions, and the concentrations 1.36 *m* and 0.17 *m* are also in the ratio of 8 to 1. Previous indications that 1.36 *m* UO_2SO_4 was less corrosive to Zircaloy-2 than was the 0.17 *m* UO_2SO_4 still appear correct. The beneficial effect of the high concentration appears greater when corrected values of power density are used.

Experiment Z-25. – This experiment[16] was with a UO_2CO_3 solution (0.01 *m* UO_2CO_3 with 0.129 *m* Li_2CO_3). The Z-25 scale contained 3.3% uranium, and only about 40% of the originally charged uranium was found in the irradiated solution. The power-density correction, calculated in the same manner as that described for Z-18 and Z-27, is indeed very large compared with the solution power density (Fig. 14.12). It should be noted that Z-25 operated at 260°C, whereas it is compared in Fig. 14.12 with 250°C data. The location of the corrected Z-25 point close to the standard curve indicates a rather small change in corrosion due to the substitution of carbonate solution for UO_2SO_4 solution. The earlier interpretation indicated a rate substantially higher in the carbonate solution than in the reference 0.17 *m* UO_2SO_4.

14.2.3 Data from Recent Autoclave Exposures

(a) Experiment L52Z-107. – This experiment was exposed for the purpose of studying the effect on Zircaloy-2 corrosion of Li_2SO_4 added to 0.17 *m* UO_2SO_4. The exposure was cut very short (34 hr with the LITR at power) because the end of the experimental rocking plug was rubbing badly and threatened severe damage to the permanent equipment at the reactor. The corrosion data are probably not very dependable and are not reported.

L52Z-107 was the first autoclave to include a Co-Al alloy as a slow-neutron flux monitor. The alloy, in the form of wire, was encased in Zircaloy-2. Prior to this time the flux in a given experiment has been determined primarily from measurements of induced activity in metal specimens. In the case of Zircaloy-2 specimens, the Zr^{95}-Nb^{95}

[32] G. H. Jenks *et al.*, *HRP Quar. Prog. Rep. Jan. 31, 1956*, ORNL-2057, p 96–98 (classified).

activity is employed. With stainless steel the Cr^{51} is measured. The technique has been to compare specimen activity with a standard sample of the given metal which has been exposed along with a specimen of cobalt in the rabbit hole of the LITR. In short, the method used to determine flux in previous bombs bases the slow-neutron flux determination on cobalt activity but involves the observation of three activities to provide one value for an unknown flux. A complication of this method in the case of Zircaloy-2 is that Zr^{95} is produced in high yield as a fission product, and the specimen must be decontaminated of this fission product with extreme care in order to avoid serious error in flux estimates. Flux determinations from Cs^{137} analyses in autoclave tests are also possible in theory. In practice, the Cs^{137} analyses have given unreasonably low and nonreproducible results and have been discarded. Probably cesium is, in part, adsorbed by the corrosion scale and lost from the solution.

The results of flux determinations in L52Z-107 by the method of measuring induced activity in the Zircaloy-2 and from induced-activity measurements in the cobalt are shown in Fig. 14.13. The flux in the open hole determined by cobalt activation is shown for comparison. Lines rather than points are plotted because the flux is not constant over the length of a given monitor. The length of a monitor is indicated by the length of a plotted line. The axial location of the autoclave and specimens is shown schematically in the lower portion of Fig. 14.13.

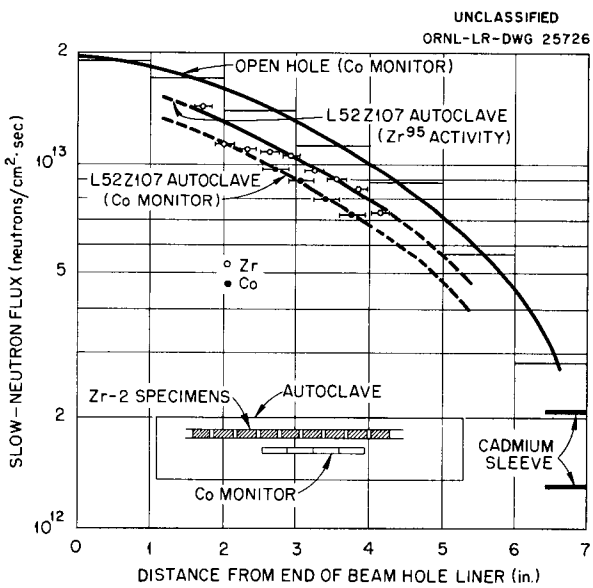

Fig. 14.13. Slow-Neutron Flux Distribution in HB-5 Multiple-Autoclave Facility.

The flux values indicated by the cobalt monitors in this autoclave are about 10 to 15% lower than those determined from measurements of the Zircaloy-2 specimens. This is considered good agreement.

A comparison of typical open-hole flux values in the three autoclave facilities employed at the LITR during the last three years is shown in Fig. 14.14. Included are the slow-neutron flux distributions in HB-6 (open hole) and in HB-5 both before (type II autoclave[33]) and after (type III autoclave[33]) the installation of the multiple-hole equipment.[34] The multiple-hole facility includes a provision for retracting the experiment into a cadmium sleeve, and the cadmium depresses the flux, particularly at the positions near the rear of the experiment. The open-hole flux in HB-6 and the relative position of the types II and III autoclaves are also shown in Fig. 14.14.

(*b*) Experiments L6Z-104, -106, and -112. – These experiments employed Zircaloy-2 autoclaves. In each test, specimens included Zircaloy-2, type 347 stainless steel and Zr–15% Nb–1.5% Sn alloy. The exposures were at 280°C. The solutions were 0.17 *m* UO_2SO_4, 0.03 *m* $CuSO_4$, and 0.03 *m* H_2SO_4 in L6Z-104 and 0.17 *m* UO_2SO_4, 0.03 *m* $CuSO_4$, and 0.06 *m* H_2SO_4 in L6Z-106 and L6Z-112. These experiments were undertaken primarily to observe the in-pile corrosion of stainless steel in a system in which the buildup of steel corrosion products in solution is minimized and in which the radiolytic-gas pressure is controlled at a low value. However, out-of-pile controls to determine the extent of corrosion in the absence of radiation are needed for the interpretation of the stainless steel data. These are not yet available.

The stainless steel specimens exposed in these tests appeared upon visual examination to be covered by a brass-colored scale similar to that found on Zircaloy-2 exposed in-pile. The usual color of stainless steel specimens after exposure

[33] K. S. Warren and R. J. Davis, *In-Reactor Autoclave Corrosion Studies – LITR. I. Outline of Methods and Procedures*, ORNL CF-57-5-110 (May 22, 1957).

[34] R. J. Davis, D. T. Jones, and F. J. Walter, *Proposed Multiple In-Pile Rocking Bomb Experiment*, ORNL CF-56-9-109 (Sept. 27, 1956).

is rust-brown. The implication that zirconium is transferred to steel surfaces will be better established by adequate scale analyses for zirconium. Zircaloy-2 corrosion in these experiments appears to be in reasonable agreement with earlier data, with the notable exception of the Zircaloy-2 specimens in L6Z-106. These pin specimens showed longitudinal fissures along their entire length. Investigation revealed that similarly located striations existed on the pins before exposure, and it appears that flaws in stock material are responsible for the preferential attack. Since deposits in the fissures were not removed during defilming, the values for average penetration as

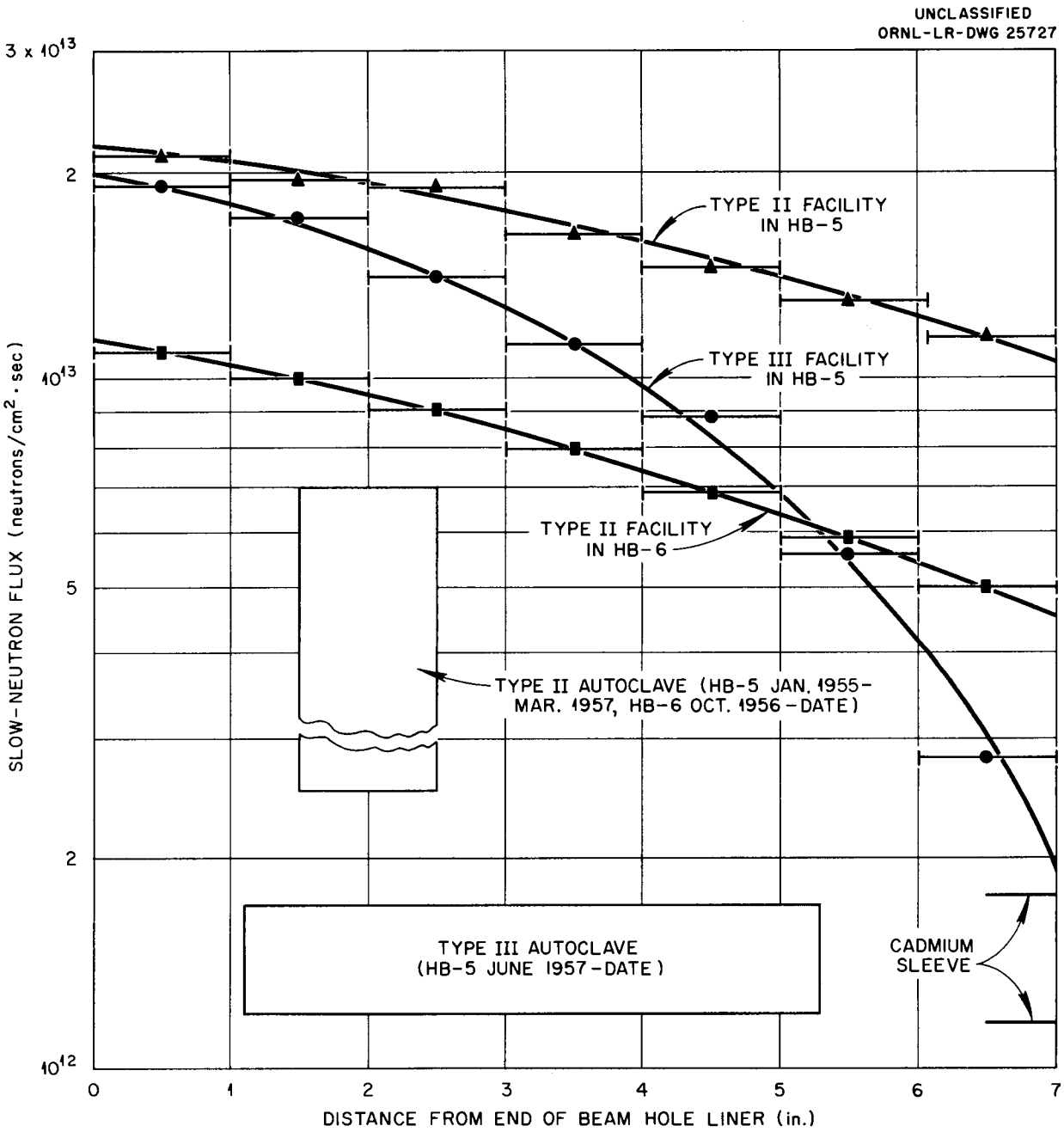

Fig. 14.14. Slow-Neutron Flux Distribution in Rocking-Autoclave Facilities at the LITR.

measured by weight loss are not meaningful. This is only the second observation of localized attack of Zircaloy-2 in in-pile autoclave tests.[32]

Samples of scale from the three types of specimens (Zircaloy-2, type 347 stainless steel, Zr-Nb-Sn alloy) in L6Z-112 were analyzed separately. The scale from the Zircaloy-2 contained 2.5% uranium, and the scale from the stainless steel and niobium alloy contained only about 0.5% uranium.

(c) Experiment L6Z-113. – This experiment was operated in order to expose samples of pure niobium metal and of sintered zirconium oxide. The zirconium oxide used was a monoclinic material, fired at 1600°C in air, density 4.6; presumably it contained no stabilizing materials. The zirconia was in the form of two short cylindrical pieces, diameter about ⅛ in. and length about ¼ in. The experimental conditions and the results of this experiment are summarized in Table 14.2.

During exposure the oxide material lost its integrity, and it was collected after the test as a loosely adherent mass. No information is available as to the stability of this material in out-of-pile solutions. However, Hess[35] has found in preliminary out-of-pile tests that unstabilized ZrO_2 falls apart in UO_2SO_4 solution at 275°C. Hence the behavior of the zirconia in this in-pile experiment was not necessarily a result of radiation exposure. The 2.8% uranium in the zirconia after exposure is about the same as the 1 to 3% uranium found in Zircaloy-2 scale from autoclaves exposed to 0.17 *m* UO_2SO_4 solution with 0.04 *m* excess acid.

During exposure the niobium pins became covered with an extremely heavy chartreuse-colored scale. It is estimated that the niobium scale was about five times as heavy as the typical Zircaloy-2 scale. The presence of the zirconia samples probably contributed somewhat to the heavy scale on the niobium specimens, although only 5.6% of the niobium scale was found to be zirconium. A large part of the niobium scale was uranium (26%) and copper (16%). The niobium specimens, even though they were apparently exposed to a very high localized power density from the 25% uranium scale, corroded only about one-third as much as the Zircaloy-2 specimens.

[35]D. N. Hess, Conversation with G. H. Jenks.

Table 14.2. Autoclave L6Z-113 Data

Solution Composition	UO_2SO_4 (*m*)	$CuSO_4$ (*m*)	H_2SO_4 (*m*)
Before exposure	0.157	0.037	0.037
After exposure	0.077	0.010	(0.023)*

Scale and Zirconia Analyses	U (%)	SO_4 (%)	Cu (%)	Zr (%)
ZrO_2	2.8	0.7	0.7	29.2
Niobium scale	25.9	0.9	16.0	5.6

Exposure Conditions and Corrosion Rate from O_2 Loss	
Temperature, °C	280
Exposure time, hr	344.8
Fission power density, w/ml	6.3
Corrosion rate, mpy	6.5

Specimen Data		
Material	Penetration from Weight Loss (mils)	Corrosion Rate (mpy)
Zircaloy-2	0.296	7.5
Niobium	0.099	2.5

*Evaluated from total sulfate determination.

The Zircaloy-2 corrosion in this experiment appears to agree well enough with other data shown in Figs. 14.9 and 14.11. To make the comparison, the measured power density of 6.3 w/ml was corrected both for uranium in the scale (assuming 2.8% as in the case of the zirconia samples) and for the large drop in uranium concentration in the solution (0.157 to 0.077 *m*). The correction was made in the manner discussed in Sec 14.2.2b in connection with Z-27. The corrected power density is 7.9 w/ml. The data in Fig. 14.9 would predict a corrosion rate of 7.9 mpy at this power density (and 280°C), which compares adequately with the 6.5 mpy determined from oxygen consumption data and with the 7.5 mpy determined from specimen weight losses.

14.3 SUPPORTING RESEARCH

Zircaloy-2 foils, 0.6 by 0.18 cm, contained in a thermal siphon loop were exposed for approximately 60 hr at 300°C to Van de Graaff electrons. The test solution was 0.04 *m* UO_2SO_4, 0.02 *m* excess H_2SO_4, and 0.01 *m* $CuSO_4$. Current densities approximately 40 $\mu a/cm^2$ at the metal surface were used, and it is estimated that the power density in the solution adjacent to the specimens was about 60 w/ml. Range curves for 1.5-Mev electrons indicate that about 0.6 w of the power put into the loop was absorbed by the 7-mil specimens.

Weight changes of $+5.8 \times 10^{-5}$ and $+2.8 \times 10^{-5}$ g, as compared with $+7 \times 10^{-6}$ g for a nonirradiated specimen, were obtained under these experimental conditions. The uncertainty in these weight values is estimated to be $\pm 2 \times 10^{-5}$ g. These weight changes give upper limits of 5 and 2 mpy for the corrosion rate on the irradiated specimens. As determined by microscopic examination, the films on the irradiated specimen are approximately 2000 to 2500 Å thick. The formation of a ZrO_2 film 2500 Å in thickness would increase the weight of a specimen by 7.9×10^{-6} g. For comparison, if the corrosion behavior of a specimen in this system is comparable to that expected in water at the same temperature, but out of radiation, an increase in weight of 2.2×10^{-5} g would be expected.[36] Hence, the results of weight and thickness measurements in this experiment do not show any significant effect of the electron irradiation on the corrosion rate of Zircaloy-2. The films on the irradiated specimens are dark gray and very adherent in appearance. Diffraction studies on these specimens are now being made.

Titanium foils were irradiated in a similar manner. At the end of a 50-hr irradiation, performed intermittently over a period of several weeks, the sample holder and samples fell down into the loop when the loop was opened and the fitting holding the sample holder removed for examination.

A new sample holder and samples were inserted. Subsequent operation of the loop resulted in a ductile failure of the loop wall. Failure of the temperature controller during the night was largely responsible, although the failure itself did not occur until the following morning, after the temperature recorder had been repaired and after additional heat had been put into the loop.

Visual examination indicated that gradual expansion of the loop wall at some elevated temperature and approximately 600 psi had occurred and that a ductile failure of the titanium resulted. A detailed study of the temperature-controller chart showed that temperature cycling, as shown by thermocouple readings, had taken place in the loop wall. The evidence indicates that temperature cycling was caused by erratic flow, or slugs of liquid formed by some impediment lodged in the loop. Recovery of the old sample holder and sample, which had been blown out through the hole in the loop wall, confirms the picture already given.

Metallographic examination[37] of specimens taken at the point of failure indicates that the metal was heated above the beta transformation temperature, about 950°C. Ductile failure resulted when the metal expanded at this temperature under the existing pressure (approximately 400 to 600 psi).

Microscopic and electron-micrograph studies are being made on both a 10-mil titanium foil specimen, irradiated for 50 hr, and a section of the 20-mil titanium loop window, which had received a radiation exposure for more than 200 hr. The film on the foil shows interference colors and is not over 1000 Å at its thickest point. The film on the outside of the loop window resembles that on the foil. The film on the inside is dark gray and approximately 20,000 to 40,000 Å thick. It is not yet known whether this is typical of the unirradiated surfaces in the rest of the loop. Crystallites of anatase titanium dioxide on the inside film are much larger than those on the outside, as indicated by spot diffraction patterns.

In additional experiments, type 347 stainless steel foils are being similarly irradiated. An exposure of 6 hr has been made on one set of samples, and a longer run of about 50 hr is being completed on a second set.

---

[36] D. E. Thomas, *Natl. Nuclear Energy Ser. Div. VII* 4, 608, esp 633 (1955).

[37] T. M. Kegley and R. L. Fitzgerald, *Metallographic Examination of ¼ in. Diameter Ti 75A Tubing Failure in Thermal Loop*, memo to M. D. Silverman (Oct. 24, 1957).

15. METALLURGY

G. M. Adamson

R. G. Berggren
E. S. Bomar
F. W. Cooke
W. J. Leonard
M. L. Picklesimer
J. J. Prislinger
P. L. Rittenhouse
R. L. Stephenson
J. K. White
J. C. Wilson

15.1 PHYSICAL METALLURGY

15.1.1 Zirconium-Alloy Development

Zirconium-base alloys containing niobium have shown the greatest promise in the development of a corrosion-resistant alloy to replace Zircaloy-2 as the HRP core-tank material. Basic physical-metallurgy studies and in-pile corrosion tests are being used to procure information necessary for the development of these alloys.

Data on the transformation occurring in the Zr-Nb-X alloy systems have been reported in four prior reports.[1-4] Age-hardening data for Zr–15% Nb–X alloys with X = 1% Al, ½% Cu, 2% Th, 1% Cr, 2% Mo, and 5% Mo were reported[4] for aging times up to 2 hr at 400°C. These alloys and others with X = 1% Ni, 5% Pd, and 3% V have now been run at 350, 400, and 500°C in the transformation machine for times up to 2 hr and in capsules for various times up to three weeks. All these ternary additions delayed the hardening transformation, with the addition of molybdenum being the most potent. With an addition of 5% Mo, no increase in hardness occurred in three weeks at any temperature. Additions of aluminum and copper lower the temperature for maximum rate of the hardening transformation to 350°C or lower.

With many of the alloys the specimens aged for 2 hr in the transformation machine were not so hard as those aged for like periods in the capsules. The major difference between these two methods is in the rate of heating to the aging temperature, the transformation machine requiring only seconds, while in the capsules it takes minutes. The higher hardening appears to have occurred at temperatures below the aging temperature.

Some progress has been made in the isothermal transformation study of the Zr–15% Nb base alloys. Specimens of Zr–15% Nb–2% Pd, previously transformed at 600°C for 24 hr, were held at 700, 800, 900, and 1000°C for times up to 30 min and mercury quenched in the isothermal transformation machine. Microstructural examination and hardness measurements are now being made. This series of specimens should yield information on the effects of time and temperature on the dissolution of the transformation products and, therefore, the time and temperature required to produce a standard and reproducible beta condition for isothermal transformation kinetics studies. Specimens of the Zr–15% Nb alloy held at various beta temperatures for various times and transformed at 400°C for 30 min are being examined.

A series of specimens of various niobium compositions with various heat treatments was submitted to the x-ray diffraction group for studies to determine the structure of the phases present and the changes of structure with aging time. A portion of this information was reported in the last report.[4] The diffraction work (performed by R. M. Steele and H. L. Yakel, Jr.) has utilized techniques involving oscillation, Weissenberg, and Debye-Scherrer diffraction patterns; single-crystal and polycrystalline wire specimens were used. The data are in Table 15.1. An analysis of the diffraction data, coupled with the hardness and metallographic data, implies a two-stage, two-transition-product decomposition mechanism for the hardening reaction, a "reversible" diffusionless transformation product ("martensitic") in the quenched specimens, and a "conventional" hypoeutectoid reaction process at the higher temperatures of transformation. A tentative explanation of the transformation mechanisms can be formulated as follows. When water-quenched from temperatures in the beta field, a small amount of

[1] G. M. Adamson *et al.*, *HRP Quar. Prog. Rep. Oct. 31, 1956*, ORNL-2222, p 114–116.

[2] G. M. Adamson *et al.*, *HRP Quar. Prog. Rep. Jan. 31, 1957*, ORNL-2272, p 119–123.

[3] G. M. Adamson *et al.*, *HRP Quar. Prog. Rep. April 30, 1957*, ORNL-2331, p 124.

[4] G. M. Adamson *et al.*, *HRP Quar. Prog. Rep. July 31, 1957*, ORNL-2379, p 122–126.

Table 15.1. X-Ray Diffraction Results for Transformed Zr-Nb and Zr–15% Nb–2% Pd Alloys[a]

Alloy Composition (wt %)	Heat Treatment[b]	Lattice Constants and Phases Present						
		Retained-Beta bcc (Å)	"Widmanstätten" bct (Å)	"Omega" bcc (Å)	Beta I bcc (Å)	Beta II bcc (Å)	Alpha Zr cph (Å)	Nb–10 Zr[c] bcc (Å)
85 Zr–15 Nb	1200°C, 3 hr, WQ	$a_0 = 3.547 \pm 0.007$ Vol = 44.6 ± 0.3 Å^3	$a_0 = 3.547 \pm 0.007$ $c_0 = 3.989 \pm 0.008$ $c/a = 1.125 \pm 0.002$ Vol = 50.2 ± 0.3 Å^3	$a_0 = 10.9 \pm 0.2$	Absent	Absent	Absent	Absent
	900°C, 1 hr, WQ	$a_0 = 3.547 \pm 0.001$	Present	Small amount	Absent	Absent	Absent	Absent
	900°C, 1 hr, WQ 400°C, 3 hr, AC	Absent	Absent	Moderate amount; $a_0 = 10.71 \pm 0.04$	$a_0 = 3.557 \pm 0.005$	$a_0 = 3.506 \pm 0.005$	Absent	Absent
	900°C, 1 hr, WQ 400°C, 24 hr, AC	Absent	Absent	Small amount; $a_0 = 10.74 \pm 0.04$	$a_0 = 3.563 \pm 0.005$	$a_0 = 3.494 \pm 0.005$	Absent	Absent
	900°C, 1 hr, WQ 500°C, 4 hr, AC	Absent	Absent	Small amount; $a_0 = 10.65 \pm 0.06$	$a_0 = 3.562 \pm 0.001$	$a_0 = 3.526 \pm 0.001$	Absent	Absent
	900°C, 1 hr, WQ 500°C, 24 hr, AC	Absent	Absent	Absent	Small amount; beta I forms alpha Zr by orientation of spots in pattern	Small amount	$a_0 = 3.224 \pm 0.004$ $c_0 = 5.152 \pm 0.006$	Absent
	900°C, 1 hr, WQ 500°C, 1 wk, AC	Absent	Absent	Absent	Absent	Absent	$a_0 = 3.230 \pm 0.004$ $c_0 = 5.146 \pm 0.006$	$a_0 = 3.31 \pm 0.01$
	900°C, 1 hr, WQ 600°C, 1 hr, AC	$a_0 = 3.549 \pm 0.002$	Absent	Absent	Absent	Absent	Small amount	Absent
	900°C, 1 hr, WQ 600°C, 1 wk, AC	$a_0 = 3.528 \pm 0.002$	Absent	Absent	Absent	Absent	Moderate amount	Absent
Zr–15 Nb–2 Pd	900°C, 1 hr WQ	$a_0 = 3.539 \pm 0.004$	Absent[d]	Small amount	Absent	Absent	Absent	Absent
	900°C, 1 hr, WQ 500°C, 4 hr, AC	$a_0 = 3.521 \pm 0.004$	Absent	Absent	Absent	Absent	Small amount	Absent
	900°C, 1 hr, WQ 500°C, 24 hr, AC	$a_0 = 3.516 \pm 0.004$	Absent	Absent	Absent	Absent	Amount equal to beta	Absent
	900°C, 1 hr, WQ 500°C, 1 wk, AC	Absent	Absent	Absent	Absent	Absent	$a_0 = 3.230 \pm 0.004$ $c_0 = 5.142 \pm 0.006$	$a_0 = 3.33 \pm 0.01$ 3/1 alpha/Nb
	900°C, 1 hr, WQ 600°C, 1 hr, AC	$a_0 = 3.539 \pm 0.001$	Absent[e]	Absent	Absent	Absent	Absent	Absent
	900°C, 1 hr, WQ 600°C, 1 wk, AC	$a_0 = 3.528 \pm 0.001$	Absent[e]	Absent	Absent	Absent	Small amount	Absent
90 Zr–10 Nb	900°C, 1 hr, WQ	$a_0 = 3.555 \pm 0.001$	Absent[d]	Moderate amount	Absent	Absent	Absent	Absent
92.5 Zr–7.5 Nb	900°C, 1 hr, WQ	$a_0 = 3.558 \pm 0.001$	Absent[d]	Considerable amount	Absent	Absent	Absent	Absent
95 Zr–5 Nb	900°C, 1 hr, WQ	Absent	Absent	Absent	Absent	Absent	Entire[f]	Absent

[a]All specimens capsulated in Vycor in partial atmosphere of purified argon, all 0.010 wire specimens.
[b]WQ = water quenched; AC = air cooled in capsule.
[c]Nominal composition.
[d]Widmanstätten platelets present by microscopy.
[e]Widmanstätten platelets absent by microscopy.
[f]Specimen entirely martensitic alpha Zr by microscopy.

a body-centered tetragonal (bct) phase is formed, either as platelets or as sheets, on the (100) planes of the retained-beta matrix during the quenching operation. This bct phase has been associated with the Widmanstätten platelet phase observed in the microstructure of the beta-quenched material, which is also observed to occur on the (100) planes of the retained-beta matrix and which disappears from the microstructure of reheated and aged specimens at the same rate as that of the bct phase from the x-ray diffraction patterns. The Widmanstätten platelet phase apparently redissolves in the beta matrix, without decomposition, upon heating the beta-quenched specimen to 300°C or above.

In addition, a second phase, which indexes with the "omega" phase reported[5] to occur in the Zr-Mo system and quite similar to that occurring in the beta-titanium alloys, forms during the quenching operation. The amount of this "omega" phase present in the beta-quenched samples decreases with increasing niobium content. The lattice structure of the "omega" phase appears to be essentially body-centered cubic (bcc), with a lattice spacing slightly larger than three times the lattice spacing of the bcc retained-beta-matrix phase. In the Zr–15% Nb alloy, the amount of "omega" phase present during aging first increases and then decreases with increasing aging time at a particular temperature.

Coincident with the increase in the amount of the "omega" phase present on aging, the retained-beta matrix seems to split into two bcc phases called beta I and beta II. The lattice spacing of the beta I phase is larger than that of the retained-beta phase, while the spacing of the beta II phase is smaller. This change in spacing is consistent with an increase in zirconium content for beta I and an increase in niobium content for beta II. The lattice spacing of beta I increases and that of beta II decreases with aging time towards the spacings found or expected for pure beta-zirconium and 90% Nb–10% Zr phases, respectively. When the composition of beta I phase has changed to approximately 5% Nb, it transforms to alpha zirconium containing niobium, as evidenced by the orientation of the spots for alpha zirconium and beta I in the oscillation diffraction patterns. The beta II phase eventually is so enriched in niobium that it transforms to the equilibrium niobium phase containing approximately 10% Zr. With the formation of alpha zirconium and the equilibrium niobium phase, the specimen has become overaged and the hardness decreases. At 550°C or above for the Zr–15% Nb alloy, the hardening type of transformation does not occur. Instead, the more conventional transformation of a hypoeutectoid system occurs, involving the precipitation of alpha-zirconium platelets in the grain boundaries, enriching the retained-beta phase in niobium, until eventually the equilibrium Nb–10% Zr phase begins to coprecipitate.

No physical picture for the formation of the two beta phases has been successfully derived. Either lines or spots which should be present in the diffraction patterns are missing for a given proposed mechanism, or lines or spots are present which cannot be accounted for by the proposed explanation. A recently obtained oscillation pattern, which was overexposed deliberately, has shown a very faint side-band occurring which had not been observed in any of the prior patterns. The pattern has not been analyzed. This observation may permit the derivation of a physical picture for the transition phase transformation.

The primary effects of the addition of small amounts of the ternary substitutional alloying elements are the lowering of the maximum temperature at which the hardening reaction can occur, an increase in incubation time for the hardening reaction at all temperatures (in some cases complete suppression seems to occur), a lowering of the temperature of maximum rate of the hardening reaction, and a definite increase in the rate of the "conventional" hypoeutectoid reaction at the higher temperatures of reaction. The addition of oxygen (which is an interstitial alloying element), by the use of sponge zirconium, speeds up all the transformation reactions.

Ingots of Zr (sponge)–15% Nb alloy were successfully extruded to $1\frac{1}{8}$-in. round stock. These bars were swaged from a furnace at 850°C to bar stock $\frac{7}{16}$ in. in diameter. After nondestructive testing, the bars were cut to $5\frac{1}{2}$-in. lengths and machined to $\frac{3}{8}$ in. in diameter and further inspected. This stock was then heat treated into two lots: (1) water quenched at 900°C and (2) water quenched at 900°C followed by two-week anneal at 550°C. From these two lots, subsize impact and tensile specimens were made for use in the first corrosion-specimen assembly for the HRT core.

[5]H. A. Robinson *et al.*, *J. Metals* 8, 1544 (1956).

15.2 MECHANICAL METALLURGY

15.2.1 Tensile Properties of Irradiated Zirconium Alloys

As a supplement to the radiation-damage work being conducted by the Solid State Division, Sec 15.5, samples of materials of interest to the HRP are irradiated in the in-pile loops operated by the Reactor Materials Research Section. These loops are operated primarily for corrosion testing and usually do not operate for long enough times to provide a sufficient fast-flux dose to cause large changes in mechanical properties by radiation damage. It is hoped, however, that it will be possible to determine whether any large radiation-induced changes occur or whether any adverse effects, such as hydrogen pickup in the samples, result from exposure to the fissioning uranyl sulfate solution at loop temperature.

Subsize tensile specimens of crystal-bar zirconium were exposed in in-pile loop L-2-15. This loop was operated at 280°C in beam hole HB-2 of the LITR with the following solution composition: 0.17 *m* UO_2SO_4, 0.028 *m* H_2SO_4, 0.015 *m* $CuSO_4$. (For further information on the loop operation, consult *HRP Quar. Prog. Rep. July 31, 1957*, ORNL-2379, p 101–114.) The estimated fast-neutron dose on the samples during the reactor exposure was between 0.7 and 1.4 × 10^{19} nvt. Samples from a single ingot were exposed to the solution both in the region of high flux (core) and in the region of low flux (in-line), and were used for control samples. Additional control samples were fabricated from other ingots made at the same time.

The tensile data obtained from these crystal-bar-zirconium samples are listed in the upper half of Table 15.2. As was previously found[4] for

Table 15.2. Tensile Data from Irradiated Zirconium Alloys

Position	Temperature (°C)	Strain Rate (in./in./min)	Tensile Strength (psi)	Proportional Limit (psi)	Reduction in Area (%)
			Crystal-Bar Zirconium – Loop L-2-15		
Core	RT*	0.05	40,800	26,700	42.0
Line	RT	0.05	41,300	21,200	50.4
Control	RT	0.05	40,000	23,500	42.9
Core	RT	0.002	39,450	21,950	50.4
Control	RT	0.05	38,100	18,800	43.9
Control	RT	0.05	41,400	23,500	52.2
Control	RT	0.002	40,800	20,400	60.2
Core	300	0.05	18,650	13,300	78.3
Line	300	0.05	20,400	18,400	78.5
Control	300	0.05	18,050	10,100	80.4
Control	300	0.05	17,000	10,400	88.3
Control	300	0.05	21,900	12,500	76.7
Control	300	0.002	18,000	11,750	97.4
			Zircaloy-3A – Loop L-4-13		
Core	RT	0.05	73,700	60,784	46.4
Control	RT	0.05	71,400	54,902	47.6
Core	300	0.05	38,196	30,980	55.2
Control	300	0.05	39,216	27,834	56.7

*RT = room temperature.

Zircaloy-2, no significant change in mechanical properties resulted from these irradiations in uranyl sulfate. The variations between core, line, and control samples are not systematic and are smaller than the variations between the various control samples. A possible small exception is the proportional limit, but additional tests will be required to show whether a small increase actually occurred. This material is sensitive to strain rate, in that a decreasing rate is accompanied by a decrease in tensile strength and proportional limit and an increase in ductility; however, these changes are independent of irradiation.

Subsize tensile specimens of Zircaloy-3A (0.2% Sn, 0.2% Fe) were irradiated in loop L-4-13. This loop operated at 250°C in LITR beam hole HB-2 with a solution containing 0.17 *m* UO_2SO_4. (Operating details are reported in *HRP Quar. Prog. Rep. April 30, 1957*, ORNL-2331, p 113–116.) The fast-neutron flux has not yet been determined in this facility, but a rough estimate has been made that the integrated fast-neutron dose was between 2 and 5×10^{18} nvt. On removal from the loop the core specimens had a purplish film which did not separate from the specimen during testing.

As shown by the data in the lower half of Table 15.2, no significant change in tensile properties of Zircaloy-3A was found under the conditions of exposure in this loop.

15.2.2 Tensile Properties of Irradiated Titanium Alloys

Along with the zirconium alloys some loop irradiation studies have been made with titanium alloys. Subsize tensile specimens of A-40 titanium were exposed in loop L-4-13, at the operating conditions discussed in Sec 15.2.1. On removal the core specimens had a straw-colored film which was very tenacious and did not separate during deformation.

Although it is not reasonable to draw conclusions from two specimens, loop irradiation appeared to cause mechanical-property changes in this alloy, Table 15.3. In both cases the tensile strength and proportional limit increased while the reduction in area decreased. No metallographic or hydrogen data are available.

The usual subsize tensile specimens of titanium alloy A-110AT were irradiated in loop L-4-16. This loop also operated in beam hole HB-4 of the

Table 15.3. Tensile Data from Irradiated Titanium Alloys

Loop Position	Temperature (°C)	Strain Rate (in./in./min)	Tensile Strength (psi)	Proportional Limit (psi)	Reduction in Area (%)
			Titanium A-40 – Loop L-4-13		
Core	RT*	0.05	53,900	37,647	73.3
Control	RT	0.05	48,000	32,549	77.7
Core	300	0.05	29,098	19,608	72.3
Control	300	0.05	19,400	10,196	84.9
			Titanium A-110AT – Loop L-4-16		
Core	RT	0.05	90,196	72,549	45.6
Line	RT	0.05	87,451	68,627	43.8
Control	RT	0.05	88,235	66,666	50.2
Control	RT	0.05	87,451	68,627	53.8
Core	300	0.05	42,039	28,235	47.0
Line	300	0.05	29,333	18,824	55.1
Control	300	0.05	33,569	22,745	71.6
Control	300	0.05	32,863	18,824	68.4

*RT = room temperature.

LITR. It circulated a solution containing 0.17 *m* UO_2SO_4 at 280°C. (Operating details have been reported in *HRP Quar. Prog. Rep. April 30, 1957*, ORNL-2331, p 118.) The estimated integrated fast-neutron dose for samples in this loop was 2.5 to 5.0 × 10^{18} nvt. The core specimens were covered with a straw-colored film which separated during pulling, while the line specimens had a charcoal-gray film which was even less adherent. The tensile data for the A-110AT alloy, listed in the lower half of Table 15.2, seem to confirm the data for A-40 titanium. Again, only single specimens were tested, but at both temperatures the tensile strength and proportional limit are higher in the core samples than in the controls, while the reduction in areas is lower. The changes are relatively small, but so are the flux doses.

15.3 WELDING DEVELOPMENT

15.3.1 Titanium Welding

Weldments have been made in ⅛-in. titanium A-110AT alloy sheet. This alloy is a high-strength ductile alloy of titanium in which aluminum and tin have been added as strengthening elements. The function of these elements is to stabilize and strengthen the predominant alpha phase by their complete solution in it.

Metallurgical examination of sheet and plate stock of titanium A-110AT received to date indicates the presence of another phase, in minor amounts, uniformly distributed within the alpha-phase matrix. This condition is similar to that seen in the two-phase high-strength alpha-plus-beta alloys, where strength is obtained with some sacrifice of ductility in the heat-affected zone of weldments.

The A-110AT titanium was welded in air by use of the usual HRP techniques developed for high-purity titanium. Weldments made in ⅛-in. plate were sectioned for microscopic examination and guided bend tests. Figure 15.1 is a photograph of root and face bends on a 2½ *T* radius. Results are considered good for a titanium alloy. The metallographic examination indicated that the thermal cycles encountered in welding sheet of this thickness caused no significant metallurgical changes in the heat-affected zone of the base metal. However, from evidence gained by equilibrium-temperature studies of titanium A-110AT base metal in the temperature range expected in the heat-affected zone of a weldment, possible loss of ductility may be encountered in heavier weldments of this material.

While it is possible to furnace-braze titanium to itself and in some cases to stainless steel, for many HRP applications it would be desirable to have a technique for torch-brazing in the field. A suitable method for torch-brazing titanium in air by use of a silver filler metal was investigated. The first requirement in such an investigation is the development of a proper flux, which will permit the brazing metal to wet the titanium metal surface and flow properly. In addition, the flux must be chemically stable at the melting and flow temperature of the filler metal and must shield the base metal and molten braze metal from the atmosphere. Fluxes currently used or recommended for titanium brazing are essentially chloride-base fluxes. There are two disadvantages in the use of such fluxes in HRP applications: (1) chloride ions may be introduced into the system and (2) these fluxes break down at the temperature of pure-silver brazing (1900 to 2000°F) and result in unacceptable oxidized joints. In view of these considerations, fluoride-base fluxes were investigated. A commercial fluoride-base flux and two others made in the laboratory were tried. The latter two were made of various proportions of sodium, potassium,

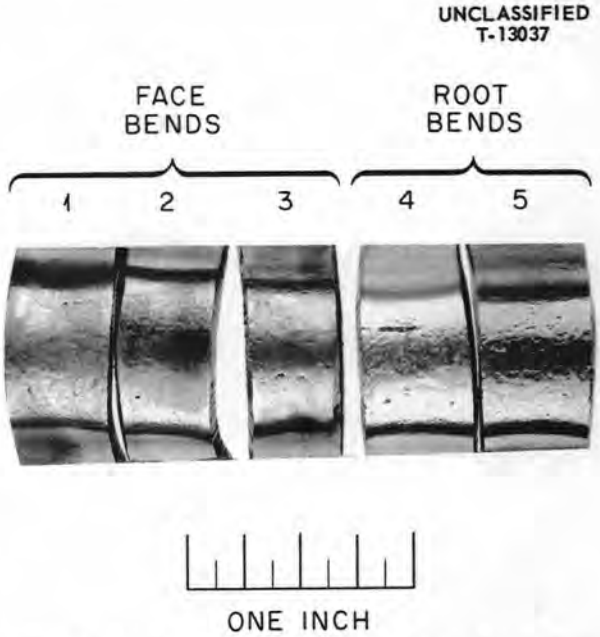

Fig. 15.1. Samples After Root- and Face-Bend Tests on A-110AT Titanium Weldments.

lithium, and silver fluorides, with a small percentage (1 to 3%) of cupric chloride or strontium chloride. A water and an alcohol paste was made of each flux. In the tests the fluxes broke down at a temperature a few hundred degrees below the melting point of silver. The titanium surface became badly oxidized; and the silver, when it melted, failed to wet the titanium. Additions of 10% potassium hydroxide failed to raise the effective operating temperature of the flux. At present, the possibility of torch-brazing titanium with braze metals acceptable to the HRP appears to be remote.

15.3.2 Stainless Steel Welding

In producing machine-welded type 347 stainless steel pipe joints in the field, it would be desirable, for obtaining simplicity of welding-equipment design, to complete a weld pass in one 360-deg rotation of the welding torch. In manual welding of fixed pipe, high-quality welds are more easily obtained with two weld passes, each covering 180 deg only, starting at the 6 o'clock position of the weld joint.

Type 347 stainless steel manual pipe welds were made in which a complete 360-deg torch traverse was used. Although this technique was more difficult than the standard technique, welds of HRP quality were obtained. These results indicate that a machine-welding apparatus, which inherently possesses much closer control of welding variables than is possible in manual welding, should experience little difference in weld quality irrespective of welding sequences used in completing a pass in pipe welds.

15.4 METAL-SOLUTION REACTIONS

15.4.1 Titanium

Under an ORNL subcontract Stanford Research Institute is studying combustion reactions between titanium and aqueous solutions. This study was prompted by the failures of titanium valve trim in the HRP dump-valve test loop. Stanford has previously shown[6] that titanium disks will be consumed completely if ruptured by 1100- to 1800-psi oxygen pressure at temperatures from 30 to 320°C.

In a continuation of the work it was shown that ignition did not take place when the disk was ruptured with water containing as much as 7200 ppm of oxygen at temperatures of 215°C. However, steam-oxygen mixtures containing 20% oxygen (180 psi) caused complete consumption of the disk at 300°C.

In a second type of test a ¼-in. tensile specimen 5 in. long was broken in a controlled atmosphere. The rod was completely consumed when fractured in 350-psi, or greater, oxygen pressure at room temperature. The critical oxygen pressure decreased to 250 psi at 300°C. While most of the work was with A-55 titanium, it appears that C-130Am, 6% Al–4% V, and A-110AT titanium alloys all behave similarly, confirming the data obtained with the rupture disks. When samples of A-55 titanium were broken in oxygen-saturated water, no reaction occurred; however, when they were broken in the steam space above the liquid, the upper half of the bar was consumed completely, but the lower half was quenched after burning approximately ½ in. below the water surface.

In a few preliminary experiments it appears that higher oxygen pressures are required for ignition in helium-oxygen mixtures than in pure oxygen.

For purposes of comparison, either rupture disks or tensile specimens of type 304 stainless steel, aluminum, magnesium, zirconium, and iron were ruptured in oxygen at pressures of 1000 psi or higher. The only material which reacted was zirconium.

15.4.2 Zirconium

A subcontract for studying metal–aqueous-solution reactions has been placed with Aerojet General Corp. The purpose of this contract is to determine whether any major differences exist between the reactions of zirconium with uranyl sulfate and those with water. Reactions between zirconium and water have been extensively studied by many laboratories.

A series of preliminary tests were made at room temperature by use of the Aerojet explosion dynamometer.[7] In these tests the reactions between molten Zircaloy-2 injected into uranyl

[6] F. E. Littman, *Reactions of Titanium With Water and Aqueous Solutions*, Stanford Research Institute Reports No. 2 and 5 (July 2 and Oct. 14, 1957).

[7] H. M. Higgins and R. O. Schultz, *The Reaction of Metals With Water and Oxidizing Gases at High Temperatures*, IDO-28,000 (April 30, 1957).

sulfate were the same as when it was injected into water.[8]

Zircaloy-2 wires were heated by resistance heating to the melting point while submerged in various media. No self-sustaining combustion reaction was found when the wires were melted in water or uranyl sulfate solution heated to 280°C and pressurized to 2000 psi with oxygen. When the sample was melted in the steam-oxygen vapor phase, it was completely consumed. There was no appreciable reaction in saturated steam at 1000 psi.

15.5 EFFECTS OF RADIATION ON STRUCTURAL METALS AND ALLOYS

15.5.1 Equipment and Facilities

Irradiation of large numbers of specimens in the MTR continued. Experiment ORNL-MTR-10-5 (elevated-temperature irradiation of carbon steels) was disassembled for test in the hot cells. Experiment ORNL-MTR-10-9, which includes over 400 tensile and impact specimens of carbon steels, was built and inserted in the MTR. Experiment ORNL-MTR-10-10 (elevated-temperature irradiation of zirconium alloys) is under construction.

The new subsize impact machine was installed in the cell, and work has started on the large backlog of specimens already irradiated. Devices for automatic temperature control and for insertion of Charpy specimens into the full-size impact machine are in the shops.

15.5.2 Test Data

Earlier tests to compare the effect of radiation on fine- and coarse-grained carbon steels of similar composition led to the conclusion that the fine-grained steel was somewhat more resistant to deleterious property changes than the coarse-grained steel.[9] The same work indicated that saturation was reached at a lower dosage with the fine-grained steel. Studies this quarter have indicated that a fine grain size alone does not make a steel more radiation resistant. Table 15.4 shows the analysis and tensile properties of three

[8] H. M. Higgins, *Reaction of Zircaloy-2 With Water and With Uranyl Sulfate Solution*, AGC-AE-36 and 37 (Aug. 3 and Oct. 1, 1957).

[9] R. G. Berggren and J. C. Wilson, *Recent Data on the Effects of Neutron Irradiation on Structural Metals and Alloys*, ORNL CF-56-11-1 (Jan. 1957).

Table 15.4. Tensile Properties of Low-Manganese Steels

(Normalized from 1700°F and Irradiated in MTR Below 200°F)

	Integrated Fast (>1-Mev) Flux (nvt)	Yield Strength (psi)	Tensile Strength (psi)	Uniform Elongation (%)	Necking Elongation (%)	Total* Elongation (%)
RH-1032 (0.21 C, 0.09 Mn,	0	57,200	78,000	17.4	10.8	28.2
0.009 P, 0.015 S, 0.18 Si,	1.7×10^{19}	87,600	90,000	3.6	10.4	14
0.009 Al, 0.14 Ti)	1×10^{20}	85,800	101,200	7.8	5.8	13.6
RH-1051 (0.07 C, 0.15 Mn,	0	27,600	51,100	29.5	15.5	45
0.011 P, 0.0295, 0.07 Si,	1.7×10^{19}	82,600	82,600	0	9.5	9.5
0.048 Al, 0.39 Cu and	1×10^{20}	97,600	98,500	0.5	8.0	8.5
0.42 Ti)						
RH-1053 (0.05 C, 0.08 Mn,	0	45,600	55,500	25	10	35
0.006 P, 0.018 S, 0.06 Si,	1.7×10^{19}	82,900	80,600**	0.5	10	10.5
0.30 Al, 0.39 Cu, 0.33 Zr)	1×10^{20}	98,400	98,000**	1.0	6.5	7.5

*Elongation in approximately 5 diameters.

**Computed from maximum load reached after yield-point elongation.

experimental heats of low-manganese steels[10] furnished by the Jones and Laughlin Steel Co. All are fine grained, and photomicrographs show them to be essentially ferritic. Two are of low-carbon content. Heat RH-1032 has a higher carbon content, more like the A-212 and A-106 steels previously tested, and has a pearlitic structure after normalizing. The low-carbon steels showed low uniform elongation after a dose of 1.7×10^{19} neutrons/cm^2 (>1 Mev); previously, low uniform elongations at this dose had been seen only in high-purity irons and E-7016 weld metal. Since all these materials are essentially ferritic in structure, it is tentatively proposed that ferrite alone rapidly loses its ductility upon irradiation and that the presence of the carbide platelets in the pearlitic steels results in a greater resistance to radiation-induced loss of ductility. Later it will be possible to compare the impact properties of the same steels.

From the fact that loss of uniform elongation is more important for engineering purposes than loss of necking elongation and because radiation tends to decrease the uniform elongation more than the necking elongation, it is concluded that the conventional elongation measured in the tensile test is less valuable than the uniform elongation in evaluating engineering materials. The conventional elongation measures the sum of the uniform and necking elongations. For many of the steels tested, the necking elongation is a substantial fraction of the conventional elongation, and the loss of uniform elongation with irradiation is partially masked. Inspection of most data on irradiated metals shows that the conventional elongation decreases rapidly with increasing dose at first but the rate of decrease then slows down. This has often been ascribed to saturation, but it is really the result of the less-sensitive necking elongation masking the change in the uniform elongation. For these reasons it appears that the uniform elongation is a much better index of ductility loss in irradiated metals than is the conventional elongation. Fortuitously, the uniform elongation is the much easier quantity to measure in a hot cell and will be the elongation used for the radiation-damage work.

[10] H. F. Beeghly, "Low Manganese Steels for Nuclear Applications," paper presented at 1st Nuclear Engineering and Science Congress held at Cleveland, Ohio, Dec. 12–16, 1955.

15.6 THORIUM OXIDE CALCINATION METHODS[11]

15.6.1 Electric and Gas-Fired Furnace Operations

A considerable number of calcinations of ThO_2 have been made at temperatures from 1000 to 1900°C. The usual procedure was to heat the material in platinum vessels in an electrical-resistor type of furnace at temperatures up to 1600°C. At higher temperatures, alumina containers and a gas-fired furnace were generally employed. The firing operation was periodic and was followed by a pulverization procedure.

The need for calcination of ThO_2 at temperatures above 1500°C in air entailed a consideration of possible container materials for the operation. Aluminum oxide containers are available and have favorable ceramic properties. Accordingly, a brief investigation was made of the possibility of contamination of powdered ThO_2 by the alumina containers. For this purpose, pressed compacts of ThO_2 were placed on flat surfaces of commercial alumina containers and were then fired for 4 hr at 1600°C. Spectrographic analyses of the products showed no increase in aluminum. It was concluded that contamination of the ThO_2 from alumina containers other than by mechanical abrasion should be rather low.

It has been thought that a brief exposure of the as-received ThO_2 to a very high temperature (3000°C) might produce in one operation calcined particles with desirable characteristics for use in a slurry blanket. Among the hoped-for properties are a very fine size (1 μ or less) and rounded particle edges, which should reduce the abrading action.

Heat sources considered for this purpose were the oxyacetylene torch, the electric arc, and the induction furnace. Preliminary tests of the first two methods were made.

15.6.2 Flame-Spray Calcination

For the oxyacetylene calcination, a metallizing gun (Metco flame spray), which employs a gravity feed, was found best. However, ThO_2 (from the oxalate process) tended to pack and was passed through the gun with difficulty, even when the gun was vibrated strongly. On the second pass there was much less difficulty.

[11] This section was submitted by C. E. Curtis of the Metallurgy Division.

Thorium oxalate and thorium formate offered less difficulty than the oxide. A thorium compound treated with acetylacetone to produce a thorium oxide–acetylacetone complex was unsatisfactory in the oxyacetylene flame-spray gun, apparently because it has a low melting temperature. Under the given conditions, three successive passes through the gun seemed necessary for complete conversion of the oxalate and formate to cubic ThO_2. The product from the oxide, formate, or oxalate consisted of fine grains which were in part clinging together in agglomerates approximately 0.5 mm in diameter; these were easily crushed to powder. In the case of thorium oxalate and formate, there was a notable volume decrease during the first passage through the gun.

Samples of flame-spray-calcined thorium oxide, formate, and oxalate have been submitted to the HRP blanket development group for tests (in toroids) of abrasive properties and ease of particle degradation.

15.6.3 Electric-Arc Calcination

The arc calcining apparatus consisted of graphite electrodes ½ in. in diameter extending into the center of a vertical refractory tube 5 in. in diameter. The powdered materials were fed through the arc by means of a vertical zircon tube, which was kept in vibration.

The product of one passage through the arc of either the oxide, formate, or oxalate contained some rather perfect spheres of ThO_2, 0.1 to 0.3 mm in diameter; many of these were transparent, iridescent, hollow bubbles, which floated on water and were carried upward by air currents; they were very fragile. Many solid opaque spheres of about the same size were formed also and appeared to be agglomerates of finer particles; they were resistant to crushing.

After three passes through the arc, the product of each of the three compounds was mostly spheres consisting of about equal proportions of the transparent hollow type and the solid opaque type.

It was concluded that the arc process produced, under the given conditions, an unsuitable product for the HRT blanket because of the comparatively large size of the spheres. It is conceivable that refinements in the apparatus might lead to the production of the submicron rounded grains desired. Uses for the transparent bubbles of ThO_2 are being sought.

15.6.4 Spheroidizing of Highly Refractory Materials

Spheres, both solid and hollow, of zirconia, alumina, hafnia, and zircon as well as of thoria (as detailed above) have been produced by arc calcination. The spheres formed were mostly under 0.3 mm in diameter in all cases. Apparently the proportion of spheres and their size and strength can be controlled, if necessary, by compacting the powder, then breaking it into agglomerates in controlled sizes before it is arc-calcined or by regulating the time period during which the ThO_2 is actually in the hot zone of the arc.

Part V

CHEMICAL ENGINEERING DEVELOPMENT

D. E. Ferguson

16. URANYL SULFATE FUEL PROCESSING

R. A. McNees P. A. Haas
J. R. Bowen R. W. Horton
S. Peterson

16.1 SOLIDS BEHAVIOR

The behavior of simulated HRT corrosion-product solids in contact with stainless steel surfaces is being investigated to determine whether corrosion-product solids will deposit irreversibly on the walls of a reactor system.

16.1.1 Loop Studies

(a) Glass-Loop Experiments. – In a series of tests in the 0.5-in.-dia glass loop, the amount of preformed ZrO_2 remaining in 0.1 *m* UO_2SO_4 solution increased as the Reynolds number of the system was increased by increasing the solution flow rate (Table 16.1). The material that came out of suspension was deposited both on the surface of the glass loop and on metal coupons in the loop.

The flow patterns caused by the presence of the metal coupons affected the solids deposition. As the system flow became more turbulent, the values determined for the densities of solids deposited on the coupons became more scattered. Change in deposition with temperature was not noticeable in the narrow range of temperatures imposed by the pressure limitations for glass pipe.

Comparison of results of analyses of samples by light transmission with counting of activated ZrO_2 indicated that a chemical or physical change occurred in the solids during the runs which gave an upward bias to the results obtained by the light-transmission method. This change could be degradation of large ZrO_2 particles, formation of colloids, or precipitation of corrosion products in the system.

(b) Loop B-2 Tests. – Steady-state and hydroclone-pot solids concentrations were determined in a test run in loop B-2 with 0.1 *m* UO_2SO_4 solution and in which hydroclone operation and addition of traced ZrO_2 were essentially continuous. Average equilibrium ZrO_2 concentrations were 380 and 2000 mg per kilogram of H_2O in the loop and hydroclone pot, respectively. These values indicate a hydroclone efficiency of 8%.

Of the ZrO_2 added to the loop, about 23% was removed in loop (bomb) samples, 23% in hydroclone-pot samples, 24% in the loop drain, and 7% in loop

Table 16.1. Effect of the Reynolds Number on Deposition of Solid ZrO_2 from 0.1 *m* UO_2SO_4

Conditions: Suspension of ZrO_2 circulating in 0.5-in.-dia glass loop; Reynolds number increased by increasing the flow rate

Run No.	Length of Run (hr)	Temperature (°C)	Reynolds No.	Ratio of Final Solids Concentration in Liquid to Original
6	30	47	3.5×10^4	0.45
7	24	47	4.3×10^4	0.60
8	36	47	5.6×10^4	0.80
9	28	47	9.3×10^4	0.70
10	30	62	9.3×10^4	0.73
11	36	77	9.3×10^4	0.70
12	30	77	9.3×10^4	0.91

washes; 22% was not recovered. The preformed ZrO_2 was added at the rate of 100 mg/hr for 220 hr of the test period. The system was shut down over the two weekends in the three-week test.

Extrapolation of these results to HRT conditions gives an estimated fuel solids concentration of 50 to 200 mg/liter if the corrosion-product solids resemble the preformed ZrO_2. Some laboratory results indicate that the true corrosion products will be larger and will settle faster than the ZrO_2 used for experimental studies, but comparison of loop B-2 and HRT parameters shows that the systems are similar in many respects (Table 16.2). Some of the differences are such that they tend to cancel out. The relatively larger HRT-CPP underflow rate and the lower HRT solids-addition rate would result in lower solids concentrations in the HRT than in the experiments.

16.1.2 Laboratory Tests

When suspensions of neutron-activated ZrO_2 in 0.04 *m* UO_2SO_4–0.02 *m* H_2SO_4 at 27°C were tumbled end over end in stainless steel tubes, 50% of the solids settled out in less than 24 hr. There was no further settling when the runs were continued up to 500 hr. The suspensions contained 55 or 110 mg of ZrO_2 per kilogram of H_2O. No effect of variation in the solids concentration, the weight of solids per unit of surface area, or the volume of suspension per unit of surface area was observed. When tubes were used that had been severely abraded with a brush and scrubbing powders, a larger fraction of the solids initially charged to the system disappeared, but after several days' agitation and two refillings with fresh suspensions, the behavior in these tubes could not be distinguished from that in other tubes less harshly treated. The studies are being continued with solids consisting of a mixture of iron, zirconium, and chromium oxides traced with either iron or zirconium tracer.

More-fundamental studies are being made at Stanford Research Institute. Data thus far obtained indicate that corrosion-product solids

Table 16.2. Comparison of Parameters of Loop B-2 and the HRT

Quantity	Units	Loop B-2 Values	HRT Values
Solids addition rate	mg/hr	100	2500
	mg/hr·liter	10	5
Hydroclone pot volume/loop volume	liters/liter	1/100	3/200
Hydroclone pot volume[a]/induced underflow rate	min	10	100
Processing time or loop volume/hydroclone flow	min	15	100
Volume/area	ft^3/ft^2	0.05	0.03
Hydroclone efficiency	%	8	8[b]
Hydroclone flow	liters/hr	40	300
Underflow pot volume	liters	0.1	8
Equilibrium circulating solids concentration	mg/liter	380	50–200[c]

[a]Based on a 1.5% induced underflow rate.

[b]The effects of the hydroclone diameter and the liquid-viscosity changes will approximately cancel.

[c]Range due to effects of underflow-pot dump cycle and/or amount of settling in HRT underflow pot.

obtained under controlled conditions in the laboratory have the same solid phases found in samples taken from circulating loops at ORNL. The crystallite sizes of these solids range from 0.03 to 0.10 μ, with nearly all solids thus far examined falling in the range 0.04 to 0.08 μ.

16.2 IODINE CHEMISTRY

The effectiveness of an iodine trap consisting of silvered-alundum Raschig rings in removing iodine from the circulating stream of the HRT mockup was demonstrated. The trap was a 6-in.-dia by 5-in.-high bed of 0.25-in. Raschig rings (2250 g) containing 48.4 g of silver. A solution containing 1.06 g of iodine traced with I^{131} was added to the high-pressure portion of the loop during 4.5 hr of operation at 280°C. The silver bed was located in the low-pressure system of the loop just ahead of the platinum recombiner. The activity of iodine at various points in the system as a function of time is shown in Fig. 16.1. The iodine activity in various parts of the bed is shown in Fig. 16.2. The efficiency of the bed under the conditions of the experiment was estimated as between 35 and 75%.

For a given gas flow rate, the fraction of incoming iodine that penetrated a silvered-alundum trap was sharply reduced by increasing the temperature of the bed (Fig. 16.3). This suggests that the absorber bed in the HRT should be operated at as high a temperature as possible in order to provide maximum protection for the platinum recombination catalyst. The apparatus used provides for generation of a flowing oxygen-steam-iodine stream of known and controlled composition, velocity, and temperature. The iodine trap was a cylinder about 1 in. in diameter filled to a depth of about 4 in. with 75 g of alundum pellets ($\frac{1}{8}$ in. dia × $\frac{1}{8}$ in. long) containing 6 mg of silver per gram of pellets.

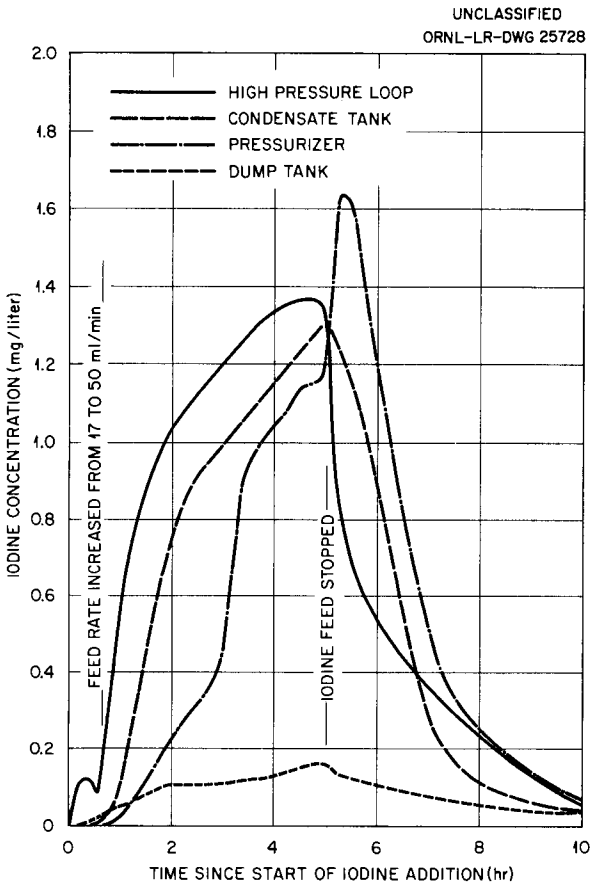

Fig. 16.1. Iodine Concentrations in HRT Mockup.

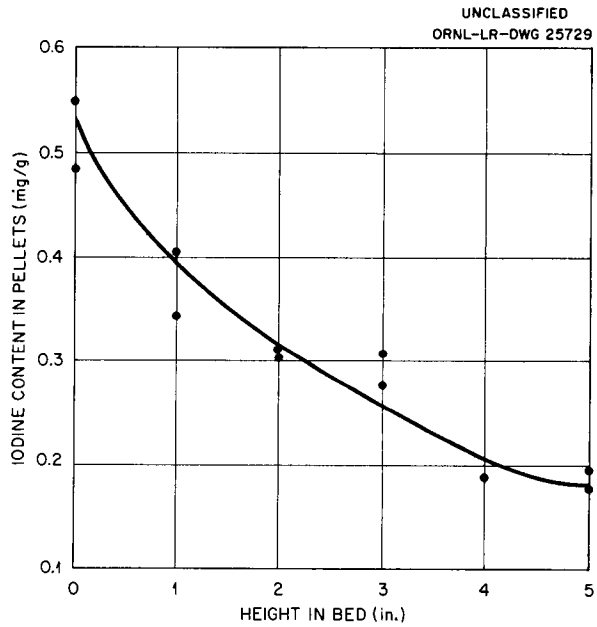

Fig. 16.2. Iodine Distribution in Mockup Silvered-Alundum Bed.

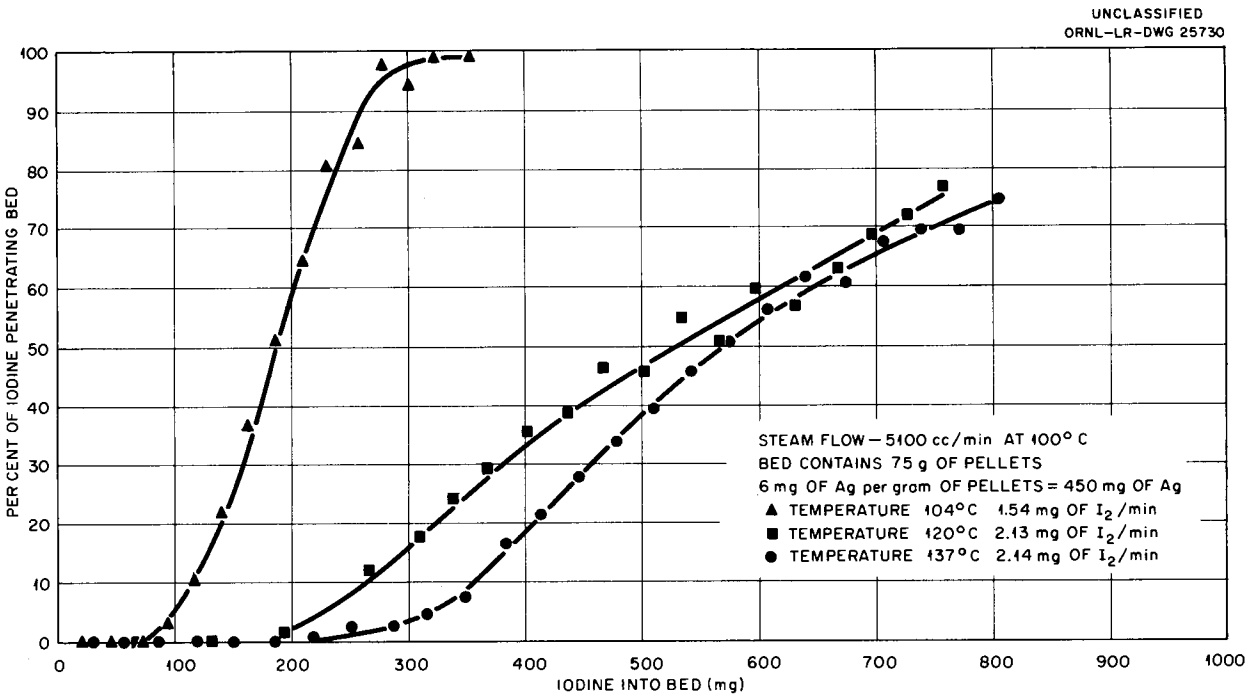

Fig. 16.3. Effect of Absorption-Bed Temperature on Removal of Iodine from a Flowing Gas Stream.

17. GASEOUS FISSION-PRODUCT DISPOSAL

R. A. McNees

R. E. Adams W. E. Browning

M. H. Lloyd

17.1 DYNAMIC STUDIES

In a single experiment on adsorption of xenon by Columbia G charcoal at room temperature, xenon was adsorbed 16.5 times as strongly as krypton, which is approximately three times the effect expected. In this study the techniques described in ORNL-2116 were used. Since the Xe^{133} tracer used contained a trace of Kr^{85}, elution curves for both elements were obtained in a single run (Fig. 17.1).

Breakthrough tests on two of the HRT charcoal beds were completed, but the quantitative results of the tests were unsatisfactory owing to occasional malfunctioning of various parts of the experimental equipment. At an oxygen flow rate of 500 cc/min, one bed showed a holdup time of 14 days for Kr^{85}; no breakthrough on the other bed was noted (Sec 6.4). The tests will be repeated, but indications are that there was no measurable bypassing of the charcoal in the bed.

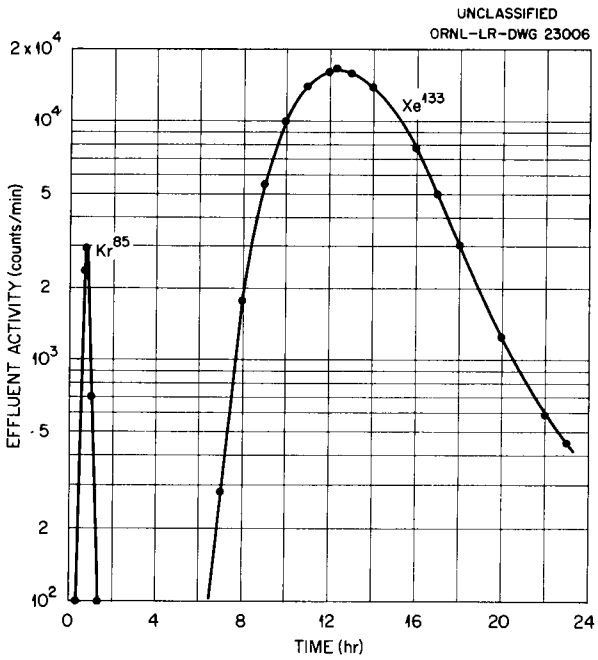

Fig. 17.1. Kr-Xe Adsorption.

17.2 EQUILIBRIUM STUDIES

Adsorption isotherms for krypton on a large number of adsorbents were reported in detail elsewhere.[1] Isotherms for some characteristic materials are shown in Fig. 17.2. Of the various inorganic adsorbents thus far tested, Linde molecular sieve 5A had the greatest capacity, with silica gel next; the other inorganics tested offer no promise of usefulness for adsorption of fission gases. The results clearly show the effect of pore size on the adsorption of krypton by inorganic adsorbents. Linde molecular sieve 4A, with the

[1] *Chem. Tech. Monthly Prog. Rep. July 1957*, ORNL-2385 (classified); *Chem. Tech. Monthly Prog. Rep. Aug. 1957*, ORNL-2400 (in press) (classified); *Chem. Tech. Monthly Prog. Rep. Sept. 1957*, ORNL-2416 (in press) (classified).

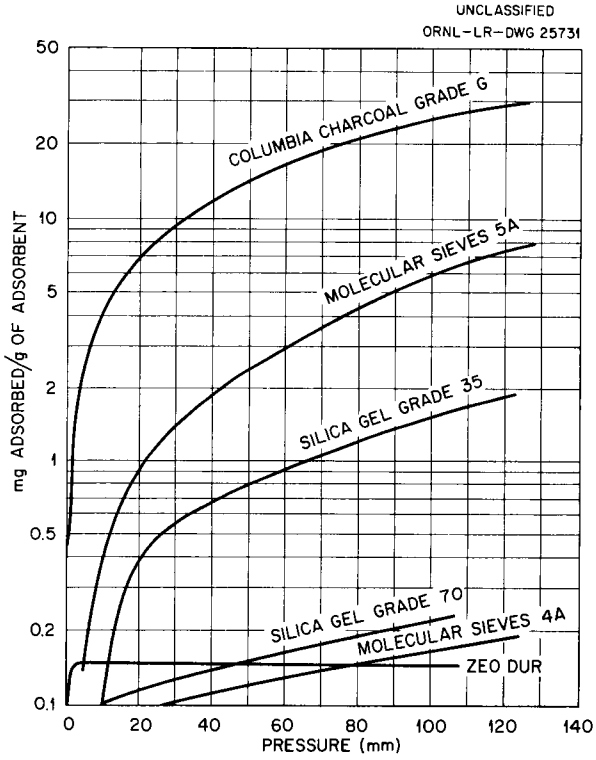

Fig. 17.2. Adsorption of Krypton on Various Materials at 28°C.

4-Å pores, cannot easily accommodate krypton (diameter ~ 4 Å) but the 5-Å pores of the 5A material can. Among silica gels, grade 35, with an average pore size of 32 Å, adsorbed five times as much krypton as grade 70, with a pore size of 140 Å. Thus, in the noncharcoal adsorbents, krypton is held most effectively by material with pores large enough to admit the atoms of gas but not so large as to lose the wall effects found in the smaller pores.

18. URANYL SULFATE BLANKET PROCESSING

R. E. Leuze P. A. Haas
J. M. Chilton S. S. Kirslis
J. W. Snider

Experimental investigations during the quarter included studies of ZrO_2 and $Zr(SO_4)_2$ behavior in the P-1 loop, in-pile irradiation of 1.4 *m* UO_2SO_4 contained in stainless steel, and spectrophotometric study of plutonium chemistry.

18.1 BEHAVIOR OF ZIRCONIUM IN THE P-1 LOOP

Several experiments were carried out in the P-1 loop in which ZrO_2 or $Zr(SO_4)_2$ was added to 1.4 *m* UO_2SO_4 circulating at 250°C under 350 to 400 psi O_2. These runs were preliminary to planned experiments to determine plutonium behavior. Zirconium was substituted for plutonium in order to determine the effectiveness of the hydroclone, the rate of solids disappearance from the circulating solution, and adsorption on metal surfaces. In nine experiments (Table 18.1) the over-all results showed that only 7.5% of the zirconium added to the loop was removed by the hydroclone; 90% was adsorbed on the loop walls. In four of these experiments preformed ZrO_2 was added; in one, dissolved $Zr(SO_4)_2$ was added; and in four, only that zirconium already in the loop was followed by analyses.

When preformed ZrO_2 was injected into the loop, the half-time of ZrO_2 disappearance from the circulating 1.4 *m* UO_2SO_4 was 2 to 4 hr. It was not possible to determine the effect of the hydroclone on this rate because of the scatter in the data. In fact, the rate of removal for run P-17 (Fig. 18.1) in which the hydroclone was not used was greater than for the runs in which the hydroclone was

Table 18.1. Zirconium Distribution in the P-1 Loop

About 10 liters of 1.4 *m* UO_2SO_4 was circulated at 250°C under sufficient oxygen to give a total pressure of 900–950 psi

Loop surface area: 46.3 ft^2 for runs P-17 to P-22
10.4 ft^2 for runs P-23 to P-25

Run No.	Time (hr)	Zirconium in Loop: Feed (g)	Zirconium in Loop: Injected Salt	Zirconium in Loop: Injected (g)	Zirconium Removed from Loop (g): Hydroclone	Zirconium Removed from Loop (g): Loop Drain	Zirconium Removed from Loop (g): Samples	Zirconium Adsorbed[a] (g)	Zirconium Material Balance (%)
P-17	64	0	ZrO_2	1.000	*b*	0.125	0.006	0.8[c]	93
-18	84	0.125	ZrO_2	2.000	0.481	0.607	0.025	1.025	101
-19	19	0.422		0	0.039		0.185	0.367	103
-20	56			0	0.016	0.019	0		
-21	33	0.019	$Zr(SO_4)_2$	1.000	0.007	0.007	0.009	0.975	98
-22A	21	0.007	ZrO_2	5.000	0.293		0.081	10.00	111
-22B	26		ZrO_2	5.000	0.281	0.357	0.085		
-23	29	0		0	0.007	0.024	0	*d*	
-24	22	0.024		0	0.002	0.004	0	*d*	
-25	78	0.004	ZrO_2	1.000	0.086	0.001	0.002	0.944[d]	103

[a]Calculated by multiplying average plutonium adsorption on coupons by loop surface area.
[b]Hydroclone not used in run P-17.
[c]Adsorption coupons not used. Adsorbed value for run P-17 estimated from subsequent runs.
[d]Adsorption coupons were not analyzed after runs P-23 and P-24.

used. Also, the effect of reducing the loop surface area from 46.3 ft^2 (runs P-17, -18, -22A in Fig. 18.1) to 10.4 ft^2 (run P-25) was less than the variation between duplicate runs.

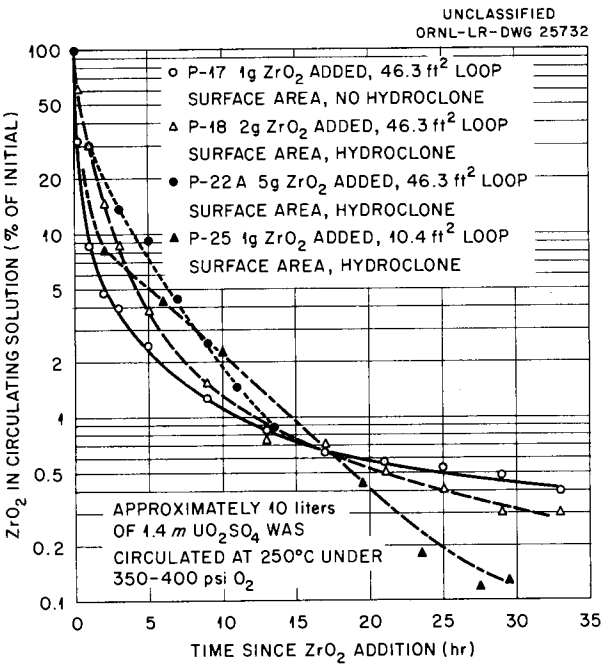

Fig. 18.1. ZrO_2 Circulating in P-1 Loop vs Time.

The amount of preformed ZrO_2 removed by the hydroclones was only 6 to 16%, compared with 85 to 90% removed by ZrO_2 adsorption on the loop walls. The hydroclone efficiency (amount of ZrO_2 removed/amount ZrO_2 passing into hydroclone) was only 10 to 20% when the ZrO_2 concentration was 10 to 100 mg/liter. Efficiency was much less at lower concentrations. When dissolved $Zr(SO_4)_2$ was allowed to hydrolyze and precipitate in the loop (run P-21, Table 18.1), essentially all the zirconium was adsorbed on the loop walls, with no more than a trace appearing in the hydroclone underflow.

For all these experiments zirconium was determined by direct counting of Zr^{95} tracer. Adsorption on loop walls was estimated by counting the zirconium activity on small adsorption coupons and multiplying the specific adsorption by the internal surface area of the loop. This area was 46.3 ft^2 in runs P-17 through P-22, when the loop was equipped with a pressurizer filled with Raschig rings, and 10.4 ft^2 in runs P-23 through P-25, after the Raschig rings were removed.

The zirconium adsorption on stainless steel, Zircaloy-2, and titanium coupons exposed during runs P-18 through P-25 was 2.6, 2.5, and 2.2 mg/in.^{2}, respectively.

18.2 LOOP P-1 OPERATION

Since the present experimental schedule does not include the use of hydrogen overpressure, the original pressurizer was removed from loop P-1 and replaced by a Raschig-ring-free pressurizer to reduce the area/volume ratio. The area/volume ratio is now approximately 1 ft^2/liter. In the original equipment both the hydrogen and oxygen addition lines became plugged with corrosion products. These lines were opened when the pressurizer was changed, but during 140 hr the oxygen line became replugged; the oxygen is now being added through the hydrogen line.

18.3 IN-PILE EXPERIMENT

When 1.4 *m* UO_2SO_4 contained in a type 347 stainless steel bomb was irradiated in the LITR at 250°C under 200 psi of oxygen, corrosion was severe after about 10 days. After 13 days the irradiation was discontinued. The excessive corrosion was probably caused by depletion of oxygen in the solution by boiling. A large amount of the uranium was reduced and precipitated as the oxide; as a result about 1% of the neptunium and about 0.1% of the plutonium remained in solution. Attempts to dissolve the precipitate were not successful, but indications are that very little of the neptunium or plutonium was in the precipitate; most was adsorbed on the bomb walls.

18.4 SPECTRUM OF PuO_2^{++}

Spectrophotometric work on the chemistry of plutonium has made use of a very intense, narrow absorption peak at 835 mμ for the determination of the plutonyl ion in solution. Considerable difficulty has been experienced in using this peak for quantitative measurements, since this value apparently does not obey either Beer's or Lambert's law.[1] This effect has been attributed to various instrumental factors such as spherical aberration, resolving power, and slit widths.

All this early work was done with Beckman DU spectrophotometers, which give spectral slit widths

[1] R. E. Connick, *Natl. Nuclear Energy Ser. Div. IV* 14B, 559 (1949).

of 45 to 50 Å in this part of the spectrum. Analysis of this peak with a Cary 14 spectrophotometer, which gives a spectral slit width of only 4 Å, showed that the peak is actually a nonsymmetrical doublet with a width of 40 Å at half peak height. With the Cary instrument both peaks of this doublet were found to follow the ideal absorption laws. Typical spectrums of this peak with each instrument are shown in Fig. 18.2.

18.5 DISPROPORTIONATION OF PLUTONIUM(IV) IN SULFATE SYSTEMS

Further work on the disproportionation[2] of Pu(IV) in concentrated uranyl sulfate solutions with the Cary spectrophotometer indicated less Pu(III) and Pu(VI) formed at 90°C than had been previously indicated with the Beckman DU at a plutonium concentration of 200 mg/liter. At a concentration of 770 mg/liter, the disproportionation reaction was largely

$$2Pu(IV) \rightleftharpoons Pu(III) + Pu(V)$$

Equilibrium was attained as fast as the sample reached temperature. At 90°C the Pu(V) (or PuO^{+}) is apparently stable. The second step in the total disproportionation,

$$Pu(IV) + Pu(V) = Pu(III) + Pu(VI)$$

evidently does not occur at this plutonium concentration in the concentrated uranyl sulfate solution.

[2]D. E. Ferguson *et al.*, *HRP Quar. Prog. Rep. Oct. 31, 1956*, ORNL-2222, p 140, esp 143.

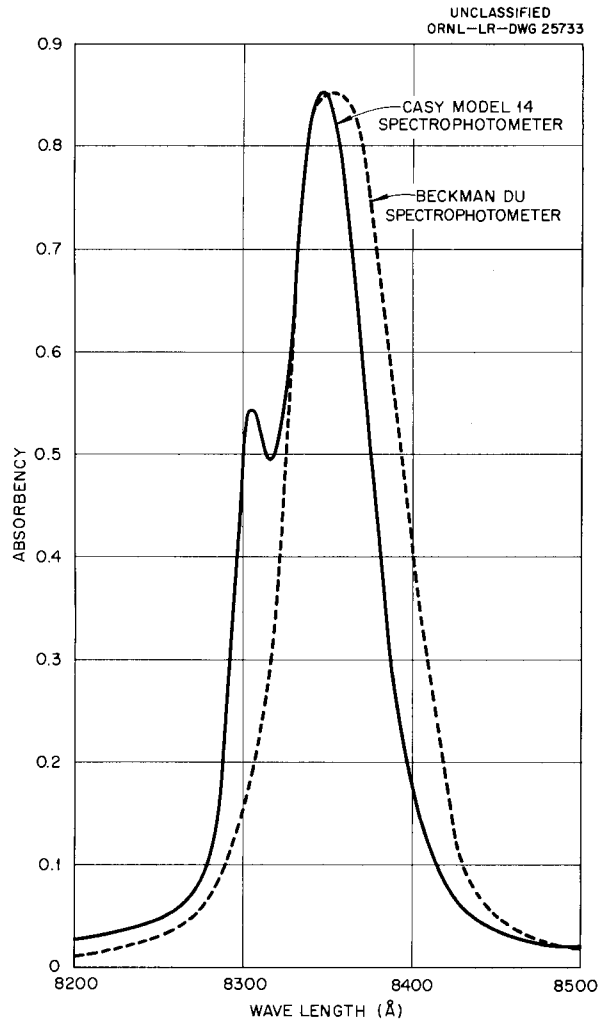

Fig. 18.2. PuO_2^{++} Spectrums Obtained with Cary Model 14 and Beckman DU Spectrophotometers.

19. THORIUM OXIDE BLANKET PROCESSING

R. E. Leuze
R. D. Baybarz

Simple methods of processing thoria slurries for removal of fission products are being investigated. Scouting studies were made to investigate possible methods of removing fission products from ThO_2 without destroying the oxide particles.

19.1 CATION ADSORPTION ON ThO_2

Cation adsorption by ThO_2 in an aqueous slurry at 250°C is a function of the surface area or calcination temperature. The decrease in the uranium adsorbed on ThO_2 from a uranyl sulfate solution as the calcination temperature increased was reported previously.[1] Adsorption of neodymium was similar (Table 19.1).

[1] R. E. Leuze and R. D. Baybarz, *HRP Quar. Prog. Rep. April 30, 1957*, ORNL-2331, p 156.

Table 19.1. Effect of ThO_2 Calcination Temperature on Neodymium Adsorption

About 0.5 g of ThO_2 slurried at 250°C in 10 ml of solution containing 2 g of $Nd(NO_3)_3$ per liter

Calcination Temperature (°C)	Neodymium Adsorption (parts per 1000 parts Th)
650	7.4
850	6.1
1000	2.4
1100	0.5

20. THORIUM OXIDE SLURRY DEVELOPMENT

J. P. McBride P. A. Haas
C. T. Bishop L. E. Morse
E. V. Jones R. L. Pearson
N. A. Krohn J. P. Phillips
C. C. Haws C. E. Schilling
W. M. Woods

20.1 OXIDE PREPARATION

20.1.1 Preparation of Small Particles

A laboratory study was initiated on the preparation of small particles. In general, the average particle size of a precipitate can be decreased, as a result of reduced solubility, by:

1. decreasing temperatures,
2. selecting solvents in which the precipitate is less soluble,
3. precipitating less-soluble salts,
4. avoiding soluble materials which increase the precipitate solubility.

The particle size can be reduced, as a result of higher "mixed" concentration at the time of precipitation, by:

1. using more concentrated feeds,
2. mixing the feeds more rapidly,
3. reducing the temperature to slow down the precipitation and allow more time for mixing.

The principal preparation variable investigated was the reagent concentration. Preliminary results with oxalate precipitated from 2 *M* $Th(NO_3)_4$ by the addition of 2 *M* $K_2C_2O_4$ were encouraging in that, with a rapid mixing technique, particles of 0.16-μ average size were prepared. However, the potassium could not be readily removed from the precipitate by simple washing or dialysis techniques. Increasing the reagent concentration by using alcohol solutions of thorium nitrate and oxalic acid yielded a large-particle product.

20.1.2 Flocculation Studies

The use of flocculants in the recovery of fine-particle solids from a thoria slurry or a thorium oxalate preparation system was investigated. Seven different flocculating agents were tested and three of these, Dow Separan 2610, Monsanto DX-908, and American Cyanamid S-3171, proved to flocculate thorium oxalate very well. Each of these agents is a synthetic polyanionic long-chain organic. By necessity, they must be completely combustible, since impurities in the final product cannot be tolerated. A spectrographic analysis of the three flocculating agents showed them to be of high purity and satisfactory for use in the production of thorium oxide.[1]

20.1.3 Flame Calcination

Flame calcination is being considered as a method of firing thoria to a temperature above its sintering point (near 1700°C) without increasing the particle size. It may also be possible to convert thoria particles to fire-polished spheres by this method of calcination.

All attempts to flame-calcine thoria to date have been unsuccessful due to an inability to disperse individual particles of thoria into the flame. Ball-milling thoria with stearic acid yielded a finely divided powder, nonaggregated to the unaided eye. This material aggregated again, however, in the feeder mechanism for the flame gun. Other methods tried unsuccessfully thus far to avoid the aggregation were an arc discharge, a beta source, and ultrasonic agitation.

In tests with various high-melting materials, it was possible to fuse and spheroidize 75- to 150-μ particles of alumina, melting point 2050°C, in a reducing oxyacetylene flame (Fig. 20.1*a* and *b*). A neutral or oxidizing flame would not spheroidize the alumina.

20.1.4 Alternate Preparation Method

An investigation of the preparation of thorium oxide from thorium hydroxide was initiated. Two preparation variables were studied, reagent concentrations and pH of the precipitating medium. Oxide products from the initial preparations were almost universally gritty, glasslike, and composed of large agglomerates. The best products were obtained by (1) using high reagent concentrations

[1] *Chem. Tech. Monthly Prog. Rep. Aug. 1957*, ORNL-2400 (in press) (classified).

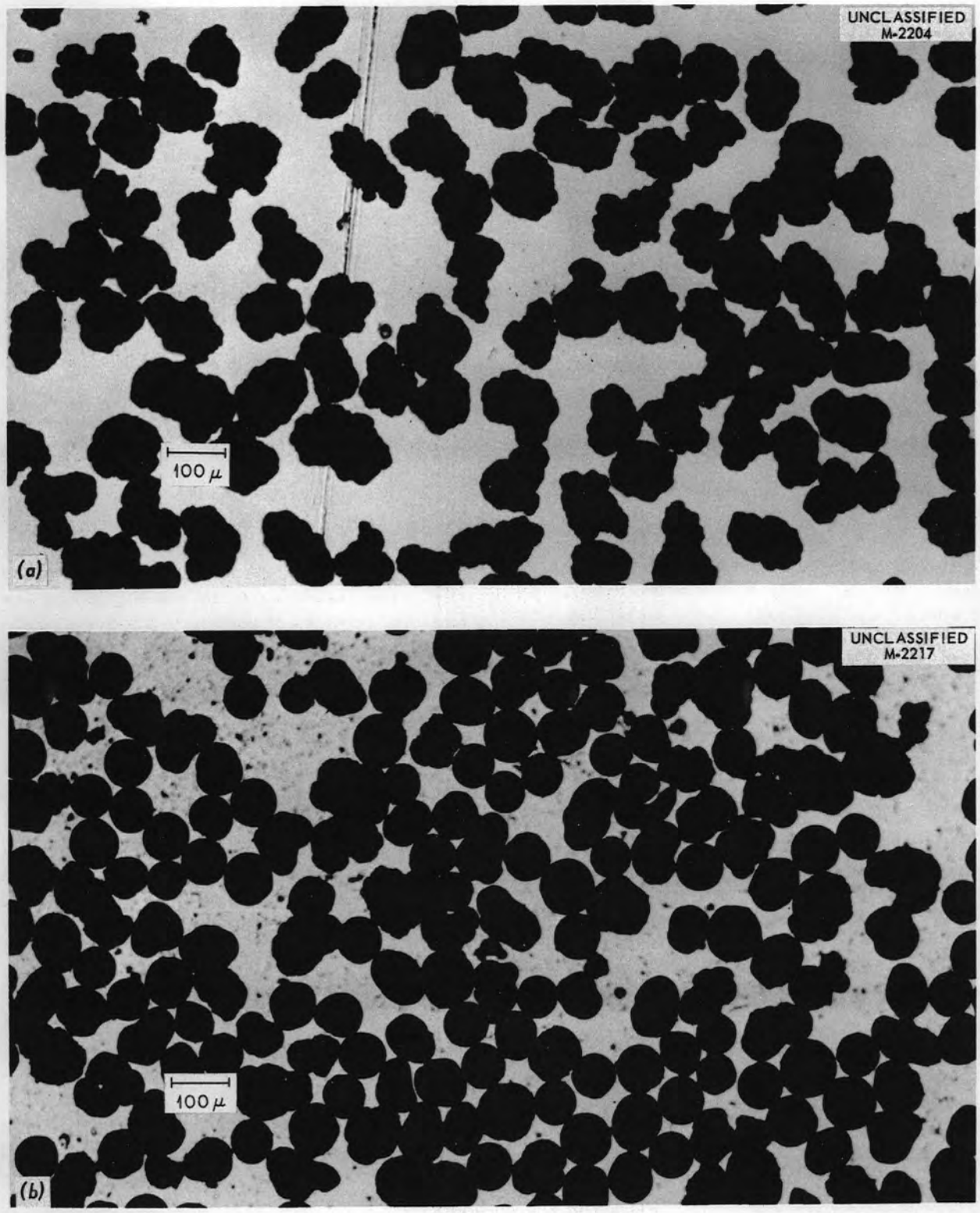

Fig. 20.1. Spheroidization of Alumina in an Oxyacetylene Reducing Flame. (*a*) Al_2O_3 as fed to flame-calcination equipment. (*b*) Al_2O_3 as recovered.

[$Th(NO_3)_4$, NH_4OH] and pH's of 6 to 9; (2) filtering rather than centrifuging the precipitated hydroxide prior to drying; and (3) washing with water as opposed to washing with dilute ammonium hydroxide. Preliminary results on washing with alcohol are particularly promising.

The studies were carried out with Thorex-product thorium nitrate solution and cp ammonium hydroxide. Preliminary experiments were made with thorium nitrate concentrations of 0.5 to 1.8 *M* and excess ammonium hydroxide (pH >10.4). These products were universally gritty and glasslike.

With pH of the final precipitation medium as the preparation variable (pH 6.1 to 8.9), aliquots of 1 *M* $Th(NO_3)_4$ and 4 *M* NH_4OH were reacted. The precipitates were washed and dried and were then fired at 650°C. None of the products were satisfactory as slurry material, but the best product was obtained at the lowest pH.

The effects of higher reagent concentration and of washing with water were investigated in a second series of experiments. The products obtained at pH's below 9 were, after firing at 650°C, in general softer than those obtained above, but after being crushed they were gritty powders.

20.1.5 Grindability of High-Fired Thorium Oxide

In order to obtain a slurry whose properties will not change as it is pumped, firing conditions necessary to prevent degradation of individual particles during pumping must be determined. The jet-impingement slurry abrasion tester was adapted to this purpose. As a slurry is degraded, the time for it to penetrate a 1-mil type 302 stainless steel shim stock increases. Oxide fired at 1400°C for 64 hr or 1600°C for 12 hr or 1800°C for 2 hr was degraded. As the temperature of firing increased, the total firing time necessary to prevent degradation decreased.

20.2 SLURRY IRRADIATION STUDIES

20.2.1 Slurry Irradiations in the LITR

The long-term irradiation of a settled slurry of 800°C-calcined micropulverized thorium oxide was terminated (experiment No. C43-1). The test was in the LITR for 15 weeks, 2091 hr of irradiation at full reactor power. When the autoclave was opened, most of the material was poured out readily as a cream-colored slurry. The autoclave was washed by adding 10 cc of water and shaking. After washing, a plug of ThO_2 was found in the top of the autoclave. It was apparently formed by drying of slurry on the walls of the autoclave above the liquid-vapor interface. This material, constituting 17% of the total solids in the autoclave, lost no weight upon drying for 48 hr at 110°C. No evidence of caking was found in the bottom of the autoclave even though the slurry solids had been in a settled condition for 15 weeks in the LITR.

Samples of the slurry that was poured from the autoclave were analyzed for fission products, corrosion products, protactinium, and U^{233}. The results (Table 20.1) showed all constituents except cesium to be with the solid phase, in agreement with the data from short-term irradiations. The U^{233} content was 0.14%.

Table 20.1. Radiochemical Analyses of Irradiated Slurries

Slurry	Amount in Supernatant (% of Total)										
	Gross β	Gross γ	Total Rare Earths	Sr	Ru	Cs	Nb	Zr	I	U^{233}	Pa
C43-1[a]	1.0	1.0	1.6	2.2	1.1	15.1	2.2	1.2	0.2	0.1	0.9
LITR-30[b]	0.2	0.6	0.2	10.0	1.4	24.6	0.1	0.1	0.3		
LITR-31[c]	0.2	0.01	0.4	3.8	0.1	12.7	0.01	0.01	0.01		
LITR-33[a]	0.1	0.01	0.5	2.5	2.2	4.4	0.1	0.2	1.0		

[a]Decayed 35 days.
[b]Decayed 32 days.
[c]Decayed 26 days.

Four short-term irradiation tests were carried out: the first (LITR-31) on a slurry of 800°C-calcined ThO_2–0.5% U^{235} prepared from the coprecipitated oxalates and containing 20,000 ppm of MoO_3 and 3000 ppm sulfate, added as $Th(SO_4)_2$. It was irradiated 343 hr. The autoclave stirrer stopped after 168 hr for no apparent reason. Unlike a similar test (LITR-30) previously reported,[2] there was no decrease in the oxygen overpressure. The slurries from both this and the previous test were brown in color, poured readily from the autoclaves, and settled slowly. The settled concentrations were both 1300 g of thorium per liter, which was in agreement with the control.

The second test (LITR-32) was on a slurry of 650°C-fired Davison Chemical Co. ThO_2 containing 750 g of thorium per kilogram of H_2O, with no additives. The autoclave leaked, resulting in the loss of all the water after approximately one week in-pile and 140 hr of irradiation. The recovered material was brown and lumpy.

The third test (LITR-33) was made on a slurry of 1600°C-fired ThO_2 which had been pumped for 268 hr at 300°C (runs BS-15 and -16). The concentration of the sample was adjusted by density measurement to 500 g of thorium per kilogram of H_2O for the in-pile test. The irradiation proceeded at 300°C without interruption for 282 hr; then the stirrer timing unit failed. After a lapse of one day for repair the stirrer was restarted without difficulty, but after 37 hr of operating time the unit again failed, and the test was stopped. In all, the experiment was in-pile for 366 hr, was stirred for 330 hr, and was irradiated at full reactor power for 336 hr. The recovered slurry was quite thick, and it was necessary to wash the autoclave to obtain good recovery.

20.2.2 Postirradiation Analyses

Analysis of the irradiated slurries showed that essentially all the fission products and corrosion products were associated with the solid phase, in agreement with previous results (Table 20.1). Corrosion-product pickup was more than five times as great in the irradiated samples as in the controls (Table 20.2).

[2] J. P. McBride *et al.*, *HRP Quar. Prog. Rep. July 31, 1957*, ORNL-2379, p 145.

Table 20.2. Corrosion Products in Irradiated Slurries

Code	Time (hr)		Corrosion Products (g/kg Th)*		
	Stirred	Irradiated	Fe	Ni	Cr
LITR-30	265	247	120	16	6
LITR-31	168	343	44	8	5
Control for 30–31	226	0	9	1	1
LITR-33	330	336	74	15	0**
Control for 33	320	0	14	3	3

*No iron or chromium was found in the supernatant. The nickel contents of the supernatants of LITR-30, -31, and -33 were 3.1, 12.8, and 3.5%, respectively, of the totals found.

**Sought repeatedly, but none found.

20.2.3 In-Pile Gas-Recombination Studies

Radiolytic-gas production and recombination rates were determined in the ORNL Graphite Reactor at 200 to 300°C for slurries of thorium-uranium oxide containing 250, 500, and 750 g of thorium per kilogram of H_2O. The oxide contained 2% U^{235} and was prepared by a 650°C calcination of 10°C-coprecipitated thorium-uranium oxalate.

Gas production rates measured by the initial pressure buildup in the autoclave at temperatures from 200 to 220°C were 1.6×10^{-4}, 3.3×10^{-4}, and 4.9×10^{-4} mole of H_2 per hour, respectively, for slurry concentrations of 250, 500, and 750 g Th/kg H_2O. Since the uranium/thorium ratio was fixed, the production rate was directly proportional to the slurry uranium concentration, with no change in *G* value as a result of changing the ThO_2 concentration. The *G* value obtained, assuming a neutron flux of 5.3×10^{11} neutrons/cm^2·sec and an energy deposition in the slurry of 170 Mev/fission, is 0.73.

Equilibrium pressures in excess of steam were the same for a given temperature regardless of slurry concentration (Fig. 20.2). Since the production rate increased linearly with slurry concentration, it can be inferred that the recombination rate was also a linear function of slurry concentration. Further

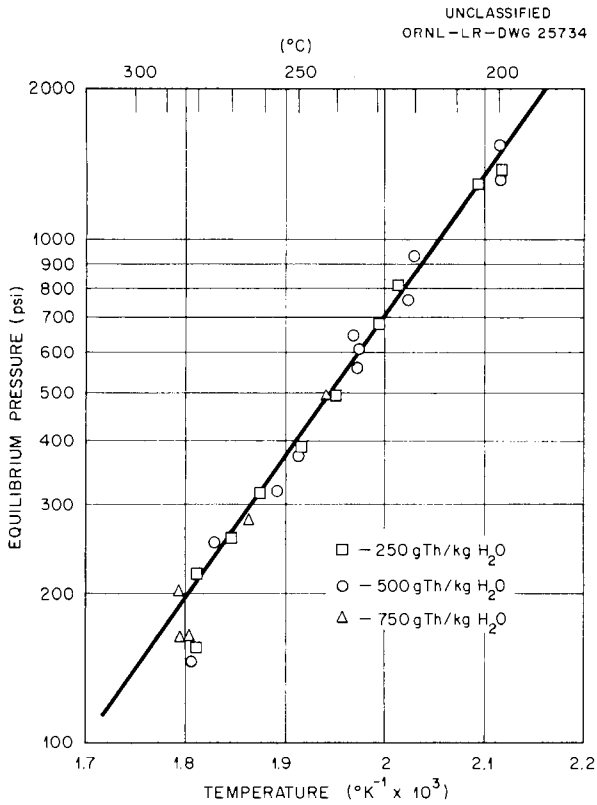

Fig. 20.2. Equilibrium Radiolytic-Gas Pressure, Excluding Steam Pressure, 1 *N* Irradiated Thorium Oxide Slurries.

measurements are being made to confirm this and to determine whether the available surface area controls the recombination rate.

20.3 GAS-RECOMBINATION STUDIES

Efforts to develop a catalyst for the recombination of radiolytic gas in thorium oxide blanket slurries continued, with studies on the effects of oxide calcination temperature and time and of pumping on the catalytic activity of MoO_3 in slurries of thorium and thorium-uranium oxide. Oxides fired at 1000°C and above provide the more effective support and promotion of MoO_3 catalytic activity.

20.3.1 Effect of Calcination Conditions on the Catalytic Activity of Aqueous Thorium-Uranium Oxide Slurries

It has been shown in previous studies[3] that the reaction rates of stoichiometric H_2-O_2 mixtures in aqueous slurries of thorium-uranium oxide prepared from the coprecipitated oxalate calcined at 1000°C for 24 hr and containing 0.05 *m* MoO_3 were much greater than the required rate of 10 moles of H_2 per hour per liter of slurry at 280°C and a partial pressure of 500 psi H_2. A study was made to determine whether the calcination time could be decreased. The results (Table 20.3) showed that calcination times of 8 to 16 hr were required to obtain satisfactory reaction rates in slurries activated by heating with hydrogen. For the slurries as prepared, calcination times greater than 16 hr and up to 24 hr were necessary for satisfactory reaction rates.

The data obtained with a slurry of a similar mixed oxide calcined at 1000°C for 4 hr at Y-12 and an additional 12 hr at ORNL support the results obtained with the 16-hr calcined oxide used in the above experiments.

Additional experiments with the mixed oxide showed that oxide calcined at 1200°C for 4 hr would

[3] *Chem. Tech. Monthly Prog. Rep. June 1957*, ORNL-2362 (classified).

Table 20.3. Effect of Calcination Conditions on the Reaction Rates of Stoichiometric H_2-O_2 Mixtures in Aqueous Slurries of Thorium-Uranium Oxide

Slurry preparation: mixed oxide (0.5% U) prepared from coprecipitated oxalates; 500 g Th/kg H_2O; 0.05 *m* MoO_3

Calcination Conditions		Combination Rate, P_{H_2} = 500 psi (moles H_2/hr·liter)	
Temperature (°C)	Time (hr)	Slurry as Prepared	Activated Slurry*
1000	4	0.1 (295°C)	0.1 (288°C)
	8	0.1 (292°C)	0.1 (293°C)
	16	0.1 (284°C)	91 (250°C)
	24	59 (250°C)	41 (250°C)
1000**	16	0.5 (284°C)	42 (247°C)
1200	4	45 (200°C)	53 (200°C)

*Slurry heated with H_2 (250 psi at 25°C) for 2 hr at 270°C.

**This sample was calcined at Y-12 (4 hr) and ORNL (12 hr).

be a satisfactory support for the catalyst. For a slurry of this oxide, reaction rates of the stoichiometric H_2-O_2 mixture in both the slurry as prepared and the hydrogen-activated slurry were well in excess of 10 moles of H_2 reacted per hour per liter at 280°C and a hydrogen partial pressure of 500 psi (Table 20.3).

The thorium-uranium oxide for these experiments was obtained by calcining thorium-uranium oxalate which had been coprecipitated at 10°C. The slurries were prepared by tumbling the dry thorium-uranium oxide and MoO_3 for 1 hr and then heating the mixture in water at 280°C for 3 hr in the presence of a small oxygen overpressure.

20.3.2 Experiments with Pumped Oxide

An 800°C-fired thorium oxide slurry (950 g of thorium per kilogram of H_2O) containing 0.05 *m* MoO_3 and 2000 ppm SO_4 (based on thorium) which had been pumped in REED loop S (run S-98) for 403 hr at 290°C had very low catalytic activity. Reaction rates in the slurry as prepared and in the hydrogen-activated slurry were less than 0.1 mole of H_2 per hour per liter of slurry at 280°C and a partial pressure of 500 psi H_2.

The thorium oxide used in this run was prepared in the Chemical Technology Division pilot plant by precipitating thorium oxalate at 70°C and finally calcining the oxide at 800°C for 4 hr. At the end of the 403-hr circulation period, the slurry contained (based on thorium) 2360 ppm Fe, 475 ppm Cr, and 380 ppm Ni as corrosion products. Low catalytic activity in the experiments reported above was characteristic of slurries prepared with thorium oxides calcined below 900°C for 24 hr. Previous experiments[4] have shown that it is unlikely that sulfate or iron affects the catalytic activity. It is believed that the low catalytic activity in these experiments resulted from low firing temperature rather than pumping and corrosion-product pickup.

20.3.3 MoO_3 Concentration Studies with 1600°C-Fired Oxide

The catalytic activity of aqueous slurries containing 1600°C-calcined ThO_2 and uranium added as the oxide or coprecipitated in the oxalate precipitation step is being studied as a function of the MoO_3 catalyst concentration. The investigation is prompted by the current interest in 1600°C-calcined materials for use in ThO_2 breeder blankets.

(a) Studies with Simple Mixtures. – Reaction rates were low with the pure 1600°C-fired ThO_2 slurry (Table 20.4). They were not significantly increased by the addition of $UO_3 \cdot H_2O$. Addition of MoO_3 to 0.024 *m* increased the reaction rate only slightly, but a marked improvement was demonstrated at 0.036 *m*. At 0.048 *m* MoO_3 the reaction rate in the hydrogen-activated slurry was 17.3 moles of H_2 per hour per liter of slurry at 291°C and a partial pressure of 500 psi H_2, which is slightly greater than the required value. These experiments will be continued to higher MoO_3 concentrations to determine the catalyst concentration at which the increase in rate levels out.

The ThO_2 used in these experiments was calcined at 1600°C for 4 hr and then circulated as a slurry for 268 hr at about 300°C in a REED loop (run BS-16). After the addition of $UO_3 \cdot H_2O$ and each 0.012 *m* MoO_3 aliquot, the slurry was heated at 280°C for 3 hr with a small oxygen overpressure.

Table 20.4. Reaction Rates of Stoichiometric H_2-O_2 Mixtures in Aqueous Slurries of Simple Mixtures of 1600°C-Calcined ThO_2 and $UO_3 \cdot H_2O$

Thorium: 500 g/kg H_2O (1600°C-4 hr calcined ThO_2)
Reaction temperature: 291°C

Slurry Composition	Combination Rate, P_{H_2} = 500 psi (moles H_2/hr·liter)	
	Slurry as Prepared	H_2-Activated Slurry*
ThO_2	<0.1	0.1
0.5% U, added as $UO_3 \cdot H_2O$	<0.1	0.21
MoO_3 additions		
0.012 *m*	0.4	0.24
0.024 *m*	0.5	0.27
0.036 *m*	1.2	3.1
0.048 *m*	5.2	17.3

*Slurry heated with hydrogen (250 psi at 25°C) for 2 hr at 270°C.

[4] J. P. McBride *et al.*, *HRP Quar. Prog. Rep. April 30, 1957*, ORNL-2331, p 157, esp 159.

(b) Studies with Thorium-Uranium Oxide Prepared from Coprecipitated Oxalates. – The catalytic behavior of the coprecipitated oxide slurry without added MoO_3 was more complex than that observed for the corresponding slurry of simple mixed oxides (Table 20.5). Hydrogen activation of the coprecipitated oxide slurry increased the rate from 0.17 mole of H_2 reacted per hour per liter of slurry at 289°C to 1.29 moles of H_2 reacted per hour per liter of slurry at 251°C. The reaction rate decreased in subsequent experiments at higher temperatures, so that at 291°C only 0.45 mole of H_2 reacted per hour per liter of slurry at a partial pressure of 500 psi H_2.

The reaction rate of the stoichiometric gas mixture in the slurry as prepared was greatly increased by the addition of 0.012 *m* MoO_3. The reaction rate was increased in the initial experiments to 29.9 moles of H_2 reacted per hour per liter at 277°C and a partial pressure of 500 psi H_2. In a second series of experiments with the same slurry, the reaction rate increased to 57.0 moles of H_2 reacted per hour per liter of slurry at 278°C. Tests with the hydrogen-activated slurry may show whether the slurry had become activated under the experimental conditions. The experiments will be continued, with increasing catalyst concentration to 0.05 *m* MoO_3.

Table 20.5. Reaction Rates of Stoichiometric H_2-O_2 Mixtures in Aqueous Slurries of 1600°C Calcined Thorium-Uranium Oxide Prepared from Coprecipitated Oxalates

500 g Th–0.5% U/kg H_2O, coprecipitated oxide calcined at 1600°C for 24 hr

Slurry Condition	Reaction Temperature (°C)	Combination Rate, P_{H_2} = 500 psi (moles H_2/hr·liter)
Slurry as prepared	289	0.17
H_2-activated slurry*	242	1.23
	251	1.29
	261	0.95
	272	0.55
	282	0.49
	291	0.45
0.012 *m* MoO_3 added (not H_2-activated)	277	29.9
	278	57.0

*Slurry heated with hydrogen (250 psi at 25°C) for 2 hr at 270°C.

20.4 SLURRY CHEMISTRY STUDIES

20.4.1 Long-Term Hydrothermal Experiments

Two aqueous slurries of thorium oxide, D-16-650-24 and LO-12 pilot-plant oxide, each at a concentration of 500 g of thorium per kilogram of H_2O, were heated at 300°C for 1500 hr in rocking stainless steel autoclaves. Samples were withdrawn at intervals, and the particle sizes, x-ray crystallite size, and specific surface areas were determined. No significant change in these properties occurred in either oxide as a result of the hydrothermal treatment, except for a pronounced decrease in average particle size in the D-16 oxide (Table 20.6).

Each of the oxide samples was refired at 900°C for 24 hr, with no change in particle size. Surface areas decreased as expected, with no significant effect of hydrothermal treatment on the LO-12 oxide but slightly higher surface areas being obtained with the D-16. Crystallite growth was not so pronounced in the hydrothermally treated oxides as has been observed in untreated oxides, and, at least with the D-16 fired oxide, the crystallite growth on refiring decreased with increasing time of hydrothermal treatment. This suggests that the failure of crystallites to grow on refiring is not wholly the result of the absence of a relic structure but may also be associated with the condition of the thoria surface.

The results indicate that the lower fired oxide is more reactive to high-temperature water than the high-fired, since both a pronounced decrease in particle size and change in crystallite-growth characteristics occurred with the 650°C-fired material as a result of the hydrothermal treatment.

20.5 THORIUM-URANIUM OXIDE STUDIES

Investigation of the effect of firing temperature from 650 to 1600°C for 24-hr firings on the properties of thorium-uranium oxide prepared from the 10°C-coprecipitated oxalates has continued. The mixed oxide studied contained 0.5 and 5% uranium.

Table 20.6. Effect of Wet-Autoclaving at 300°C on the Characteristic Properties of Thorium Oxide

Oxide	Autoclaving Time (hr)	Average Particle Size (μ)		X-Ray Crystallite Size (Å)		Surface Area (m^2/g)	
		As Removed from Autoclave	After Refiring at 900°C for 24 hr	As Removed from Autoclave	After Refiring at 900°C for 24 hr	As Removed from Autoclave	After Refiring at 900°C for 24 hr
D-16-650	0	2.5	2.8	130	619	35	8
	100	2.6	3.0	121	375	35	9
	250	2.0	2.7	124	388	35	13
	500	1.6	1.8	125	257	33	10
	1200	1.3	1.5	141	232	31	13
	1500	1.1	1.3	129	261	32	13
LO-12-800	0	4.5		225	570	17	
	100	4.1	5.0	231	341	20	10
	250	4.3	4.7	217	326	20	9
	500	3.7	4.7	241	370	19	9
	1200	3.5	5.0	243	318	19	10
	1500	4.0	4.3	255	360	18	9

20.5.1 Uranium Content

It has been speculated that oxyacetylene firing of a coprecipitated thorium-uranium oxide at 1400 or 1600°C might result in appreciable uranium losses by volatilization. However, the uranium content remained constant up to 1600°C for 24-hr firings, with a mean value of 0.54 ± 0.05 g of uranium per kilogram of thorium.

The result was similar with the thorium-uranium oxide containing 5% uranium in the range 650 to 1300°C (Table 20.7). The average uranium content was 5.07 ± 0.07 g per kilogram of thorium.

20.5.2 Tap Densities

Tap-density data were obtained by measuring the minimum attainable volume of a weighed sample of oxide by tapping it sharply on a firm surface until no further volume change occurred. The tap densities as a function of firing temperature of two

Table 20.7. Effect of Firing Temperature on Some Properties of Thorium-Uranium 10°C-Coprecipitated Oxides

Conditions: g U/100 g Th = 5.07
Initial decomposition of 10°C-coprecipitated oxalates at 650°C, 2-hr firing time

Firing Temperature (°C)	Uranium Content (g U/100 g Th)	X-Ray Crystallite Size (Å)	Specific Surface Area (m^2/g)
650	5.08	94	17.0
800	4.99	140	7.3
900	5.16	535	2.3
1000	5.14	1764	1.5
1200	5.02	2500	0.91
1300	5.02	2500	0.62

thorium-uranium oxides, prepared from the 10°C-coprecipitated oxalates, containing 0.5 and 5% uranium are shown in Fig. 20.3.

The presence of uranium promoted incipient sintering, since at low uranium content (0.54 g U/100 g Th) the curve starts out much flatter in the range 650 to 1000°C, whereas at tenfold higher concentration the slope is considerably higher.

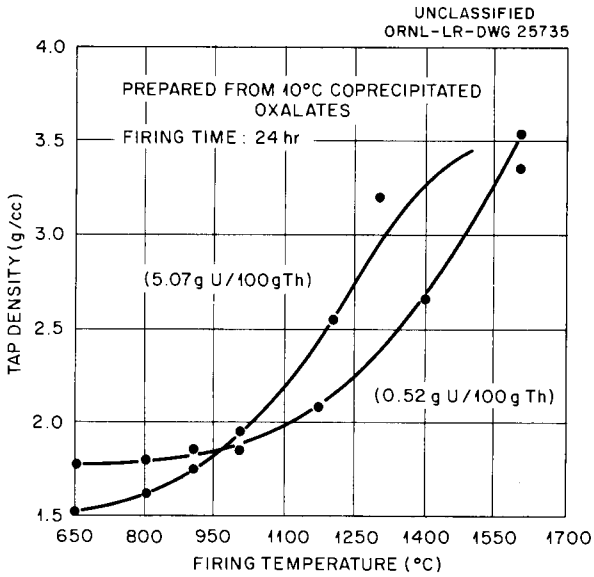

Fig. 20.3. Tap Density of Thorium-Uranium Oxides as a Function of Firing Temperature.

For a similar pure ThO_2 sample (TO-10) fired for 12 hr, the tap density was essentially unchanged in the range 650 to 1300°C. The differences in incipient sintering between the two thorium-uranium oxides may be compared by observing from the curves the temperature at which a 10% increase in tap density is produced when compared with the initial value at 650°C. The value 10% represents about twice the estimated experimental error. The sintering temperatures thus found were 1070 and 840°C, respectively, for 5.07 and 0.54 g of uranium per 100 g of thorium. For the 12-hr-fired pure oxide the sintering temperature was 1520°C.

The effect of firing time at 1600°C was investigated for oxide containing 5.07 g of uranium per 100 g of thorium and for TO-10 pure oxide for comparison, since in the latter case the effect was known to be slight. Figure 20.4 shows that for the uranium-bearing oxide, firing time at 1600°C is

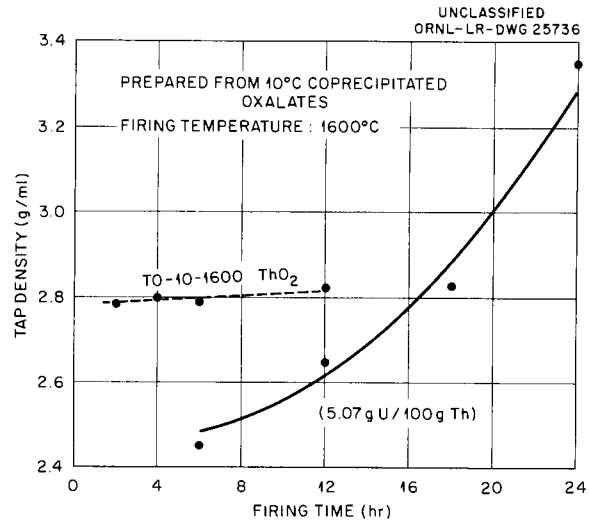

Fig. 20.4. Effect of Firing Time on Tap Density of Coprecipitated Thorium-Uranium Oxide.

a relatively more important variable than in the case of extremely pure ThO_2.

20.5.3 Particle Size

The mean Stokes diameters, as measured by the neutron activation-sedimentation technique are shown graphically in Fig. 20.5 for temperatures in the range 650 to 1600°C (24-hr firings). The data do not permit a quantitative estimate of sintering temperatures to be made similar to those determined by tap density. However, the same general trend is established, namely that for the uranium-rich sample sintering takes place even at the lower end of the temperature range, as indicated by the steep slope of the curve at that point. The slope of the curve for the low-uranium sample (0.54 g U/100 g Th) is much flatter up to about 1000°C, indicating relatively little particle-to-particle sintering in the range 650 to 1000°C.

20.5.4 Crystallite Size and Surface Area

The results of Table 20.7 show the usual increase in crystallite size and decrease in surface area which accompanied an increase in firing temperature for the mixed oxide in the range 650 to 1300°C. The fact that changes were somewhat

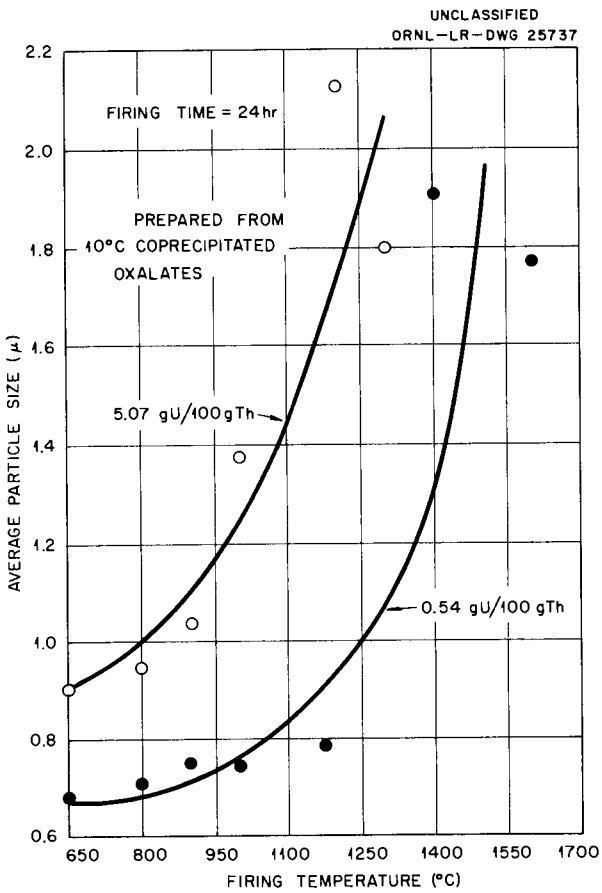

Fig. 20.5. Effect of Firing Temperature on the Average Particle Size of Thorium-Uranium Oxides.

steeper than for the mixed oxide previously reported,[5] which contained 0.54 g of uranium per 100 g of thorium, indicates again that increasing the uranium content decreases the temperature at which sintering occurs.

20.5.5 Abrasive Characteristics

The penetration rates on the abrasion tester obtained with the two mixed oxides are shown in Table 20.8. Both mixed oxides showed a sharp increase in penetration rate with increasing firing temperature. Abrasiveness as measured by the penetration rate appears to increase with increasing uranium content.

[5]J. P. McBride *et al.*, *HRP Quar. Prog. Rep. April 30, 1957*, ORNL-2331, p 157, esp 161.

Table 20.8. Effect of Firing Temperature on Jet Abrasion Rate of Coprecipitated Thorium-Uranium Oxides

Conditions: Samples prepared by firing 10°C-coprecipitated oxalates at 650°C for 2 hr; refired for 24 hr at temperature stated

Slurry concentration 250 to 300 g Th/kg H_2O

One-mil type 302 stainless steel shim-stock target

Firing Temperature (°C)	Jet Abrasion Rate (μin./sec)	
	0.54 g U/100 g Th	5.07 g U/100 g Th
650	*	0.63
800	*	3.0
900	0.99	17.1
1000	2.63	24.4
1170	11.6	
1200		27.2
1300		29.4
1400	11.2	
1600	8.9	

*Too low to be measured.

20.6 SLURRY VISCOSITY AND HINDERED SETTLING[6]

Analyses of data obtained in measuring the viscosity of thoria slurries indicate a straight-line relation between the logarithm of the ratio of viscosity of a thoria suspension and water at specified reciprocal absolute temperatures. For thoria concentrations of 200, 400, and 700 g per kilogram of H_2O, the viscosity–reciprocal-temperature curves parallel each other (Fig. 20.6). The general equation fitting these curves is

$$\left(\frac{\eta}{\mu_0}\right)_T = ae^{b/T} ,$$

[6]Work supervised by J. M. Dalla Valle.

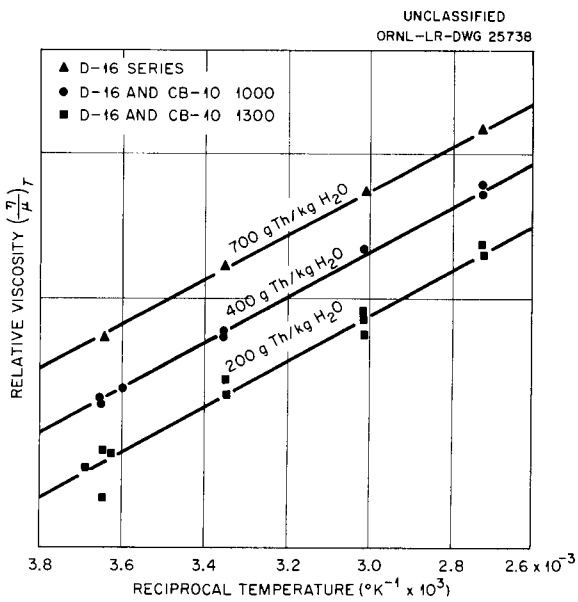

Fig. 20.6. Relation Between Slurry Relative Viscosity and Reciprocal Absolute Temperature.

where $(\eta/\mu_0)_T$ is the ratio of the viscosity property of the slurry to the viscosity of water at absolute temperature T, and a and b are constants.

The values of the constant a depend on the concentration of the suspension:

Concentration (g Th/kg H_2O)	Constant a
200	1.15
400	1.35
700	1.65

The viscosities of the thorium oxide slurries containing 200 to 700 g of thorium per kilogram of H_2O in the temperature range 25 to 90°C are related to the hindered-settling rates by the equation

$$\eta = A\, U_0\, e^{\frac{2.85 \times 10^3}{T}} ,$$

where η is the viscosity in centipoises, U_0 the settling rate in cm/sec, and T the absolute temperature. The proportionality constant, A, is characteristic of the oxide used and for the oxides tested was 0.003.

20.7 SURFACE-CHEMISTRY STUDIES[7]

Isotherms for adsorption of carbon dioxide on thoria were obtained for thoria which had been degassed at 450°C. Rates of desorption were also obtained for several temperatures. The desorption rates show a linear decrease with the logarithm of time. Attempts are being made to interpret the data theoretically, and various significant constants are being calculated. An interesting correlation was made between some adsorption and desorption constants. It is possible that the behavior of the gas on the surface is associated with an overlapping charge field built up following adsorption. It seems possible that both enthalpy and entropy play a part in adsorption, entropy becoming more important as the temperature is increased.

In a study of adsorption on thoria from sulfuric acid solutions, isotherms at 4°C showed an apparent surface saturation of four hydrogen ions and two sulfate ions per surface site. This result is tentatively explained as a displacement of two hydroxyl groups per surface site by hydrogen sulfate groups. The stoichiometry is complicated by the dissolution of thoria in sulfuric acid solutions more concentrated than 0.02 N, even at 4°C. Studies in sodium hydrogen sulfate solutions now under way should overcome this difficulty.

Differential infrared studies of thoria surfaces show bands at 8.3, 8.9, and 9.6 μ which can be attributed to adsorbed sulfates. Inspection of available spectra shows most resemblance to heavy-metal sulfates. The carbonate, hydrogen sulfate, and sulfate of thorium were synthesized, and the x-ray and infrared spectra of these compounds were obtained in addition to those of thorium hydrogen sulfate and thorium nitrate. The spectra of adsorbates on the thoria surface are very similar to the thorium hydrogen sulfate spectrum. Carbon dioxide adsorbed on thoria from the air was tentatively identified by infrared bands at 5.7 and 14.4 μ. Absolute identification of these spectra depends on matching of x-ray reflection spectra with spectra known to be characteristic of these compounds.

[7]Work done by M. E. Wadsworth, University of Utah, under subcontract.

21. IN-PILE SLURRY LOOP

W. E. Unger

T. A. Arehart
L. J. King
B. B. Klima
W. F. Schaffer

One of the most important parts of the development of fluid-fuel power reactors is the testing of fuels and materials of construction in environments which duplicate as nearly as practical the environments expected in the reactor. The most useful tool for performing these tests is the forced-circulation in-pile loop. A strong mutual interest in loops and ThO_2 slurry fuels by both ORNL (HRP) and Westinghouse–Pennsylvania Power and Light (PAR) served as a strong incentive for the two projects to collaborate on a common program.

A cooperative effort has been in effect since January 1957. The PAR Project has assumed the responsibility for designing, developing, and fabricating a loop that will circulate slurries in concentrations up to 500 g/liter. The PAR Project will also provide the necessary auxiliaries. HRP personnel will operate the loop in the ORR and will conduct the postirradiation examination of loops and contents.

21.1 SLURRY SAMPLING

An unsolved problem is that of taking a representative sample. ORNL has designed a sample valve and is testing an ultrasonic agitator to keep the ThO_2 suspended in the sample aliquot. The unit is a magnetostrictive type manufactured by Acoustica Associates, Inc., which operates at 25 kc and has a power output of 400 w. In glass apparatus, the unit appears capable of maintaining small quantities of slurry in suspension.

21.2 IN-PILE LOOP FACILITY DESIGN

The large size of the slurry loop requires a special south reactor facility plug. A series of shielded chambers are also to be provided to enclose the auxiliary equipment associated with the slurry loop.

The primary slurry loop is located entirely within reactor beam hole HS-1 (Fig. 21.1) and is enclosed in a vapor-tight stainless steel container designed to hold the pressure if the primary loop and high-pressure coolant system should rupture. The vapor container is 128 in. long, with a major diameter of 27 in. and a minor diameter at the front of $9\frac{3}{4}$ in.

The south facility plug, 77 in. long, 65 in. OD, contains two beam holes, HS-1, and a smaller 10-in. hole, HS-2. Twenty inches of aluminum pellets and $\frac{1}{4}$ in. of boral make up the thermal shield; the remainder is barytes concrete. The whole assembly is water cooled.

A mockup of the loop vapor container and beamhole liner was fabricated and installed in Building 4501 to determine design feasibility. Preliminary experimentation indicated that the 5600-lb loop can be inserted into and removed from the beamhole liner of the ORR with ease.

Equipment chambers A, B, C, D, and E house the loop auxiliaries (Figs. 21.1 to 21.3). These chambers, individually shielded by lead ranging in thickness from 8 to 12 in., are located outside the biological shield of the ORR.

Chamber A houses the disconnects for the process, instrument, and service lines to the loop and loop sampler. It is $5\frac{1}{2} \times 5\frac{1}{2} \times 1\frac{1}{2}$ ft deep and is located immediately behind the loop. Entrance is gained by means of a 4-ft-thick 70%-iron-filled concrete shield door.

Chamber B houses the loop off-gas system. It contains the gas holdup tanks, the valves, and the piping required to dispose of the radioactive gases from the loop and to obtain samples of the gases. The chamber is $5\frac{1}{2} \times 4\frac{1}{2} \times 4$ ft deep.

Chamber C contains the high-pressure cooling-water system, which consists of two recirculating pumps, an air-to-water heat exchanger and radiator, a water reservoir, a pressurizer, and the associated valves and piping. The chamber is $5\frac{1}{2} \times 5\frac{1}{2} \times 4\frac{1}{4}$ ft deep.

Chamber D houses the slurry dump system. It contains the dump and wash tanks and associated valves and piping. The cell is $8 \times 5 \times 3\frac{1}{2}$ ft deep and is the most heavily shielded chamber.

Chamber E houses the two vacuum pumps and is separated from the other chambers to permit servicing of the pumps as required. This chamber, situated on top of chamber B, is $2 \times 3\frac{1}{3} \times 2$ ft deep.

21.3 SEGMENTING FACILITY

The dismantling cell (in Building 3026) for power-reactor-development experiments (Fig. 21.4) will be used for segmenting the loop for inspection and removal of corrosion coupons. Detailed examination of the coupons and pieces of equipment will be done in other existing hot cells. The dismantling facility will consist of two large cells equipped with manipulators, windows, and hoists, plus additional implements provided for handling the slurry loop:

1. a 12-ft-long, 3-ft-wide movable work table complete with rollers, vises, and other handling equipment;
2. two abrasive-wheel cut-off saws, one with a 24-in. and one with a 16-in. blade;
3. decontamination equipment which consists of tanks, sprays, and an ultrasonic cleaner.

21.4 SCHEDULES

June 1, 1958, has been established for the start of in-pile operation of the slurry loop. Over-all engineering design of the in-pile loop facility is approximately 20% complete.

Engineering design of the segmenting facility is proceeding according to schedule, and the bulk of it will be completed by November 15, 1957, although some of the small-tool design could extend into February 1958.

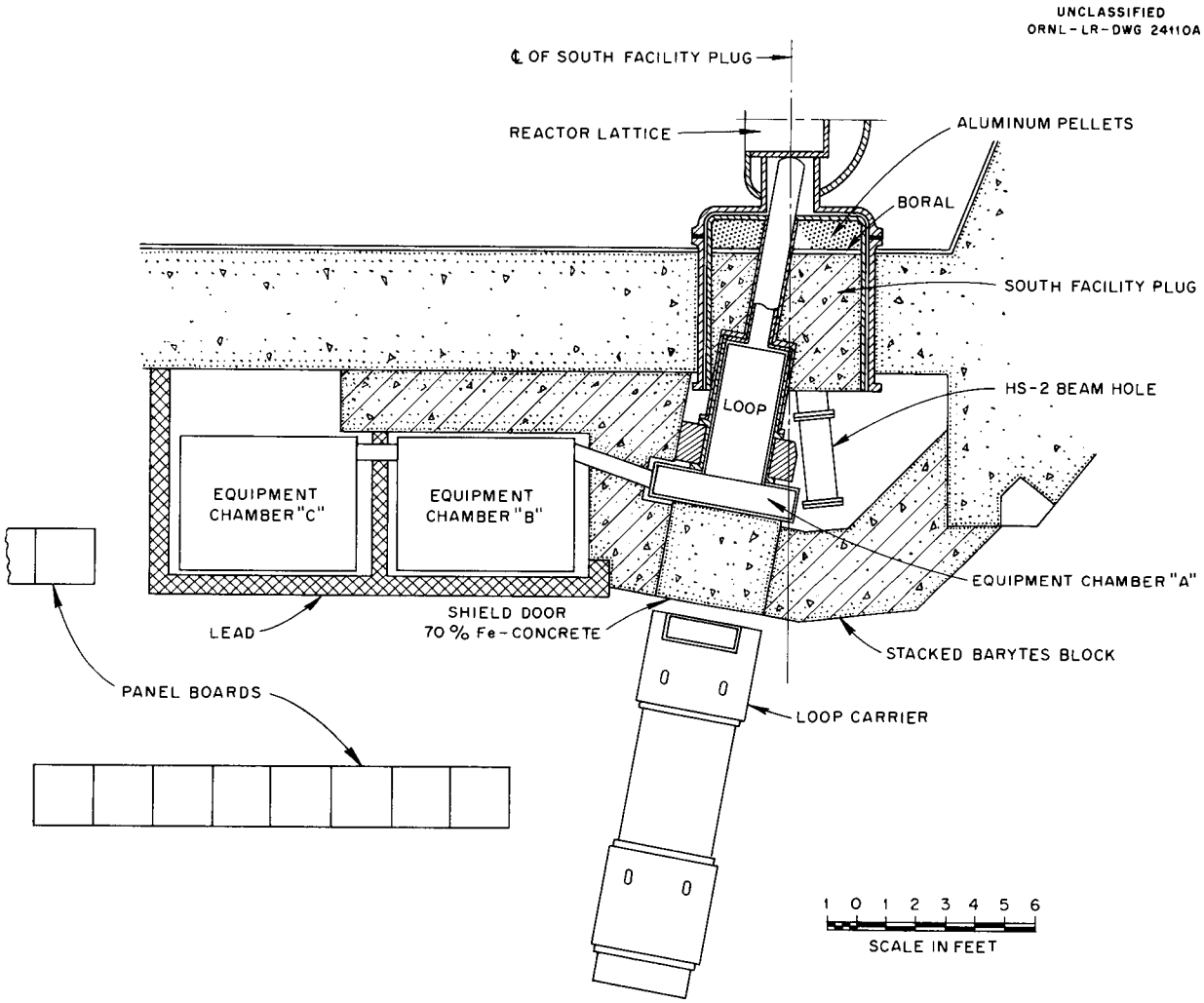

Fig. 21.1. Plan of Equipment – Operating Floor.

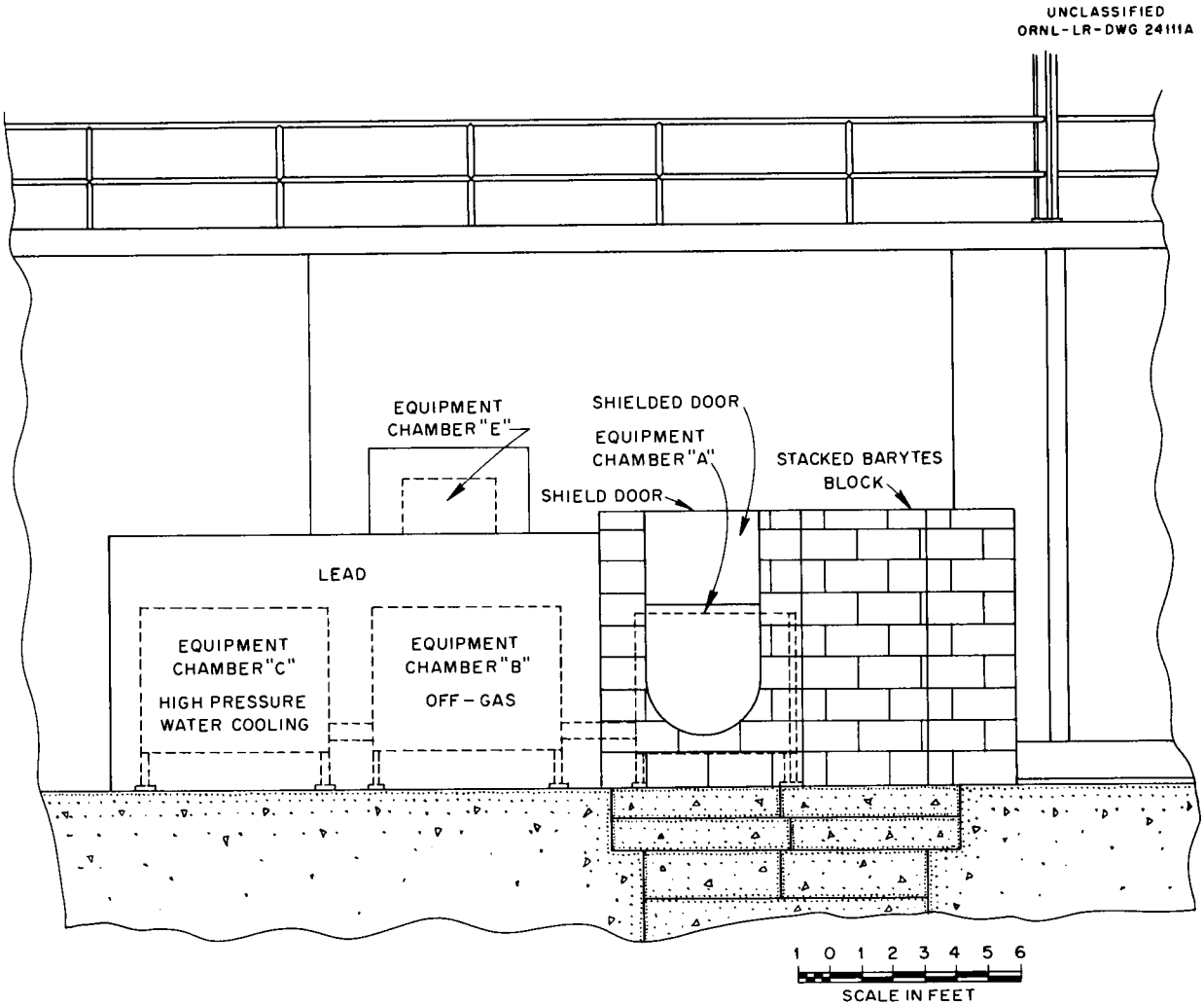

Fig. 21.2. Elevation of Equipment – Operating Floor.

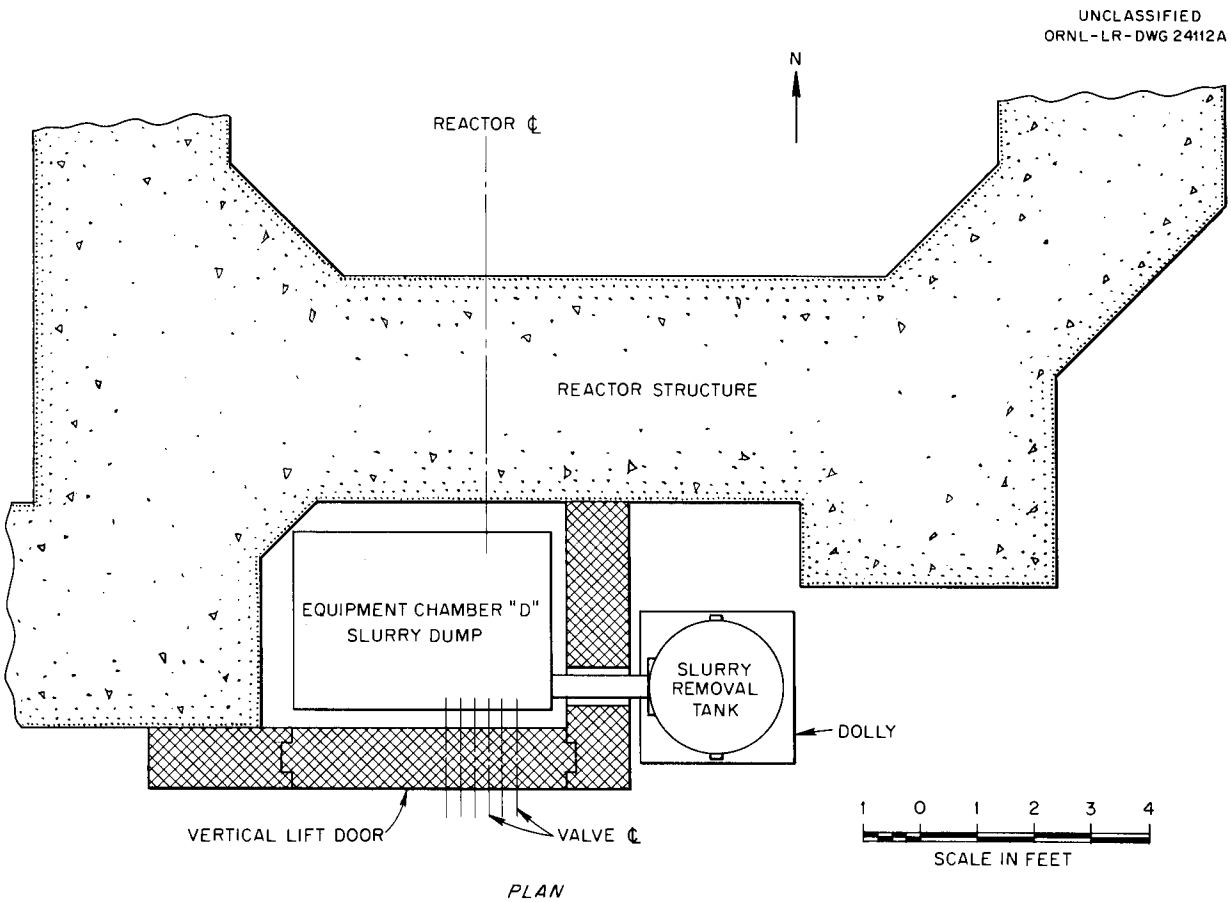

Fig. 21.3. Loop Equipment in ORR Basement.

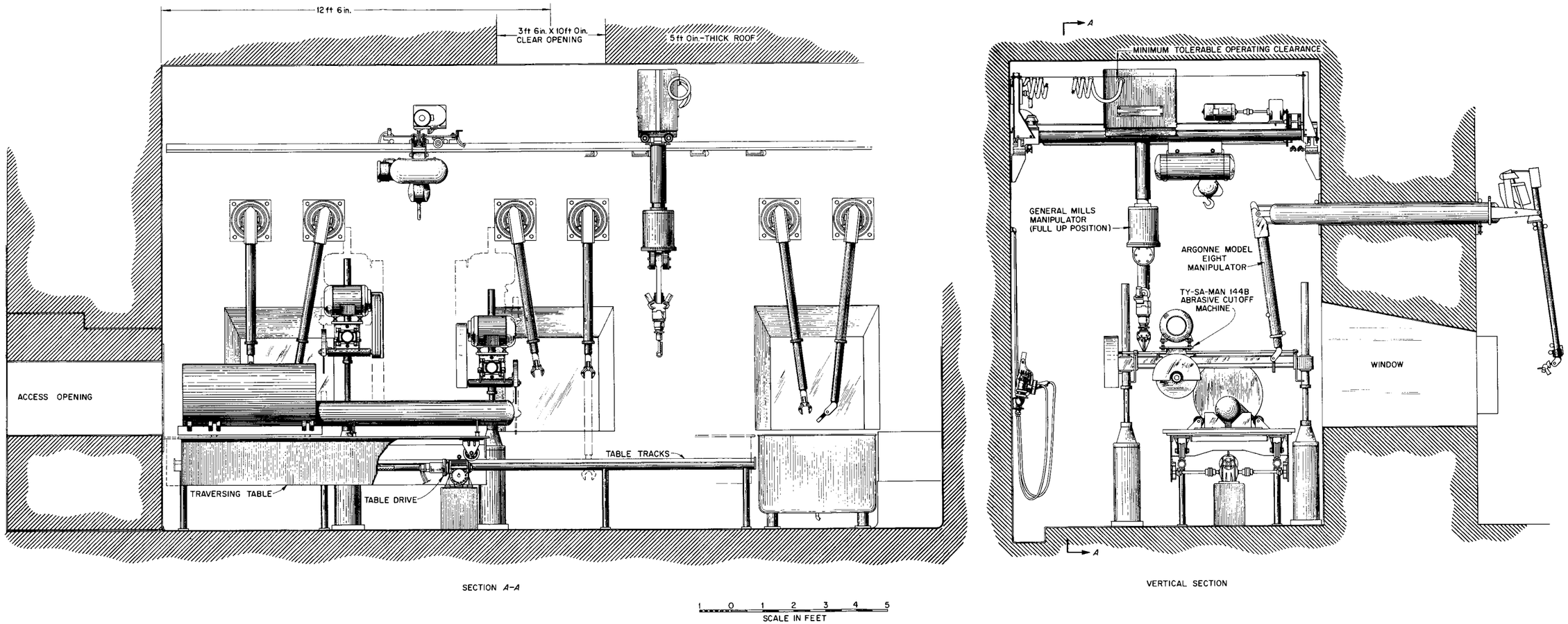

Fig. 21.4. Segmenting-Cell Equipment Layout.

Part VI

SUPPORTING CHEMICAL RESEARCH

E. H. Taylor

22. AQUEOUS SYSTEMS AT ELEVATED TEMPERATURES

W. L. Marshall

F. E. Clark J. S. Gill R. Slusher

22.1 TWO-LIQUID-PHASE TRANSITION TEMPERATURES IN THE SYSTEM $CuSO_4$-UO_2SO_4-H_2SO_4-H_2O

Data are presented in Tables 22.1 to 22.5 to show the two-liquid-phase transition temperatures for the system $CuSO_4$-UO_2SO_4-H_2SO_4-H_2O. These data, in addition to the results previously reported,[1] give essentially a complete representation of the liquid-liquid immiscibility occurring in the temperature range 285 to 374°C. Furthermore, the regions are defined in which one of the two liquid phases is replaced by a solid or solids. The solids in general are basic (as opposed to acidic) single and double salts of copper and uranium. The general nature and composition of these basic salts are described in detail in a previous report.[1] In general, the mode of formation of the solid was found to be the same as described previously. There is a relatively long induction period before precipitation starts, and the rate of approach to equilibrium is relatively slow. In contrast to this behavior of the solids, the formation of two immiscible phases occurs in less than a second at the specified phase transition temperature and is reversible with equal rapidity. The transition temperatures presented in Tables 22.1 to 22.5 for two-liquid-phase behavior are believed to be accurate to ±1°C, which is approximately the accuracy of temperature measurement using an iron-constantan thermocouple connected to a recording potentiometer.

The experimental methods were essentially the same as reported previously.[1] Solutions of known composition were prepared, and portions of these solutions were sealed in individual 2-mm-ID silica tubes with silica rod extensions. A silica tube containing solution was inserted into a liquid salt bath of an $NaNO_3$, KNO_3, and $LiNO_3$ eutectic mixture, and the top end of its extension was connected to an on-off vibrator unit as used previously. The temperature of the bath was raised or lowered, and the temperature was determined at which a second liquid phase appeared or disappeared. Thermal gradients were kept to a minimum by the use of an efficient stirrer within the liquid salt bath. Gradients were found to exist in several types of aluminum-cylinder heater units used previously, and consequently the change to a liquid salt bath was considered desirable to eliminate this particular uncertainty. The previous data at 29.11 mole % excess sulfuric acid were redetermined, and the revised values are included in Table 22.4. The difference in recorded transition temperature between the past and revised data for any particular composition was in the range of 0 to +3°C.

The actual experimental data are given in Tables 22.1 to 22.5. The preparation of the master and dilute solutions has been described in detail in the previous report.[1] Briefly, the primary solutions of various weight ratios, $CuSO_4/UO_2SO_4$, were obtained by mixing exact weights of the master solutions. Consequently, the dilutions were prepared by exact weight dilutions with H_2O of the various primary solutions. All reported temperature values are for the appearance or disappearance of a second liquid phase. In the few data in which both a solid phase and a temperature are listed, a very small amount of the specified solid was observed in addition to the two liquid phases.

The blue-green solid listed in the tables apparently is antlerite, $3CuO{\cdot}SO_3{\cdot}2H_2O$. As yet, however, no x-ray diffraction patterns have been obtained from the small amounts of solid to compare with the established pattern for antlerite. This solid would appear in the more dilute solutions at temperatures more than 100°C below the two-liquid-phase temperatures, thus substantiating previous observations of the existence of a steep cliff near the dilute region.[1] The red solid appearing at low H_2SO_4 and $CuSO_4$ concentrations does not coincide with previous observations on the behavior of the system UO_3-H_2SO_4-H_2O, and at present its identity is unknown. Presumably, it is a uranium-containing solid phase which is either zippeite, $2UO_3{\cdot}SO_3{\cdot}5H_2O$, a form similar to zippeite, or a questionable reaction product of the silica-tube

[1] C. H. Secoy *et al.*, *HRP Quar. Prog. Rep. Jan. 31, 1957*, ORNL-2272, p 163.

Table 22.1. Phase Transition Temperatures (°C); Part A

Master solutions: (a) 17.17% $CuSO_4$, 0.00 mole % excess H_2SO_4
(b) 47.64% UO_2SO_4, 0.00 mole % excess H_2SO_4

Weight Ratio, Solution/H_2O	Weight Ratio, $CuSO_4/UO_2SO_4$									
	8/2	7/3	6/4	5½/4½	5/5	4/6	3/7	2/8	1/9	0/10
10/0		Blue-green solid	Blue-green solid	287	287	287	287.5	288.5	289.5	291
9/1			Blue-green solid	Blue-green solid	286	286		287		290
8/2			Blue-green solid	Blue-green solid	285.5	285.5		286		289
7/3				Blue-green solid	Blue-green solid	285		285.5		288
6/4					Blue-green solid	284.5		285		287
5/5					Blue-green solid	285		285		287
4/6					Blue-green solid	286		286		287.5
3/7					Blue-green solid	288 + red solid		289		289.5
2/8				Blue-green solid	Blue-green solid	292.5 + red solid		292.5 + red solid		293
1/9	Blue-green solid				Blue-green solid	Blue-green and red solid		302 + red solid		302.7
0.75/9.25						Blue-green solid	Red solid	Red solid		Yellow solid
0.5/9.5						Blue-green and red solid	Red solid	Red solid	Red solid	312
0.25/9.75							Red solid	Red solid	Red solid	Yellow solid

Table 22.2. Phase Transition Temperatures (°C); Part B

Master solutions: (a) 17.24% $CuSO_4$, 9.91 mole % excess H_2SO_4
(b) 47.05% UO_2SO_4, 9.91 mole % excess H_2SO_4

Weight Ratio, Solution/H_2O	Weight Ratio, $CuSO_4/UO_2SO_4$								
	8/2	7/3	6/4	5/5	4/6	3/7	2/8	1/9	0/10
10/0	Blue-green solid	306.5	305.5	305	304.5	305	305.5	307	308.5
9/1		305		303					305.5
8/2	Blue-green solid		301.5		300.5		301		303
7/3		301.5		300					300.5
6/4			299.5		297.5		297.5		298.5
5/5		Blue-green solid		297.5					297.5
4/6			300		297		296.5		297
3/7				299.5					298
2/8			Blue-green solid		302		300.5		300.5
1/9	Blue-green solid	Blue-green solid	Blue-green solid	Blue-green solid	311		309.5		309
0.75/9.25	Blue-green solid	Blue-green solid	Blue-green solid	Blue-green solid	313	313	313	313	313
0.5/9.5	Blue-green solid	Blue-green solid	Blue-green solid	Blue-green solid	321	320	319	319	319
0.25/9.75	Blue-green solid	Blue-green solid	Blue-green solid	Blue-green solid	332	332	331	331	

container and UO_3. The amount of red solid produced is very small and is somewhat difficult to observe. Neither the blue-green nor the red solids are observed to redissolve under the experimental conditions. The qualitative description indicates only the type of solid to be found near the isotherm intersections of two-liquid-phase composition curves with the particular solid.

The data in Tables 22.1 to 22.5 were plotted on graphs of $CuSO_4$ vs UO_2SO_4 concentration, and from these graphs temperature contour lines (isotherms) were drawn. The resulting curves are shown in Fig. 22.1 at each of the several concentrations of excess H_2SO_4 and in the system containing no excess H_2SO_4. Also shown are the areas in which blue-green and red solids are stable and the approximate concentration lines of stability between two liquid layers and solid. The figures show graphically the regions of two-liquid-phase stability for $CuSO_4$-UO_2SO_4-H_2SO_4-H_2O and indicate the maximum temperature limits for homogeneous stability for various compositions in this system. Also shown are the approximate concentrations proposed for HRT operation and for an

Table 22.3. Phase Transition Temperatures (°C); Part C

Master solutions: (a) 16.90% $CuSO_4$, 19.25 mole % excess H_2SO_4
(b) 46.29% UO_2SO_4, 19.25 mole % excess H_2SO_4

Weight Ratio, Solution/H_2O	Weight Ratio, $CuSO_4/UO_2SO_4$													
	9/1	8½/1½	8/2	7½/2½	7/3	6½/3½	6/4	5½/4½	5/5	4/6	3/7	2/8	1/9	0/10
10/0	326	324.5	323	322.5	321.5	320	320	321	320	321	321.5	324	324.5	327
9/1	323		320		318.5		317			316.5				322
8/2	Blue-green solid	319	318				314		313.5					317
7/3		Blue-green solid		314	313			312.5		310.5				313.5
6/4	Blue-green solid		314.5		311.5		310		309					310
5/5				311.5	310.5			309.5		307				307.5
4/6	Blue-green solid		Blue-green solid				308		306.5					308.5
3/7				Blue-green solid	311			309.5		306				306.5
2/8	Blue-green solid				Blue-green solid		312		309.5	309				310.5
1/9				Blue-green solid		Blue-green solid	319		317.5	316				315
0.75/9.25	Blue-green solid		Blue-green solid		Blue-green solid		Blue-green solid		320	319	318	317	317	317
0.5/9.5	Blue-green solid		Blue-green solid		Blue-green solid		Blue-green solid		325	325	325	323	322	322
0.25/9.75	Blue-green solid		Blue-green solid		Blue-green solid		Blue-green solid		337	335	335	333	334	334

Table 22.4. Phase Transition Temperatures (°C); Part D

Master solutions: (a) 16.64% $CuSO_4$, 29.11 mole % excess H_2SO_4
(b) 45.63% UO_2SO_4, 29.11 mole % excess H_2SO_4

Weight Ratio, Solution/H_2O	Weight Ratio, $CuSO_4/UO_2SO_4$													
	10/0	9½/½	9/1	8½/1½	8/2	7½/2½	7/3	6/4	5/5	4/6	3/7	2/8	1/9	0/10
10/0	347.5	342.5	341.7	339	338	337	337	334	335	336	336	336.5	339.5	343.5
9/1	342.2		337		335.5		332	330.5	329.5	329.5				334
8/2	340		334		331.5		328.5	326	325	325				329
7/3	338.2		332		328		325	323	322	321				324
6/4	Blue-green solid	332.2	330		325.5		322	320.2	319	318.2				319
5/5		Blue-green solid	328.5	324.5	323.5		320.5	318	316.5	315.5				316
4/6			327	323.5	322.5		319.5	316	315	314				313.5
3/7			Blue-green solid	323.5	322		319	316	315	313.5				312.2
2/8				Blue-green solid	323.5		318.5	316.5	313.5	313.5				313
1/9			Blue-green solid		Blue-green solid		Blue-green solid	323	318	318				318.5
0.75/9.25			Blue-green solid		Blue-green solid		Blue-green solid	327	327	325	325	322	320	320
0.5/9.5			Blue-green solid		Blue-green solid		Blue-green solid	331	331	331	329	329	327	327
0.25/9.75			Blue-green solid		Blue-green solid		Blue-green solid	Blue-green solid	339	339	339	339	340	339

Table 22.5. Phase Transition Temperatures (°C); Part E

Master solutions: (a) 16.53% $CuSO_4$, 38.75 mole % excess H_2SO_4
(b) 45.36% UO_2SO_4, 38.75 mole % excess H_2SO_4

Weight Ratio, Solution/H_2O	Weight Ratio, $CuSO_4/UO_2SO_4$										
	10/0	9/1	8/2	7/3	6/4	5/5	4/6	3/7	2/8	1/9	0/10
10/1	361	355	351.5	350.2	349	349.5	349	350.5	352.5	355	358
9/1	357.5	351		345	344			343.5	345		353.5
8/2	355	348	344			338		338	339		347
7/3	352	345		336.5	335						338.5
6/4	349.5	341.5	337.5			329.5		328	328.5		331.5
5/5	347	339		330.5	327.5	326					327.5
4/6	345	336.5	332	328.5	325.5	323.5		321.5	321		324
3/7	344	335.5	331	327	324	322		320	319.5		321.5
2/8	Blue-green solid	Blue-green solid	332	328	325	322.5		320.5	320		320
1/9	Blue-green solid	Blue-green solid	336.5	333.5	330	328		326	325		324.5
0.75/9.25		Blue-green solid	Blue-green solid	334	330	330	328	327	326	326	326
0.5/9.5		Blue-green solid	Blue-green solid	339	336	336	333	332	332	330	330
0.25/9.75		Blue-green solid	Blue-green solid	Blue-green solid	347	343	343	342	342	340	340

arbitrary solution in the low-concentration range. If D_2O is substituted for H_2O in this system, the indicated transition temperature will probably be lowered by approximately 10°C. This opinion is based on previous investigations of UO_2SO_4-D_2O two-liquid-phase transitions[2] and on comparison of solubility behavior of D_2O and H_2O salt systems.

Immiscibility transition temperatures will, in all probability, be changed by the addition of small amounts of other components such as $NiSO_4$ and fission products. Further investigations should establish some degree of change and should estimate other effects incurred on this system by additional components. In this respect, study of HRT-solution composition regions is to be emphasized.

[2]C. H. Secoy, chap. 4.3, p 559, in *Reactor Handbook*, declassified ed., ed. by J. F. Hogerton and R. C. Grass, Technical Information Service, AEC, 1955.

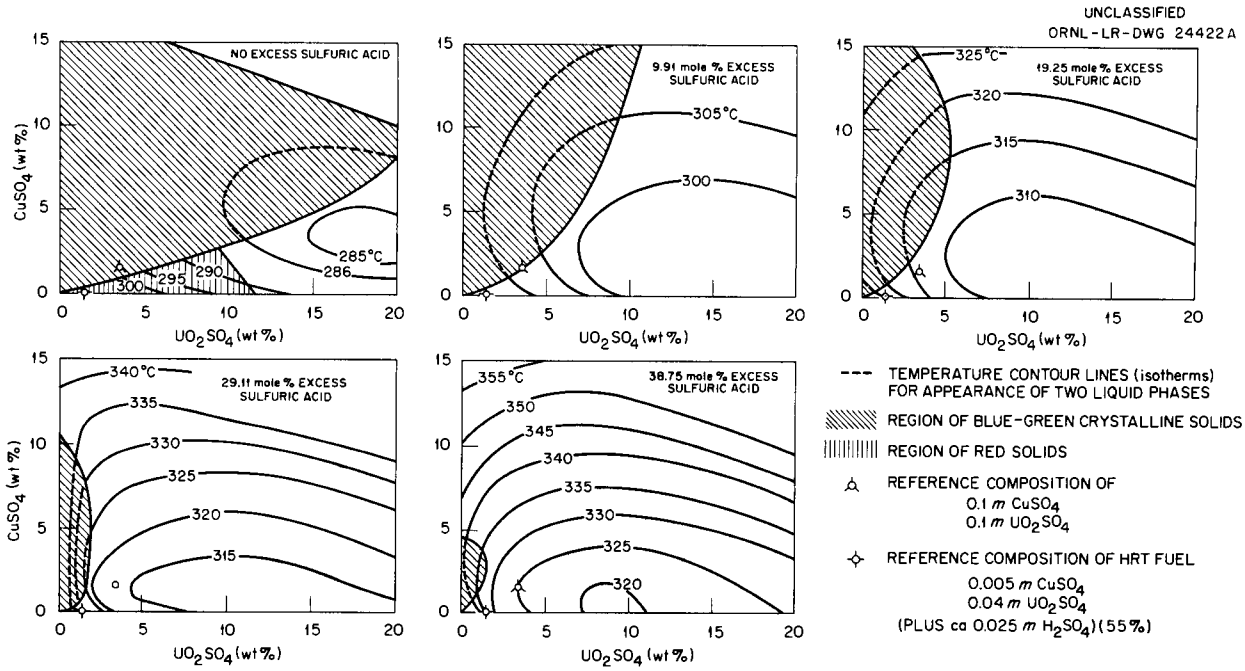

Fig. 22.1. Phase-Transition Temperatures in Solutions Containing Cupric Sulfate, Uranyl Sulfate, and Sulfuric Acid.

Part VII

ANALYTICAL CHEMISTRY

M. T. Kelley

23. ANALYTICAL CHEMISTRY

O. Menis

R. G. Ball
C. M. Boyd
G. Goldstein
H. P. House
D. L. Manning
R. H. Powell

23.1 ANALYSIS OF SOLUTIONS OF URANYL SULFATE

23.1.1 Determination of Arsenic

A spectrophotometric method[1] has been applied to the determination of very low concentrations (5 to 100 μg/ml) of arsenic in solutions of uranyl sulfate. Arsenic(V) is reacted in a 0.15 *M* sulfuric acid solution with ammonium molybdate, thereby forming a heteropoly arsenomolybdic acid. The arsenomolybdic acid is reduced with 1,2,4-aminonaptholsulfonic acid to "molybdenum blue." The concentration of arsenic is calculated from the absorbancy measurements, which are made at a wavelength of 840 mμ. Uranium does not interfere in this determination; therefore no prior separation is required. From 0.2 to 4 μg of arsenic per milliliter in the solution used for the absorbancy measurement can be determined by this method with a coefficient of variation of about 3%.

23.1.2 Pyrolytic Separation and Spectrophotometric Determination of Ruthenium

A method was devised for the separation of microgram quantities, 10 to 100 μg, of ruthenium as a nitroso salt, chloride or sulfate, from uranyl sulfate and its subsequent determination colorimetrically. Decomposition of the nitroso salt and separation of the ruthenium are accomplished by pyrolysis for 1 hr at 1000°C in a stream of moist oxygen. The ruthenium, which volatilizes as the tetraoxide, is absorbed and reduced to the trivalent state in a 1 *M* HCl solution saturated with sulfur dioxide. β-Nitroso-γ-naphthol is added, after which the solution is boiled for about 10 min to accelerate development of a blue-colored ruthenium-β-nitroso-γ-naphthol complex and to expel excess sulfur dioxide. After cooling the solution, the absorbancy of this complex, from which the ruthenium concentration is calculated, is measured at 560 mμ. From 0.2 to 6 μg of ruthenium per milliliter in the solution used for the absorbancy measurement can be determined by the method with a coefficient of variation of approximately 3%. This method is at least four times as sensitive as the flame-photometric method for ruthenium.[2] The pyrolytic separation is more effective than the conventional oxidation-distillation procedure, in that the nitroso salts of ruthenium are more quantitatively separated by the pyrolytic method.

23.1.3 Determination of Cerium

A redox titration procedure[3] for macro quantities of cerium was adapted to the determination of microgram quantities of cerium. Cerium(III) is oxidized to cerium(IV) by titration with 0.0002 *N* potassium permanganate. The end point of the titration is established photometrically. From 50 to 200 μg of cerium in a titration volume of 40 ml can be determined by this procedure with a coefficient of variation of about 6%. Uranium does not interfere in the titration; consequently, no separation is required.

23.1.4 Spectrophotometric Determination of Antimony

A spectrophotometric method which was used by Ward and Lakin[4] for the determination of antimony in soils and rocks has been applied to the estimation of small amounts (<10 ppm) of antimony in uranyl sulfate. The method was found to be applicable to the determination of 0.1 to 1 μg of antimony. Uranium in amounts equal to 10,000 times that of the antimony can be tolerated.

23.1.5 Spectrophotometric Titration of Bismuth

A volumetric titration procedure which was used by Malat, Suk, and Ryba[5] for the determination of

---

[1] E. B. Sandell, *Colorimetric Determination of Traces of Metals*, p 137, Interscience, New York, 1944.

[2] O. Menis *et al.*, *HRP Quar. Prog. Rep. July 31, 1957*, ORNL-2379, p 171.

[3] T. L. Marple, E. P. Przyblowicz, and D. N. Hume, *Anal. Chem.* **28**, 1892 (1956).

[4] F. N. Ward and H. W. Lakin, *Anal. Chem.* **26**, 1168 (1954).

[5] M. Malat, V. Suk, and O. Ryba, *Collection Czechoslov. Chem. Commun.* **19**, 258 (1954).

macro amounts of bismuth was adapted to the estimation of microgram quantities of bismuth in uranyl sulfate. In titrating solutions of uranyl sulfate which contain microgram amounts of bismuth, a spectrophotometric method is used to detect the end point, since the visual end point is too indistinct, and, in addition, colored ions such as UO_2^{++} obscure the end point. As much as 30 mg of sulfate, as uranyl sulfate, can be tolerated by utilizing a back-titration procedure. The absorbancy measurements are made at a wavelength of 575 mμ. From 20 to 100 μg of bismuth can be titrated by this procedure with a coefficient of variation of the order of 5%. Of the metals which interfere in this titration, Fe(III), Zn, Sb, Hg, In, and Ga, only Fe(III) is usually encountered in solutions of uranyl sulfate and can be eliminated by reducing it to Fe(II) with hydrazine nitrate in a boiling solution which contains a trace of Cu^{++} as catalyst.

23.2 ANALYSIS OF THORIUM OXIDE

23.2.1 Determination of Cobalt

A more sensitive method for the determination of cobalt in concentrations of the order of 1 ppm or less in slurries of thorium oxide was desired in anticipation of excessive corrosion of pump components. A survey of chromogenic reagents for cobalt revealed that 1-(2-pyridylazo)-2-naphthol (PAN) appeared to possess the specified degrees of sensitivity and selectivity.[6] These properties were confirmed experimentally; it was found that quantities as low as 0.5 μg of Co(III) can be determined by reacting cobalt with PAN at a pH of 5, extracting the green-colored cobalt-PAN chelate into 5 ml of chloroform, and then finally measuring the absorbancy of the extract. Beer's law is obeyed over the range of 0.5 to 7 μg of cobalt in the 5 ml of organic extract which is used for the absorbancy measurement. The coefficient of variation is of the order of 5%. With the exception of copper, 100-μg quantities of common metals which are ordinarily encountered in contaminated slurries of thorium oxide do not interfere in the method. By applying an anion exchange technique[7] for the removal of microgram quantities of cobalt from a thorium matrix prior to its spectrophotometric determination, 0.1 ppm of cobalt can be determined by this method when a 5-g sample of slurry is taken for analysis.

23.2.2 Separation of Fluoride by Pyrolysis

For the purpose of determining fluoride in reactor materials, ThO_2 and UO_3, and in clays which are under test as possible suspending agents,[8] development work has been continued on the application of a pyrolytic technique for the separation of fluoride from these materials.[9] The sample is mixed with a selected oxide and pyrolyzed in a stream of moist oxygen at 480 to 1000°C in an apparatus of special design (see Fig. 23.1). The temperature of pyrolysis is dependent on the oxide which is used. The fluoride is volatilized from the mixture, absorbed in an alkaline solution, and then determined either by acidimetric titrimetry or by a colorimetric method. The following oxides have been demonstrated as being effective accelerators in releasing the fluoride at the temperature indicated.

Accelerator	Optimum Temperature of Pyrolysis (°C)
U_3O_8	1000
WO_3	825
Nb_2O_5	750
MoO_3	600
V_2O_5	480

Of these oxides, WO_3, V_2O_5, and U_3O_8 have been found to be the most satisfactory accelerators. The fluoride can be removed by volatilization from a number of readily decomposable inorganic fluorides, such as AlF_3 and ZrF_4, by direct pyrolysis in moist oxygen without the addition of an accelerator.

A new principle was applied to a number of clays and silicates which makes it possible to release fluoride with relative ease from highly refractory materials. This principle is based on the fusion and metathesis of refractory materials, whereby fluoride is converted to NaF which in the

[6] K. L. Cheng and R. H. Bray, *Anal. Chem.* **27**, 782 (1955).

[7] K. A. Kraus, F. Nelson, and G. W. Smith, *J. Phys. Chem.* **58**, 11 (1954).

[8] L. M. Doney and C. D. Lynch, *Clays as Suspending Agents for Thoria Slurries*, ORNL CF-57-10-23 (Oct. 4, 1957).

[9] R. H. Powell, *Anal. Chem. Ann. Prog. Rep. Dec. 31, 1956*, ORNL-2218, p 44 (classified).

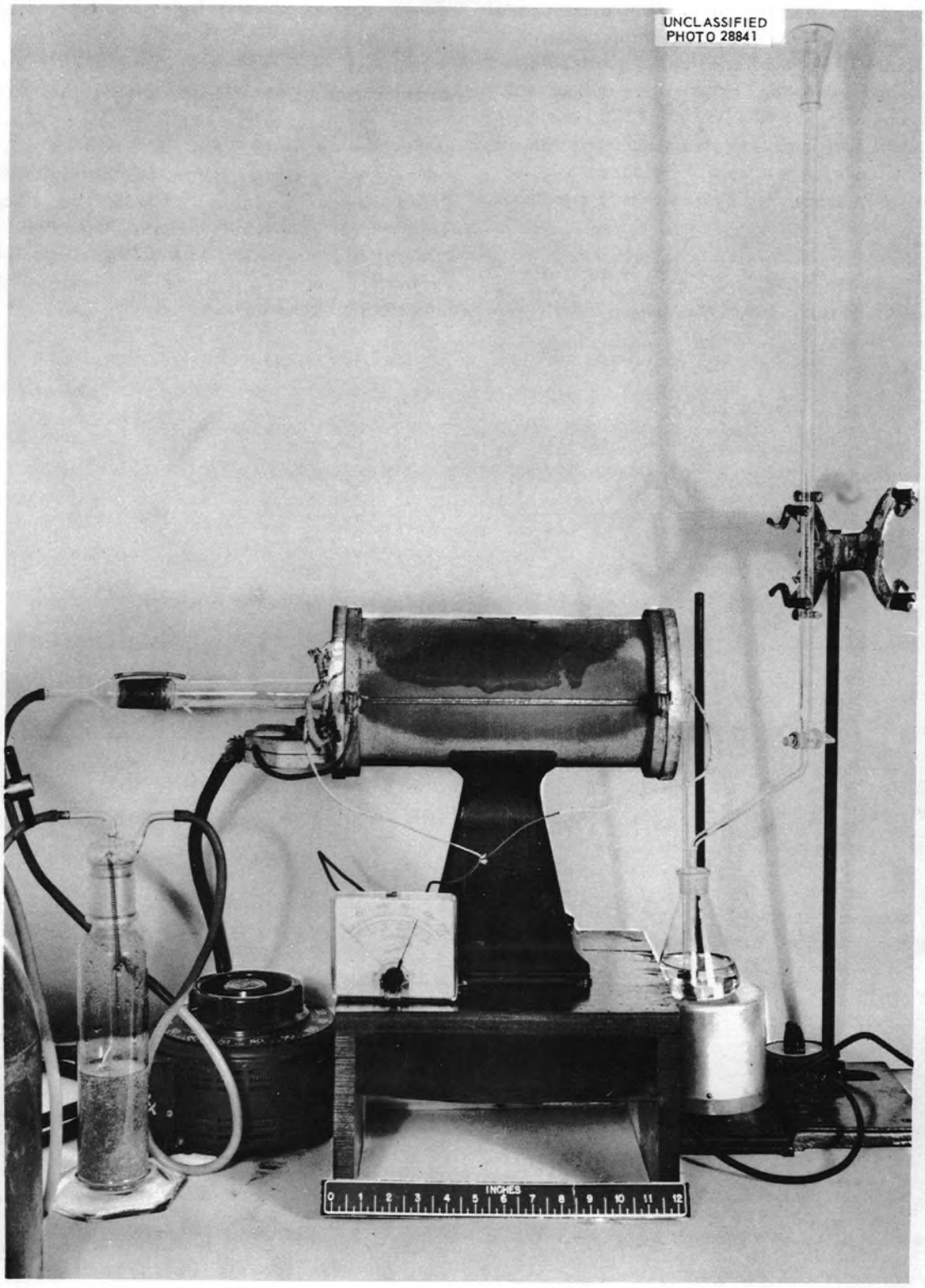

Fig. 23.1. Pyrolysis Apparatus.

presence of the accelerator is then decomposed and releases HF. The suspending materials, which included montmorillanite, attapulgite, ceramic and synthetic clays, were mixed with a flux consisting of Na_2WO_4 plus WO_3 and then heated until fusion and pryolysis occurred. In all cases, the fluoride was readily released and subsequently was determined by a colorimetric method.

[10] O. Menis, H. P. House, and C. M. Boyd, *Particle-Size Distribution of Thorium Oxide by Centrifugal Sedimentation Methods*, ORNL-2345 (Aug. 5, 1957).

23.2.3 Particle-Size Distribution in the Range of 10 to 50 μ

The Andreasen sedimentation method[10] for the determination of particle-size distribution was extended to include fractions of particulate matter within the range of 10 to 50 μ. This was accomplished by following the sedimentation rate of thorium oxide in mixtures of water and glycerol. The viscosity of such mixtures is higher by an order of 10 centipoises, thus making it possible to extend the upper limit to which measurements of particle size can be made.

OAK RIDGE NATIONAL LABORATORY
HOMOGENEOUS REACTOR PROJECT

NOVEMBER 1, 1957

PROJECT DIRECTOR
R. B. BRIGGS — D

ASSOCIATE PROJECT DIRECTOR
C. E. WINTERS** — D
A. L. GUNNELS, SEC. — REE

TECHNICAL ASSISTANT
F. KERTESZ — REE

PROJECT EDITOR
W. D. REEL — TI

DESIGN AND ENGINEERING
R. N. LYON, ASSISTANT DIRECTOR — REE
T. S. CARLSMITH, SEC. — REE

DESIGN
W. R. GALL, SECTION CHIEF — REE
M. I. LUNDIN, ASSISTANT SECTION CHIEF — REE

MECHANICAL DESIGN
F. C. ZAPP, GROUP LEADER — REE
F. C. BOWEN — VITRO
C. A. BURCHSTED — REE
C. J. CLAFFEY — REE
C. W. COLLINS — REE
E. M. GUGLIELMO — VITRO
A. C. PHILLIPS — VITRO
R. G. PITKIN — VITRO
R. E. SCHAPPEL — REE
D. D. TARR — VITRO
W. L. WRIGHT — REE

PROCESS DESIGN
R. C. ROBERTSON, GROUP LEADER — REE
J. C. BOLGER — REE
E. H. GIFT — REE
H. A. MCLAIN — ORSORT
R. O. MAAK — FOSTER WHEELER

HRE-3 MECHANICAL DESIGN
R. H. CHAPMAN, GROUP LEADER — REE
D. W. VROOM — REE

HRE-3 SITE AND STRUCTURES
J. N. ROBINSON — REE

PLANT LAYOUT AND DRAFTING
C. L. SEGASER, GROUP LEADER — REE
W. ROBINSON — REE
H. H. BRADFORD — REE
R. L. CAUBLE — REE
C. W. DAY — REE
J. P. DILORENZO — REE
F. GUNNESS — REE
A. R. KERR — REE
W. B. KRICK — REE
A. S. LUDLOW — REE
C. A. ROBERTS — REE
R. D. SATTERFIELD — REE
R. H. SIGLER — REE
W. G. STERLING — REE

COMPONENT DEVELOPMENT
I. SPIEWAK, SECTION CHIEF — REE

HEAT EXCHANGERS, MECHANICAL ENGINEERING PROBLEMS
J. S. CULVER, GROUP LEADER — REE
B. D. DRAPER — TVA
P. P. HOLZ — REE
I. K. NAMBA — REE
H. C. ROLLER — REE
T. L. CASTILE — REE
T. M. CATE — REE
A. B. DAFFRON — REE
H. C. LeTELLIER — REE

CIRCULATING PUMPS
C. H. GABBARD, GROUP LEADER — REE
J. M. BAKER — REE
J. C. MOYERS — REE
H. R. PAYNE — REE
C. C. HURTT — REE
R. J. LOCKETT — REE

FEED PUMPS AND VALVES
E. C. HISE, GROUP LEADER — REE
R. BLUMBERG — REE
J. P. HURST — REE
G. A. WINDLE — REE

CORE AND BLANKET, CHEMICAL ENGINEERING PROBLEMS
C. G. LAWSON, GROUP LEADER — REE
B. A. HANNAFORD — REE
J. K. HAYES — COMBUSTION
J. E. MOTT — REE
D. L. SNYDER — REE
R. GOODMAN — REE
S. R. WEST — REE

SYSTEMS DEVELOPMENT
R. B. KORSMEYER, SECTION CHIEF — REE
F. N. PEEBLES, ASSISTANT SECTION CHIEF — REE

COMPONENT AND SLURRY TESTING
R. VAN WINKLE, GROUP LEADER — REE
R. B. GALLANER — REE
C. H. GIBSON — REE
C. F. VANDENBULCK — UCNC
C. M. FITZPATRICK — REE

HRT CORE MOCKUP
P. H. HARLEY, GROUP LEADER — REE
D. E. WILLIS — REE
W. M. PARKS — REE
L. E. PENTON — REE
T. R. WILSON — REE

SLURRY BLANKET DEVELOPMENT
L. F. PARSLEY, GROUP LEADER — REE
V. L. KENYON* — REE
R. E. CARNES — REE

OPERATIONS
A. N. SMITH, GROUP LEADER — REE
T. L. BOSWELL — REE
B. R. CHILCOAT — REE
J. T. DICKIE — REE
C. A. GIFFORD — REE
C. A. MCLAUGHLIN — REE
H. G. MOORE — REE
R. E. POTTER — REE
D. H. WALLACE — REE

SPECIAL ASSIGNMENT
M. RICHARDSON — REE

INSTRUMENTATION AND CONTROLS
D. S. TOOMB, SECTION CHIEF — I&C

HRT
J. R. BROWN, GROUP LEADER — I&C
R. M. PIERCE* — TVA
R. W. BORGERS — I&C

HRP SUPPORTING FACILITIES
D. G. DAVIS, GROUP LEADER — I&C
S. J. BALL — I&C
G. W. GREENE — I&C
J. D. GRIMES — TVA
P. G. HERNDON — I&C
J. A. RUSSELL — I&C
R. M. BURNETT — I&C
M. A. MEACHAM — I&C
P. E. SMITH — I&C

VALVES AND ACTUATORS
A. M. BILLINGS, GROUP LEADER — I&C
E. H. BELL — I&C
B. J. JONES — I&C
P. F. HURAY — I&C
A. J. SHARENBERGER* — I&C

INSTRUMENT DEVELOPMENT
R. L. MOORE, GROUP LEADER — I&C
H. D. WILLS — I&C

RESEARCH AND ANALYSIS
P. R. KASTEN, SECTION CHIEF — REE

HRE-3 REACTOR PHYSICS
M. W. ROSENTHAL, GROUP LEADER — REE
B. E. PRINCE — REE

FLOW VISUALIZATION AND SCALE-UP STUDIES
H. C. CLAIBORNE, GROUP LEADER — REE
W. R. MIXON — REE

TRANSPORT PROPERTIES OF SLURRIES
D. G. THOMAS, GROUP LEADER — REE
L. L. BENNETT — REE
R. H. NIMNO — REE
P. H. HAYES — REE
R. M. SUMMERS — REE

PHYSICAL CHEMISTRY OF SLURRIES
C. S. MORGAN — REE
B. G. SUTTON — REE

STRESS ANALYSIS AND CLOSURE RESEARCH
R. O. CHEVERTON, GROUP LEADER — REE
T. H. MAUNEY — REE
E. VOLK — COMBUSTION

REACTOR ANALYSIS AND LONG RANGE PLANNING
T. B. FOWLER — REE
S. JAYE — REE
M. P. LIETZKE — REE
C. W. NESTOR, JR. — REE
M. TOBIAS — REE

REACTOR MATERIALS RESEARCH
E. G. BOHLMANN, ASSISTANT DIRECTOR — REE
T. F. KELLY, SEC. — REE
B. H. BOLEN, STENO. — REE
R. E. WACKER, RECORDS — REE

SOLUTIONS
J. C. GRIESS, ASSISTANT SECTION CHIEF — REE

LOOPS
R. S. GREELEY, GROUP LEADER — REE
S. R. BUXTON — REE
J. E. JACKSON — REE
W. H. HINDS — REE

LABORATORY STUDIES
J. L. ENGLISH, GROUP LEADER — REE
D. N. HESS — REE
P. D. NEUMANN — REE
L. L. FAIRCHILD — REE
H. L. BARKER — REE
P. B. DAVIS — REE
B. L. JOHNSON — REE
H. R. TINCH — REE
J. L. UNDERWOOD — REE

SLURRIES
E. L. COMPERE, ASSISTANT SECTION CHIEF — REE

LOOPS
S. A. REED,* GROUP LEADER — REE
F. E. McDANIEL — REE

TOROIDS
S. A. REED* — REE
R. F. BENSON — REE
B. H. PARKS — REE
G. G. WARNER — REE

IN-PILE BOMBS
L. F. WOO — REE

ENGINEERING
H. C. SAVAGE, ASSISTANT SECTION CHIEF — REE

SOLUTIONS
S. E. BOLT, GROUP LEADER — REE
W. C. ULRICH — REE

IN-PILE MOCKUPS
J. R. HART, LEADER — REE
C. H. BURBAGE — REE
H. F. HENDERSON — REE
R. W. RAY — REE
B. W. SCOTT — REE

100A LOOP OPERATIONS
J. F. WINESETTE* — REE
L. L. ALLEN — REE
C. M. BURCHELL — REE
C. L. FRANCIS — REE
J. B. FRENCH — REE
D. G. GATES — REE
J. W. GOOCH — REE
T. R. RAYBURN — REE
W. H. WAGNER — REE

SLURRIES
D. T. JONES, GROUP LEADER — REE
D. W. HUBBARD — REE
R. M. WARNER — REE

IN-PILE TOROIDS
J. D. BARNES — REE

100A LOOP OPERATIONS
J. F. WINESETTE* — REE
C. R. BENSON — REE
G. A. MOORE — REE
L. G. PHELPS — REE
A. E. PUGH — REE

REACTOR OPERATIONS
R. A. LORENZ, GROUP LEADER — REE
J. W. BROWN — REE
V. A. DECARLO — REE
F. J. WALTER‡ — REE
V. R. BULLINGTON — REE
W. E. TEICHERT, A SHIFT LEADER — REE
C. E. ROBERTS — REE
E. H. GUINN, B SHIFT LEADER — REE
D. M. SMITH — REE
A. L. SUTTON, C SHIFT LEADER — REE
R. A. JONES — REE
R. M. WALLER — REE
J. W. MYERS, D SHIFT LEADER — REE
J. W. MOSIER — REE
R. G. ROSS — REE

RADIATION
G. H. JENKS, SECTION CHIEF — REE

IN-PILE LOOPS
J. R. McWHERTER, GROUP LEADER — REE
J. E. BAKER — REE
J. C. BANTER — REE
S. H. WHEELER — REE

IN-PILE BOMBS
R. J. DAVIS, GROUP LEADER — C
F. A. KNOX — REE
K. S. WARREN — C
J. L. RUTHERFORD — REE

SUPPORTING RESEARCH
A. L. BACARELLA — C
M. D. SILVERMAN — C
W. C. YEE‡ — C

REMOTE EVALUATION
A. R. OLSEN — REE
B. W. McCOLLUM, SHIFT LEADER — REE
W. J. SCHILL — REE
W. H. SMITH, JR. — REE
J. C. THOMPSON — REE

METALLURGY
G. M. ADAMSON, SECTION CHIEF — M

METALLURGICAL RESEARCH
M. L. PICKLESIMER, LEADER — M
P. L. RITTENHOUSE — M
R. L. STEPHENSON — M
P. J. JONES — M
G. C. NELSON — M
M. A. WHEELER — M

METALLURGICAL ENGINEERING
E. S. BOMAR, LEADER — M
F. W. COOKE — M
E. A. FRANCO-FERREIRA** — M
W. J. LEONARD — M
J. J. PRISLINGER — M
J. K. WHITE — M
C. H. WOOTKE — M
C. M. SMITH — M
J. J. WOODHOUSE — M

METALLOGRAPHY
R. S. CROUSE,** LEADER — M
T. M. KEELEY, JR. — M
W. J. WERNER** — M
E. R. BOYD — M
B. F. DAY** — M
R. L. FITZGERALD — M
T. J. HENSON** — M
L. G. SPRADER** — M

RADIATION DAMAGE
R. C. BERGGREN — SS
J. C. WILSON — SS
F. W. GRIZZEL — SS

SUBCONTRACTS
AEROJET GENERAL CORPORATION
HOUDRY PROCESS CORPORATION
OHIO STATE UNIVERSITY
RICE INSTITUTE
STANFORD RESEARCH INSTITUTE
SYRACUSE UNIVERSITY
TULANE UNIVERSITY
UNIVERSITY OF TENNESSEE
UNIVERSITY OF UTAH
UNIVERSITY OF VIRGINIA

INDUSTRIAL PARTICIPATION
COMBUSTION ENGINEERING, INC.
FOSTER WHEELER
PENNSYLVANIA POWER AND LIGHT COMPANY
PUERTO RICO WATER RESOURCES AUTHORITY
TENNESSEE VALLEY AUTHORITY
UNION CARBIDE NUCLEAR COMPANY, NEW YORK

AC ANALYTICAL CHEMISTRY DIVISION
C CHEMISTRY DIVISION
CT CHEMICAL TECHNOLOGY DIVISION
D DIRECTOR'S DIVISION
E&M ENGINEERING AND MECHANICAL DIVISION
I&C INSTRUMENTATION AND CONTROLS DIVISION
M METALLURGY DIVISION
REE REACTOR EXPERIMENTAL ENGINEERING DIVISION
SS SOLID STATE DIVISION
TI TECHNICAL INFORMATION DIVISION
* DUAL CAPACITY
** PART TIME ON PROJECT
† ON LOAN FROM DUKE UNIVERSITY
‡ SPECIAL ASSIGNMENT

CHEMICAL TECHNOLOGY
O. E. FERGUSON,* PROGRAM LEADER — CT
I. LOOPE, SEC. — CT
R. WILLIAMS, SEC. — CT

CHEMICAL DEVELOPMENT
D. E. FERGUSON,* SECTION CHIEF — CT

BLANKET PROCESSING
R. E. LEUZE, PROBLEM LEADER — CT
R. D. BAYBARZ — CT
J. M. CHILTON — CT
S. S. KIRSLIS — CT
J. H. GROOVER — CT
R. L. HICKEY — CT
O. K. TALLENT — CT

CORE PROCESSING
R. A. McNEES, PROBLEM LEADER — CT
M. H. LLOYD — CT
S. PETERSON — CT
J. E. DAVIDSON — CO-OP, UNIV. OF TENN.
W. B. HOWERTON — CT

THORIUM BLANKET STUDIES
J. P. McBRIDE, PROBLEM LEADER — CT
E. V. JONES — C
N. A. KROHN — CT
K. M. McCORKLE — CT
L. E. MORSE — CT
R. L. PEARSON — CT
C. E. SCHILLING — CT
C. W. GREENE — CT
P. P. HAYDON — CT
W. J. LEE — CO-OP, GEORGIA TECH.
W. L. PATTISON — CT
H. F. SOARD — CT

DESIGN
W. E. UNGER, ASSISTANT SECTION CHIEF — CT

PROCESS DESIGN
B. F. BOTTENFIELD — CT
J. C. SUDOATH — CT
H. O. WEEREN — CT

PROJECT DESIGN
G. B. BERRY** — E&M
F. C. McCULLOUGH — CT
E. B. BRIDGES** — E&M
J. D. CUPP** — E&M
J. W. DAY — E&M
H. W. FALLON** — E&M
L. C. HUBBARD — E&M
J. H. MANNEY** — E&M
F. L. PEISHEL** — E&M
J. PHILLIPS** — E&M
K. F. STOOKSBURY** — E&M
J. H. THOMPSON — E&M
J. N. WHEELER** — E&M

LOOP DESIGN
T. A. AREHART — CT
B. B. KLIMA — CT
L. J. KING — CT
W. F. SCHAFFER — CT

INSTRUMENTATION
C. S. LISSER — I&C

PILOT PLANT
R. B. LINDAUER,** SECTION CHIEF — CT

SLURRY PREPARATION
E. M. SHANK, PROBLEM LEADER — CT
C. V. ELLISON — CT

UNIT OPERATIONS
P. A. HAAS, GROUP LEADER — CT

CORE PROCESSING
K. O. JOHNSSON — CT
E. L. YOUNGBLOOD — CT
R. D. ARTHUR — CT
R. C. EARLY — CT

UO_2SO_4 BLANKET PROCESSING
J. W. SHIDER — CT
F. N. McLAIN — CT
D. A. McWHIRTER — CT
G. E. WOODALL — CT

THORIUM BLANKET STUDIES
C. C. HAWS — CT
W. M. WOODS — CT
V. L. FOWLER — CT
S. G. KENT, III — CT

CHEMICAL RESEARCH
E. H. TAYLOR,** DIRECTOR — C
H. A. STEINKE, SEC. — C

FUEL SOLUTION CHEMISTRY
H. F. McDUFFIE, GROUP LEADER — C
W. L. MARSHALL, GROUP LEADER — C
J. S. GILL — C
G. M. HEBERT — C
R. SLUSHER — C
H. H. STONE — C
F. H. SWEETON — C

RADIATION CHEMISTRY
C. J. HOCHANADEL,** GROUP LEADER — C
J. W. BOYLE** — C
H. A. MAHLMAN** — C

HEAVY ELEMENT CHEMISTRY
R. W. STOUGHTON,** GROUP LEADER — C
J. HALPERIN** — C
M. H. LIETZKE** — C
W. C. WAGGENER** — C

INORGANIC SOLUTION CHEMISTRY
K. A. KRAUS,** GROUP LEADER — C
T. A. CARLSON** — C
H. O. PHILLIPS** — C

ANALYTICAL CHEMISTRY
MYRON T. KELLEY,** DIRECTOR
C. D. SUSANO,** ASSOCIATE DIRECTOR
K. A. ODOM, SEC. — AC

CORROSION ANALYTICAL LABORATORY
O. MENIS,* SUPERVISOR — AC
H. P. HOUSE, ASSISTANT SUPERVISOR — AC

RESEARCH
O. MENIS,* GROUP LEADER — AC
C. M. BOYD — AC
R. H. POWELL — AC
D. L. MANNING, GROUP LEADER — AC
R. G. BALL — AC
G. GOLDSTEIN — AC
T. C. RAINS, GROUP LEADER — AC
I. B. RUBIN — AC

SERVICES
C. K. TALBOTT, GROUP LEADER — AC
D. E. CARPENTER — AC
N. M. FERGUSON — AC
F. L. LAYTON — AC
T. P. BACON — AC
W. D. CLAPP, JR. — AC
C. A. CLARK — AC
P. S. GOODWIN — AC
B. D. HICKS — AC
A. H. MATTHEWS — AC
T. G. MILLER — AC
V. S. NORMAN — AC
E. ONKST — AC
C. M. WILSON — AC

HRT AND IN-PILE LOOP ANALYSES
U. KOSKELA, SUPERVISOR — AC
L. G. FARRAR, ASSISTANT SUPERVISOR — AC
J. E. ATTRILL — AC
C. P. BAKER — AC
R. E. CORCORAN — AC
S. R. DINSMORE — AC
J. L. MOTTERN — AC
G. M. CAMPBELL — AC
G. I. GAULT — AC
M. H. McCORQUODALE — AC
J. SLESSINGER, JR. — AC
W. R. WARREN — AC
H. L. WEBB — AC
H. L. WHITTINGTON — AC

HRT DEVELOPMENT
P. F. THOMASON, GROUP LEADER — AC
R. E. BIGGERS — AC
F. J. MILLER — AC
S. A. REYNOLDS, GROUP LEADER — AC
T. H. HANDLEY — AC

HIGH RADIATION LABORATORY
C. L. BURROS — AC

HOMOGENEOUS REACTOR TEST
S. E. BEALL, PROJECT ENGINEER — REE
B. EUBANK, SEC. — REE
M. SWANK, SEC. — CT

REACTOR PLANNING
S. I. KAPLAN, GROUP LEADER — REE
J. R. BUCHANAN — CT

SPECIAL ASSIGNMENT
H. M. McLEOD — CT

PLANT OPERATIONS
J. W. HILL, JR., CHIEF — REE
R. SMITH — REE
J. R. ENGEL, SUPERVISOR — CT
R. J. HARVEY — REE
H. K. SEARCH — PA. POWER AND LIGHT CO.
H. D. CURTIS — REE
D. T. GODWIN — REE
A. L. JOHNSON — REE
L. P. PUGH — REE
J. O. FLYNN, SUPERVISOR — REE
H. F. BAUMAN — CT
N. C. BRADLEY — CT
E. D. BOLLING — REE
W. T. BOSTIC — CT
E. W. BROWN — CT
T. G. HILL — REE
J. O. KOLB, SUPERVISOR — REE
N. A. BROWN — TVA
D. F. FRECH — REE
J. E. EVE — REE
R. J. SHANNON — CT
L. J. SHERSKY — CT
J. E. WOLFE — REE
G. W. RIVENBARK, SUPERVISOR — REE
D. F. BRULEY — CT
T. H. GLADNEY — TVA
R. H. GUYMON — CT
H. L. BROWN — REE
R. J. HUNTER — REE
F. L. ROUSER — REE
J. L. STEPP — REE

REACTOR MATERIALS AND CHEMISTRY
D. M. RICHARDSON, GROUP LEADER — REE
J. D. JONES — REE

CHEMICAL PLANT
W. D. BURCH, GROUP LEADER — CT
W. L. ALBRECHT — TVA
R. H. WINGET — CT
W. A. LINDSEY — CT
R. E. TRENT — CO-OP, UNIV. OF TENN.

PERFORMANCE STUDIES
R. VAN WINKLE, GROUP LEADER — REE
J. A. WATTS — REE

REACTOR ANALYSIS
P. N. HAUBENREICH, GROUP LEADER — REE
J. HERNANDEZ — PUERTO RICO WATER RESOURCES AUTHORITY

MAINTENANCE PLANNING
W. TERRY, SUPERVISOR — REE
T. E. HAYNES — REE
G. H. JOHNSTONE — REE

INSTRUMENTATION
K. W. WEST, GROUP LEADER — I&C
R. M. PIERCE* — TVA
A. J. SHARENBERGER* — I&C

PERSONNEL SUMMARY

	FULL TIME	PART TIME	INDUSTRIAL PARTICIPATION
ADMINISTRATION	7	4	
ANALYTICAL CHEMISTRY	43		
CHEMICAL RESEARCH	7	10	
CHEMICAL TECHNOLOGY	50	10	
DESIGN AND ENGINEERING	118		7
HOMOGENEOUS REACTOR TEST	43		5
REACTOR MATERIALS RESEARCH	99	6	
TOTAL	367	30	12